US Army Corps of Engineers

TECHNICAL REPORT HL-91-7

(2)

DEVELOPMENT AND VERIFICATION OF A THREE-DIMENSIONAL NUMERICAL HYDRODYNAMIC, SALINITY, AND TEMPERATURE MODEL OF CHESAPEAKE BAY

Volume I

MAIN TEXT AND APPENDIX D

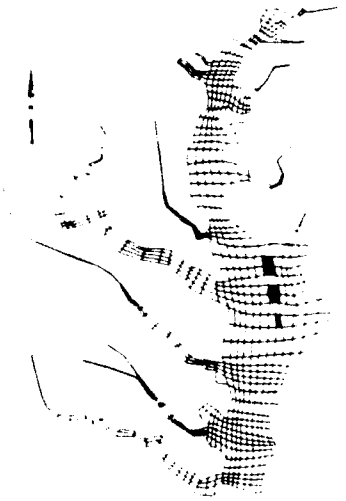

by

B. H. Johnson, R. E. Heath, B. B. Hsieh

Hydraulics Laboratory

and

K. W. Kim, H. L. Butler

Coastal Engineering Research Center

DEPARTMENT OF THE ARMY
Waterways Experiment Station, Corps of Engineers
3909 Halls Ferry Road, Vicksburg, Mississippi 39180-6199

August 1991
Final Report

Prepared for US Army Engineer District, Baltimore
Baltimore, Maryland 21203-1715

HYDRAULICS LABORATORY

Destroy this report when no longer needed. Do not return it to the originator.

The findings in this report are not to be construed as an official Department of the Army position unless so designated by other authorized documents.

The contents of this report are not to be used for advertising, publication, or promotional purposes. Citation of trade names does not constitute an official endorsement or approval of the use of such commercial products.

REPORT DOCUMENTATION PAGE

Form Approved
OMB No. 0704-0188

1. AGENCY USE ONLY *(Leave blank)*	2. REPORT DATE	3. REPORT TYPE AND DATES COVERED
	August 1991	Final report

4. TITLE AND SUBTITLE
Development and Verification of a Three-Dimensional Numerical Hydrodynamic, Salinity, and Temperature Model of Chesapeake Bay; Volume I: Main Text and Appendix D

5. FUNDING NUMBERS

6. AUTHOR(S)
B. H. Johnson, K. W. Kim, R. E. Heath, B. B. Hsieh, H. L. Butler

7. PERFORMING ORGANIZATION NAME(S) AND ADDRESS(ES)
USAE Waterways Experiment Station, Hydraulics Laboratory and Coastal Engineering Research Center, 3909 Halls Ferry Road, Vicksburg, MS 39180-6199

8. PERFORMING ORGANIZATION REPORT NUMBER
Technical Report HL-91-7

9. SPONSORING/MONITORING AGENCY NAME(S) AND ADDRESS(ES)
USAED, Baltimore, PO Box 1715, Baltimore, MD 21203-1715

10. SPONSORING/MONITORING AGENCY REPORT NUMBER

11. SUPPLEMENTARY NOTES
A limited number of copies of Appendixes A-C are published under separate cover. Copies of this report and the appendixes are available from National Technical Information Service, 5285 Port Royal Road, Springfield, VA 22161

12a. DISTRIBUTION/AVAILABILITY STATEMENT
Approved for public release; distribution is unlimited

12b. DISTRIBUTION CODE

13. ABSTRACT *(Maximum 200 words)*

A time-varying three-dimensional (3-D) numerical hydrodynamic model of Chesapeake Bay has been developed to provide flow fields to a 3-D water quality model of the bay. The water surface, 3-D velocity field, salinity, and temperature are computed. Major physical processes affecting bay circulation and vertical mixing are modeled. A particular feature of the model is the solution of transformed equations on a boundary-fitted grid in the horizontal plane.

The 3-D model has been verified through application to six data sets. The first three were about 1 month long each and represented a dry summer condition, a spring runoff, and a fall wind-mixing event. The last three were yearlong simulations for the years of 1984, 1985, and 1986. These years represent a wet, dry, and average freshwater inflow year, respectively. A major storm in November 1985 over the lower portion of the bay resulted in a 200-year flood on the James River and served to demonstrate the ability of the model to simulate extreme events. Results from these applications demonstrate that the model is a good representation of the hydrodynamics of the Chesapeake Bay and its major tributaries.

14. SUBJECT TERMS		15. NUMBER OF PAGES
Chesapeake Bay Hydrodynamics	Numerical model Three-Dimensional	193

17. SECURITY CLASSIFICATION OF REPORT	18. SECURITY CLASSIFICATION OF THIS PAGE	19. SECURITY CLASSIFICATION OF ABSTRACT	20. LIMITATION OF ABSTRACT
UNCLASSIFIED	UNCLASSIFIED		

PREFACE

The study described herein and the preparation of this report were conducted during 1988–91 for the US Army Engineer District, Baltimore, by the US Army Engineer Waterways Experiment Station (WES) under the general supervision of Mr. F. A. Herrmann, Jr., Chief of the Hydraulics Laboratory; Dr. J. R. Houston, Chief of the Coastal Engineering Research Center; and Messrs. M. B. Boyd, Chief of the Waterways Division (WD), Hydraulics Laboratory; W. H. McAnally, Chief of the Estuaries Division (ED), Hydraulics Laboratory; and H. Lee Butler, Chief of the Research Division (RD), Coastal Engineering Research Center. Dr. Robert W. Whalin, Technical Director, WES, was the director of the study; and Mr. D. L. Robey, Chief of the Ecosystem Research and Simulation Division (ERSD), Environmental Laboratory, was the Study Manager. Mr. Butler was the coordinator for the Hydrodynamics Modeling Team.

Drs. B. H. Johnson, WD, and K. W. Kim, RD, prepared this report with assistance from Mr. R. E. Heath, Math Modeling Branch, WD; Dr. B. B. Hsieh, ED; and Mr. Butler. Dr. Y. P. Sheng of University of Florida was a consultant in the early phases of the study.

The June–July 1980 data presented in the report were obtained from Dr. W. Boicourt of the Horn Point Environmental Laboratories in Cambridge, MD. Dr. A. Blumberg of HydroQual, Inc., Mahwah, NJ, provided the April 1983 and September 1983 data sets. These data were primarily collected by the National Ocean Service.

This report was edited by Mrs. M. C. Gay, Information Technology Laboratory, WES.

Commander and Director of WES during preparation of this report was COL Larry B. Fulton, EN. Technical Director was Dr. Robert W. Whalin.

The report should be cited as follows:

Johnson, B. H., Kim, K. W., Heath, R. E., Hsieh, B. B., and Butler, H. L. 1991. "Development and Verification of a Three-Dimensional Numerical Hydrodynamic, Salinity and Temperature Model of Chesapeake Bay," Technical Report HL-91-7, US Army Engineer Waterways Experiment Station, Vicksburg, MS.

CONTENTS

* A limited number of copies of Appendixes A through C are published under separate cover. Copies are available from National Technical Information Service, Springfield, VA 22161.

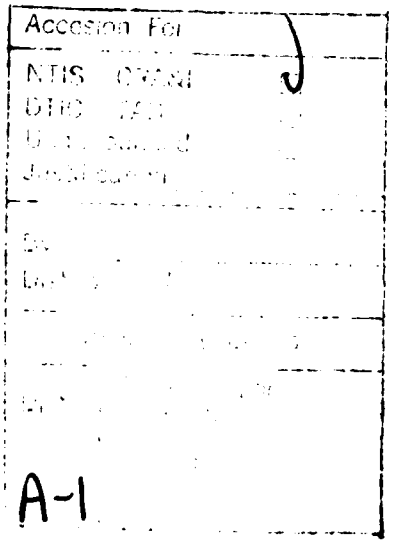

CONVERSION FACTORS, NON-SI TO SI (METRIC)
UNITS OF MEASUREMENT

Non-SI units of measurement used in this report can be converted to SI (metric) units as follows:

Multiply	By	To Obtain
cubic feet	0.02831685	cubic metres
feet	0.3048	metres

DEVELOPMENT AND VERIFICATION OF A THREE-DIMENSIONAL NUMERICAL HYDRODYNAMIC, SALINITY, AND TEMPERATURE MODEL OF CHESAPEAKE BAY

PART I: INTRODUCTION

Background

1. The Chesapeake Bay is one of the Nation's most valuable natural resources. It supports important commercial and recreational fisheries, transportation, industry, recreation, and tourism, and provides irreplaceable habitat for marine resources and wildlife. However, the estuary has been subjected to increasing environmental stress in recent decades, and the productivity and beauty of the Chesapeake Bay have significantly declined. In 1983, the US Environmental Protection Agency (USEPA) identified major contributing factors to the bay's decline as inputs of nutrients and toxicants from point and nonpoint sources, changes in land use within the basin with resulting modification of the watershed and resource habitat, and concurrent impacts of natural events such as floods and droughts (USEPA 1983a, 1983b). Because population within the bay drainage basin is still increasing, and development pressures will continue into the foreseeable future, it is necessary that strategies are developed to reverse the present bay decline and to accommodate future growth in an environmentally sound manner.

2. The Chesapeake Bay Program (CBP), established in 1983, provides a management structure through which the activities of state and Federal agencies, as well as those of private citizens, can be coordinated toward the goal of bay restoration. A number of tools have been developed by the CBP that will assist in the planning, implementation, and evaluation of these strategies. Among these tools are the following: a baywide long-term monitoring program to determine water quality conditions and trends; a comprehensive Chesapeake Bay data base; and a series of numerical models to evaluate alternative control strategies and to guide the establishment of pollutant reduction goals. In June 1985, the CBP Implementation Committee approved a modeling strategy that called for phased development of these models. Phase I was the refinement, computer code conversion, and updating of the existing Chesapeake Bay Watershed Model, which predicts the delivery of nutrients to the estuary from point and nonpoint sources above the fall line and nonpoint

sources below the fall line. Phase II was the development of a steady-state (coarse grid) water quality model of the bay to assess general response of the system to nutrients and the relative importance of various processes. The third phase of the modeling strategy consisted of a three-dimensional (3-D), time-varying, hydrodynamic, and water quality model for the bay and tributaries that could provide a detailed assessment of the system's response to nutrient inputs and other parameters varied realistically over time and space. The 3-D model represents the means through which proposed management actions can be tested before implementation, allowing more cost-effective selection of appropriate strategies.

Purpose

3. It has been acknowledged that water quality impacts in the Chesapeake Bay cannot be successfully assessed without an accurate description of the hydrodynamic processes. Thus, the purpose of this study was the development and subsequent verification of a 3-D hydrodynamic model of Chesapeake Bay. The particular hydrodynamic computer code employed is called CH3D (Curvilinear Hydrodynamics in Three Dimensions). The basic code was developed by Sheng (1986) for the US Army Engineer Waterways Experiment Station (WES) but has been extensively modified in its application to Chesapeake Bay. As its name implies, CH3D makes hydrodynamic computations on a curvilinear or boundary-fitted planform grid. Physical processes impacting baywide circulation and vertical mixing that are modeled include tides, wind, density effects (salinity and temperature), freshwater inflows, turbulence, and the effect of the earth's rotation. Adequately representing the vertical turbulence is crucial to a successful simulation of stratification, destratification, and anoxia in the bay. The boundary-fitted coordinates feature of the model provides enhancement to fit the deep navigation channel and irregular shoreline configuration of the bay and permits adoption of an accurate and economical grid schematization.

Scope

4. The Chesapeake Bay is one of the largest estuaries in the world. As shown in Figure 1, the main bay extends approximately 300 km north from the

ocean entrance to the Susquehanna River. The average depth of the bay is about 8 m, although a natural channel with depths greater than 15 m traverses the bay for more than 60 percent of its length. The bay is irregular in shape, varying in width from 6.4 km between Annapolis, MD, and Kent Island, in the Upper Chesapeake Bay, to 48.3 km in the middle bay off the Potomac River. The bay is long enough to accommodate one complete tidal wave at all times.

5. The numerical grid employed in the 3-D hydrodynamic model is shown in Figure 2. There are 734 active horizontal cells and a maximum of 15 vertical layers, resulting in over 4,000 computational cells. To capture the important features of the hydrodynamic processes and bathymetry in the bay, grid resolution is 1.52 m vertical and approximately 10 km longitudinal and 3 km lateral. Major tributaries, i.e., the James, York, Rappahannock, Potomac, Patuxent and Susquehanna Rivers, are modeled fully 3-D in the lower reach and two-dimensional (2-D) in the upper reach with a single cell spanning the width of the tributary. Based upon an average inflow of 70,000 cfs, typically about 90 percent of the fresh water in the bay enters by these rivers.

6. A successful verification of the hydrodynamic model requires sets of synoptic data. These sets must contain freshwater inflows and their temperature on the major tributaries; tides at the bay entrance as well as at various interior stations; meteorological data at one or more stations from which the surface wind stress and heat flux can be determined; and currents, temperature, and salinity at several locations throughout the bay as well as at the ocean boundary.

7. The bay being so large contributes to the fact that there is a lack of synoptic data throughout the bay and its tributaries. Three relatively extensive synoptic data sets were identified for use in the initial verification of the 3-D model. These data sets were collected during June-July 1980, April 1983, and September 1983. The 1980 data were collected and provided by Dr. William Boicourt of the Horn Point Environmental Laboratories at Cambridge, MD, and the 1983 data were collected primarily by the National Ocean Service (NOS) and provided by Dr. Alan Blumberg of HydroQual, Inc, Mahwah, NJ. The 1980 data set represents low inflow conditions and is a good characterization of the summer circulation that may occur in any year. The spring 1983 data represent conditions during a large spring runoff event, whereas the fall 1983 data set contains a strong wind-mixing event that resulted in a destratification of the bay. This process was aided by a rapid cooling of the surface

waters. Final verification of the 3-D model was achieved through yearlong simulations of the years 1984, 1985, and 1986. These years represent high, low, and average freshwater inflows, respectively. Table 1 summarizes conditions existing during each of these simulation periods.

8. Results from each of these six simulations are presented. It should be noted that results from the June-July 1980 and April 1983 simulations are from the application of an earlier version of the final model. Thus, these results should be viewed only in a qualitative sense. Application to the fall 1983 data is discussed in detail since this data set guided the modifications resulting in the model that was finally applied to the yearlong production simulations. These yearlong simulations also served as additional verification of the 3-D model since no additional adjustment of model coefficients was made. Only selected results from the yearlong simulations are presented. Complete results are given in Appendixes A-C.

9. Before discussing verification results, a limited discussion of the numerical model is provided. For more information, see Johnson et al. (1991).

PART II: MODEL DESCRIPTION

Boundary-Fitted Equations

10. To better resolve complex geometries in the horizontal directions, the Chesapeake Bay 3-D model makes computations on the boundary-fitted or generalized curvilinear planform grid shown in Figure 2. This necessitates the transformation of the governing equations into boundary-fitted coordinates (ξ,η).* If only the (x,y) coordinates are transformed, a system of equations similar to those solved by Johnson (1980) for vertically averaged flow fields is obtained. However, in the Chesapeake Bay model, not only are the (x,y) coordinates transformed into the (ξ,η) curvilinear system but also the velocity is transformed such that its components are perpendicular to the (ξ,η) coordinate lines. This is accomplished by employing the following definitions for the components of the Cartesian velocity (u,v) in terms of contravariant components $\bar{u}$ and $\bar{v}$.

$$u = x_\xi \bar{u} + x_\eta \bar{v} \tag{1}$$

$$v = y_\xi \bar{u} + y_\eta \bar{v} \tag{2}$$

With the governing equations written in terms of the contravariant components of the velocity, boundary conditions can be prescribed on a boundary-fitted grid in the same manner as on a Cartesian grid since $\bar{u}$ and $\bar{v}$ are perpendicular to the curvilinear cell faces; e.g., at a land boundary, either $\bar{u}$ or $\bar{v}$ is set to zero.

11. Initially the vertical dimension was handled through the use of what is commonly called a sigma stretched grid. However, with the grid resolution shown in Figure 2, it was observed that stratification in the deep channels could not be maintained during long-term simulations on Chesapeake Bay. With a sigma stretched grid, the bottom layer in one column communicates

---

* For convenience, symbols and unusual abbreviations are listed and defined in the Notation (Appendix D).

with the bottom layer in an adjacent column. Thus, if depth changes are rather coarsely resolved, channel stratification cannot be maintained. As a result, the governing equations were rederived for solution on the Cartesian or z-plane in the vertical direction.

12. With both the Cartesian coordinates and the Cartesian velocity transformed, the following boundary-fitted equations for $\bar{u}$, $\bar{v}$, w, S, and T to be solved in each vertical layer are obtained:

$$\frac{\partial h\bar{u}}{\partial t} = -h\left[\frac{G_{22}}{J^2}\frac{\partial \zeta}{\partial \xi} - \frac{G_{12}}{J^2}\frac{\partial \zeta}{\partial \eta}\right] + \frac{h}{J}\left(G_{12}\bar{u} + G_{22}\bar{v}\right) + \frac{R_o x_\eta}{J^2}\left[\frac{\partial}{\partial \xi}\left(Jy_\xi h\bar{u}\bar{u}\right.\right.$$

$$\left. + Jy_\eta h\bar{u}\bar{v}\right) + \frac{\partial}{\partial \eta}\left(Jy_\xi h\bar{u}\bar{v} + Jy_\eta h\bar{v}\bar{v}\right)\Big] - \frac{R_o y_\eta}{J^2}\left[\frac{\partial}{\partial \xi}\left(Jx_\xi h\bar{u}\bar{u} + Jx_\eta h\bar{u}\bar{v}\right)\right.$$

$$\left. + \frac{\partial}{\partial \eta}\left(Jx_\xi h\bar{u}\bar{v} + Jx_\eta h\bar{v}\bar{v}\right)\right] - R_o\left[\left(w\bar{u}\right)_{top} - \left(w\bar{u}\right)_{bot}\right]$$

$$+ E_v\left[\left(A_v\frac{\partial \bar{u}}{\partial z}\right)_{top} - \left(A_v\frac{\partial \bar{u}}{\partial z}\right)_{bot}\right] - \frac{R_o h}{Fr_D^2}\left[\int_z^\zeta\left(\frac{G_{22}}{J^2}\frac{\partial \rho}{\partial \xi}\right.\right.$$

$$\left.\left. - \frac{G_{12}}{J^2}\frac{\partial \rho}{\partial \eta}\right)dz\right] + \text{Horizontal Diffusion} \qquad (3)$$

$$\frac{\partial h\bar{v}}{\partial t} = -h\left[-\frac{G_{21}}{J^2}\frac{\partial \zeta}{\partial \xi} + \frac{G_{11}}{J^2}\frac{\partial \zeta}{\partial \eta}\right] - \frac{h}{J}\left(G_{11}\bar{u} + G_{21}\bar{v}\right) - \frac{R_o x_\xi}{J^2}\left[\frac{\partial}{\partial \xi}\left(Jy_\xi h\bar{u}\bar{u}\right.\right.$$

$$\left. + Jy_\eta h\bar{u}\bar{v}\right) + \frac{\partial}{\partial \eta}\left(Jy_\xi h\bar{u}\bar{v} + Jy_\eta h\bar{v}\bar{v}\right)\Big] + \frac{R_o y_\xi}{J^2}\left[\frac{\partial}{\partial \xi}\left(Jx_\xi h\bar{u}\bar{u} + Jx_\eta h\bar{u}\bar{v}\right)\right.$$

$$\left. + \frac{\partial}{\partial \eta}\left(Jx_\xi h\bar{u}\bar{v} + Jx_\eta h\bar{v}\bar{v}\right)\right] - R_o\left[\left(w\bar{v}\right)_{top} - \left(w\bar{v}\right)_{bot}\right]$$

$$+ E_v\left[\left(A_v\frac{\partial \bar{v}}{\partial z}\right)_{top} - \left(A_v\frac{\partial \bar{v}}{\partial z}\right)_{bot}\right] - \frac{R_o h}{Fr_D^2}\left[\int_z^\zeta\left(-\frac{G_{21}}{J^2}\frac{\partial \rho}{\partial \xi} + \frac{G_{11}}{J^2}\frac{\partial \rho}{\partial \eta}\right)dz\right]$$

$$+ \text{Horizontal Diffusion} \qquad (4)$$

$$w_{top} = w_{bot} - \frac{1}{J}\left[\frac{\partial J\bar{u}h}{\partial \xi} + \frac{\partial J\bar{v}h}{\partial \eta}\right] \tag{5}$$

$$\frac{\partial hS}{\partial t} = \frac{E_v}{Pr_v}\left[\left(K_v \frac{\partial S}{\partial z}\right)_{top} - \left(K_v \frac{\partial S}{\partial z}\right)_{bot}\right] - \frac{R_o}{J}\left[\frac{\partial hJ\bar{u}S}{\partial \xi} + \frac{\partial hJ\bar{v}S}{\partial \eta}\right]$$

$$- R_o\left[(wS)_{top} - (wS)_{bot}\right] + \text{Horizontal Diffusion} \tag{6}$$

$$\frac{\partial hT}{\partial t} = \frac{E_v}{Pr_v}\left[\left(K_v \frac{\partial T}{\partial z}\right)_{top} - \left(K_v \frac{\partial T}{\partial z}\right)_{bot}\right] - \frac{R_o}{J}\left[\frac{\partial hJ\bar{u}T}{\partial \xi} + \frac{\partial hJ\bar{v}T}{\partial \eta}\right]$$

$$- R_o\left[(wT)_{top} - (wT)_{bot}\right] + \text{Horizontal Diffusion} \tag{7}$$

where

$$G_{22} = x_\eta^2 + y_\eta^2$$

$$J = x_\xi y_\eta - x_\eta y_\xi$$

$$G_{12} = G_{21} = x_\xi x_\eta + y_\xi y_\eta$$

$$G_{11} = x_\xi^2 + y_\xi^2$$

Equations 3–7 have been written in terms of dimensionless variables where

h = layer thickness

t = time

ζ = water-surface elevation

w = vertical component of velocity

ρ = water density

S = salinity

T = temperature

The dimensionless parameters R_o, E_v, Fr_D, Fr, and Pr_v are defined as

$$R_o = U_r/fX_r$$

$$E_v = A_{vr}/fZ_r^2$$

$$Fr_D = Fr/[(\rho_r - \rho_o)/\rho_o]^{1/2}$$

$$Fr = U_r/(gZ_r)^{1/2}$$

$$Pr_v = A_{vr}/K_{vr}$$

where

A_v, K_v = vertical turbulent eddy coefficients

f = Coriolis parameter

g = acceleration due to gravity

and the quantities U_r, ρ_r, X_r, Z_r, A_{vr}, and K_{vr} are arbitrary reference values of the velocity, density, horizontal and vertical dimensions, vertical viscosity, and vertical diffusivity, respectively. An equation of state relating the water density to the salinity and temperature closes the system.

13. As noted, there are a maximum of 15 vertical layers in the Chesapeake Bay model. Each is 1.52 m thick except for the top layer, which varies with the tide. The water-surface slope terms in Equations 3 and 4 are evaluated from similar transformed equations for the vertically averaged flow field. The horizontal diffusion terms are quite lengthy and thus are not listed here, but are included in Johnson et al. (1991). It might be noted that initially the convective terms in the momentum equations resulted in unstable solutions due to being written with velocity squared terms present (see Sheng 1986). However, writing these terms as presented in Equations 3 and 4 solved this problem.

Boundary Conditions

14. The boundary conditions at the free surface are

$$A_v \left(\frac{\partial \bar{u}}{\partial z} , \frac{\partial \bar{v}}{\partial z} \right) = \left(\frac{\tau_{s_\xi}}{\rho} , \frac{\tau_{s_\eta}}{\rho} \right) = \left(C W_\xi^2 , C W_\eta^2 \right) \tag{8}$$

$$\frac{\partial T}{\partial z} = \frac{Pr_v}{E_v} K (T - T_e) \tag{9}$$

$$\frac{\partial S}{\partial z} = 0 \tag{10}$$

whereas the boundary conditions at the bottom are

$$A_v \left(\frac{\partial \bar{u}}{\partial z} , \frac{\partial \bar{v}}{\partial z} \right) = \left(\frac{\tau_{b_\xi} , \tau_{b_\eta}}{\rho} \right)$$

$$= \frac{U_r}{A_{vr}} Z_r C_d \left(\bar{u}_1^2 + \bar{v}_1^2 \right)^{1/2} (\bar{u}_1, \bar{v}_1) \tag{11}$$

$$\frac{\partial T}{\partial z} , \frac{\partial S}{\partial z} = 0 \tag{12}$$

where

$\tau_{s_\xi}, \tau_{s_\eta}$ = components of surface shear stress

C = surface drag coefficient

W = wind speed

K = surface heat exchange coefficient

T_e = equilibrium temperature

$\tau_{b_\xi}, \tau_{b_\eta}$ = components of bottom shear stress

C_d = bottom friction coefficient

$\bar{u}_1, \bar{v}_1$ = horizontal velocity components next to the bottom

With z_1 equal to one-half the bottom layer thickness, C_d is given by

$$C_d = k^2 \left\{ \left[\ln \ (z_1/z_o) \right] \right\}^{-2} \tag{13}$$

where k is the von Karman constant and z_o is the bottom roughness height. As presented by Garratt (1977), the surface drag coefficient is computed from

$$C = (0.75 + 0.067 W) \times 10^{-3} \tag{14}$$

with the maximum allowable value being 0.003. The surface heat exchange coefficient K and the equilibrium temperature T_e are computed from meteorological data as discussed by Edinger, Brady, and Geyer (1974).

15. Along the shoreline where river inflow occurs, the freshwater inflow and its temperature are prescribed and the salinity is assumed to be zero. At an ocean boundary, the water-surface elevation is prescribed along with time-varying vertical distributions of salinity and temperature. During flood, the specified values of salinity and temperature are employed, whereas during ebb, interior values are advected out of the grid. Along a solid boundary, the normal component of the velocity and the viscosity and diffusivity are set to zero.

Numerical Solution Algorithm

16. Finite differences are used to replace derivatives in the governing equations, resulting in a system of linear algebraic equations to be solved. As discussed by Johnson et al. (1991), both external and internal mode equations are solved.

17. The external mode consists of equations for the water-surface elevation ζ and vertically integrated contravariant unit flows $\bar{U}$ and $\bar{V}$. All of the terms in the transformed vertically averaged continuity equation are treated implicitly, whereas only the water-surface slope terms in the transformed vertically averaged momentum equations are treated implicitly. Those terms treated implicitly are weighted between the new and old time-steps. The resulting finite difference equations are then factored such that a ξ-sweep followed by an η-sweep of the horizontal grid yields the solution at the new time-step.

18. The internal mode consists of computations from Equations 3-7 for the three velocity components $\bar{u}$, $\bar{v}$, and w; salinity; and temperature. The only terms treated implicitly are the vertical diffusion terms in all equations and the bottom friction and surface slope terms in the momentum equations. Values of the water-surface elevations from the external mode are used to evaluate the surface slope terms in Equations 3 and 4. As a result, the extremely restrictive speed of a free-surface gravity wave is removed from the stability criteria. Upwind differencing is used to represent the convective terms in the momentum equations, whereas a spatially third-order scheme

developed by Leonard (1979) called QUICKEST is used to represent the advective terms in Equations 6 and 7 for salinity and temperature.

19. It should be noted that once the $\bar{u}$ and $\bar{v}$ velocity components are computed, they are slightly adjusted to ensure the conservation of mass. This is accomplished by forcing the sum of $\bar{u}$ over the vertical to be the vertically averaged velocity $\bar{U}/H$ and the sum of $\bar{v}$ over the vertical to equal $\bar{V}/H$. where H is the total water depth.

20. A staggered grid is used in both the horizontal and vertical directions of the computational domain. In the horizontal directions, a unit cell consists of a ζ-point in the center, a $\bar{u}$-point to its left, and a $\bar{v}$-point to its bottom. In the vertical direction, the vertical velocities are computed on the upper and lower cell faces. Temperature, salinity, and density are computed at the center of the 3-D cell.

Turbulence Parameterization

21. Vertical turbulence is handled by using the concept of eddy viscosity and diffusivity to represent the velocity and density correlation terms that arise from a time averaging of the governing equations. These eddy coefficients are computed from mean flow characteristics using a simplified second-order closure model originally developed by Donaldson (1973). The closure model has been further developed and applied to various types of flows by Lewellen (1977) and Sheng (1982, 1986). A discussion of the implementation of the turbulence model taken from Sheng* follows.

22. Basically all second-order closure models solve the Reynolds stress equations in addition to the equations for the mean flow. These equations can be found in any textbook on turbulence and thus are not reproduced here. Assuming local equilibrium of turbulence, the Reynolds stress equations can be greatly simplified since there is no time evolution nor spatial diffusion of the second-order correlations. If one considers only the vertical turbulent transport, these equations can be expanded into

---

* Y. P. Sheng. 1990. "A Simplified Second Order Closure Model of Turbulent Transport." Unpublished paper prepared for US Army Engineer Waterways Experiment Station, Vicksburg, MS.

$$\frac{q}{\Lambda}\,\overline{u'u'} + \frac{q^3}{3\Lambda}\,(2b-1) + 2\,\overline{u'w'}\,\frac{\partial\bar{u}}{\partial z} = 0 \qquad (15)$$

$$\frac{q}{\Lambda}\,\overline{v'v'} + \frac{q^3}{3\Lambda}\,(2b-1) + 2\,\overline{v'w'}\,\frac{\partial\bar{v}}{\partial z} = 0 \qquad (16)$$

$$\frac{q}{\Lambda}\,\overline{w'w'} + \frac{q^3}{3\Lambda}\,(2b-1) + \frac{2g}{\bar{\rho}}\,\overline{w'\rho'} = 0 \qquad (17)$$

$$\frac{q}{\Lambda}\,\overline{u'v'} + \overline{u'w'}\,\frac{\partial\bar{v}}{\partial z} + \overline{u'w'}\,\frac{\partial\bar{u}}{\partial z} = 0 \qquad (18)$$

$$\frac{q}{\Lambda}\,\overline{u'w'} + \overline{w'w'}\,\frac{\partial\bar{u}}{\partial z} + \frac{q}{\bar{\rho}}\,\overline{u'\rho'} = 0 \qquad (19)$$

$$\frac{q}{\Lambda}\,\overline{w'w'} + \overline{w'w'}\,\frac{\partial\bar{v}}{\partial z} + \frac{q}{\bar{\rho}}\,\overline{v'\rho'} = 0 \qquad (20)$$

$$\frac{bsq}{\Lambda}\,\overline{\rho'\rho'} + \overline{w'\rho'}\,\frac{\partial\bar{\rho}}{\partial z} = 0 \qquad (21)$$

$$\frac{Aq}{\Lambda}\,\overline{u'\rho'} + \overline{u'w'}\,\frac{\partial\bar{\rho}}{\partial z} + \overline{w'\rho'}\,\frac{\partial\bar{u}}{\partial z} = 0 \qquad (22)$$

$$\frac{Aq}{\Lambda}\,\overline{v'\rho'} + \overline{v'w'}\,\frac{\partial\bar{\rho}}{\partial z} + \overline{w'\rho'}\,\frac{\partial\bar{v}}{\partial z} = 0 \qquad (23)$$

$$\frac{Aq}{\Lambda}\,\overline{w'\rho'} + \overline{w'w'}\,\frac{\partial\bar{\rho}}{\partial z} + \frac{q}{\bar{\rho}}\,\overline{\rho'\rho'} = 0 \qquad (24)$$

where

$$b = 0.125\ ,\quad s = 1.8\ ,\quad A = 0.75$$

and

$$q = \left(\overline{u'u'} + \overline{v'v'} + \overline{w'w'}\right)^{1/2} \qquad (25)$$

where u', v', and w' are the turbulent velocity fluctuations and the overbar indicates time averaging. These equations can be manipulated to produce an equation relating the turbulent kinetic energy and the macroscale of turbulence Λ to the mean flow shear and stratification (given by the Richardson number Ri):

$$3A^2b^2sQ^4 + A[(bs + 3b + 7b^2s)Ri - Abs(1 - 2b)]Q^2 + b(s + 3 + 4bs)Ri^2 + (bs - A)(1 - 2b)Ri = 0 \tag{26}$$

where

$$Ri = - \frac{\frac{g}{\rho}\frac{\partial \bar{\rho}}{\partial z}}{\left(\frac{\partial \bar{u}}{\partial z}\right)^2 + \left(\frac{\partial \bar{v}}{\partial z}\right)^2} \tag{27}$$

and

$$Q = \frac{q}{\Lambda\sqrt{(\partial \bar{u}/\partial z)^2 + (\partial \bar{v}/\partial z)^2}} \tag{28}$$

23. As discussed by Sheng,* it can also be shown that the following relations hold:

$$\overline{u'w'} = - \frac{\frac{\partial \bar{u}}{\partial z}\Lambda}{q}\frac{1 + \frac{\bar{\omega}}{A}}{1 - \bar{\omega}}\overline{w'w'} \tag{29}$$

$$\overline{v'w'} = - \frac{\frac{\partial \bar{v}}{\partial z}\Lambda}{q}\frac{1 + \frac{\bar{\omega}}{A}}{1 - \bar{\omega}}\overline{w'w'} \tag{30}$$

$$q^2b = \left[\frac{1 + \frac{\bar{\omega}}{A}}{Q^2(1 - \bar{\omega})} + \bar{\omega}\right]\overline{w'w'} \tag{31}$$

---

* 1990, op. cit.

where

$$\omega = \frac{Ri}{AQ^2} \tag{32}$$

and

$$\bar{\omega} = \frac{\omega}{1 - \frac{\omega}{bs}} \tag{33}$$

Thus, after the velocity shear and flow stratification are determined, q can be computed using Equations 26 and 28. $\overline{w'w'}$ is then determined from

$$\overline{w'w'} = \frac{\frac{q^2}{2} - q^2 b}{\frac{3}{2}(1 - 2\bar{\omega})} \tag{34}$$

Finally, after Λ is prescribed, $\overline{u'w'}$ and $\overline{v'w'}$ can be computed from Equations 29 and 30 and the vertical eddy coefficients can be determined from

$$A_v = \frac{-\overline{u'w'}}{\frac{\partial \bar{u}}{\partial z}} = \frac{\Lambda}{q} \frac{A + \bar{\omega}}{A(1 - \omega)} \overline{w'w'} \tag{35}$$

$$K_v = \frac{-\overline{\rho'w'}}{\frac{\partial \rho}{\partial z}} = \frac{\Lambda}{q} \frac{bs}{(bs - \omega)A} \overline{w'w'} \tag{36}$$

If the Richardson Number Ri never exceeds a critical value of 0.55 at any vertical position in the water column, the initial distribution of Λ at a vertical position z is computed from $0.65z$ such that Λ is zero at both the surface and the bottom with its maximum value occurring at middepth. However, if a pycnocline does exist ($Ri \geq 0.55$), then the initial distribution

of Λ is computed such that Λ is zero at the surface, at the pycnocline, and at the bottom with maximum values occurring halfway between the surface and the pycnocline and the bottom. This initial distribution is then modified by the three basic constraints below:

$$\left| \frac{d\Lambda}{dz} \right| \leq 0.65 \tag{37}$$

$$\Lambda \leq \frac{q}{N} = \frac{q}{\left(-\frac{g}{\rho} \frac{\partial \rho}{\partial z} \right)^{0.5}} \tag{38}$$

$$\Lambda \leq Q_{cut} \left(z_{q=qmax} - z_{q=qmax/2} \right) \tag{39}$$

where N is the Brunt-Vaisala frequency. Equation 39 states that Λ is less than a fraction of the spread of turbulence as measured by the distance between the location of a maximum q^2 to where q^2 is equal to 25 percent of the maximum. The coefficient Q_{cut} is on the order of 0.15 to 0.25.

PART III: APPLICATION WITH AN EARLY VERSION OF THE MODEL TO THE JUNE-JULY 1980 AND APRIL 1983 DATA SETS

Strategy

24. Verification of the 3-D model was conducted in various phases. Initially, simplified problems for which closed form solutions could be written were simulated to aid in assessing model performance as well as to guide needed model modifications. The next phase involved employing data that had been collected on a physical model of the Chesapeake Bay in Maryland. However, because these data do not contain wind effects, the effort devoted to this phase of the verification process was minimal. Ultimately the verification of any numerical model must be conducted using sets of field data. In addition, it is desirable that the various sets of field data represent different physical conditions that are considered important and routinely occur in the system being modeled.

25. A preliminary study of synoptic field data available on Chesapeake Bay revealed three fairly extensive data sets that were each approximately 1 month long. As described in paragraph 7, the first, collected during June-July 1980 by Dr. Boicourt, represents dry summer conditions on Chesapeake Bay. The next two were collected by the NOS during 1983. One set, collected during April 1983, represents a relatively large freshwater runoff into the bay, whereas the other, collected during September 1983, captured an important wind-mixing event. These data sets are summarized in Table 1.

26. Model development during this study was an ongoing exercise, e.g., the rederivation of the convective terms, the incorporation of the QUICKEST scheme, the incorporation of the ability to compute temperature, and the solution of the governing equations on the z-plane rather than the sigma-plane. Therefore, it is difficult to state the differences between the version (or versions) of the model applied to the June-July 1980 and April 1983 data sets and the final version applied to the September 1983 data set and the yearlong simulations since changes were made, often on a daily basis. However, major differences included correcting an error in the coding of the advection scheme near inflow boundaries, applying a three-point smoothing equation to effectively diffuse the vertical turbulence, computing the surface heat exchange coefficients with wind data adjusted to reflect over-water winds, specifying

time-varying salinity and temperature at the ocean boundary, and distributing ungaged inflows below the fall lines of the tributaries. Since these individual differences were incorporated over a period of time during many simulations of the September 1983 data set, it is difficult to ascertain the impact of each individually. However, an inspection of the September 1983 verification results reveals that collectively they resulted in a much better matching of the computed results with the field data.

27. Application to the three month-long data sets are discussed in two parts. Results from the June-July 1980 and April 1983 applications are presented first with minimal discussion before presenting results from the September 1983 application. Because an earlier version of the model was applied to these two data sets, these applications should not be viewed as verification efforts. As noted, the version of the model and values of model coefficients applied to the September 1983 data set were the same as applied to the yearlong simulations. Thus, this application is considered much more important and as a result is discussed in more detail in Part IV. Results from the June-July 1980 and April 1983 data sets should be viewed in a qualitative sense as demonstrating basic behavior of the model rather than a quantitative verification of the model.

June-July 1980

Description of field data

28. As discussed by Blumberg et al. (1991), velocity, salinity, and temperature data were available from Boicourt at several locations.* Data at the four stations (M3, WT4, SP2, BB1) shown in Figure 3 were selected for comparison with model results. These data were measured at either a 10-min or 30-min interval.

29. Wind data at Norfolk International Airport and at the Baltimore-Washington International Airport (BWI) at 3-hour intervals were available for the June-July 1980 period.** The wind data are given in terms of wind direction and speed. Hourly tidal height, corrected to the National Geodetic Vertical Datum (NGVD), were available at six locations: Havre de Grace, MD

---

* Personal Communication with W. Boicourt of Horn Point Environment Laboratories, Cambridge, MD.

** Personal Communication with National Climatic Data Center, Asheville, NC.

(HdG); Colonial Beach, VA (COL); Annapolis, MD (ANN); Solomons, MD (SOL); Hampton Roads, VA (HRd); and Chesapeake Bay Tunnel, VA (CBT).* The locations of these gages are also shown in Figure 3. Average daily riverflow data at the tributary fall lines were obtained from the US Geological Survey Water Resources Data reports (USGS 1981a and b).

Initial conditions

30. To save on computation time, the initial 3-D salinity and temperature fields were constructed to be as close to reality as possible. The procedure used is discussed in more detail in Part IV. The initial velocity field was taken to be zero and the water surface was taken to be at mean sea level.

Boundary forcing data

31. Boundary forcings consist of tides, winds, freshwater inflows, and the exchange of heat at the water surface. The tide imposed at the ocean boundary (M3) is shown in Figure 4. In addition to the tide at the ocean boundary, vertical distributions of salinity and temperature were also prescribed. However, in this application these distributions were not allowed to vary with time. Thus, on inflow the values prescribed in the initial conditions became the boundary conditions. In all applications, since data were not available, the Chesapeake and Delaware Canal was closed.

32. Daily freshwater inflows (Figure 5) were prescribed at the head of all major tributaries. All of these flows were quite low. The time-varying temperature of each inflow was taken to be the equilibrium temperature computed from meteorological data at the Patuxent River Naval Station (PAX).**

33. Wind stress in the lower to middle bay was computed from linearly interpolated wind data from the Norfolk and BWI stations. North of the BWI station, only wind data from the BWI station were used. Wind vectors from the Norfolk and BWI stations are presented in Figures 6 and 7, respectively. These data have been adjusted to reflect over-water winds. This was accomplished by multiplying the north-south and east-west components of the wind at the three stations by factors obtained from Goodrich (1985). For the Norfolk winds these factors were 1.53 and 1.85, respectively; and for the Patuxent and BWI winds, the factors used were 2.03 and 1.40.

---

* Personal Communication with National Ocean Service, Rockville, MD.
** Personal Communication with National Climatic Data Center, Asheville, NC.

34. As previously noted, the surface heat exchange is handled through the concept of an equilibrium temperature and a surface heat exchange coefficient as discussed by Edinger, Brady, and Geyer (1974). These were computed from meteorological data taken at the Patuxent Naval Air Station and are presented in Table 2.*

Verification results

35. With the boundary forcings and initial state described previously, computations were made on the numerical grid shown in Figure 2. The initial salinity and temperature fields were frozen for the first 7 days. Computed salinity, temperature, and velocity were saved at the locations previously noted. Computed water-surface elevations were saved at the interior tide stations noted in Figure 3.

36. Comparisons of the computed and recorded tide at Hampton Roads, VA, and Solomons, Annapolis, and Havre de Grace, MD, are presented in Figures 8-11. Generally, the amplitudes match well and reflect wind effects as well as the astronomical tide. Phasing differences can be seen in the results at Havre de Grace (Figure 11).

37. A comparison at three depths of the major velocity component at the ocean entrance (M3) is presented in Figure 12. A similar plot at three depths of the along-bay component of the flow velocity at station WT4 is given in Figure 13. In these plots, the u-velocity is the along-bay component, and the v-velocity is the across-bay component. Comparisons of computed and recorded salinities and temperature at station WT4 are given in Figures 14 and 15, respectively. Comparisons of computed and recorded velocity, salinity, and temperature at station SP2 are presented in Figures 16-18, and at station BB1 in Figures 19-21.

38. Velocity comparisons are generally favorable, especially if one considers that the recorded velocity occurs at a point, whereas the model velocity represents an average over a large computational cell. The salinity and temperature comparisons are not as good. However, as previously noted, these results were generated with an early version of the model. The excellent results presented in Part IV for the September 1983 data set are from the latest version of the model in which the various modifications discussed in paragraph 26 have been made. Once again it should be noted that the surface

---

* Personal Communication with National Climatic Data Center, Asheville, NC.

heat exchange data presented in Table 1 were generated without correcting the Patuxent wind data to account for winds over water. This correction resulted in a much better comparison of temperatures during the September 1983 application. Due to time and funding constraints, the 1980 data set was not rerun using the latest version of the model.

April 1983

39. Data for this application were obtained from a circulation survey of Chesapeake Bay conducted by NOS during April 1983* and are discussed in detail by Blumberg et al. (1991). This data set represents conditions during a large spring runoff event.

Description of field data

40. As shown in Figure 22, current meter data were available for four stations: bay entrance (BE), midbay (MB), Wolf Trap (WT), and Bay Bridge (BB). These data include current direction and amplitude, water temperature, pressure, and conductivity. The data were measured at a 10-min interval. The temperature and conductivity were used to compute salinity from the following expression**:

$$S = (\{[(-1.02527 * RF + 4.81236) * RF - 9.04061] * RF + 11.95364\} * RF + 28.29988) * RF \quad (40)$$

where

$$RF = RT + RT * RD * TF * (BR + TF + FRT) * 10^{-5}$$

and

$$RT = C/CKT$$

$$RD = RT - 1.0$$

$$BR = \{[(-26.9 * RD + 3.09) * RD - 8.52] * RD + 67.1\}$$

$$FRT = -0.25 * RD * TF$$

with

$$CKT = (\{[(-2.217 * 10^{-8} * T - 2.5813 * 10^{-5}) * T + 4.6704 * 10^{-3}] * T + 0.86062\} * T + 29.0473$$

---

* Personal Communication with National Ocean Service, Asheville, NC.
** Personal Communication with Alan Blumberg, HydroQual, Mahwah, NJ.

$$TF = T - 15.0$$

and

T = temperature, °C

C = conductivity, mmhos/cm

S = salinity, ppt

41. Hourly wind data at the Patuxent River Naval Air Station and the Norfolk International Airport were available for the April 1983 period.* These data include wind direction and wind amplitude. Figures 23 and 24 present wind data from these two stations. Locations of the stations are shown in Figure 22. These data have been adjusted to represent over-water winds as discussed in paragraph 33.

42. Daily riverflow data at the tributary fall lines were obtained from the US Geological Survey Water Resources Data reports for the April 1983 period (USGS 1984a and b). These data are presented in Figure 25 for the James, York, Rappahannock, Potomac, Patuxent, Patapsco, Susquehanna, and Choptank Rivers.

43. Hourly tidal height data at six locations were available from NOS for the April 1983 period.** The location of these gages is given in Figure 22. The values have been corrected to NGVD. The boundary tide at CBT is given in Figure 26.

44. Equilibrium temperatures and surface heat transfer coefficients computed from meteorological data at the Patuxent River Naval Air Station for the April 1983 period are presented in Table 3.* As with the 1980 data set, the Patuxent winds were not adjusted to reflect over-water winds in the surface heat exchange computations.

Verification results

45. Initial conditions were generated as in the 1980 application (paragraph 30).

46. Comparisons of the recorded and computed tides at Hampton Roads and Colonial Beach, VA, and Solomons, Annapolis, and Havre de Grace, MD, are presented in Figures 27-31, respectively. Results are quite good except at

---

* Personal Communication with National Climatic Data Center, Rockville, MD.

** Personal Communication with National Ocean Service, Asheville, NC.

Havre de Grace. The reason for the much larger computed tidal range at Havre de Grace over the last half of the month is not clear. This behavior at Havre de Grace was not nearly as pronounced in the 1980 application (Figure 11).

47. Comparisons of computed and recorded velocities at stations BE and WT are presented in Figures 32 and 33, and comparisons of velocity, salinity, and temperature at stations MB and BB (Figure 22) are presented in Figures 34-39. Again, it should be remembered that recorded velocities are point values, whereas computed velocities are all cell-averaged values. In addition, the previous comments concerning the use of an early version of the model and erroneous surface heat exchange data are applicable.

Conclusions

48. Based upon an overall comparison of model results with field data at several locations, the general conclusion after these two applications was that the 3-D hydrodynamic model responded to boundary forcings in a reasonable fashion. After correcting model deficiencies during the September 1983 application (Part IV) and after accounting for ungaged tributary inflows and the adjustment of the Patuxent wind data in the computation of the surface heat exchange, comparisons of computed and field data improved substantially for the September 1983 application. As a result, confidence in the ability of the model to accurately compute the 3-D hydrodynamics of the Chesapeake Bay was increased. This confidence was increased even more during the yearlong simulations discussed in Part V.

PART IV: VERIFICATION OF THE FINAL MODEL TO THE SEPTEMBER 1983 DATA SET

49. These data illustrate the destratification of the Chesapeake Bay waters during a strong wind event with a subsequent restratification as the wind abated. In addition, rapid cooling of the surface waters near the middle of the month contributed to the destratification process.

Description of Field Data

50. As with the April 1983 data, current meter data were available for four long-term stations: bay entrance (BE), Wolf Trap (WT), midbay (MB), and Bay Bridge (BB).* These locations are shown in Figure 40. These data include current direction and amplitude, water temperature, pressure, and conductivity. They were measured at a 10-min time interval. The temperature and conductivity were used to compute salinity from Equation 40.

51. Hourly wind data at the Patuxent River Naval Air Station and wind data at Norfolk International Airport at 3-hour intervals were available for the September 1983 period.** The wind data are given in terms of wind direction and speed. Hourly tidal height, corrected to NGVD, at seven locations were obtained from NOS: Havre de Grace, MD (HdG), Colonial Beach, VA (COL), Lewisetta, VA (LEW), Annapolis, MD (ANN), Solomons, MD (SOL), Hampton Roads, VA (HRd), and Chesapeake Bay Tunnel, VA (CBT).* The locations of these gages are also shown in Figure 40. Average daily riverflow data at the tributary fall lines were obtained from the US Geological Survey Water Resources Data reports (USGS 1984a and b).

Initial Conditions

52. To save on computation time, the initial 3-D salinity and temperature fields were constructed to be as close to reality as possible. These were established by using the available field data. The value for each individual cell of the 3-D grid was first set to be that of the nearest field data point. The resulting 3-D fields of salinity and temperature were then

---

* Personal Communication with National Ocean Service, Asheville, NC.
** Personal Communication with National Climatic Data Center, Rockville, MD.

smoothed several times using a three-point smoothing equation. Figures 41 and 42 show the vertical structure of the prescribed salinity field at stations MB and BB. Based upon the limited field data available, it can be seen that initial stratification of the bay is represented well. The initial velocity field was taken to be zero and the water surface was taken to be at mean sea level.

Boundary Forcing Data

53. As for the 1980 and April 1983 applications, boundary forcings consist of tides, winds, freshwater inflows, and the exchange of heat at the water surface. The tide imposed at the ocean boundary (CBT) is shown in Figure 43. In addition to the tide at the ocean boundary, time-varying vertical distributions of salinity and temperature were also prescribed using the field data at station BE. Recall that in the previous applications these vertical distributions were constant in time. As previously noted, since data were not available, the Chesapeake and Delaware Canal was closed.

54. Daily freshwater inflows were prescribed at the head of all major tributaries. All of these flows were quite low, with over half of the total freshwater inflow coming from the Susquehanna River. These inflows are shown in Figure 44. The time-varying temperatures of these inflows were also prescribed. The salinity of the tributary inflows was taken to be zero.

55. Wind stress in the lower to middle bay was computed from linearly interpolated wind data from the Norfolk and Patuxent stations. North of the Patuxent station, only wind data from the Patuxent station were used. Wind vectors from these two stations are presented in Figures 45 and 46 and have been adjusted to represent over-water winds.

56. As previously noted, the surface heat exchange was computed as described in paragraph 34. Unlike the previous two applications discussed, the wind data employed in the computation of the surface heat exchange data presented in Table 4 were adjusted to represent over-water winds.

Model Coefficients

57. The horizontal eddy viscosity and diffusivity coefficients are prescribed along with parameters connected with the computation of the

vertical turbulence coefficients and the bottom drag coefficient. The bottom roughness was set such that the bottom drag coefficient was computed to have a value of 0.0028 throughout the bay. Values for the horizontal eddy viscosity and diffusivity were taken to be zero. Background values for the vertical eddy viscosity and diffusivity were set to be 10 cm^2/sec and 0.005 cm^2/sec, respectively. These same values were used in the previous two applications.

58. As discussed in Part II, the vertical turbulence model contains one free parameter, Q_{cut}, that can be varied. However, its value should be in the range of 0.15-0.25. In this range, the computed eddy coefficients were fairly insensitive to variations in Q_{cut}. Thus, Q_{cut} was set to 0.20. The other three parameters, b, A, and S, are considered to be constants. However, several runs with the September 1983 data set were made in which the values of these parameters were varied. The basic conclusion drawn from these results was that the default values should not be changed and these parameters should indeed be considered model constants.

Verification Results

59. With these boundary forcings and initial state, computations were made on the numerical grid shown in Figure 2. The initial salinity and temperature fields were frozen for the first 5 days. Computed salinity, temperature, and velocity were saved at the locations of the current meter stations in Figure 40 for comparison with the field data. Computed water-surface elevations were saved at the six interior tide stations noted in Figure 40. Furthermore, monthly averaged velocity vectors were computed for comparison with observed long-term circulation patterns in Chesapeake Bay.

60. In addition to time series plots showing a visual comparison of model results to field data, difference measures have also been computed. Bias is described by the mean bias error (MBE) defined as

$$MBE = \frac{\sum_{i=1}^{N} (M_i - O_i)}{N} \tag{41}$$

where

N = number of data points

M_i = model results

O_i = observed data

Average difference is described by the root mean square error (RMSE) or perhaps the mean absolute error (MAE). These are defined by the following:

$$RMSE = \sqrt{\frac{\sum_{i=1}^{N} (M_i - O_i)^2}{N}} \tag{42}$$

$$MAE = \frac{\sum_{i=1}^{N} |M_i - O_i|}{N} \tag{43}$$

Finally, the average relative error (ARE) is defined as

$$ARE = \frac{\sum_{i=1}^{N} |M_i - O_i|}{\sum_{i=1}^{N} O_i} \tag{44}$$

61. Comparison of the computed and recorded tides at Hampton Roads, Lewisetta, and Colonial Beach, VA, and Solomons, Annapolis, and Havre de Grace, MD, are presented in Figures 47-52. Table 5 presents a comparison of model and observed maximum flood and minimum ebb water surface elevations, along with a comparison of the timing of the peaks, at these stations. Low water at Hampton Roads is consistently computed to be too high; however, the range at most other stations is about right, except for Havre de Grace. As with all the simulations, the computed range at that station is too high. Around the middle of the month the computed water surface at most stations experiences too much setup. This is probably due to an inaccuracy in the wind data or perhaps a barometric disturbance that is not modeled. The effect of the wind shift around the 20th of the month is quite evident in the water surface plots in the upper bay. Figures 53-58 are similar water-surface plots but with all frequencies below 36 hours filtered from the results. Thus, these plots illustrate a comparison of recorded and computed water-surface elevations due to nonastronomical events, e.g., wind and freshwater runoff. The difference measures for the surface elevations are presented in Table 6.

The bias is positive at all stations and is generally about 0.05 m or less. The difference error is less than about 0.1 m at all stations except Havre de Grace. This is a unique station located at the head of the bay in the Susquehanna Flats which are not represented well in the model.

62. Figures 59–62 illustrate the ability of the numerical model to reproduce flow velocity well. The impact of the sudden shift in the wind around the 20th of the month can clearly be seen at stations MB and BB. Table 7 presents a comparison of model and observed along-bay currents near the surface at maximum flood and minimum ebb. Table 8 presents the difference measures for the velocity. From an inspection of the time series plots, it appears the difference error is caused more by phase errors than by range errors.

63. Salinity and temperature results are presented at the three interior stations shown in Figure 40 in Figures 63–65 and 66–68, respectively. The salinity plots at stations MB and BB demonstrate that the vertical turbulence closure model responds reasonably well to the wind-mixing event. As a result of the turbulence generated by the velocity shear created by the wind, the bay destratified but then began to restratified within a few days. To adequately capture this event, it was found that some diffusion of the turbulence generated was required. This was accomplished by using a three-point smoothing equation on the eddy viscosity and diffusivity coefficients generated by the turbulence model discussed in Part II. With k being the vertical layer indicator and D representing either the eddy viscosity or diffusivity, the following equation is employed:

$$D_k = \frac{D_{k-1} + D_k + D_{k+1}}{3} \tag{45}$$

Figure 69 shows the salinity at the MB station without the three-point smoothing. A comparison with Figure 64b clearly demonstrates the impact of employing such a smoothing scheme. Difference measures for the salinity are presented in Table 9. Generally, the mean bias is less than 1 ppt with the difference error also less than 1 ppt, except at Wolf Trap. Difference measures for the temperature are presented in Table 10. Generally, the absolute error as well as the mean bias error is less than 0.5°C.

64. Since flow fields generated by the hydrodynamic model are to be used in the long-term computation of water quality parameters, it is important to demonstrate the ability of the model to compute the proper residual circulation of the bay. Figure 70 shows the computed monthly averaged near-surface and near-bottom currents in the bay. Note the classical gravitational circulation, with the surface water flowing toward the ocean and bottom water moving up the bay. Figure 71 is a similar plot that was constructed by Blumberg, from records of field data collected by NOS at various locations over a period of time from 1976 to 1983.* Only those records of at least 15 days in length were employed in constructing these plots. Note that the magnitude of the model-computed near-surface and near-bottom residual currents is in the 5- to 10-cm/sec range as is that for the field data. Although one should not necessarily expect results representing an average of data collected from 1976 to 1983 to agree with the computed monthly averaged circulation for September 1983, it can be seen that in a qualitative sense these results do justify placing confidence in the model's ability to compute the residual circulation of the bay.

65. Computed nondimensional eddy diffusivity at the midbay and Bay Bridge stations before the use of Equation 45 are presented in Figures 72 and 73. The values plotted should be multiplied by 10 cm^2/sec to yield dimensional values. An inspection of the computed coefficients shows values of perhaps 500-1,000 cm^2/sec being sustained for a couple of days during the wind-mixing event. These plots also illustrate the importance of shear stresses at the boundaries in the generation of turbulence.

Conclusions

66. Based upon an overall comparison of model results with available field data at several locations, the general conclusion is that the 3-D model is a good representation of the hydrodynamics of the Chesapeake Bay. This is further qualitatively substantiated by the excellent agreement of the computed monthly averaged flow field with average circulation values determined from field data collected by NOS during 1976-83.

---

* Personal Communication with Dr. Alan Blumberg, HydroQual, Inc., Mahwah, NJ.

PART V: MODEL VERIFICATION ON AN ANNUAL TIME SCALE

67. Hydrodynamics for the years of 1984, 1985, and 1986 are required as input to the 3-D water quality model of Chesapeake Bay. These years represent high, low, and average freshwater inflow years, respectively. A 1-year simulation of the hydrodynamics using a computational time-step of 5 min takes about 10 hr on a CRAY Y-MP computer. Sequences of these hydrodynamics will be constructed to drive long-term (decades) water quality simulations.

68. For each of these years, near-surface and near-bottom salinity and temperature data at approximately 2-week intervals were available throughout the bay and its major tributaries.* These data, as well as tide data,** were used as additional verification of the hydrodynamic model.

69. Time series plots of water level, salinity, and temperature as well as seasonally averaged longitudinal transects of salinity along the main bay and its major tributaries have been constructed. The location of these transects is given in Figure 74.

1984 Simulation

Boundary conditions

70. The 1984 year was broken into five seasons as follows for the purpose of generating seasonally averaged longitudinal transects of salinity:

Season 1 ⇒ 1 Jan-25 Mar
Season 2 ⇒ 26 Mar-10 Jun
Season 3 ⇒ 11 Jun-27 Aug
Season 4 ⇒ 28 Aug-25 Nov
Season 5 ⇒ 26 Nov-31 Dec

Time series results and boundary forcing data are presented for a portion of the year. The ocean boundary tide at the Chesapeake Bay Tunnel is shown in Figure 75. Wind forcing data that have been corrected to reflect over-water winds based on recorded winds at the Norfolk and BWI Airports are presented in

---

* Personal Communication, 1989, with Chesapeake Bay Liaison Office, US Environmental Protection Agency, Annapolis, MD.

** Personal Communication with National Ocean Service, Asheville, NC.

Figures 76 and 77.* Freshwater inflows on the James, Potomac, Patuxent, and Susquehanna Rivers are shown in Figure 78 (USGS 1985a and b). Surface heat exchange data for season 5 are listed in Table 11.

Results

71. Locations for which results are presented are shown in Figure 79. Complete results are given in Appendix A. A typical comparison of computed and recorded water level at Annapolis, MD, is given in Figure 80. Figure 81 is an expanded view of this comparison near day 301 for two tidal cycles.

72. Salinity comparisons are given at four main bay stations as well as stations on the James, Potomac, and Patuxent Rivers for the last 3 months of 1984. Station EE 3.5 was located in a relatively shallow area, about 4.5 m, on the eastern side of the bay. As can be seen in Figure 82, very little stratification ever appears in either the field data or model results. The Wolf Trap station (station CB 6.3) was in the same location as in the September 1983 data set. Figure 83 indicates the water column can be alternately well mixed and partially stratified. The midbay station, CB 5.1, was located in the deep natural channel traversing Chesapeake Bay and thus basically remained stratified throughout the year, although the degree of stratification depended upon the degree of turbulence and the amount of freshwater inflow. Figures 84 and 85 show the ability of the 3-D model to reproduce the stratification throughout the year. The bay bridge station, CB 3.3W, was located nearer the saline front and thus experienced greater fluctuation. As illustrated in Figure 86, the water column at this station experiences a great deal of apparent mixing and subsequent restratification. The numerical model reproduces these events extremely well. Difference measures for the main bay stations are presented in Table 12. The average relative error is about 10 percent for the salinity computations.

73. Figure 87 illustrates the comparison of computed and recorded salinity near the mouth of the James River. Model results indicate the water column is stratified throughout the year. However, some of the field data imply a well-mixed condition at times. The exact reason for this discrepancy is unknown. The coarseness of the grid prohibits modeling localized topographic effects. In addition, errors in the specification of the local wind may be a factor.

---

* Personal Communication with National Climatic Data Center, Rockville, MD.

74. Figures 88 and 89 show salinity comparisons on the Potomac (LE 2.2) and Patuxent (LE 1.1) Rivers, respectively. These results serve to demonstrate that conditions on the tributaries are represented reasonably well. An inspection of the numerical grid in Figure 2 reveals the rather coarse discretization of the tributaries. With this grid resolution it is encouraging that conditions are reproduced as well as they are on the tributaries. The spatially third-order QUICKEST scheme employed in the salt and temperature transport equation is primarily responsible for this success. Difference measures on the tributaries are given in Table 12 and show that the average relative error is approximately 15–20 percent.

75. Temperature comparisons at the same stations are given in Figures 90–96. These results demonstrate the adequacy of the surface heat exchange formulation in modeling temperatures in Chesapeake Bay. With the bay being so large, if more than one meteorological station had been employed, these results would likely have been even better. Difference measures for both the main bay and the tributaries are given in Table 13. It can be seen that the average relative error is generally less than 10 percent in the main bay and less than 15 percent in the tributaries.

76. Seasonally averaged longitudinal transects of salinity have been constructed from both model results and the field data. The location of these transects are shown in Figure 74. Results for seasons 4 and 5 for both main bay transects and the James and Potomac Rivers are given in Figures 97–100. When viewing these results it should be remembered that the seasonally averaged field data generally involve only four or five values and in some cases only one value. The range of the field data is shown by the vertical lines drawn through the average value at each location where data were available. The locations of the mouths of the Potomac and Patapsco Rivers are noted.

77. The final set of plots of 1984 results are presented in Figures 101–104. Data from all of the main bay stations and all of the tributary stations have been grouped together separately to illustrate a comparison of computed and recorded stratification, as reflected by the difference in salinity between the top and bottom layers, for the complete year. As shown in Figures 101 and 103, a linear regression analysis shows the square of the correlation coefficient R^2 to be above 0.80 for both the main bay and tributary stations. An inspection of Figures 102 and 104 reveals that the error in

the computed stratificatien is less than about 1 ppt for approximately 70 percent of the time.

1985 Simulation

Boundary conditions

78. The 1985 year was broken into the following five seasons for the purpose of generating seasonally averaged longitudinal transects of salinity:

Season 1 ⇒ 1 Jan–28 Feb

Season 2 ⇒ 1 Mar–30 Apr

Season 3 ⇒ 1 May–15 Jul

Season 4 ⇒ 16 Jul–18 Sep

Season 5 ⇒ 19 Sep–31 Dec

79. Boundary forcing data are presented for season 4 of 1985. The ocean boundary tide at the Chesapeake Bay Tunnel is given in Figure 105 with the wind data at the Norfolk and BWI airports presented in Figures 106 and 107. Freshwater inflows for season 4 on the James, Potomac, Patuxent and Susquehanna Rivers are shown in Figure 108 (USGS 1986a,b). Surface heat exchange data for season 4 are listed in Table 14.

Results

80. Locations for which results are presented are shown in Figure 109. Complete results are given in Appendix B. A comparison of computed and recorded water level at Colonial Beach, VA, is given in Figure 110. This comparison is typical of results at other stations. Figure 111 is an expanded view of this comparison near day 201 for two tidal cycles.

81. Salinity comparisons are given at four main bay stations as well as stations on the James, Potomac, and Patuxent Rivers for season 4. These stations are the same ones for which 1984 results were presented. Plots showing salinity comparisons at the main bay stations are given in Figures 112–115. A comparison of Figure 114 and Figure 84 reveals a greater stratification in the midbay during 1984. This is because 1984 was a higher freshwater inflow year. Note that the numerical model computes the reduced stratification in 1985 quite well. The apparent mixing and subsequent restratification observed in the 1984 data at the Bay Bridge station can also be seen in the 1985 results

presented in Figure 115. Once again the model does an excellent job of reproducing these events.

82. Salinity comparisons on the James, Potomac, and Patuxent Rivers are presented in Figures 116-118. Generally, these results show a good reproduction of conditions on the James and Patuxent Rivers. It does appear from Figure 117 that higher saline conditions than are reflected in the field data are computed in the lower Potomac River during season 4. An inspection of results at this station for the complete year (see Appendix B) reveals that this is true for most of the year. The coarseness of the grid in the tributaries which results in an inadequate representation of the channel is probably responsible for the increased error at some tributary locations. Temperature results at the same stations are presented in Figures 119-125 for season 4. Difference measures for both salinity and temperature are given in Tables 12 and 13. It appears the model did a slightly better job in 1984. However, it should be noted that fewer field data were available in 1984 for comparison.

83. During 1985, salinity and temperature data were collected at 1-m intervals at several locations.* These have been used along with model results to construct Figure 126 showing a comparison of computed and recorded vertical profiles of water density at station CB 5.1 at six times during the year. These results demonstrate that the model maintains the proper vertical stratification with the pycnocline in approximately the correct location.

84. Seasonally averaged salinities have been computed along the transects shown in Figure 74. Results for season 4 for both main bay transects as well as the James and Potomac Rivers are presented in Figures 127-130. Once again it should be remembered that the field data used to compute the seasonal averages were very sparse.

85. Figures 131-134 illustrate a comparison of computed and recorded stratification for the complete year for the main bay and tributary stations. A linear regression analysis shows the square of the correlation coefficient to be above 0.70 for both sets of stations. The error in the computed stratification is less than 1 ppt for approximately 70 percent of the time.

86. One final result is presented for the 1985 simulation. During the

---

* Personal Communication with Chesapeake Bay Liaison Office, US Environmental Protection Agency, Annapolis, MD.

early part of November, a major storm moved over the lower Chesapeake Bay. As illustrated in Figure 135, this resulted in a peak flow of nearly 6,000 m^3/sec on the James River. Figure 136 reveals that the numerical model computed virtually salt-free surface waters for the entire James River at the flood peak. Although field data were not available at the time of peak flow, it can be seen that the model does an excellent job of reproducing salinities immediately before and after. These results serve to demonstrate that the numerical model does an excellent job of reproducing extreme events.

1986 Simulation

Boundary conditions

87. The 1986 year was broken into the following five seasons for the purpose of generating seasonally averaged longitudinal transects of salinity:

Season 1 ⇒ 1 Jan–16 Feb

Season 2 ⇒ 17 Feb–3 May

Season 3 ⇒ 4 May–2 Aug

Season 4 ⇒ 3 Aug–9 Nov

Season 5 ⇒ 10 Nov–31 Dec

Time series results and boundary forcing data are presented for a portion of the year. The ocean boundary tide at the Chesapeake Bay Tunnel is shown in Figure 137.* Wind forcing data corrected to reflect the wind over open water are given in Figures 138 and 139. As in 1984 and 1985, these data are from the Norfolk and BWI Airports.** Freshwater inflows on the James, Potomac, Patuxent, and Susquehanna Rivers are given in Figure 140 (USGS 1987a and b). Surface heat exchange data for season 4 are listed in Table 15.

Results

88. Locations at which results are presented are shown on Figure 141. Complete results are given in Appendix C. A comparison of computed and recorded water level at Solomons, MD, is given in Figure 142 with an expanded plot of a couple of tidal cycles near day 201 presented in Figure 143. The reason for the "roughness" in the second computed ebb is unclear but is

---

* Personal Communication with National Ocean Service, Asheville, NC.

** Personal Communication with National Climatic Data Center, Rockville, MD.

probably related to the rapidly changing wind direction illustrated in Figure 139.

89. As for the previous 2 years, salinity comparisons are given for four main bay stations plus stations on the James, Potomac, and Patuxent Rivers. These are shown in Figures 144-150. Results at the shallow eastern shore station EE 3.5 are not reproduced quite as well as in the previous 2 years. However, results at the remaining stations exhibit the same excellent reproduction of actual salinity values as well as the observed stratification patterns. Difference measures are given in Table 12 and demonstrate that the verification for all 3 years is approximately the same.

90. Temperature comparisons at these same stations are presented in Figures 151-156. Generally, these comparisons appear to be about as good as previous results presented for 1984 and 1985. As reflected by the mean bias error in Table 13, the computed temperatures are consistently too cold. Note, however, that temperature inversions are generally reproduced well. Again, it should be remembered that the surface heat exchange data are computed using meteorological data from the Patuxent River Naval Station* and then applied uniformly over the complete grid.

91. The longitudinal plots of seasonally averaged salinities for the two main bay transects and those on the James and Potomac Rivers are given in Figures 157-160. The main bay transects are reproduced extremely well. The coarseness of the grid in the tributaries results in the tributary transects not comparing as well.

92. The final results presented are the plots illustrating the ability of the model to reproduce the stratification, as reflected by the salinity, of the main bay and tributaries in an overall average sense. These results are shown in Figures 161-164. The squares of the correlation coefficients from a linear regression analysis of results for both the main bay and the tributaries are 0.79 and 0.89, respectively. The error in the computed stratification is generally less than 1 ppt for 70 percent of the time.

---

* Personal Communication with National Climatic Data Center, Rockville, MD.

PART VI: SUMMARY AND CONCLUSIONS

Summary

93. A time-varying 3-D numerical hydrodynamic model of Chesapeake Bay has been developed, verified, and applied in a production mode to yield year-long flow fields to drive a 3-D water quality model. The hydrodynamic model, CH3D, makes computations on a curvilinear or boundary-fitted planform grid. Physical processes impacting baywide circulation and vertical mixing that are modeled include tides, wind, density effects (salinity and temperature), freshwater inflows, vertical turbulence, and the effect of the earth's rotation.

94. A successful verification of the hydrodynamic model required sets of synoptic data representing a range of events. Three relatively extensive synoptic data sets were identified. Each of these data sets was approximately 1 month long. The June-July 1980 set represented dry summer conditions and was collected and provided by Dr. William Boicourt of the Horn Point Environment Laboratories in Cambridge, MD. The April 1983 and September 1983 data sets were collected by NOS and provided by HydroQual, Inc. The April data reflected a large spring runoff, whereas the September data contained a wind-induced mixing event that was aided by a temperature inversion. Application of the model to the June-July 1980 and April 1983 data sets involved an early version of the model, whereas verification to the September 1983 data set was with the final version of the model. Verification of the model consisted of comparing recorded and computed water levels, flow velocities, salinities, and temperatures. These comparisons were made through an analysis of time series plots as well as computed difference measures.

95. With the successful simulation of these data sets, the 3-D model was then employed in a production mode. Yearlong simulations of 1984, 1985, and 1986 were made to provide flow fields to drive long-term water quality computations. These simulations also provided additional verification of the model through comparisons of computed tides, salinities, and temperatures at several interior stations with field data. Since salinity is a conservative substance and local concentrations depend heavily upon the flow transport process, if the salinity comparison is good, then it is reasonable to assume the flow is approximately correct. Obviously diffusion of salt (numerical or

real) plays a part also, especially near saline fronts such as those on the tributaries.

Conclusions

96. Two basic conclusions can be drawn. Based upon an overall comparison of model results with available field data from the six simulations presented, it has been demonstrated that the 3-D hydrodynamic model behaves well and is a good representation of the hydrodynamics of the Chesapeake Bay. This has been demonstrated over virtually all types of events that occur in the bay, e.g., a 200-year flood event on the James River during November 1985. For the three yearlong simulations the average relative error in the computed salinity in the main bay is about 10 percent, whereas in the tributaries it is 15-20 percent. The coarseness of the grid in the tributaries is obviously the major reason for the increased error. The average relative error for the temperature is slightly less than for the salinity. This study has also demonstrated that yearlong 3-D hydrodynamic computations to drive water quality models are feasible. A 1-year simulation on the Chesapeake Bay grid using a time-step of 5 minutes takes about 10 hours on a CRAY Y-MP computer.

97. Other conclusions relate to the modeling approach taken. The major problem encountered with the horizontal boundary-fitted transformation concerned the convection terms in the momentum equations. Initially these terms were derived such that velocity squared terms were present. With this form, stable solutions were not possible on irregular grids. However, after deriving these terms such that only gradients of velocity squared terms appeared, this problem was eliminated. The use of a sigma grid in the vertical resulted in excess advection of salt from the deep channels to the shallows. Therefore, to maintain stratification in the channels over long periods of simulation, computations are now made on the z-plane.

98. The obvious benefit of generating solutions on boundary-fitted grids is that geometric features are modeled more accurately and economically. The price for this is the increased complexity of the equations. However, since the equations are differenced on a transformed regular grid, this poses no particular problem. Use of the contravariant velocity results in a more straightforward differencing of the equations since the same type staggered

grid employed in Cartesian models can be used. In addition, boundary conditions are more easily applied.

REFERENCES

Blumberg, A. F., Johnson, B. H., Heath, R. E., Hsieh, B. B., Pankow, V. R., Kim, K. W., and Butler, H. L. 1991. "Data Employed in the Development of a Three-Dimensional, Time-Varying, Numerical Model of Chesapeake Bay," Technical Report HL-91-1, US Army Engineer Waterways Experiment Station, Vicksburg, MS.

Donaldson, C. duP. 1973. "Atmospheric Turbulence and the Dispersal of Atmospheric Pollutants," Workshop on Micrometeorology, D. A. Haugen, ed., American Meteorological Society, Science Press, Boston, pp 313-390.

Edinger, J. E., Brady, D. K., and Geyer, J. C. 1974. "Heat Exchange and Transport in the Environment," Report 14, EPRI Publication No. 74-049-00-3, Prepared for Electric Power Research Institute, Palo Alto, CA.

Garratt, J. R. 1977. "Review of Drag Coefficients Over Oceans and Continents," Monthly Weather Review, Vol 105, pp 915-929.

Goodrich, D. M. 1985. "On Stratification and Wind Induced Mixing in Chesapeake Bay," PhD Dissertation, State University of New York, Stony Brook, NY, 134 pp.

Johnson, B. H. 1980. "VAHM - A Vertically Averaged Hydrodynamic Model Using Boundary-Fitted Coordinates," Miscellaneous Paper HL-80-3, US Army Engineer Waterways Experiment Station, Vicksburg, MS.

Johnson, B. H., Kim, K. W., Heath, R. E., and Butler, H. L. 1991. "User's Guide for the Chesapeake Bay Three-Dimensional Numerical Hydrodynamic Model," Technical Report HL-91-1, US Army Engineer Waterways Experiment Station, Vicksburg, MS.

Leonard, B. P. 1979. "A Stable and Accurate Convective Modeling Procedure Based on Upstream Interpolation," Computer Methods in Applied Mechanics and Engineering, Vol 19, pp 59-98.

Lewellen, W. S. 1977. "Use of Invariant Modeling," Handbook of Turbulence, W. Frost, ed., Plenum Press, New York, Vol 1, pp 237-280.

Sheng, Y. P. 1982. "Hydraulic Applications of a Second-Order Closure Model of Turbulent Transport," Applying Research to Hydraulic Practice, P. Smith, ed., American Society of Civil Engineers, New York, pp 106-119.

_____. 1986. "A Three-Dimensional Mathematical Model of Coastal, Estuarine and Lake Currents Using Boundary Fitted Grid," Report No. 585, A.R.A.P Group of Titan Systems, New Jersey, Princeton, NJ.

US Environmental Protection Agency. 1983a. "Chesapeake Bay: A Framework for Action," V. T. Tippie et al., technical coordinators, US Environmental Protection Agency, Region III, Philadelphia, PA.

US Environmental Protection Agency. 1983b. "Chesapeake Bay: A Profile of Environmental Change," D. A. Flemmer et al., technical coordinators, US Environmental Protection Agency, Region III, Philadelphia, PA.

US Geological Survey. 1981a, 1984-1987 inclusive. "Water Resources Data, Maryland," Water Years 1980, 1983-1986 inclusive, Towson, MD.

US Geological Survey. 1981b, 1984-1987 inclusive. "Water Resources Data, Virginia," Water Years 1980, 1983-1986 inclusive, Richmond, VA.

Table 1

Summary of Conditions During Simulation Periods

Period	Inflow Conditions	Wind Conditions	Model Used	Comments
Jun–Jul 1980	Dry summer conditions	Normal	Early version	Data from Boicourt. Overland winds used in computation of surface heat exchange. Boundary temp and salt constant in time.
Apr 1983	Spring runoff	Normal	Early version	Data from NOS. Overland winds used in computation of surface heat exchange. Boundary temp and salt constant in time.
Sep 1983	Low	Wind-mixing event	Final version	Data from NOS. Entire bay well mixed during wind event. Over-water winds used in surface heat exchange computations. All boundary conditions time varying.
1984	High	Wide range	Final version	Data from NOS and USEPA. Over-water winds used in surface heat exchange computations. All boundary conditions time varying. Little data first 6 months.
1985	Low	Wide range	Final version	Data from NOS and USEPA. Overwater winds used in surface heat exchange computations. All boundary conditions time varying. Extreme inflow event in November on lower bay.
1986	Average	Wide range	Final version	Data from NOS and USEPA. Overwater winds used in surface heat exchange computations. All boundary conditions time varying.

Table 2

1980 Surface Heat Exchange Data

Date	Equilibrium Temperature °C	Surface Transfer Coefficient Watts/m^2/°C
6/23/80	24.7	58.2
6/24/80	24.4	90.6
6/25/80	23.5	80.2
6/26/80	22.3	59.8
6/27/80	21.7	31.0
6/28/80	24.1	23.9
6/29/80	22.9	28.6
6/30/80	26.9	49.7
7/01/80	27.3	36.6
7/02/80	27.9	29.8
7/03/80	28.0	32.0
7/04/80	26.8	48.0
7/05/80	24.7	69.1
7/06/80	24.1	47.1
7/07/80	22.2	47.5
7/08/80	24.2	34.4
7/09/80	23.4	47.7
7/10/80	23.6	31.3
7/11/80	23.4	55.7
7/12/80	26.7	43.6
7/13/80	25.9	63.9
7/14/80	24.3	24.8
7/15/80	21.3	38.6
7/16/80	22.8	52.7
7/17/80	21.3	24.6
7/18/80	19.5	33.8
7/19/80	21.7	25.9
7/20/80	23.6	25.3
7/21/80	25.4	28.5
7/22/80	27.6	31.5
7/23/80	27.2	29.2
7/24/80	26.6	40.1
7/25/80	25.3	44.9
7/26/80	26.4	42.8
7/27/80	26.3	45.9
7/28/80	27.8	30.3
7/29/80	25.7	42.8
7/30/80	25.4	35.2
7/31/80	25.5	43.1

Table 3

April 1983 Surface Heat Exchange Data

Date	Equilibrium Temperature °C	Surface Transfer Coefficient Watts/m^2/°C
4/01/83	13.8	15.7
4/02/83	9.6	21.7
4/03/83	14.2	29.4
4/04/83	16.2	17.4
4/05/83	14.6	11.8
4/06/83	13.7	12.4
4/07/83	14.6	12.8
4/08/83	16.7	13.6
4/09/83	12.6	23.0
4/10/83	13.8	18.7
4/11/83	12.4	21.9
4/12/83	18.2	15.3
4/13/83	15.7	19.2
4/14/83	13.1	29.2
4/15/83	13.6	33.9
4/16/83	12.1	27.7
4/17/83	14.3	18.6
4/18/83	9.9	18.7
4/19/83	4.6	26.2
4/20/83	6.5	28.4
4/21/83	18.4	15.1
4/22/83	19.1	15.8
4/23/83	14.7	19.6
4/24/83	12.4	29.6
4/25/83	7.4	30.6
4/26/83	15.2	25.3
4/27/83	20.9	18.9
4/28/83	21.8	27.1
4/29/83	17.9	32.6
4/30/83	17.9	38.8

Table 4

September 1983 Surface Heat Exchange Data

Date	Equilibrium Temperature °C	Surface Transfer Coefficient Watts/m^2/°C
9/01/83	24.2	41.7
9/02/83	23.6	31.4
9/03/83	27.2	20.0
9/04/83	26.0	45.1
9/05/83	28.7	34.8
9/06/83	28.8	41.4
9/07/83	29.4	27.8
9/08/83	23.4	27.9
9/09/83	26.5	25.1
9/10/83	26.9	29.5
9/11/83	25.8	42.2
9/12/83	25.4	42.9
9/13/83	21.3	43.4
9/14/83	17.1	46.2
9/15/83	18.1	38.1
9/16/83	19.4	29.9
9/17/83	22.3	32.8
9/18/83	22.6	29.6
9/19/83	23.4	49.3
9/20/83	23.4	60.5
9/21/83	20.8	62.9
9/22/83	12.9	46.5
9/23/83	15.4	21.0
9/24/83	15.7	22.3
9/25/83	20.6	13.5
9/26/83	18.2	13.3
9/27/83	21.3	18.7
9/28/83	17.5	40.4
9/29/83	14.5	54.8
9/30/83	16.9	58.3
9/31/83	20.8	22.4
10/1/83	19.9	19.3

Table 5

Comparison of Model and Observed Water Surface at Maximum Flood and Minimum Ebb

Station	Maximum Flood		Minimum Ebb	
	$\lvert E_m - E_o \rvert$ m	$\lvert t_m - t_o \rvert$ min	$\lvert E_m - E_o \rvert$ m	$\lvert t_m - t_o \rvert$ min
Hampton Roads	0.026	12.55	0.104	26.42
Lewisetta	0.085	47.50	0.061	50.63
Colonial Beach	0.058	31.25	0.055	30.00
Solomons	0.113	48.51	0.058	50.00
Annapolis	0.085	15.65	0.073	18.51
Havre de Grace	0.192	160.85	0.098	171.06

Note: E_m = computed water-surface elevation at maximum flood (minimum ebb)
E_o = observed water-surface elevation at maximum flood (minimum ebb)
t_m = computed time to maximum flood (minimum ebb)
t_o = observed time to maximum flood (minimum ebb)

Table 6

Difference Measures for the September 1983 Water-Surface Elevations

Station	MBE m	RMSE m	MAE m
Hampton Roads	0.066	0.095	0.074
Lewisetta	0.016	0.098	0.077
Colonial Beach	0.013	0.106	0.088
Solomons	0.067	0.127	0.101
Annapolis	0.026	0.111	0.085
Havre de Grace	0.051	0.377	0.328

Table 7

Comparison of Model and Observed Near-Surface Along-Bay Current at Maximum Flood and Minimum Ebb

Station	Maximum Flood		Minimum Ebb	
	$\lvert V_m - V_o \rvert$ cm/sec	$\lvert t_m - t_o \rvert$ min	$\lvert V_m - V_o \rvert$ cm/sec	$\lvert t_m - t_o \rvert$ min
Wolf Trap	10.97	32.23	15.81	35.47
Mid Bay	8.78	28.61	10.62	25.36
Bay Bridge	6.95	81.84	7.80	86.74

Note: V_m = Computed along-bay current near the surface at maximum flood (minimum ebb)
V_o = Observed along-bay current near the surface at maximum flood (minimum ebb)
t_m = Computed time to maximum flood (minimum ebb)
t_o = Observed time to maximum flood (minimum ebb)

Table 8

Difference Measures for the September 1983 Along-Bay Component of Velocity

Station	Level	MBE cm/sec	RMSE cm/sec	MAE cm/sec
Wolf Trap	Near surface	-2.17	23.12	19.18
Midbay	Near surface	-0.61	12.03	9.81
	Near bottom	-0.06	10.73	8.26
Bay Bridge	Near surface	-5.24	21.43	18.31
	Near bottom	-14.21	18.97	16.79

Table 9

Difference Measures for the September 1983 Salinities

Station	Level	MBE ppt	RMSE ppt	MAE ppt	ARE %
Wolf Trap	Near surface	1.28	2.17	1.54	10.22
Midbay	Near surface	0.26	0.67	0.55	4.57
	Near bottom	-0.57	1.19	0.87	5.91
Bay Bridge	Near surface	0.14	0.69	0.53	5.15
	Near bottom	-0.08	1.73	1.03	8.14

Table 10

Difference Measures for the September 1983 Temperatures

Station	Level	MBE °C	RMSE °C	MAE °C	ARE %
Wolf Trap	Near surface	-0.60	0.89	0.76	3.60
Midbay	Near surface	-0.17	0.48	0.41	1.94
	Near bottom	0.12	0.38	0.32	1.55
Bay Bridge	Near surface	0.20	0.71	0.52	2.91
	Near bottom	-0.10	0.21	0.12	0.83

Table 11

Surface Heat Exchange Data, Season 5, 1984

Date	Equilibrium Temperature °C	Surface Transfer Coefficient Watts/m^2/°C
11/26/84	5.3	13.0
11/27/84	5.6	13.9
11/28/84	10.6	55.0
11/29/84	3.3	32.9
11/30/84	4.9	23.8
12/01/84	6.4	27.5
12/02/84	4.8	15.0
12/03/84	8.0	22.1
12/04/84	1.1	17.6
12/05/84	0.5	25.2
12/06/84	1.1	36.6
12/07/84	-4.4	35.0
12/08/84	0.3	20.2
12/09/84	3.8	10.0
12/10/84	3.8	10.3
12/11/84	5.3	19.0
12/12/84	4.1	17.1
12/13/84	7.8	14.1
12/14/84	8.6	14.4
12/15/84	8.5	15.4
12/16/84	6.7	17.1
12/17/84	10.5	20.1
12/18/84	13.0	16.4
12/19/84	9.1	19.1
12/20/84	6.8	10.8
12/21/84	6.1	22.0
12/22/84	11.4	53.3
12/23/84	2.3	20.6
12/24/84	4.0	21.5
12/25/84	3.4	33.5
12/26/84	1.0	9.3
12/27/84	3.5	11.9
12/28/84	11.4	30.6
12/29/84	13.6	51.5
12/30/84	9.9	30.2
12/31/84	9.5	31.1

Table 12

Salinity Statistics for Yearlong Simulations

	Main Bay				Tributaries			
Year	MBE ppt	MAE ppt	RMSE ppt	ARE %	MBE ppt	MAE ppt	RMSE ppt	ARE %
				Near Surface				
1984	-0.05	1.21	1.45	10.13	-0.20	1.54	1.85	17.25
1985	0.90	1.49	1.93	11.43	1.09	1.66	2.04	16.32
1986	0.25	1.52	1.87	12.29	0.32	1.60	2.04	15.02
				Near Bottom				
1984	-0.64	1.72	2.12	10.44	-0.09	2.36	2.83	19.94
1985	1.12	1.78	2.34	12.11	1.27	2.31	2.99	18.30
1986	-0.16	1.35	1.68	8.74	0.24	2.23	2.65	13.40

Table 13

Temperature Statistics for Yearlong Simulations

	Main Bay				Tributaries			
Year	MBE °C	MAE °C	RMSE °C	ARE %	MBE °C	MAE °C	RMSE °C	ARE %
				Near Surface				
1984	-1.48	1.56	1.79	8.45	-1.90	2.07	2.20	11.06
1985	-1.73	1.97	2.25	12.76	-2.03	2.06	2.28	12.11
1986	-1.61	1.72	2.04	11.62	-1.97	2.09	2.40	14.92
				Near Bottom				
1984	-0.42	1.14	1.35	6.79	-1.28	1.70	1.92	9.70
1985	-1.01	1.45	1.70	9.99	-1.53	1.75	2.00	10.94
1986	-1.03	1.34	1.63	9.60	-1.61	1.91	2.32	14.74

Table 14

Surface Heat Exchange Data, Season 4, 1985

Date	Equilibrium Temperature °C	Surface Transfer Coefficient Watts/m^2/°C
7/16/85	27.1	35.8
7/17/85	24.0	40.2
7/18/85	29.9	21.3
7/19/85	25.5	38.4
7/20/85	27.6	32.6
7/21/85	27.4	29.0
7/22/85	25.1	43.1
7/23/85	22.2	34.3
7/24/85	24.8	31.4
7/25/85	24.6	65.0
7/26/85	24.2	88.8
7/27/85	25.0	26.2
7/28/85	27.5	24.9
7/29/85	26.4	17.8
7/30/85	26.7	38.2
7/31/85	25.5	53.2
8/01/85	21.9	40.1
8/02/85	22.5	33.7
8/03/85	27.9	18.9
8/04/85	24.9	27.5
8/05/85	23.2	32.8
8/06/85	23.1	28.7
8/07/85	23.2	56.0
8/08/85	25.3	30.1
8/09/85	27.8	28.3
8/10/85	26.1	35.7
8/11/85	30.7	20.4
8/12/85	24.6	33.1
8/13/85	25.3	44.2
8/14/85	26.3	44.2
8/15/85	24.9	60.5
8/16/85	27.1	33.5
8/17/85	22.0	35.6
8/18/85	21.2	63.1
8/19/85	24.3	49.8
8/20/85	27.5	20.9
8/21/85	21.9	35.5
8/22/85	23.0	22.1
8/23/85	26.2	17.4
8/24/85	19.5	54.5
8/25/85	21.8	50.8
8/26/85	24.6	44.5
8/27/85	23.6	33.2

(Continued)

Table 14 (Concluded)

Date	Equilibrium Temperature °C	Surface Transfer Coefficient Watts/m^2/°C
8/28/85	23.6	37.5
8/29/85	23.0	53.3
8/30/85	22.4	74.2
8/31/85	20.1	55.3
9/01/85	20.5	56.1
9/02/85	22.9	57.3
9/03/85	26.0	36.2
9/04/85	26.1	41.5
9/05/85	28.1	34.2
9/06/85	27.0	44.7
9/07/85	30.7	21.1
9/08/85	28.9	20.3
9/09/85	27.0	30.4
9/10/85	28.2	27.6
9/11/85	20.6	35.0
9/12/85	17.4	28.5
9/13/85	13.0	43.3
9/14/85	16.3	27.3
9/15/85	18.7	19.3
9/16/85	20.4	19.1
9/17/90	20.8	21.7
9/18/90	22.9	15.0
9/19/90	22.5	20.5

Table 15

Surface Heat Exchange Data, Season 4, 1986

Date	Equilibrium Temperature °C	Surface Transfer Coefficient Watts/m^2/°C
8/03/86	24.7	33.0
8/04/86	26.3	30.2
8/05/86	26.5	34.1
8/06/86	23.9	53.6
8/07/86	26.0	36.9
8/08/86	24.3	50.7
8/09/86	25.8	39.2
8/10/86	25.2	56.1
8/11/86	22.9	52.3
8/12/86	20.5	34.3
8/13/86	20.2	50.3
8/14/86	24.2	42.4
8/15/86	26.2	42.4
8/16/86	26.6	55.6
8/17/86	25.5	60.6
8/18/86	23.7	72.8
8/19/86	24.5	32.7
8/20/86	21.4	83.9
8/21/86	22.7	56.0
8/22/86	23.8	32.0
8/23/86	22.6	52.7
8/24/86	20.1	62.2
8/25/86	21.7	26.3
8/26/86	23.3	50.4
8/27/86	22.9	86.7
8/28/86	16.3	55.9
8/29/86	16.9	30.5
8/30/86	18.2	31.2
8/31/86	20.9	64.3
9/01/86	20.9	51.9
9/02/86	19.7	33.6
9/03/86	20.9	57.3
9/04/86	21.3	73.3
9/05/86	21.4	34.8
9/06/86	24.3	39.9
9/07/86	24.5	20.1
9/08/86	17.3	29.8
9/09/86	19.2	23.1
9/10/86	19.5	47.4
9/11/86	22.0	50.4

(Continued)

Table 15 (Continued)

Date	Equilibrium Temperature °C	Surface Transfer Coefficient Watts/m^2/°C
9/12/86	22.2	31.5
9/13/86	19.5	29.8
9/14/86	20.5	39.7
9/15/86	20.1	34.2
9/16/86	15.8	19.3
9/17/86	13.2	17.9
9/18/86	15.1	35.1
9/19/86	19.5	30.0
9/20/86	19.9	21.7
9/21/86	21.6	23.5
9/22/86	19.3	22.2
9/23/86	21.8	26.6
9/24/86	22.9	27.2
9/25/86	24.8	40.2
9/26/86	25.6	39.6
9/27/86	21.6	25.4
9/28/86	19.2	34.9
9/29/86	22.4	33.2
9/30/86	23.6	23.1
10/01/86	23.9	27.1
10/02/86	23.7	39.1
10/03/86	22.2	47.0
10/04/86	23.0	40.4
10/05/86	20.6	50.7
10/06/86	12.7	28.6
10/07/86	14.0	20.9
10/08/86	17.7	39.5
10/09/86	21.0	26.1
10/10/86	10.1	45.1
10/11/86	12.2	105.3
10/12/86	15.4	97.2
10/13/86	17.9	32.4
10/14/86	18.4	29.6
10/15/86	8.8	44.7
10/16/86	12.1	61.5
10/17/86	11.4	39.8
10/18/86	10.4	50.7
10/19/86	10.3	53.7
10/20/86	11.7	48.5
10/21/86	12.5	47.2
10/22/86	15.1	48.7
10/23/86	16.7	82.3
10/24/86	14.3	55.8

(Continued)

Table 15 (Concluded)

Date	Equilibrium Temperature °C	Surface Transfer Coefficient Watts/m^2/°C
10/25/86	11.7	32.5
10/26/86	16.1	33.4
10/27/86	16.8	48.5
10/28/86	13.7	34.2
10/29/86	12.9	36.1
10/30/86	13.5	33.7
10/31/86	9.3	37.6
11/01/86	14.6	21.9
11/02/86	14.7	28.6
11/03/86	8.1	26.1
11/04/86	10.9	25.9
11/05/86	9.3	31.7
11/06/86	9.4	30.4
11/07/86	10.8	21.8
11/08/86	16.2	32.6
11/09/86	16.7	65.4

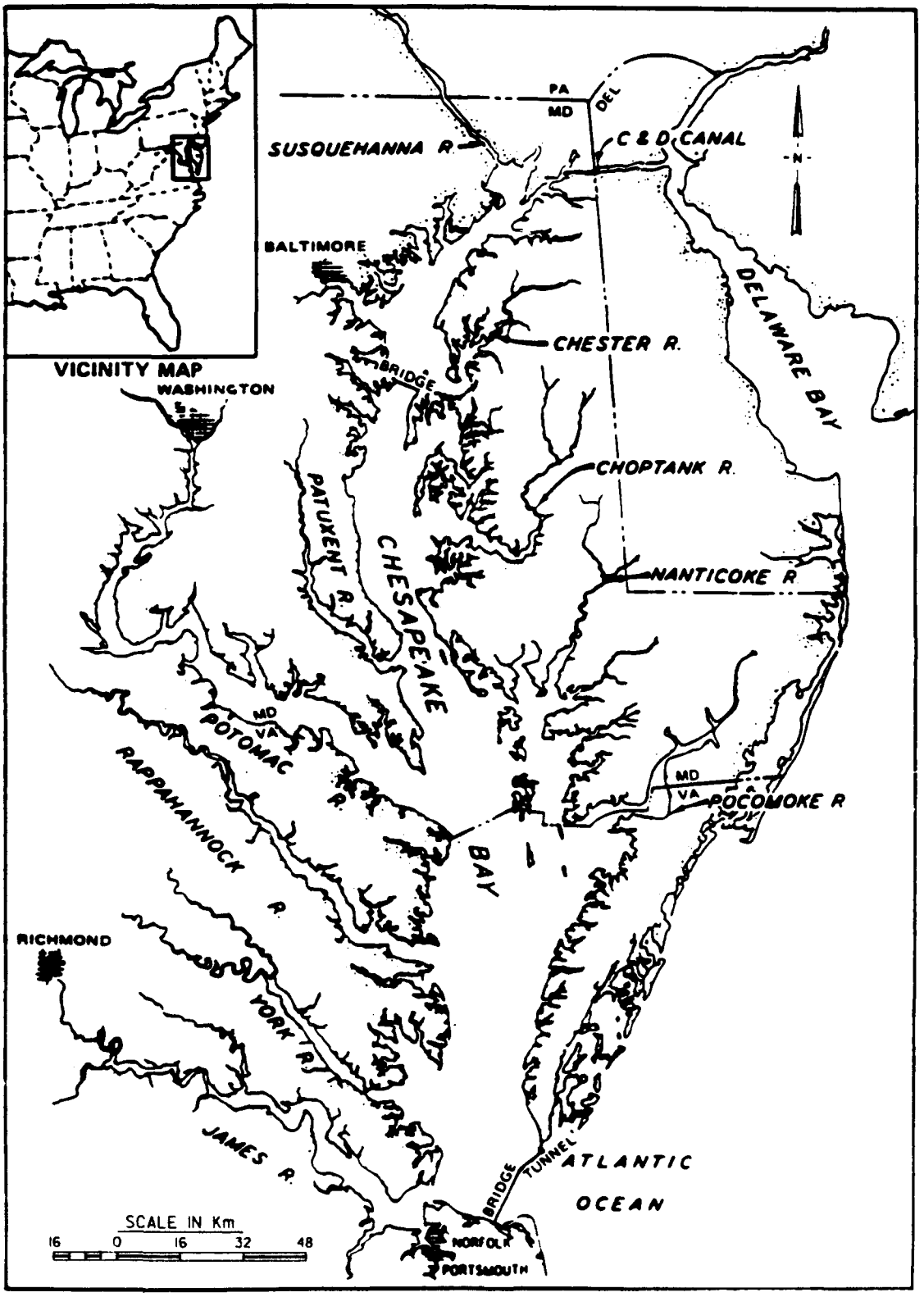

Figure 1. Chesapeake Bay

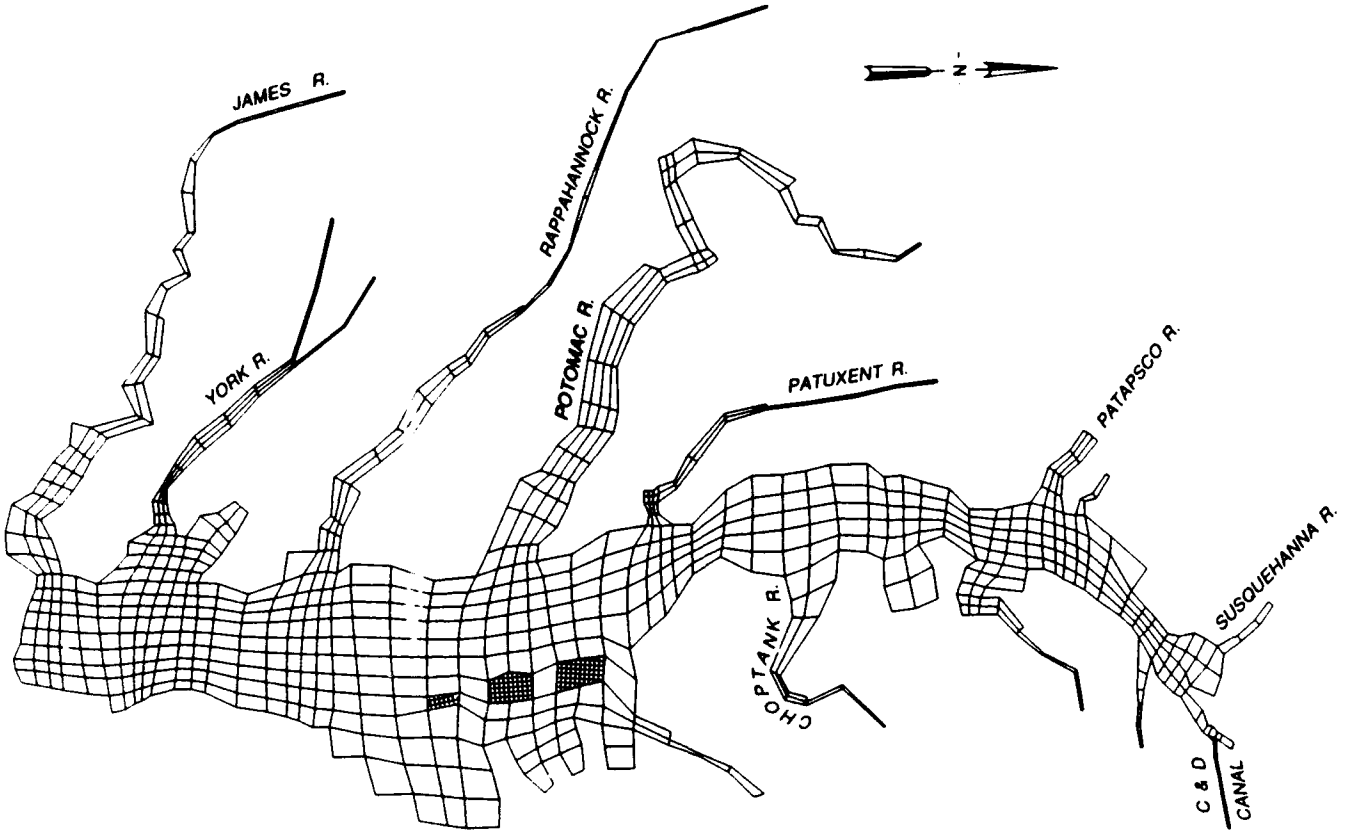

Figure 2. Planform boundary-fitted grid of Chesapeake Bay

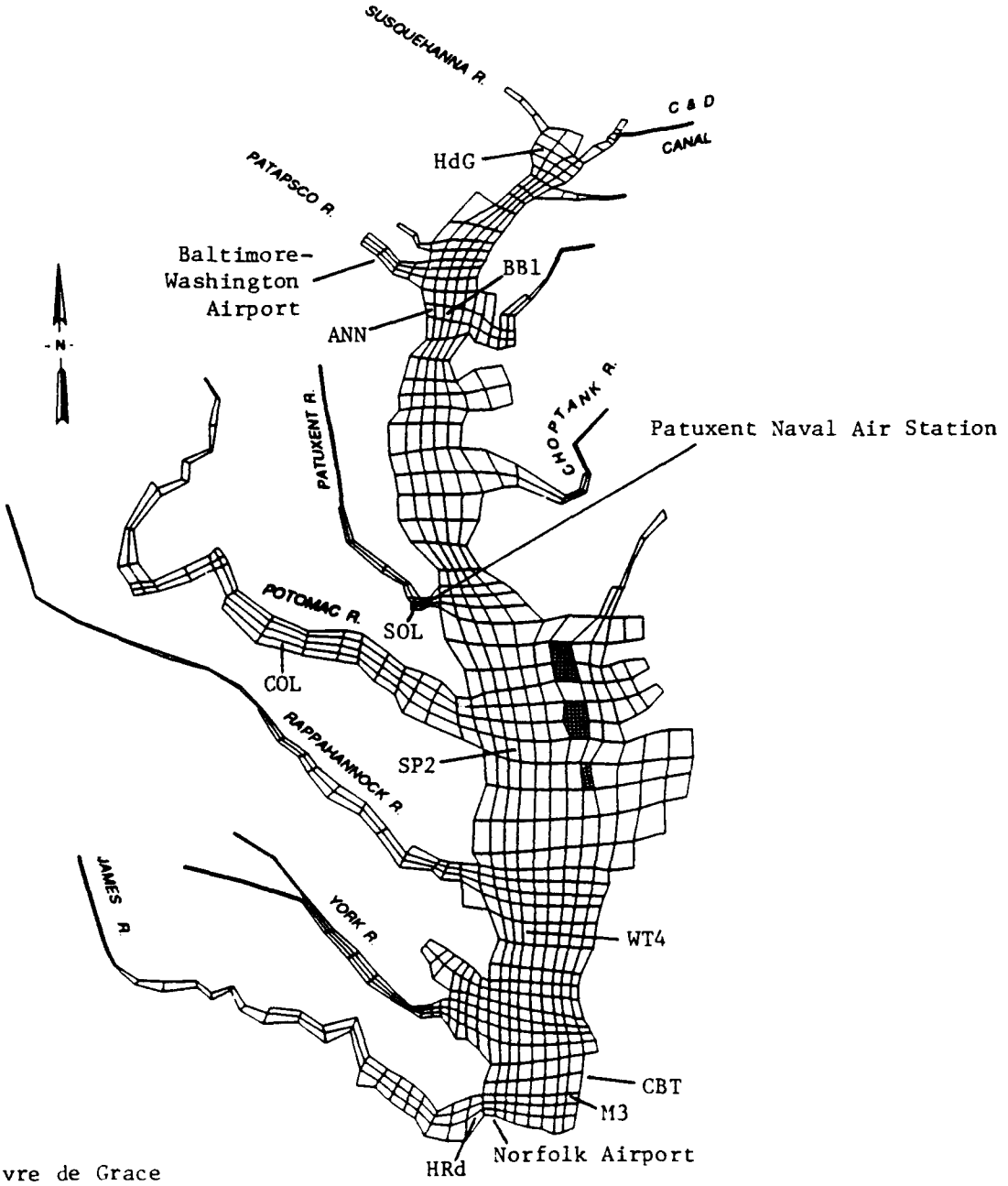

HdG - Havre de Grace
ANN - Annapolis
SOL - Solomons
COL - Colonial Beach
HRd - Hampton Roads
CBT - Chesapeake Bay Tunnel

Figure 3. Location of stations for 1980 data set

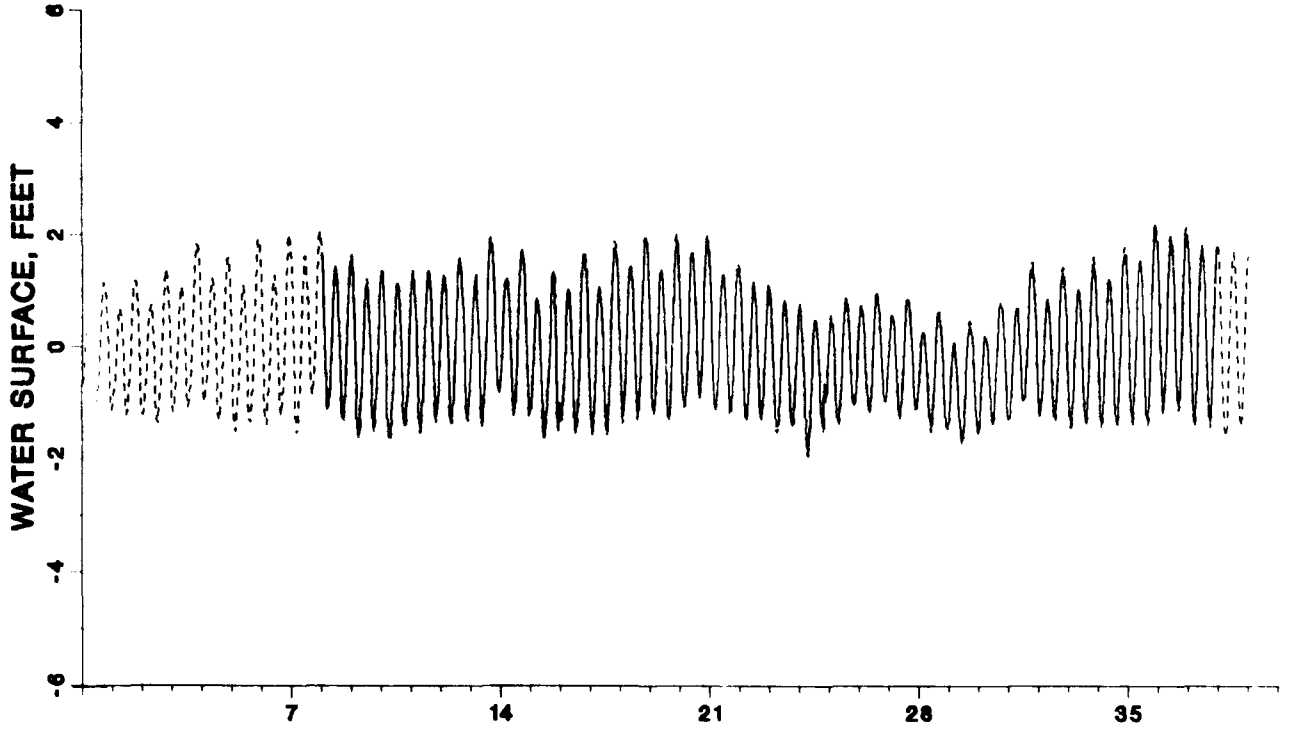

Figure 4. Ocean boundary tide at the Chesapeake Bay Tunnel during June–July 1980

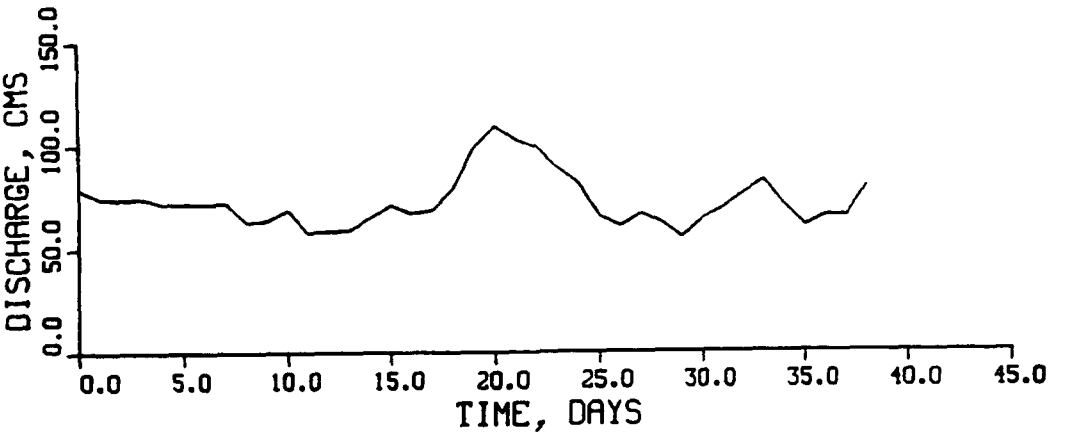

a. James River

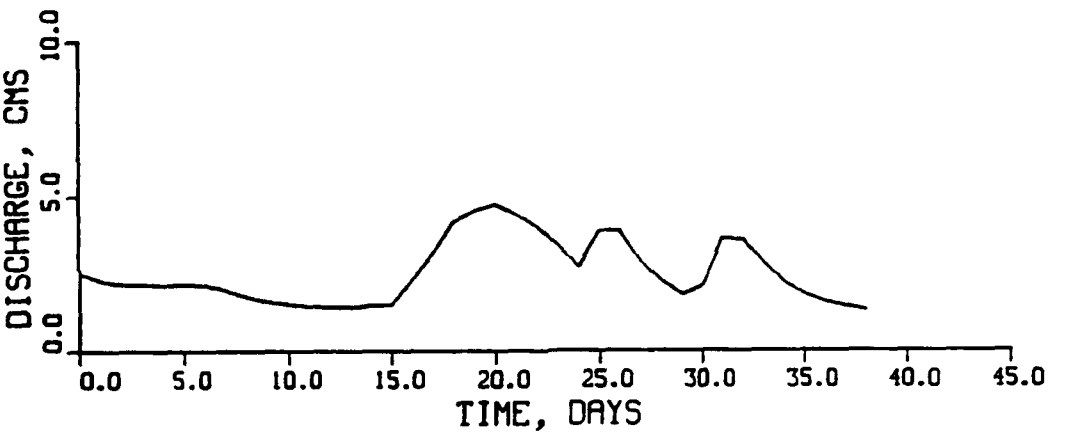

b. Mattaponi River

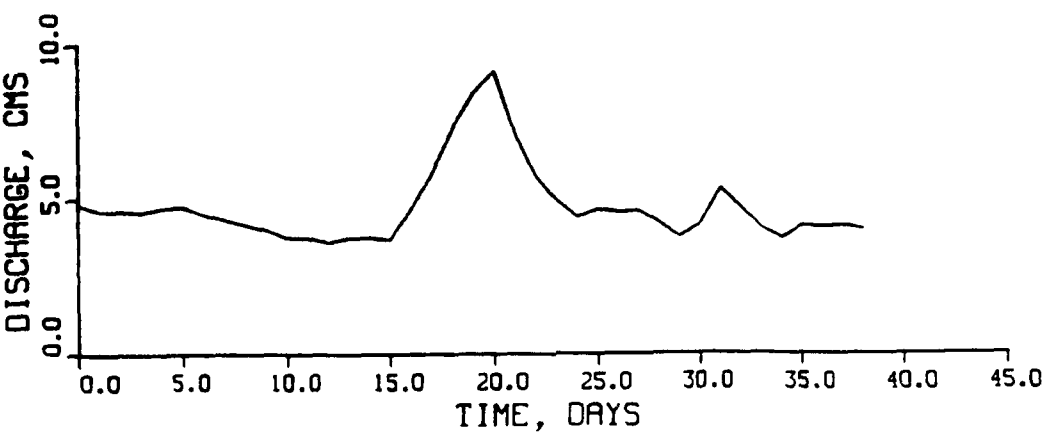

c. Pamunkey River

Figure 5. Freshwater inflows during June–July 1980. Day 0 is 23 June. (Sheet 1 of 3)

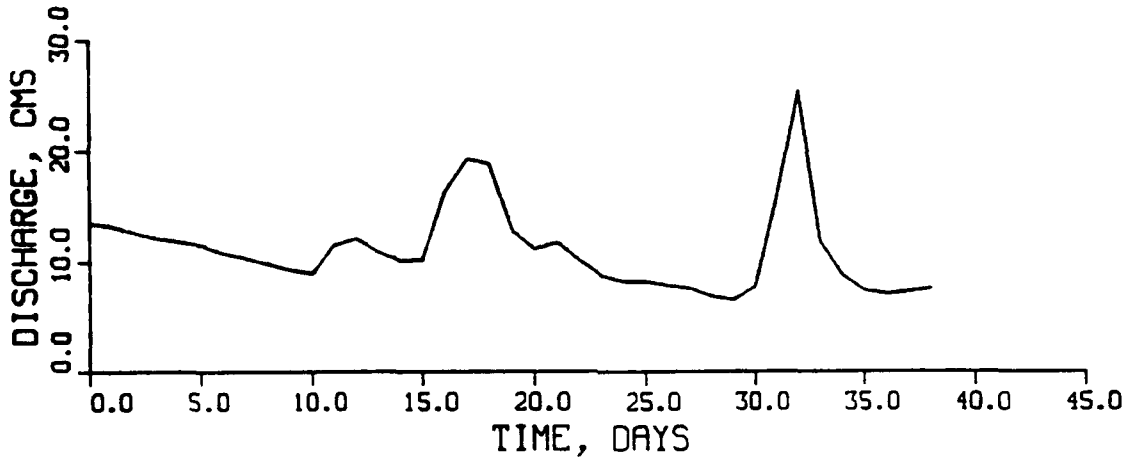

d. Rappahannock River

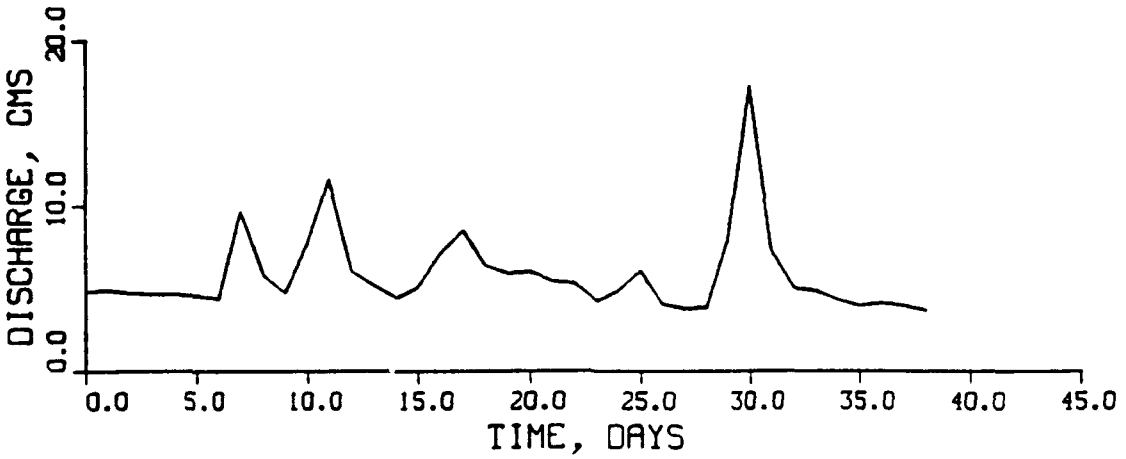

e. Patuxent River

Figure 5. (Sheet 2 of 3)

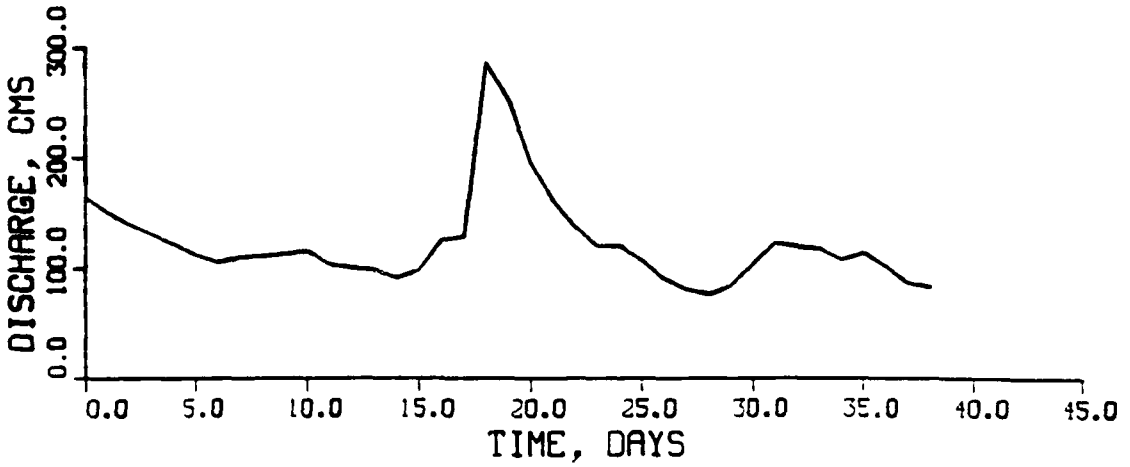

f. Potomac River

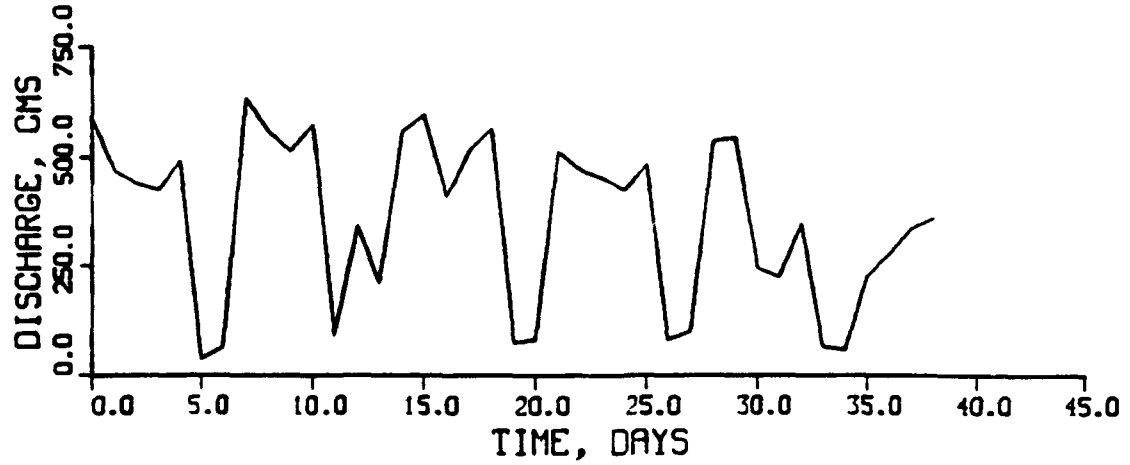

g. Susquehanna River

Figure 5. (Sheet 3 of 3)

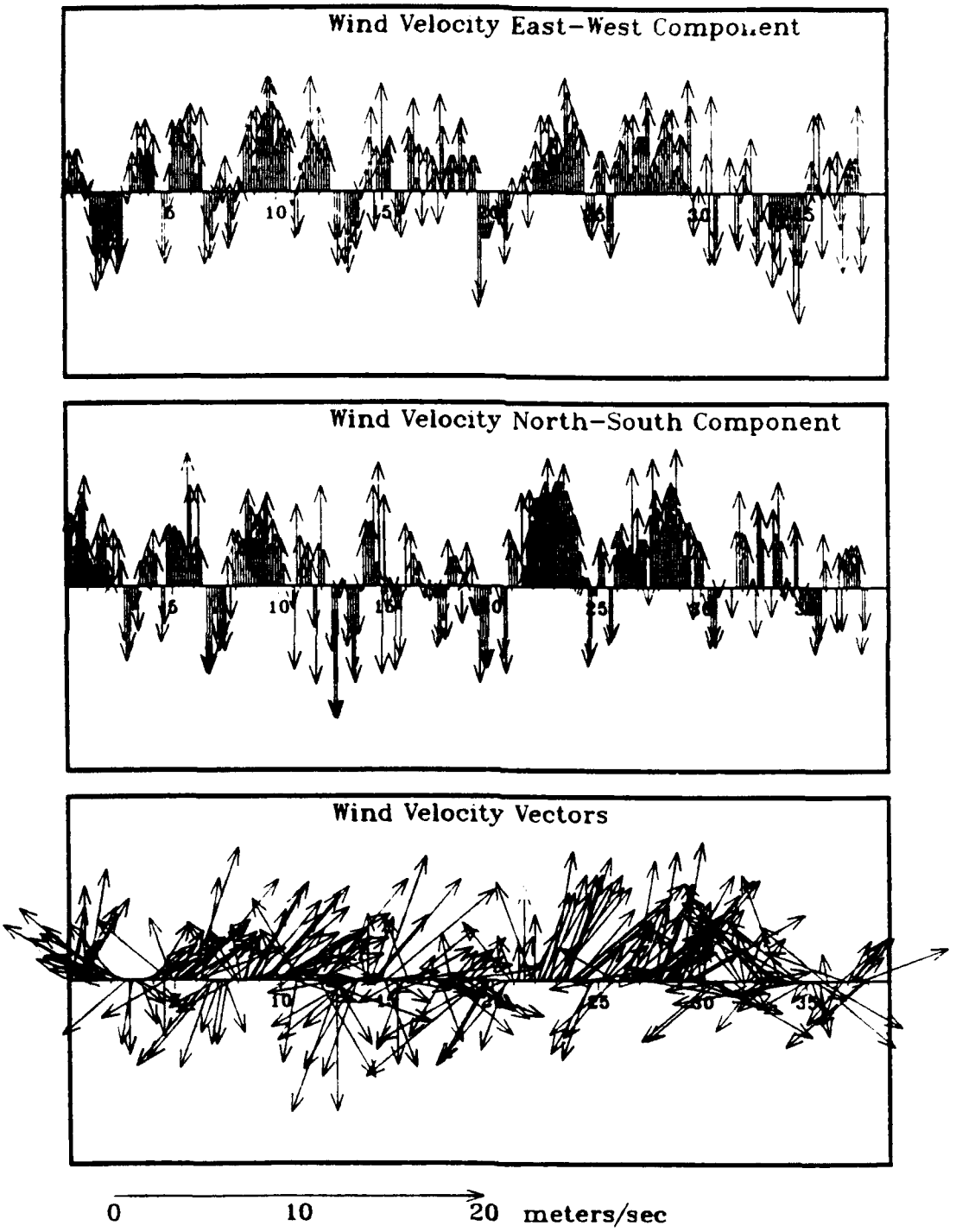

Figure 6. Wind data at Norfolk International Airport during June–July 1980. Day 0 is 23 June.

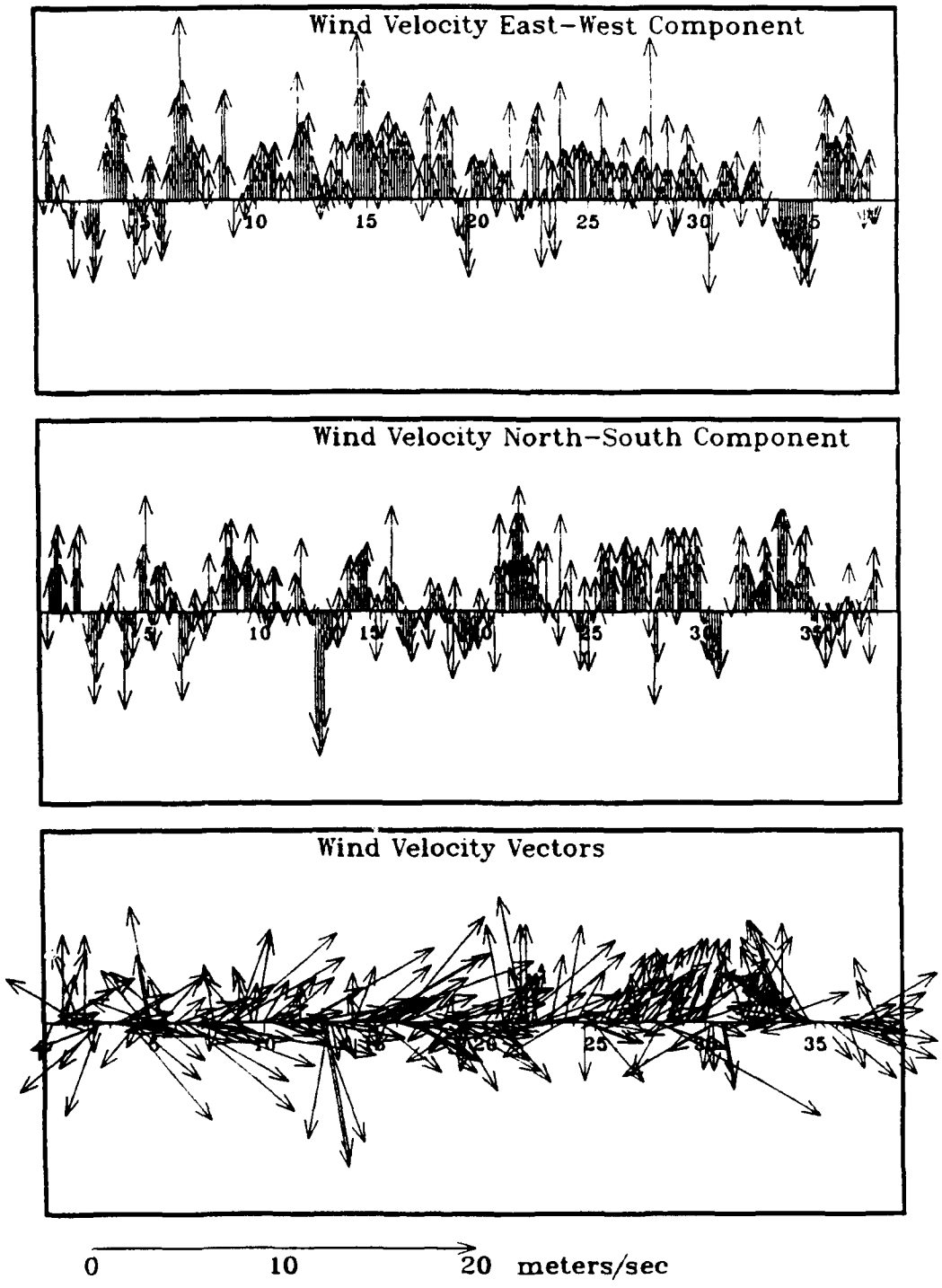

Figure 7. Wind data at BWI station during June-July 1980. Day 0 is 23 June.

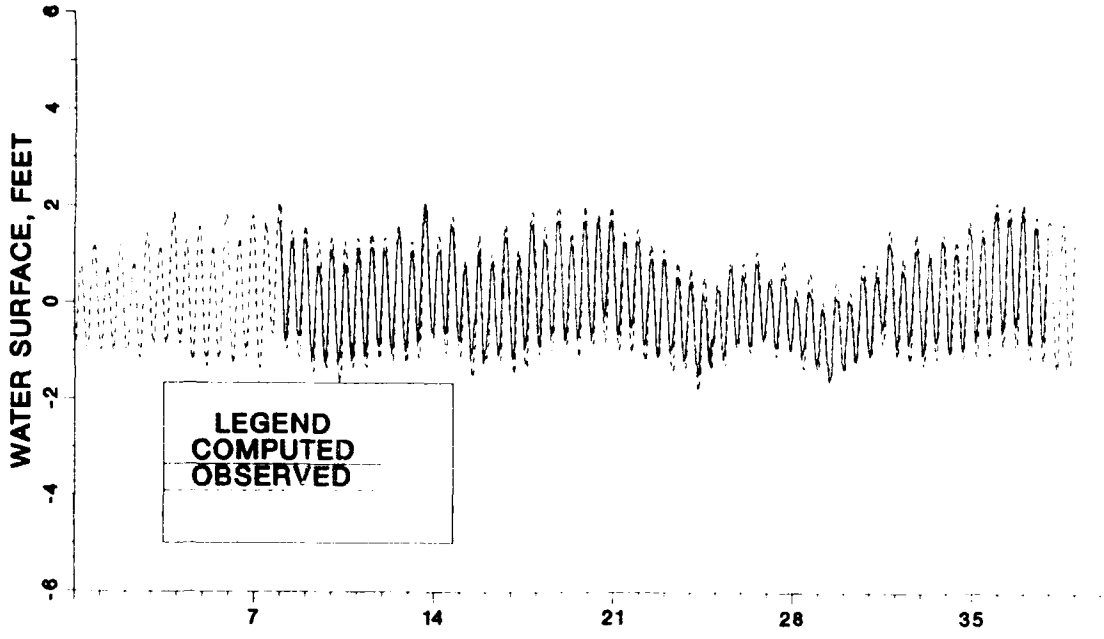

Figure 8. Comparison of computed and recorded tide at Hampton Roads, VA, during June–July 1980. Day 0 is 23 June.

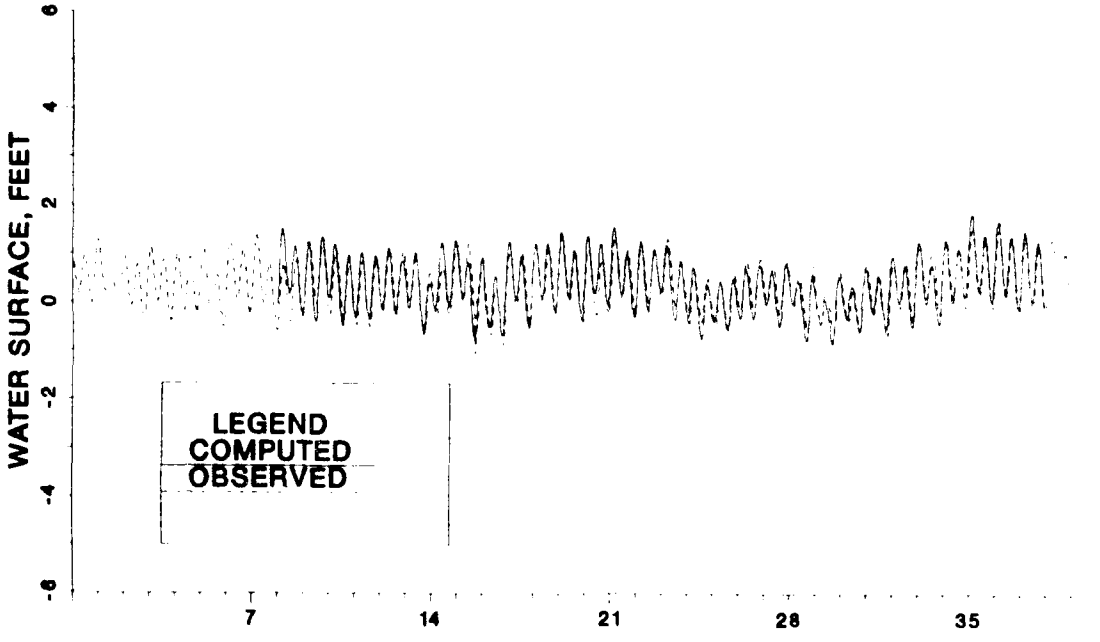

Figure 9. Comparison of computed and recorded tide at Solomons, MD, during June–July 1980. Day 0 is 23 June.

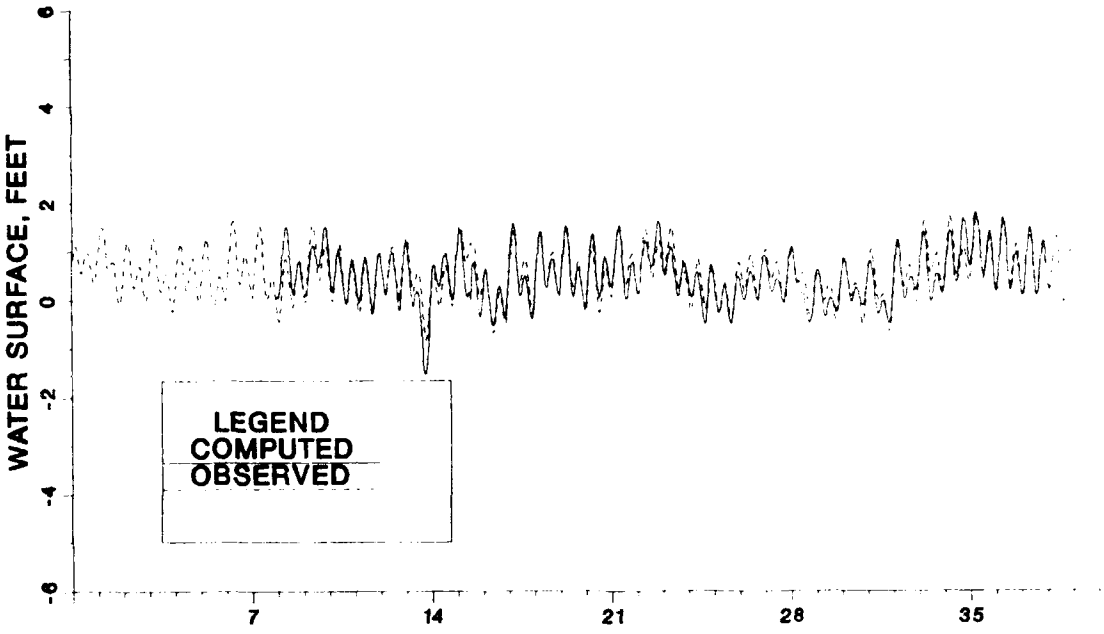

Figure 10. Comparison of computed and recorded tide at Annapolis, MD, during June-July 1980. Day 0 is 23 June.

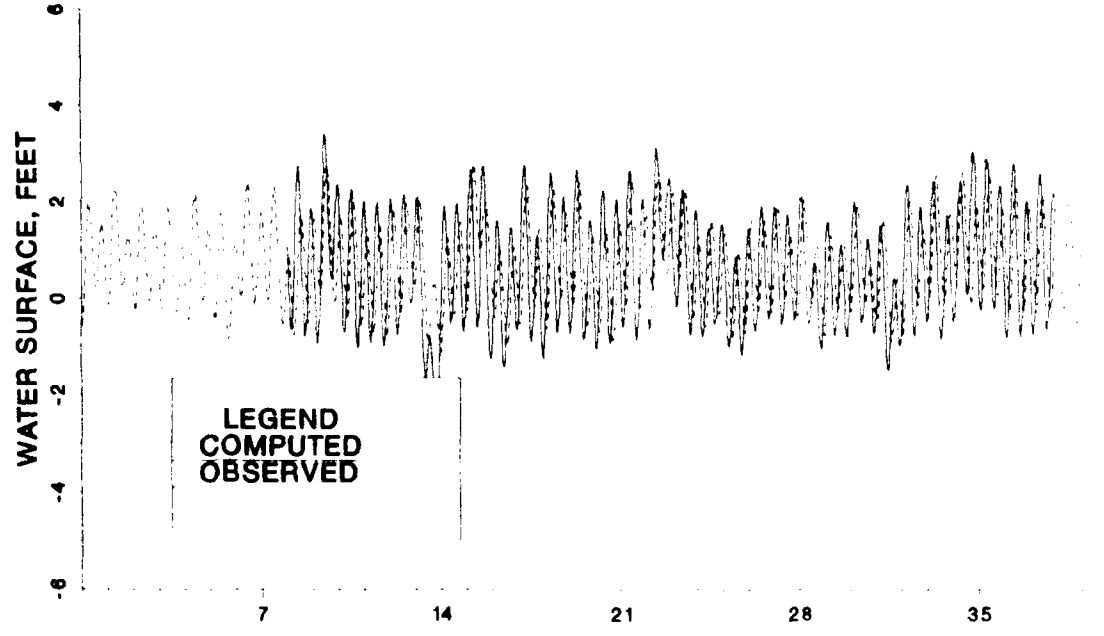

Figure 11. Comparison of computed and recorded tide at Havre de Grace, MD, during June-July 1980. Day 0 is 23 June.

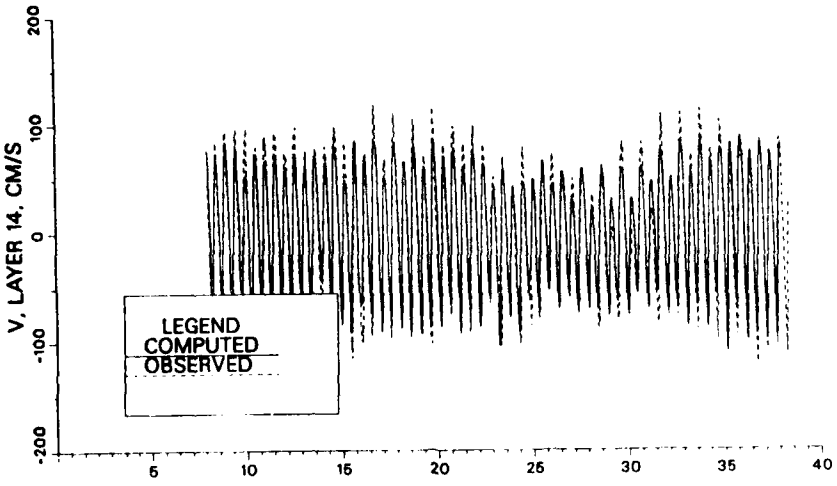

a. Depth = 7.5 ft

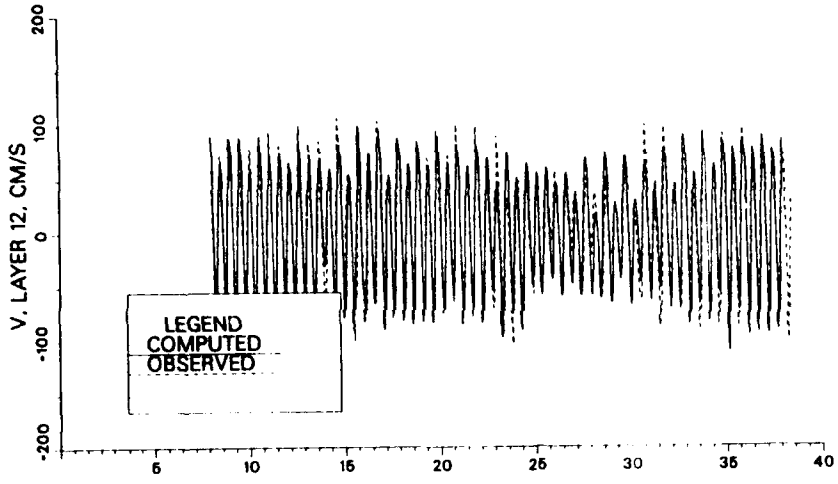

b. Depth = 17.5 ft

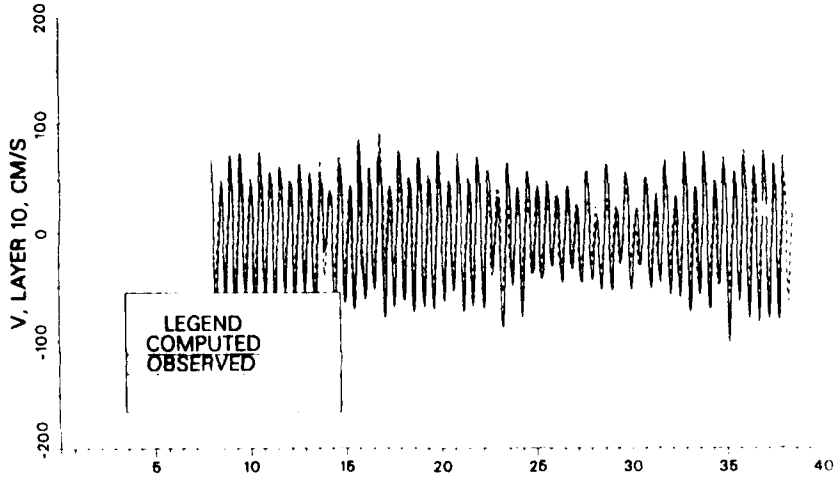

c. Depth = 27.5 ft

Figure 12. Comparison of computed and recorded velocity at station M3 during June-July 1980. Day 0 is 23 June.

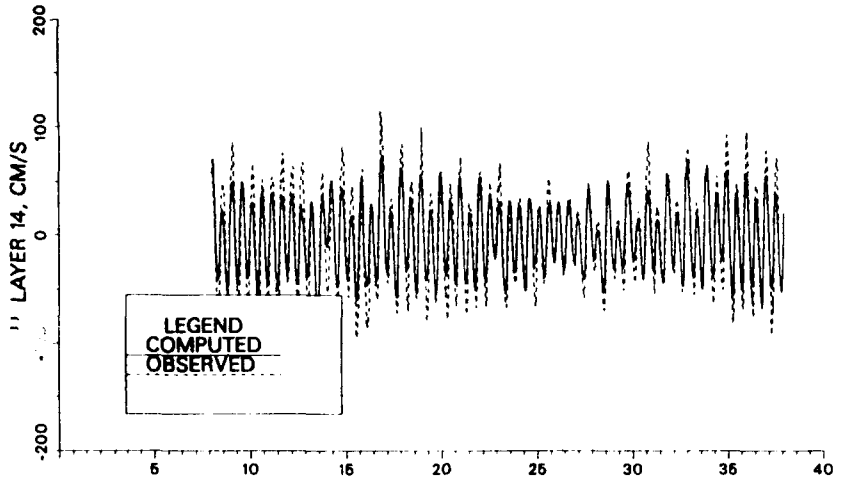

a. Depth = 7.5 ft

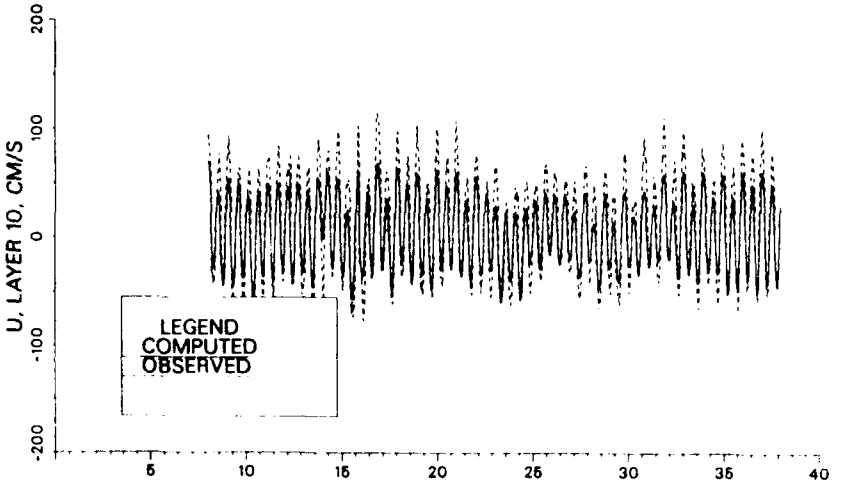

b. Depth = 27.5 ft

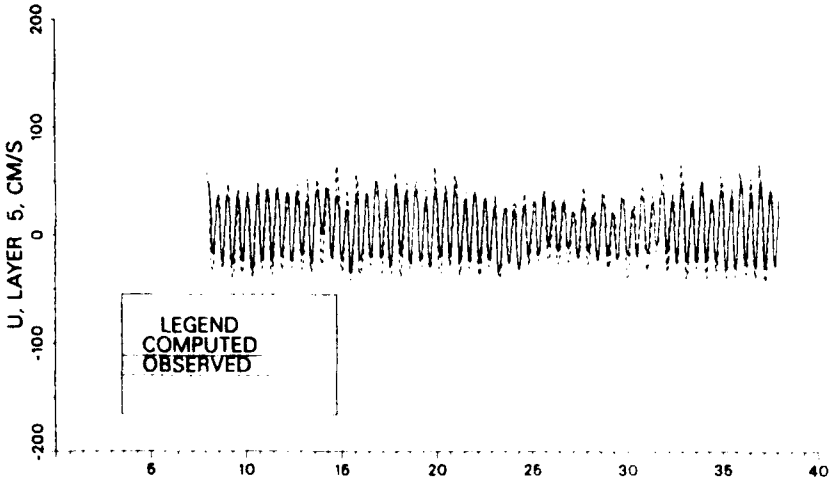

c. Depth = 52.5 ft

Figure 13. Comparison of computed and recorded velocity at station WT4 during June–July 1980. Day 0 is 23 June.

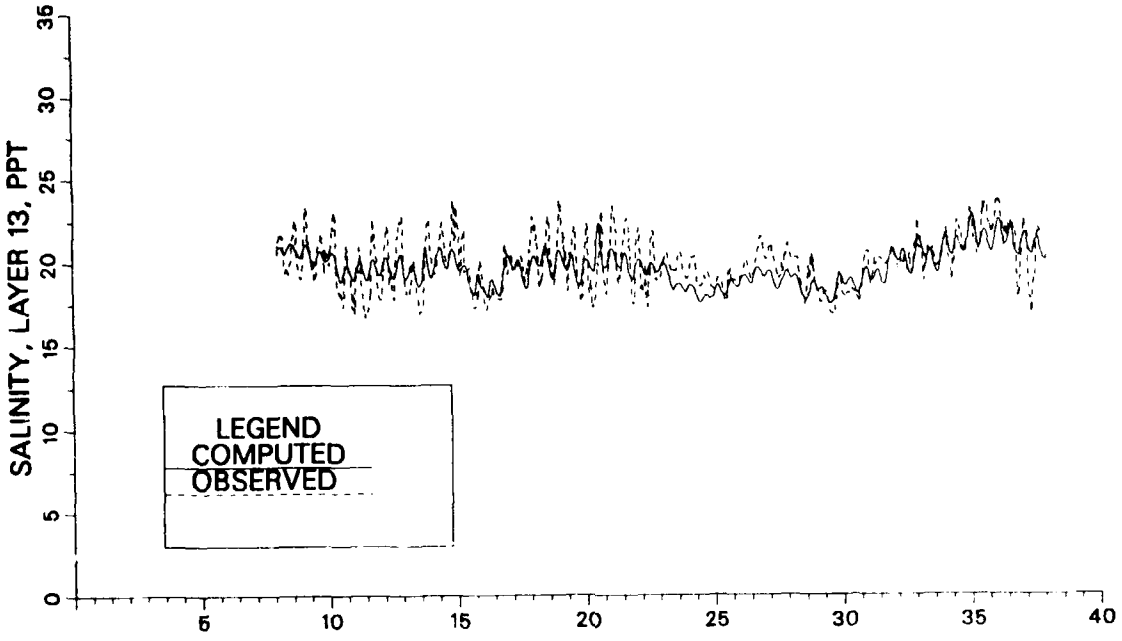

a. Depth = 12.5 ft

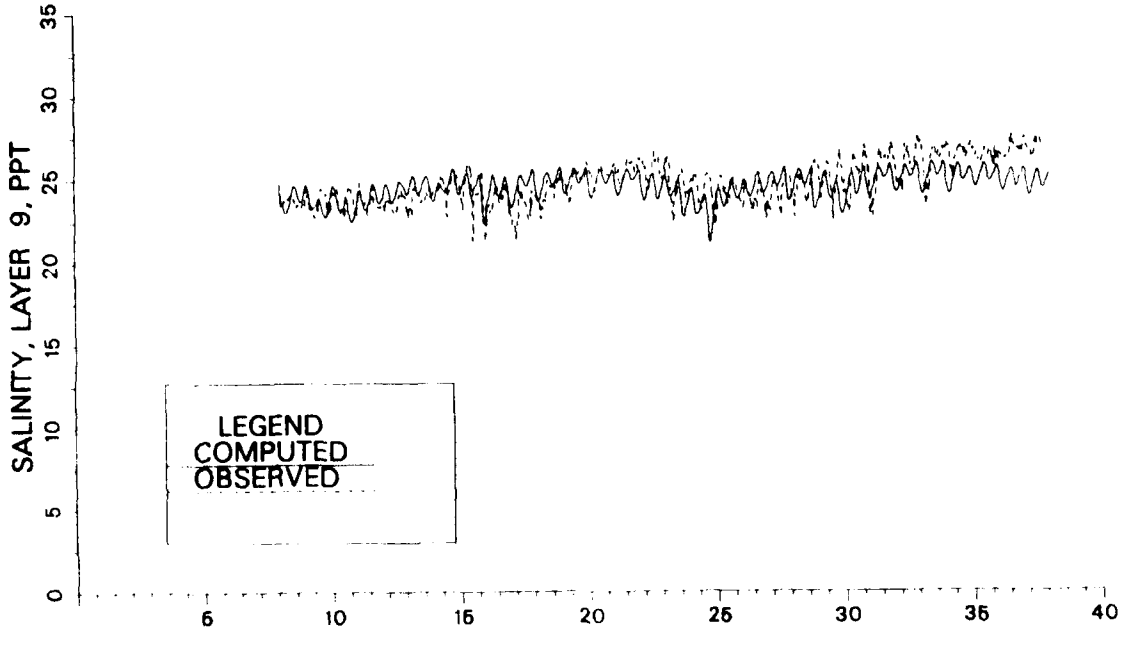

b. Depth = 32.5 ft

Figure 14. Comparison of computed and recorded salinity at station WT4 during June–July 1980. Day 0 is 23 June.

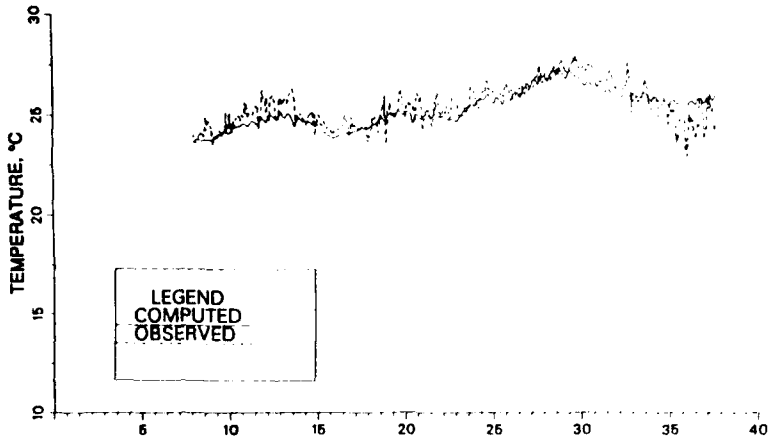

a. Depth = 12.5 ft

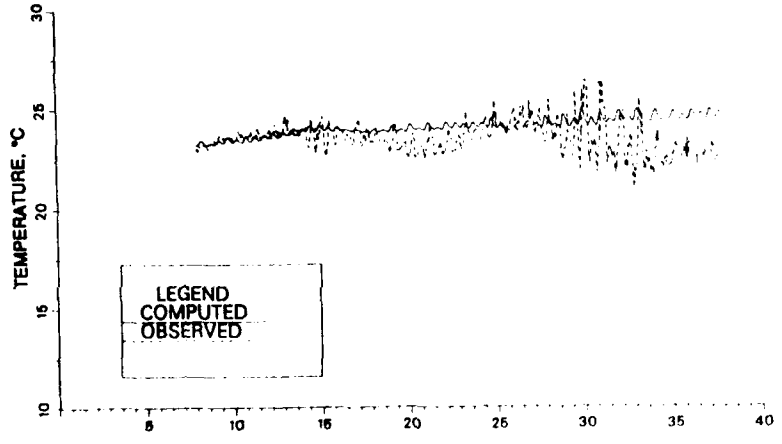

b. Depth = 32.5 ft

c. Depth = 57.5 ft

Figure 15. Comparison of computed and recorded temperature at station WT4 during June–July 1980. Day 0 is 23 June.

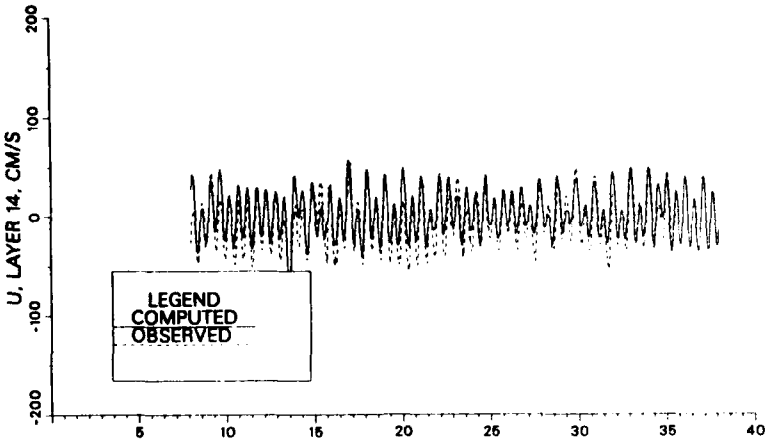

a. Depth = 7.5 ft

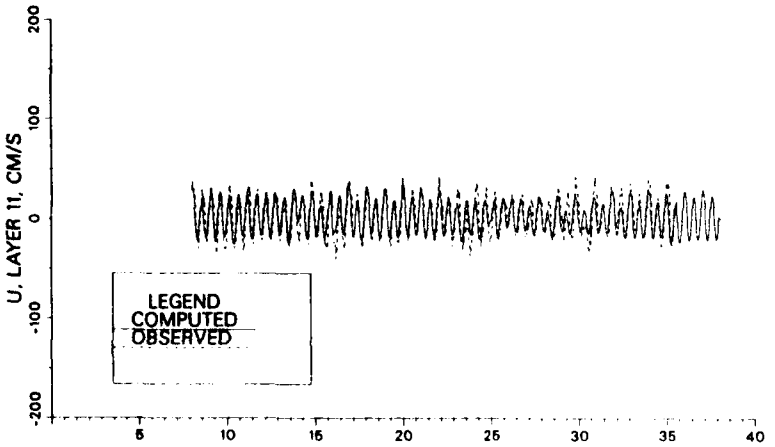

b. Depth = 22.5 ft

Figure 16. Comparison of computed and recorded velocity at station SP2 during June–July 1980. Day 0 is 23 June.

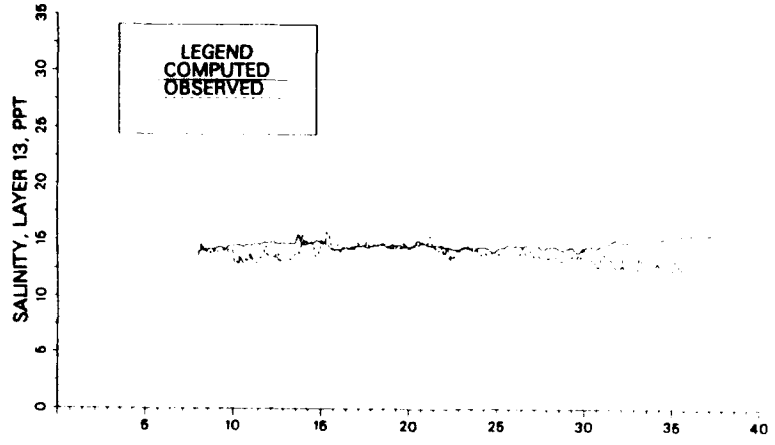

Figure 17. Comparison of computed and recorded salinity at station SP2 at a depth of 12.5 ft during June–July 1980. Day 0 is 23 June.

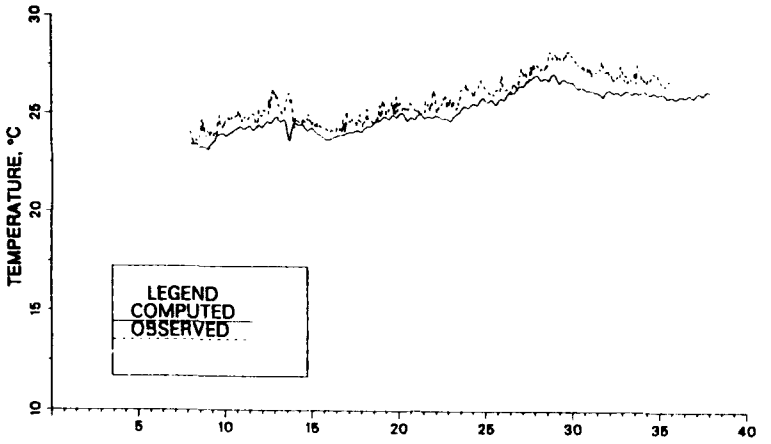

a. Depth = 12.5 ft

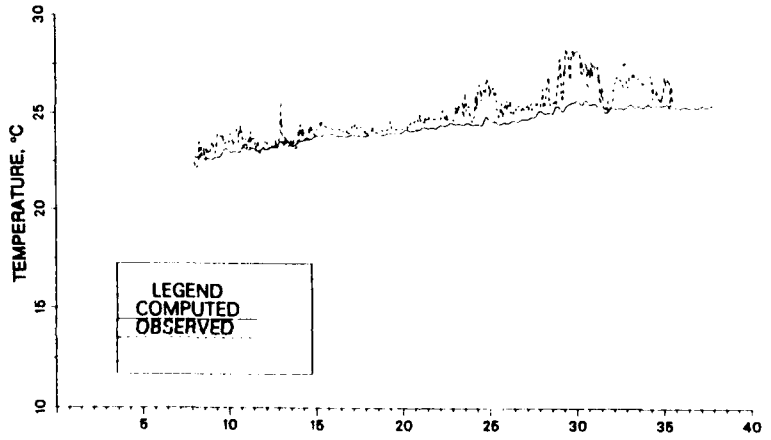

b. Depth = 22.5 ft

Figure 18. Comparison of computed and recorded temperature at station SP2 during June-July 1980. Day 0 is 23 June.

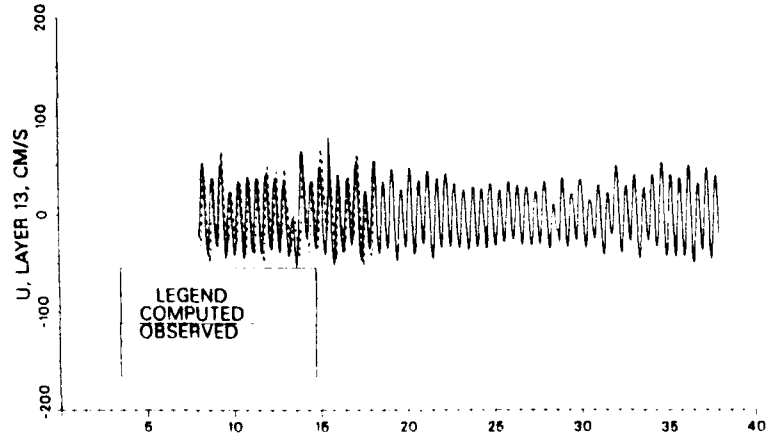

Figure 19. Comparison of computed and recorded velocity at station BB1 at a depth of 12.5 ft during June-July 1980. Day 0 is 23 June.

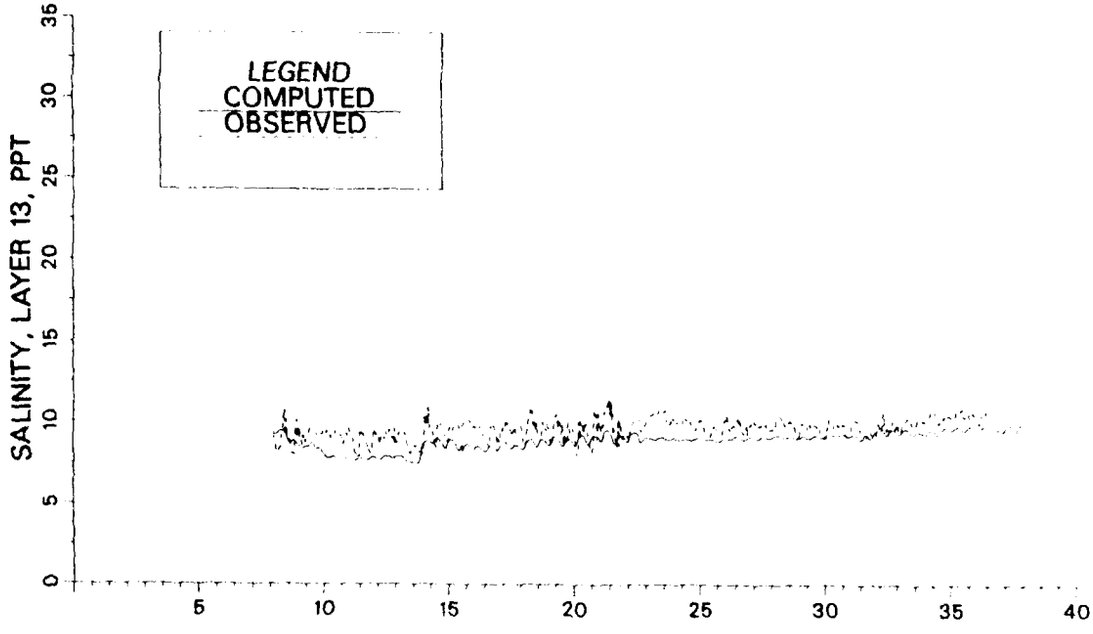

a. Depth = 12.5 ft

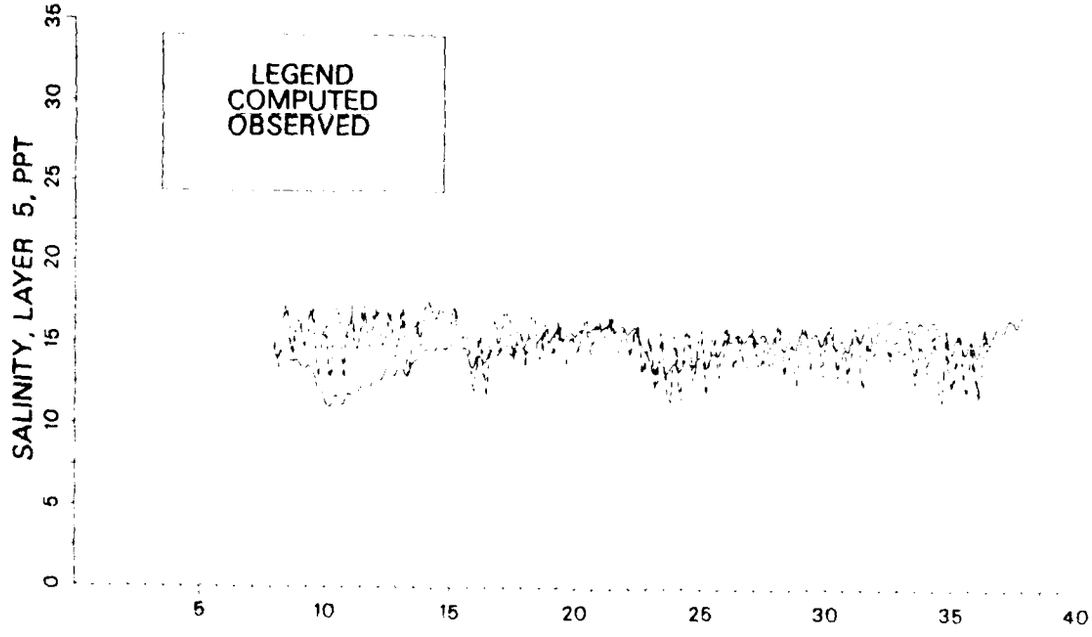

b. Depth = 52.5 ft

Figure 20. Comparison of computed and recorded salinity at station BB1 during June–July 1980. Day 0 is 23 June.

a. Depth = 12.5 ft

b. Depth = 52.5 ft

Figure 21. Comparison of computed and recorded temperature at station BB1 during June-July 1980. Day 0 is 23 June.

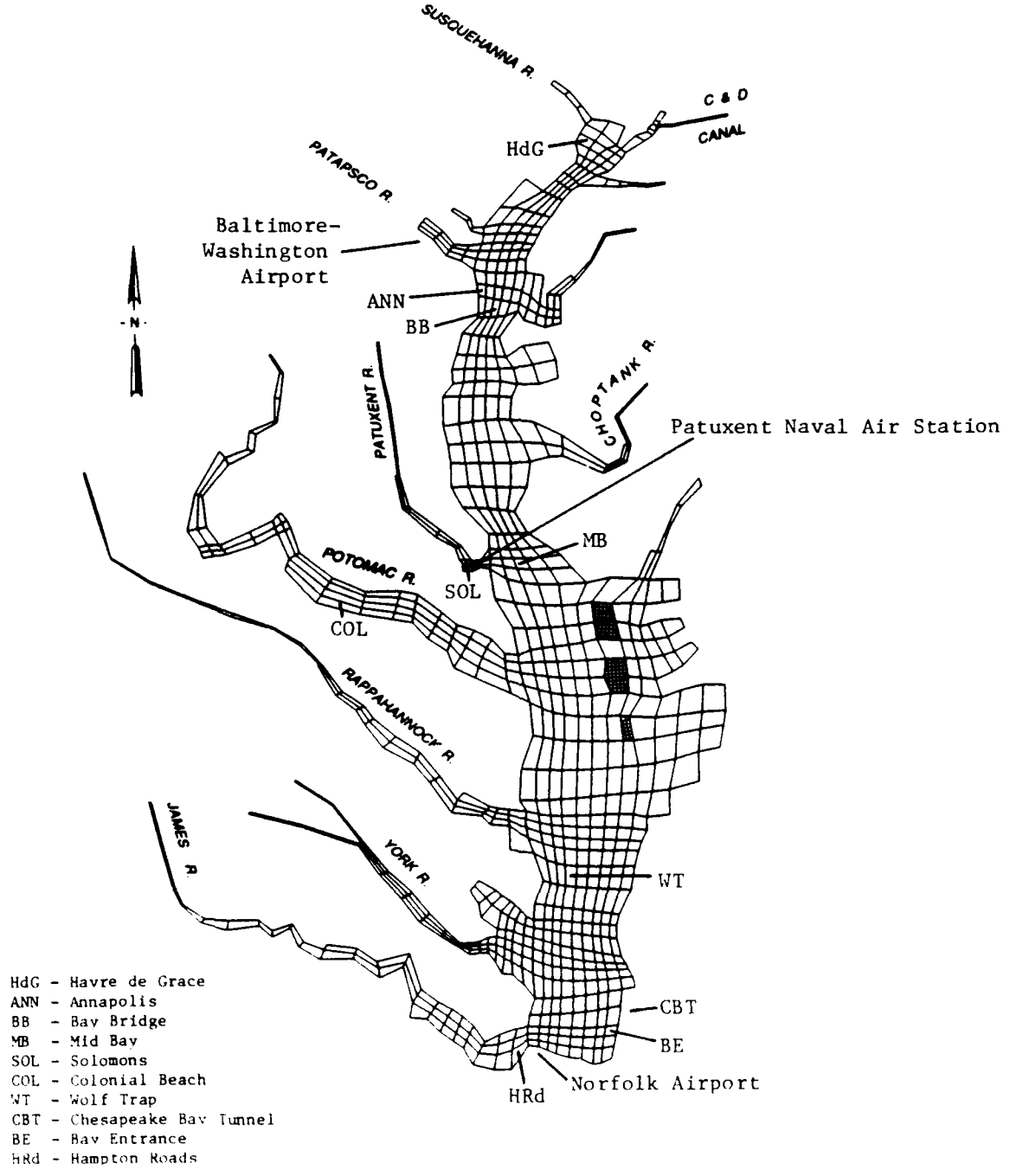

Figure 22. Location of data stations for April 1983 data set

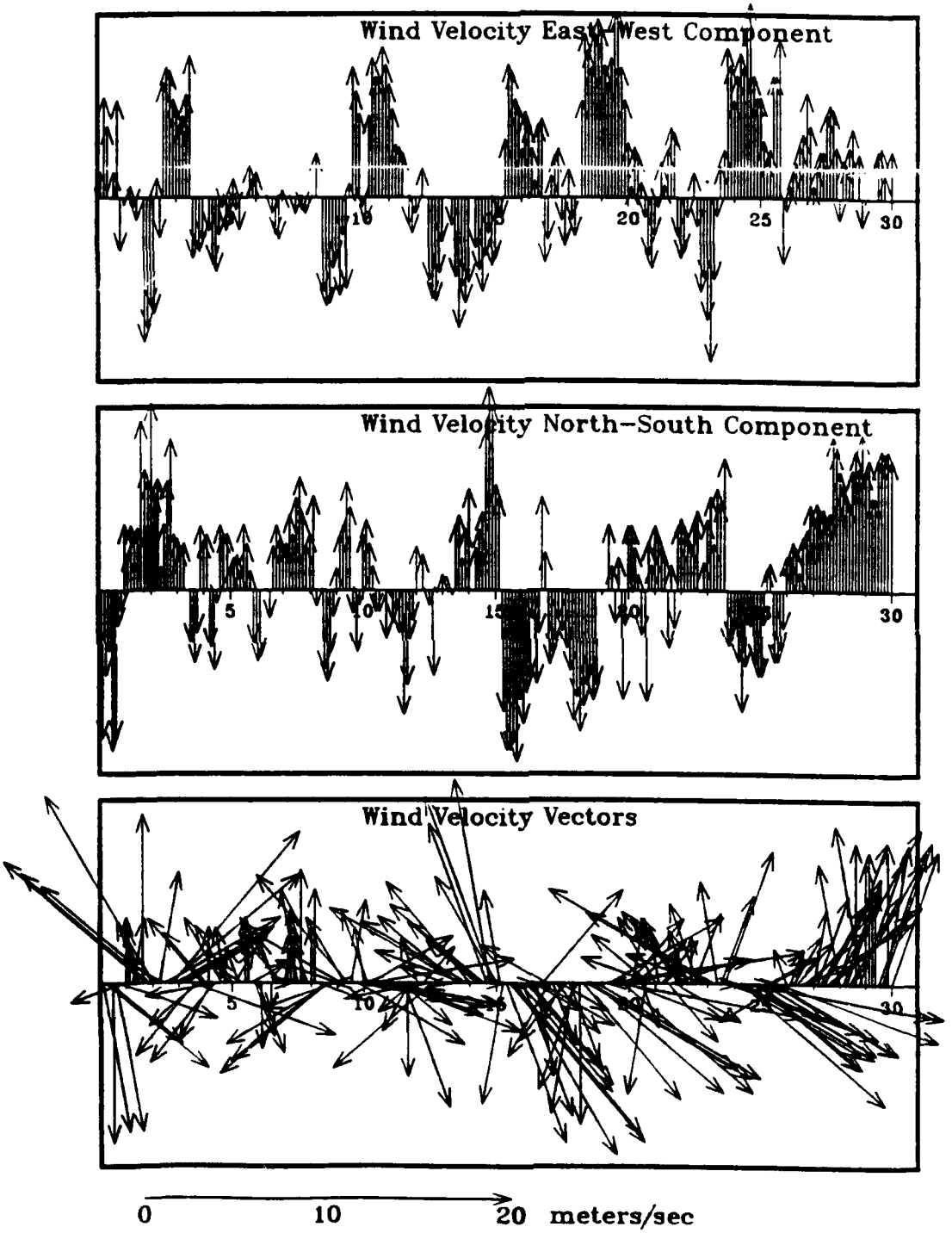

Figure 23. Wind data at Patuxent River Naval Air Station during April 1983. Day 0 is 1 April.

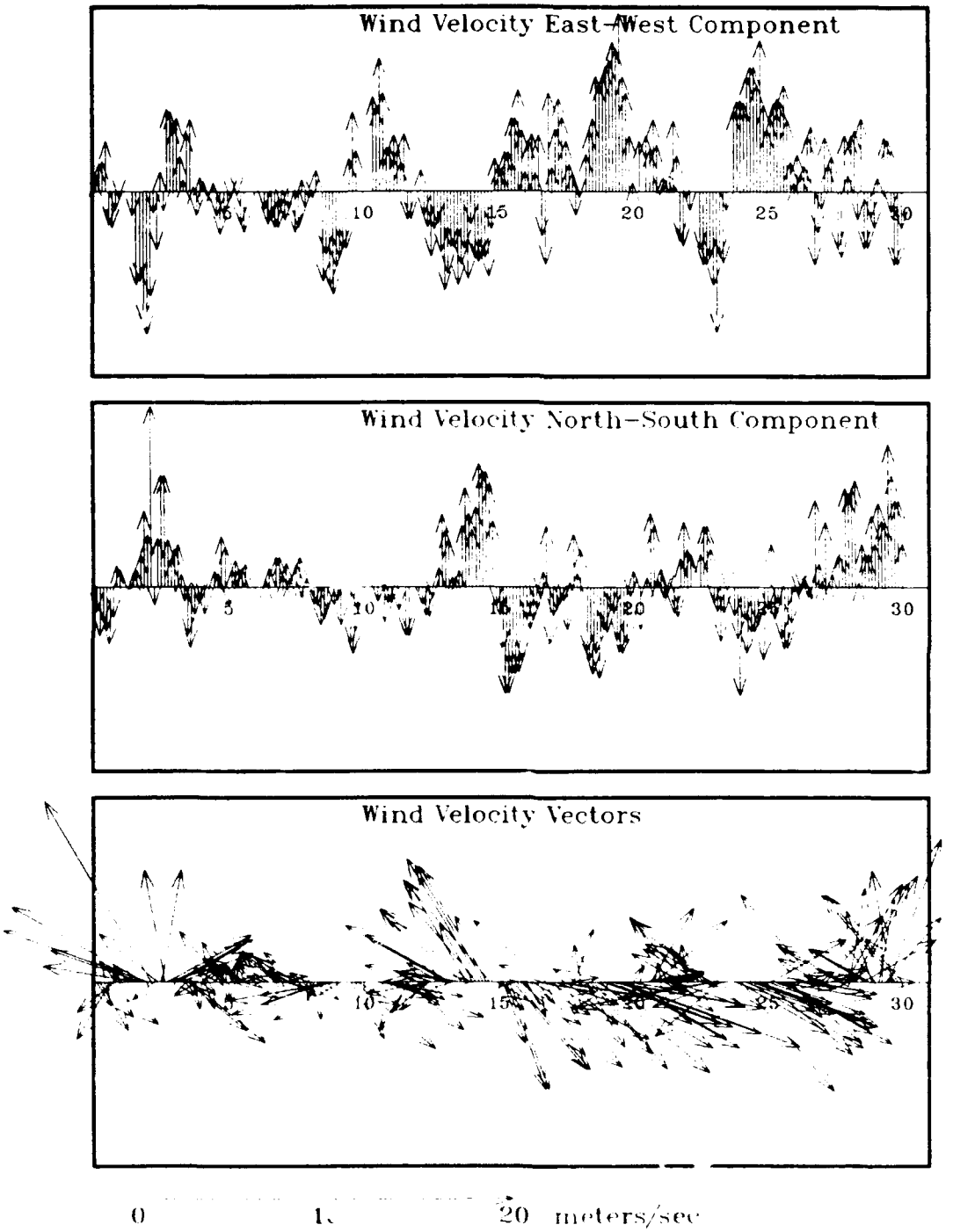

Figure 24. Wind data at Norfolk International Airport during April 1983 Day 0 is 1 April.

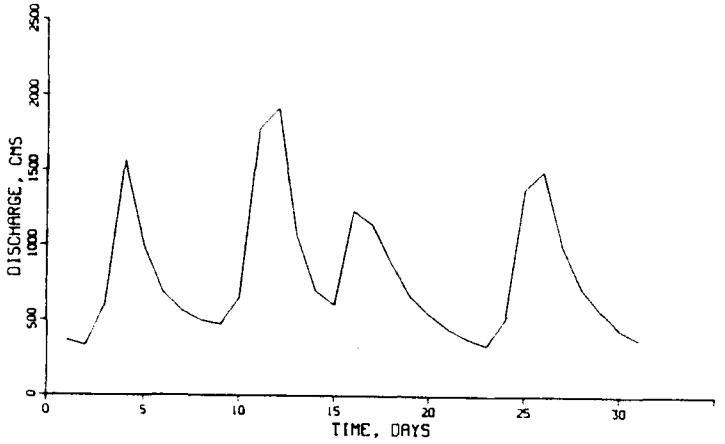

a. James River

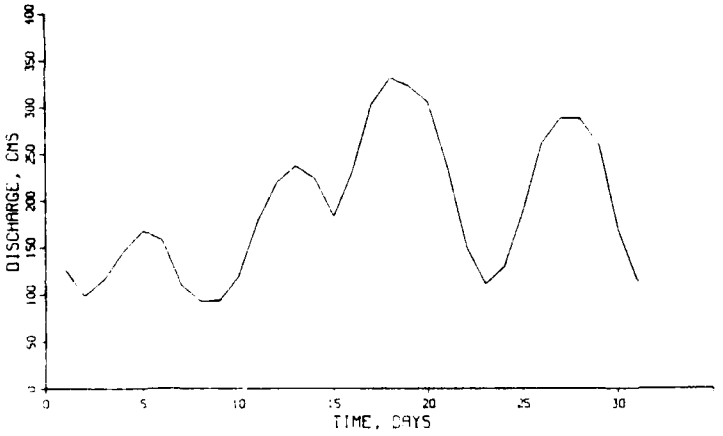

b. York River

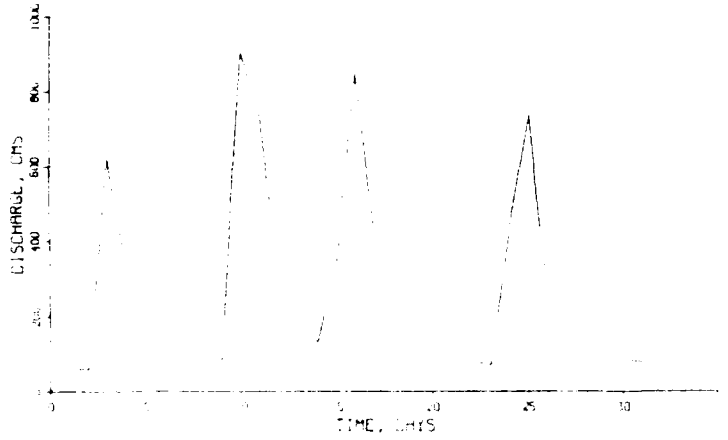

c. Rappahannock River

Figure 25. Freshwater inflows during April 1983. Day 0 is 1 April. (Sheet 1 of 3)

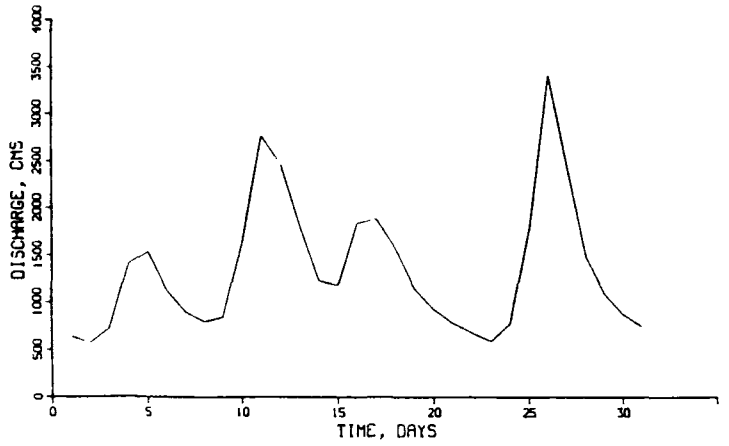

d. Potomac River

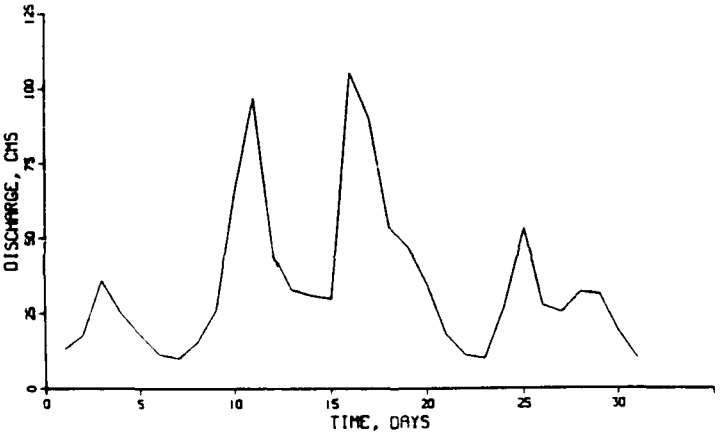

e. Patuxent River

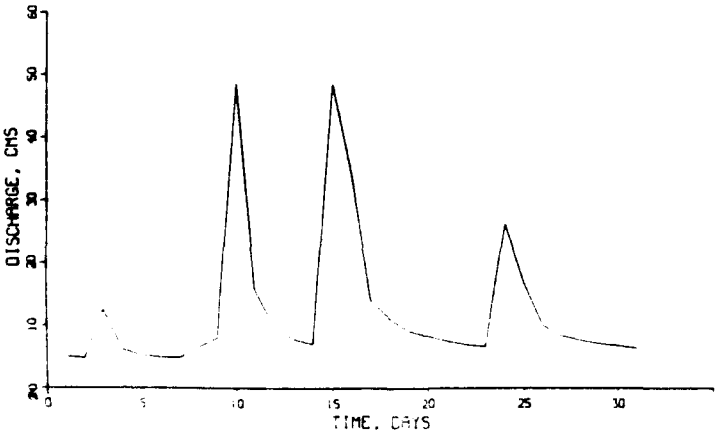

f. Patapsco River

Figure 25. (Sheet 2 of 3)

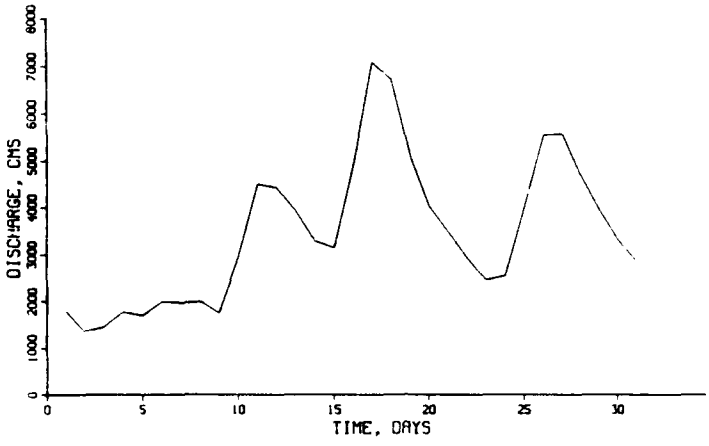

g. Susquehanna River

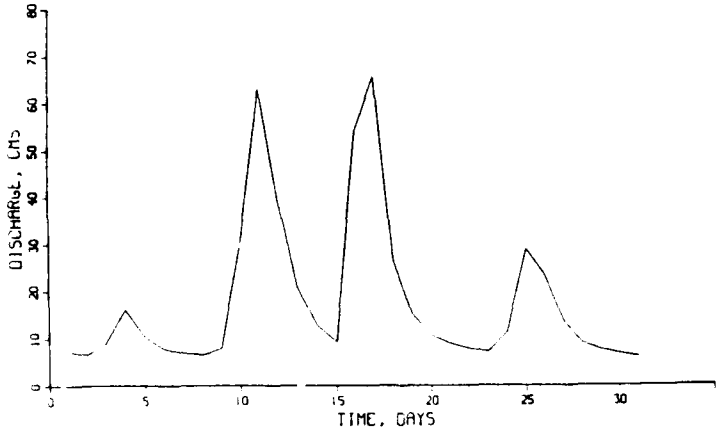

h. Choptank River

Figure 25. (Sheet 3 of 3)

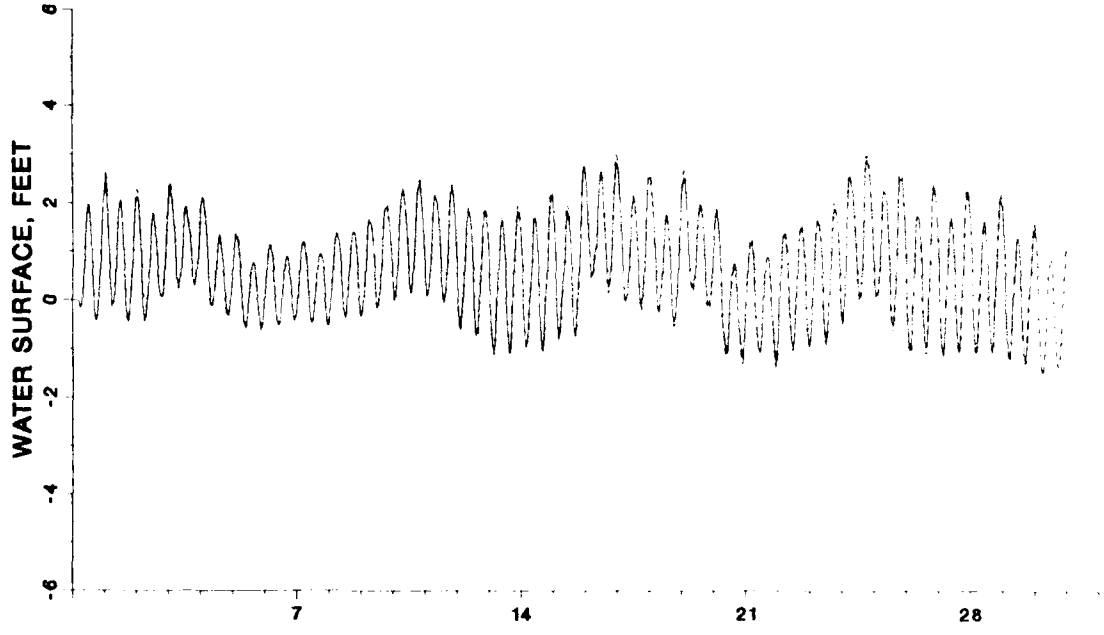

Figure 26. Ocean boundary tide at Chesapeake Bay Tunnel during April 1983

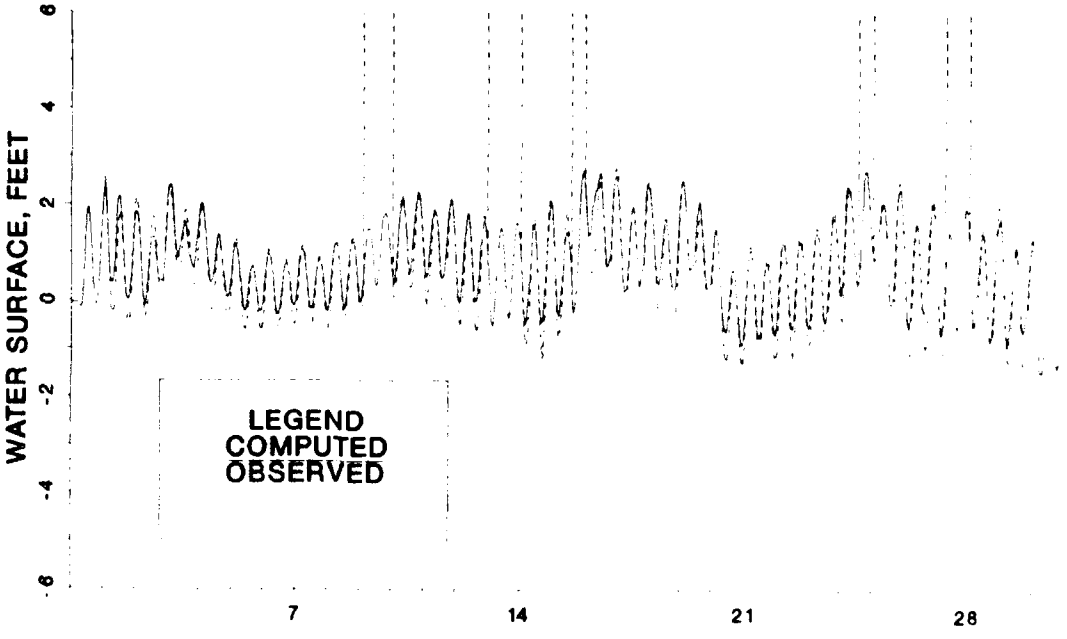

Figure 27. Comparison of computed and recorded tides at Hampton Roads, VA, during April 1983

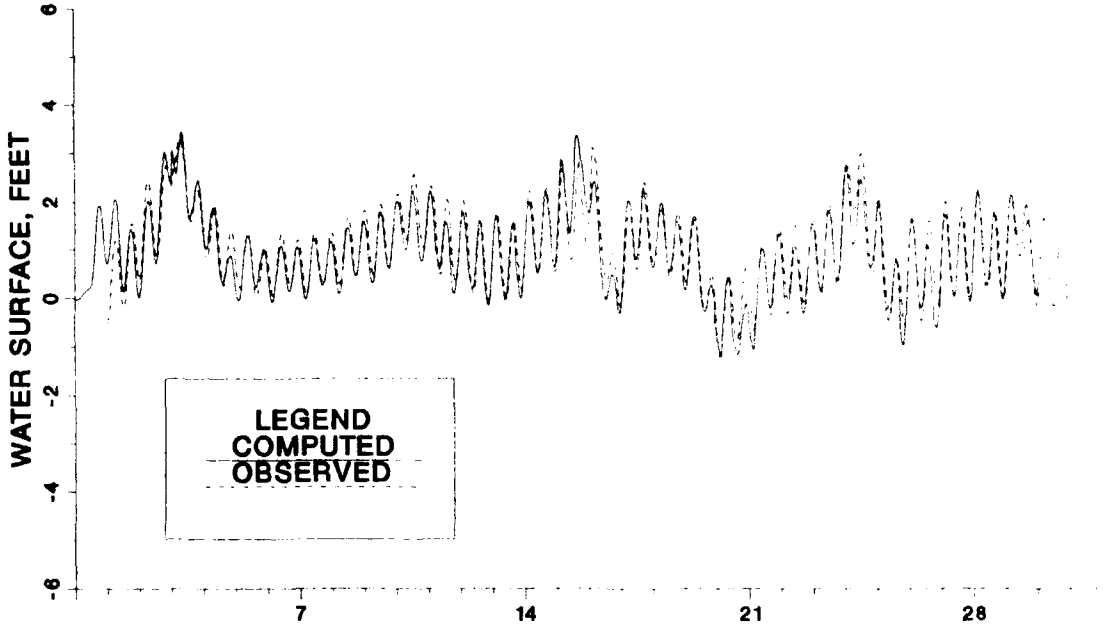

Figure 28. Comparison of computed and recorded tides at Colonial Beach, VA, during April 1983

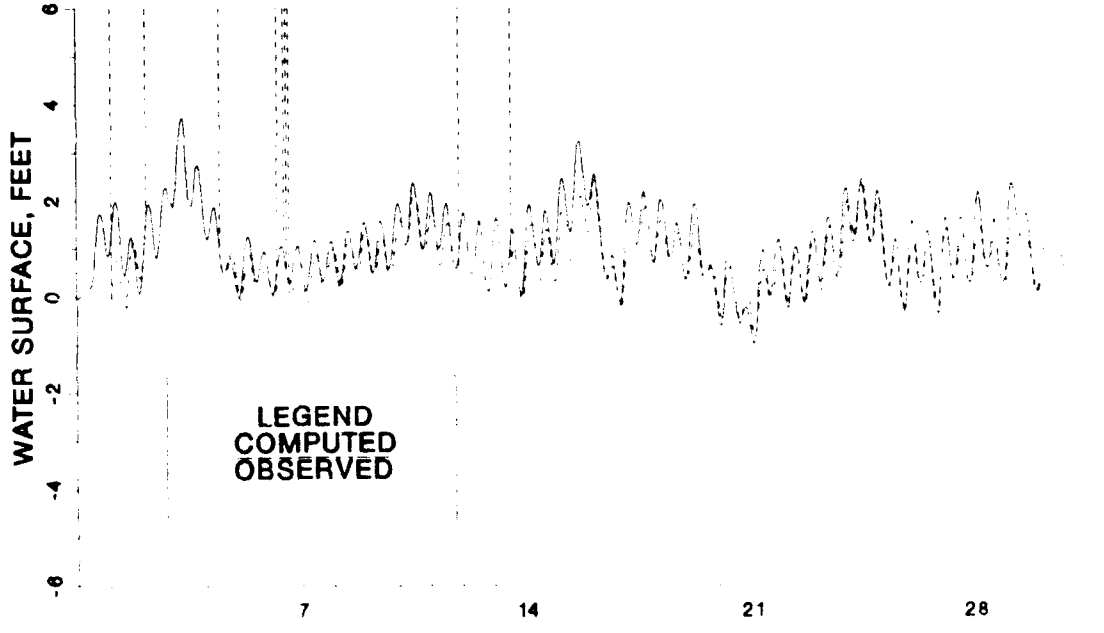

Figure 29. Comparison of computed and recorded tides at Solomons, MD, during April 1983

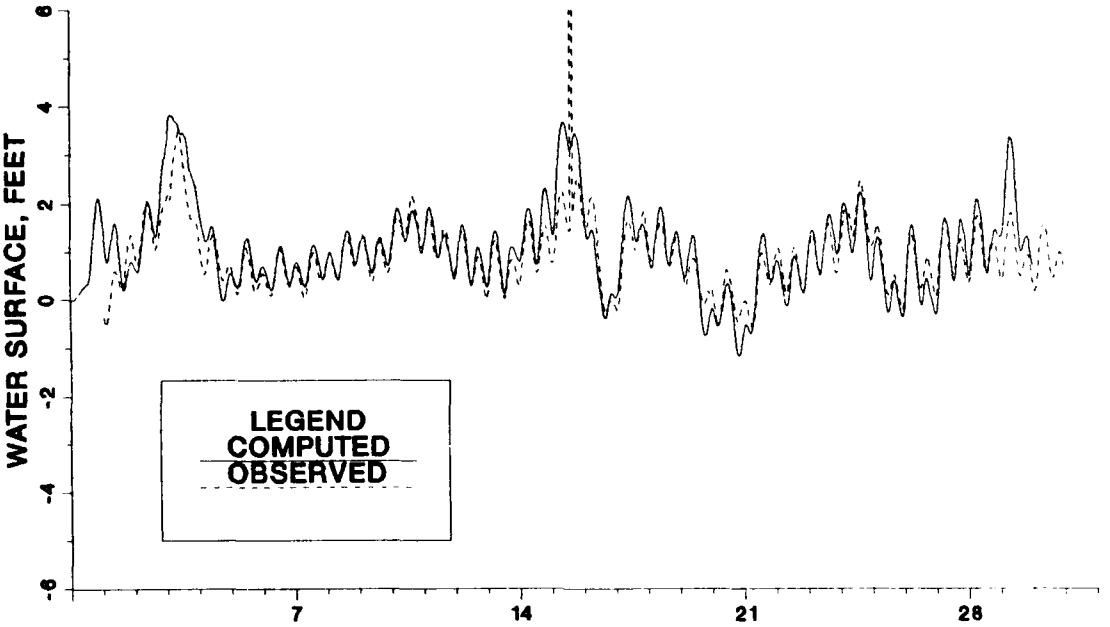

Figure 30. Comparison of computed and recorded tides at Annapolis, MD, during April 1983

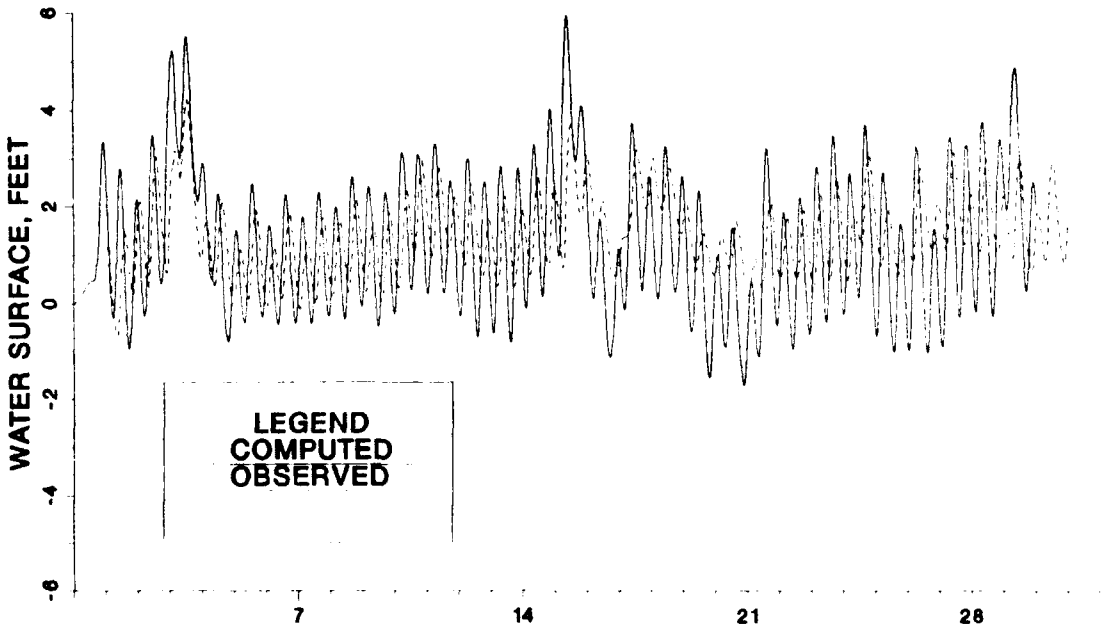

Figure 31. Comparison of computed and recorded tides at Havre de Grace during April 1983

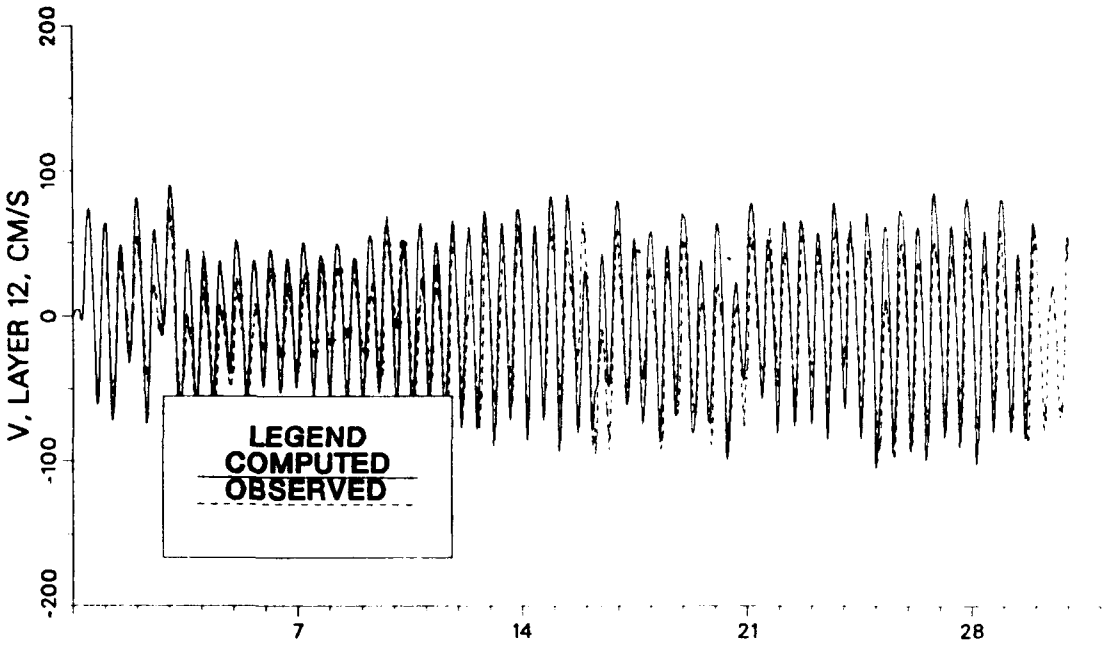

a. Depth = 17.5 ft

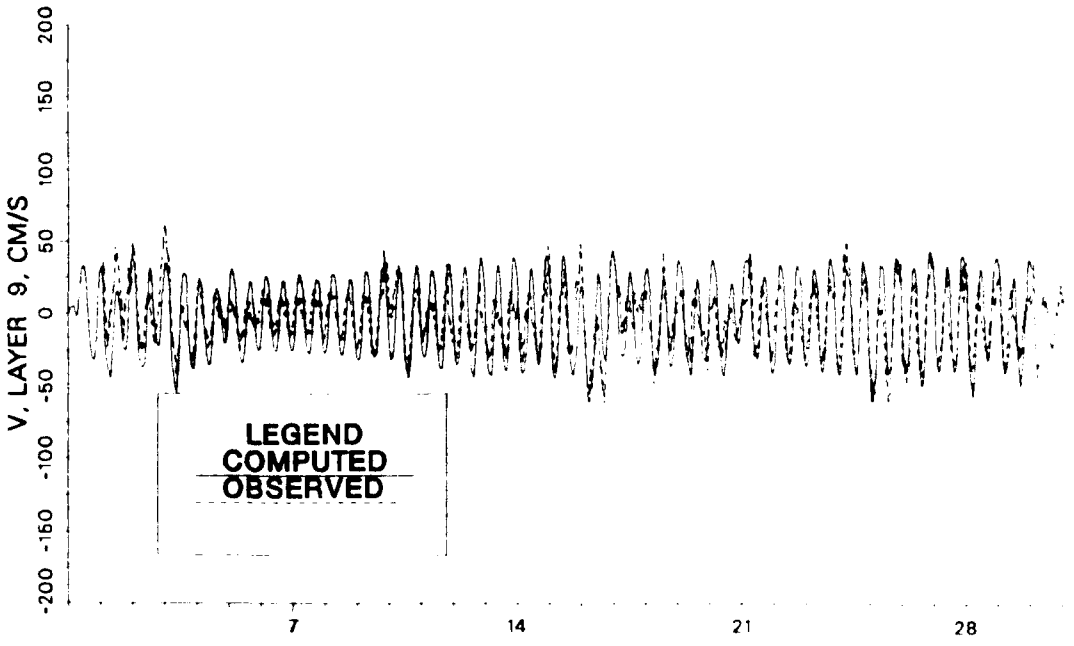

b. Depth = 32.5 ft

Figure 32. Comparison of computed and recorded velocity at station BE during April 1983

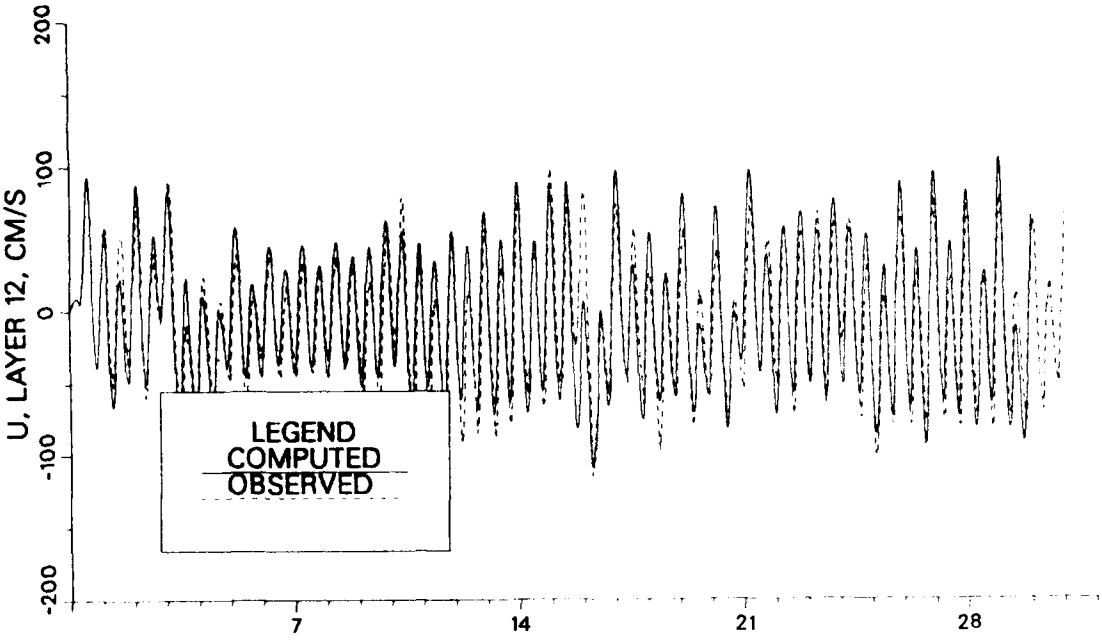

a. Depth = 17.5 ft

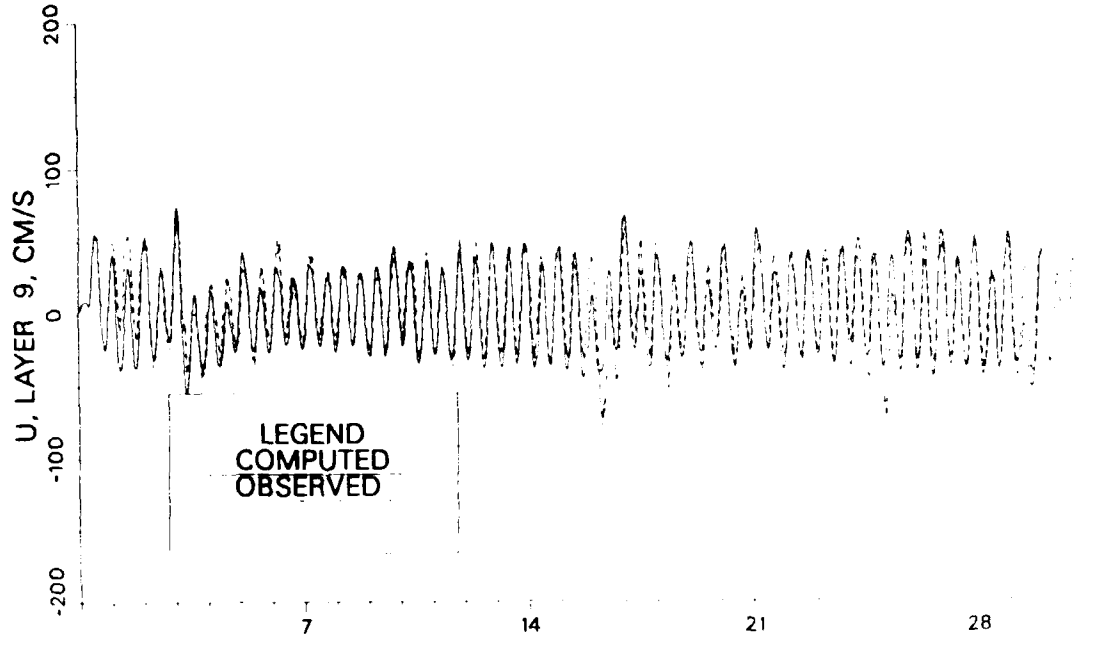

b. Depth = 32.5 ft

Figure 33. Comparison of computed and recorded velocity at station WT during April 1983

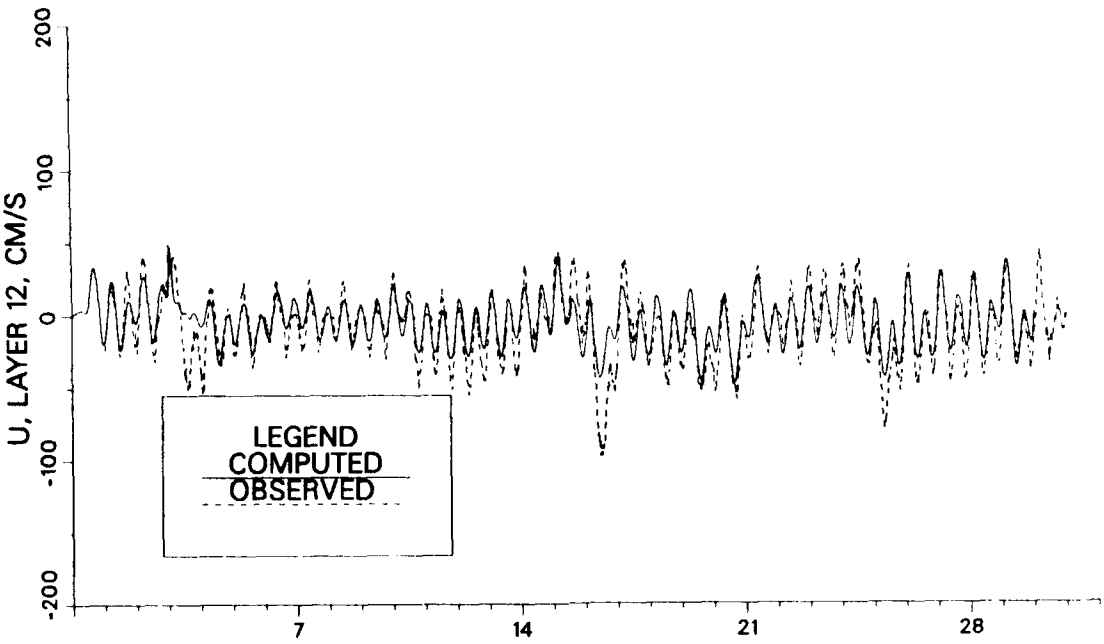

a. Depth = 17.5 ft

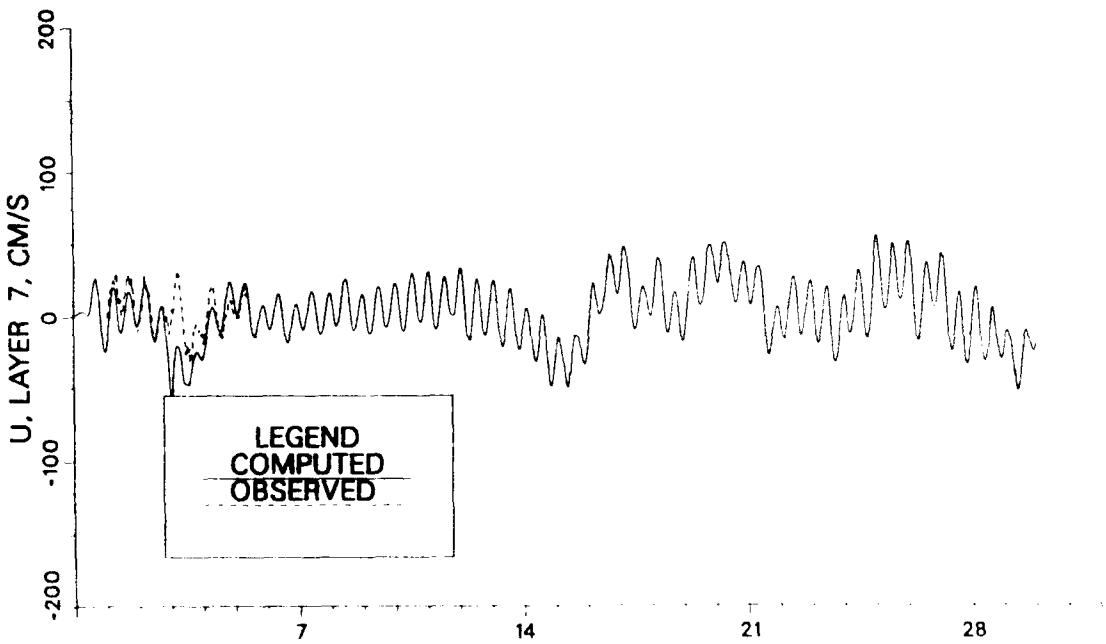

b. Depth = 42.5 ft

Figure 34. Comparison of computed and recorded velocity at station MB during April 1983

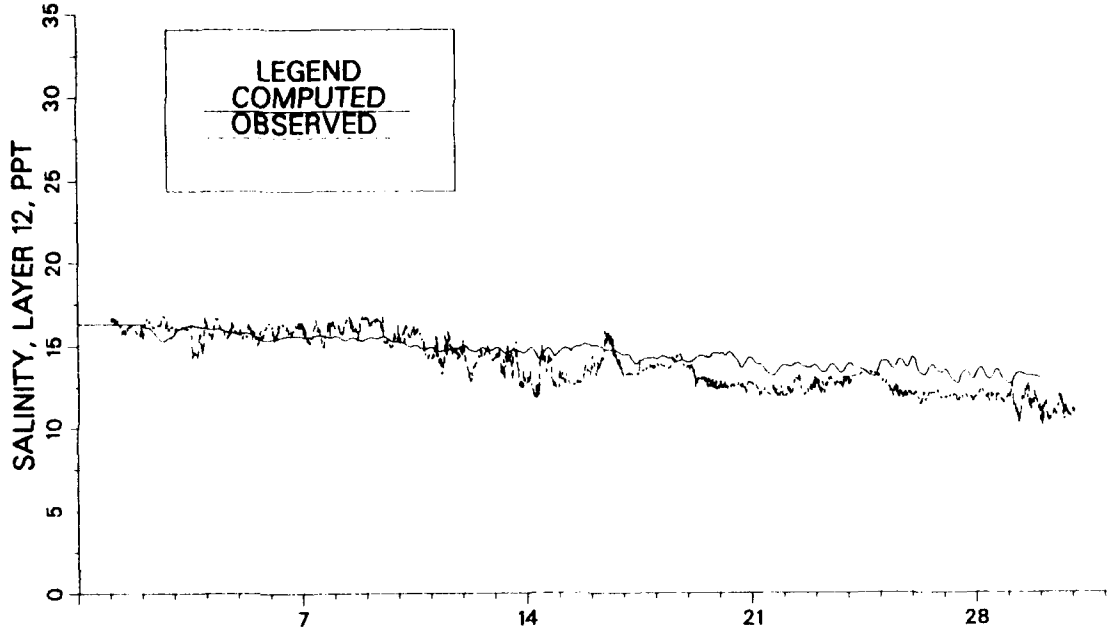

a. Depth = 17.5 ft

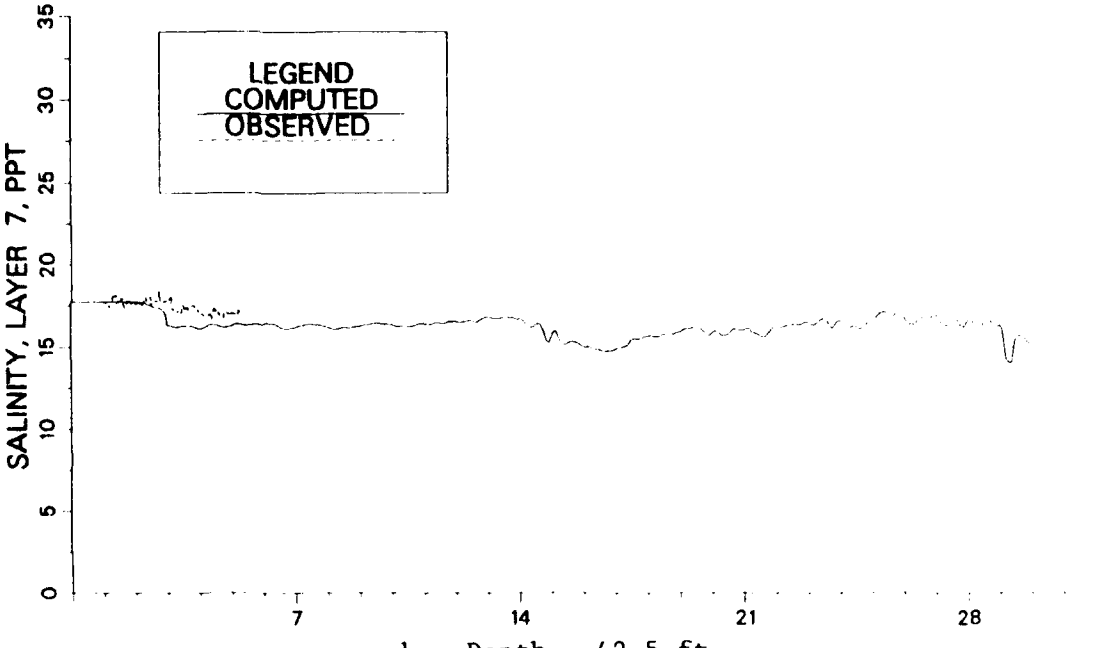

b. Depth = 42.5 ft

Figure 35. Comparison of computed and recorded salinity at station MB during April 1983

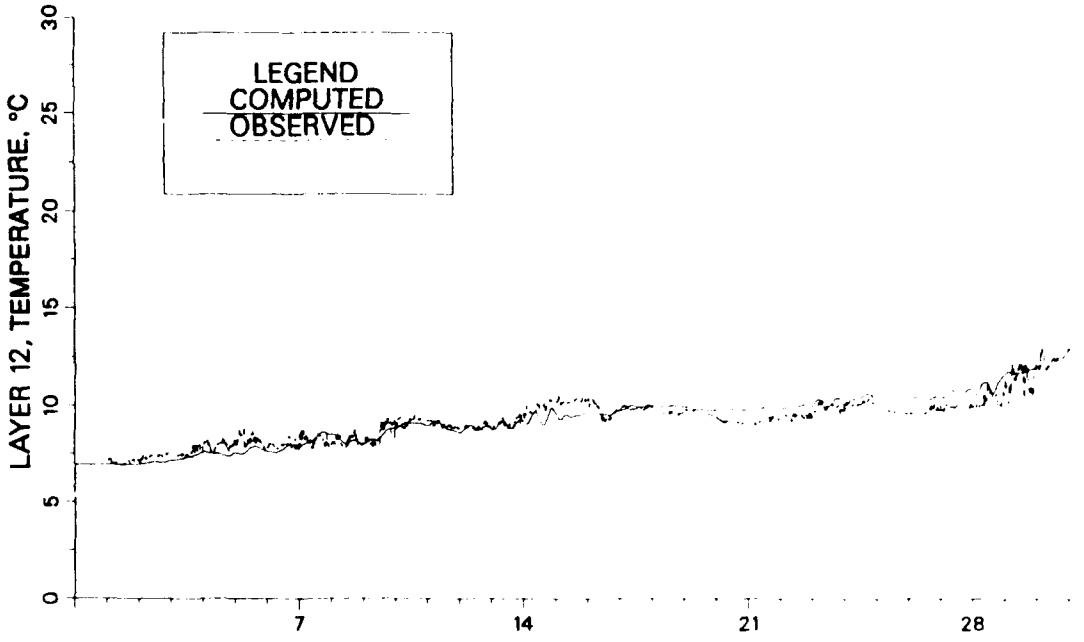

a. Depth = 17.5 ft

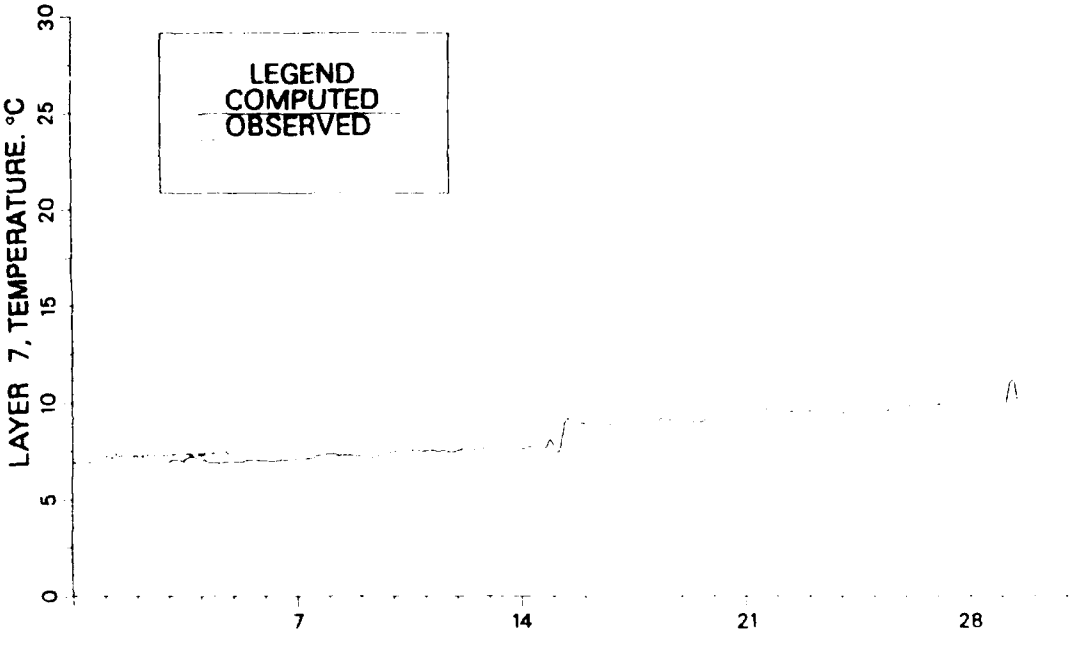

b. Depth = 42.5 ft

Figure 36. Comparison of computed and recorded temperature at station MB during April 1983

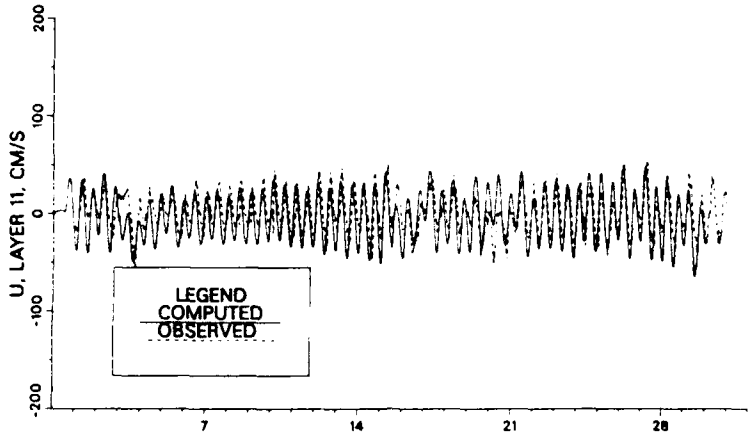

a. Depth = 22.5 ft

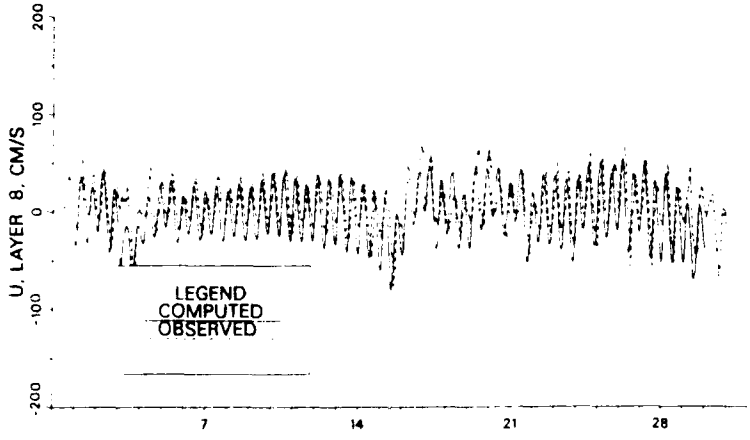

b. Depth = 37.5 ft

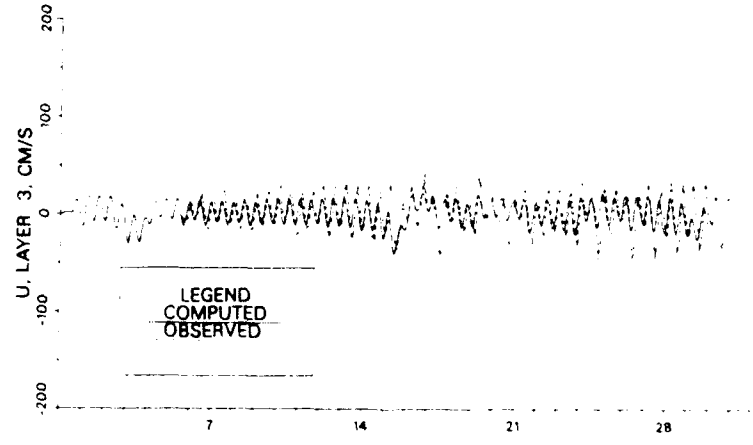

c. Depth = 62.5 ft

Figure 37. Comparison of computed and recorded velocity at station BB during April 1983

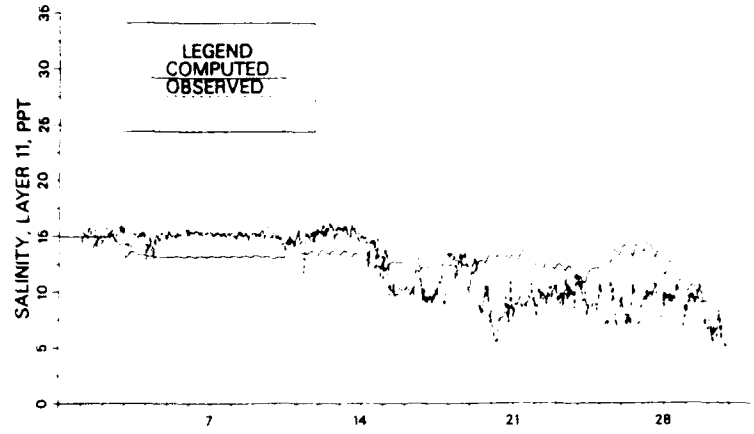

a. Depth = 22.5 ft

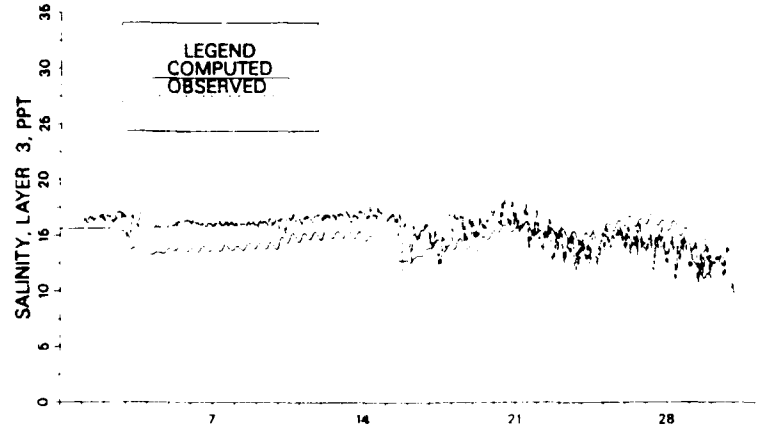

b. Depth = 37.5 ft

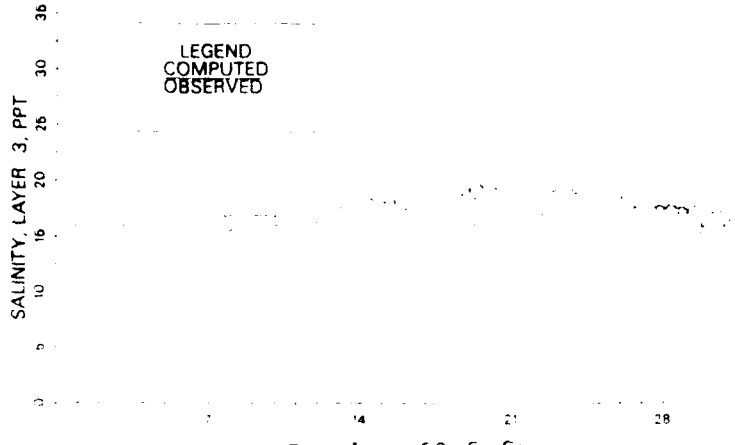

c. Depth = 62.5 ft

Figure 38. Comparison of computed and recorded salinity at station BB during April 1983

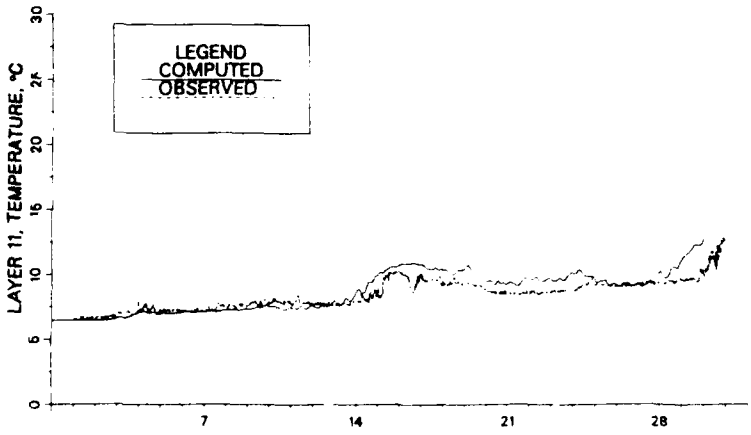

a. Depth = 22.5 ft

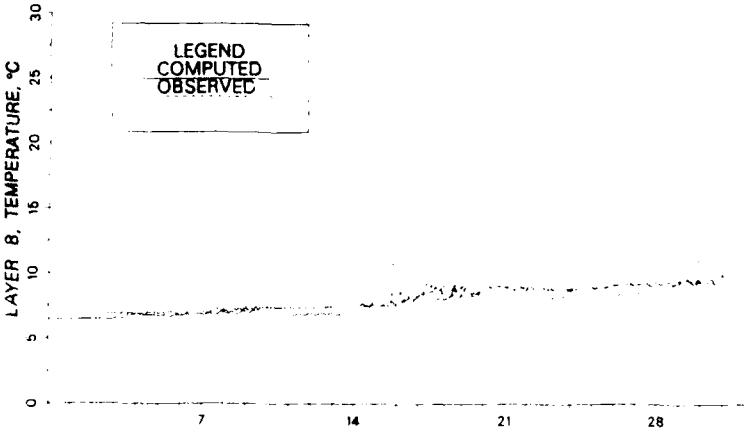

b. Depth = 37.5 ft

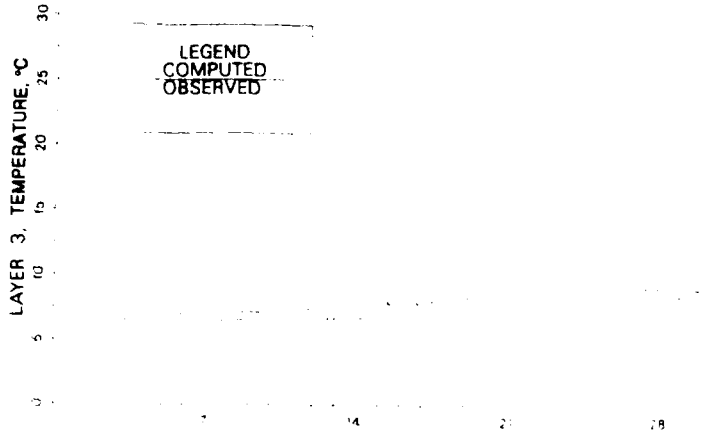

c. Depth = 62.5 ft

Figure 39. Comparison of computed and recorded temperature at station BB during April 1983

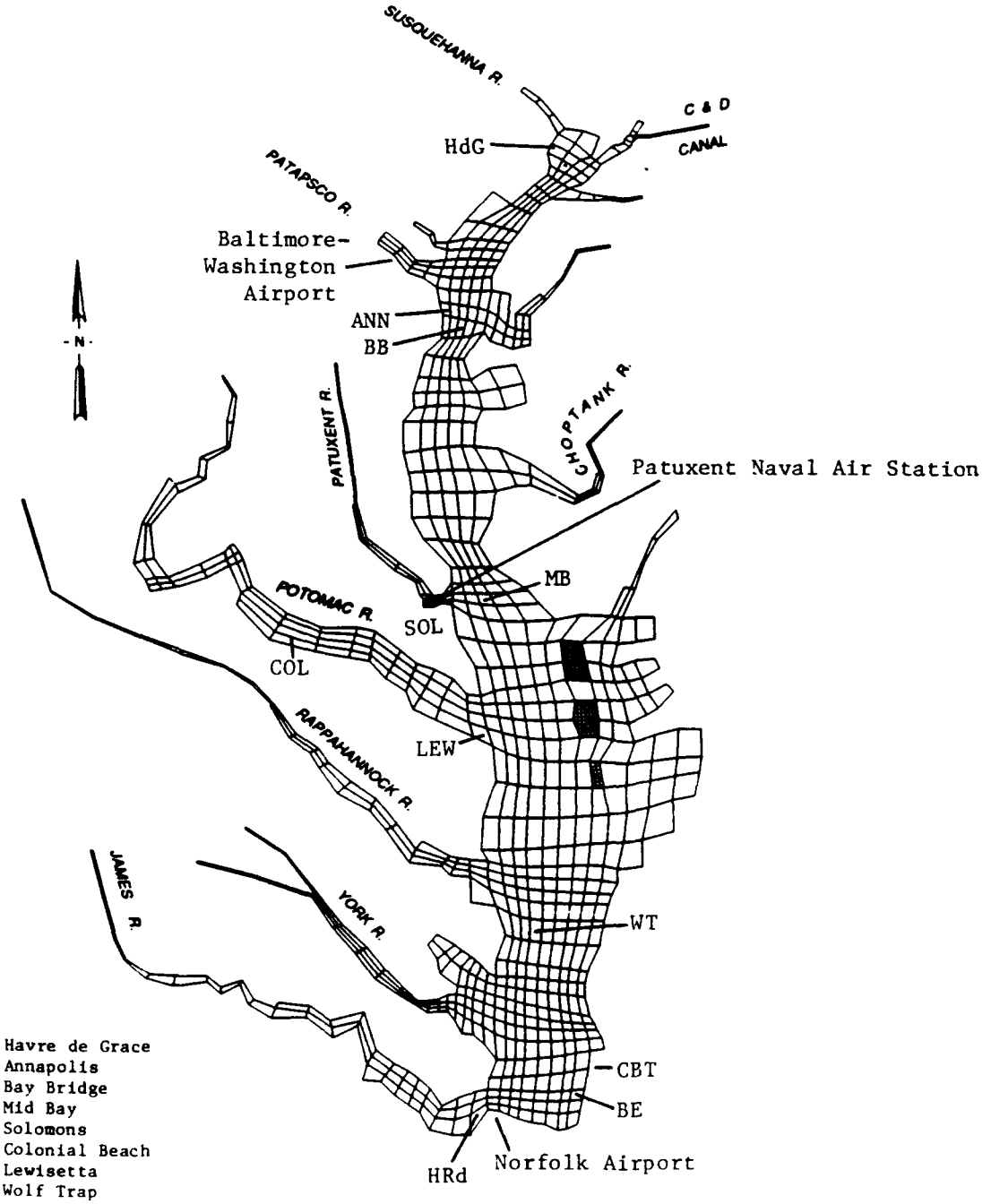

HdG - Havre de Grace
ANN - Annapolis
BB - Bay Bridge
MB - Mid Bay
SOL - Solomons
COL - Colonial Beach
LEW - Lewisetta
WT - Wolf Trap
CBT - Chesapeake Bay Tunnel
BE - Bay Entrance
HRd - Hampton Roads

Figure 40. Data stations for September 1983 data set

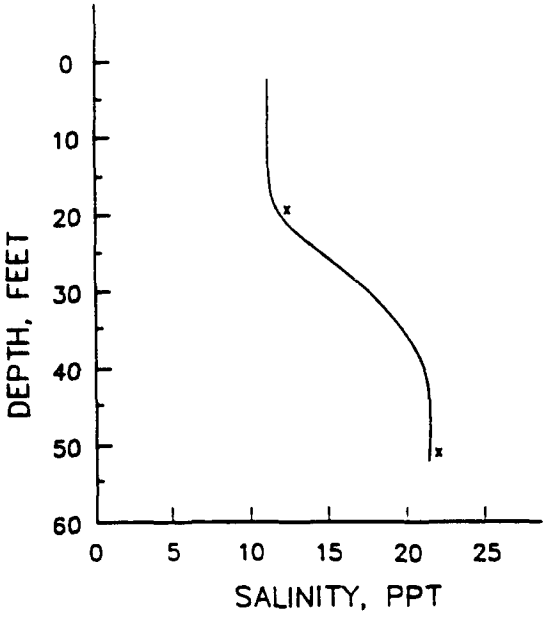

Figure 41. Initial salinity profile at station MB on 1 September 1983

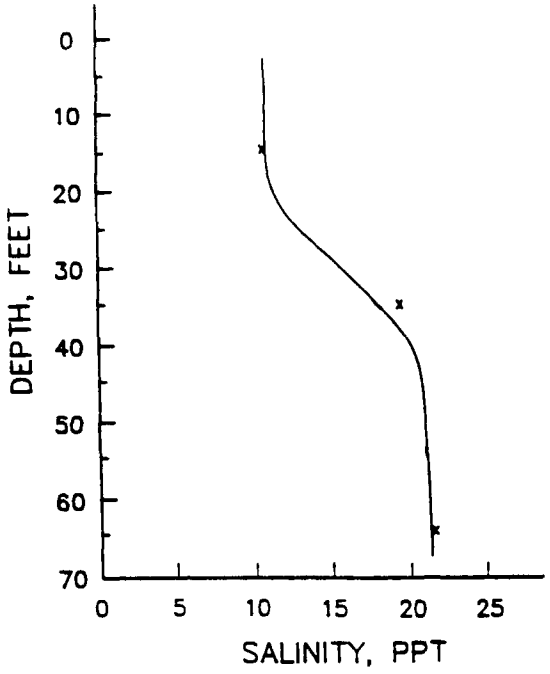

Figure 42. Initial salinity profile at station BB on 1 September 1983

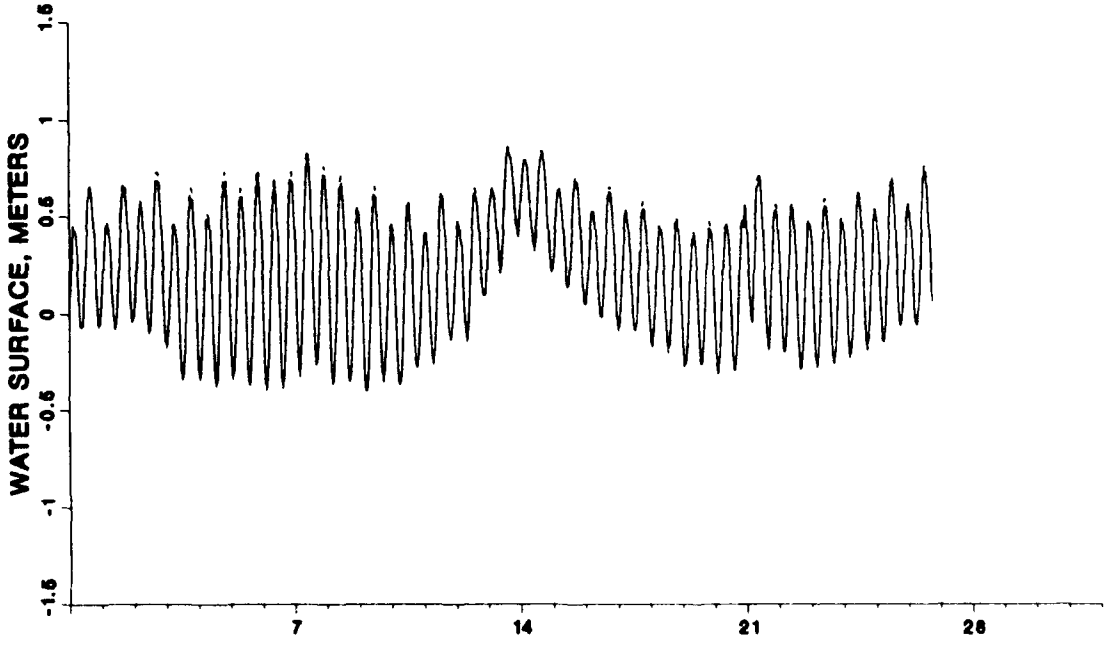

Figure 43. Ocean boundary tide at Chesapeake Bay Tunnel during September 1983

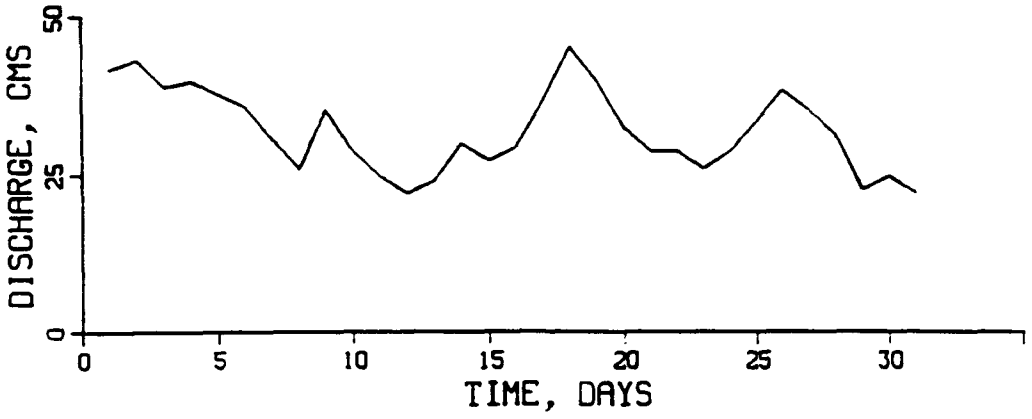

a. James River

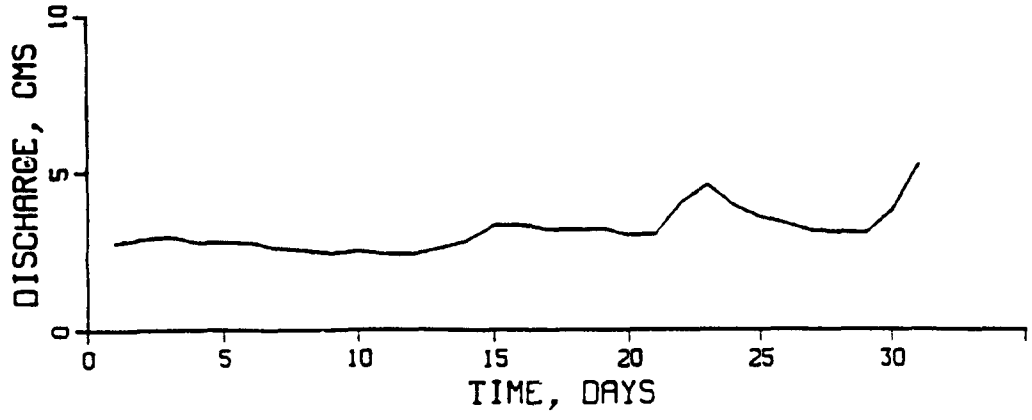

b. York River

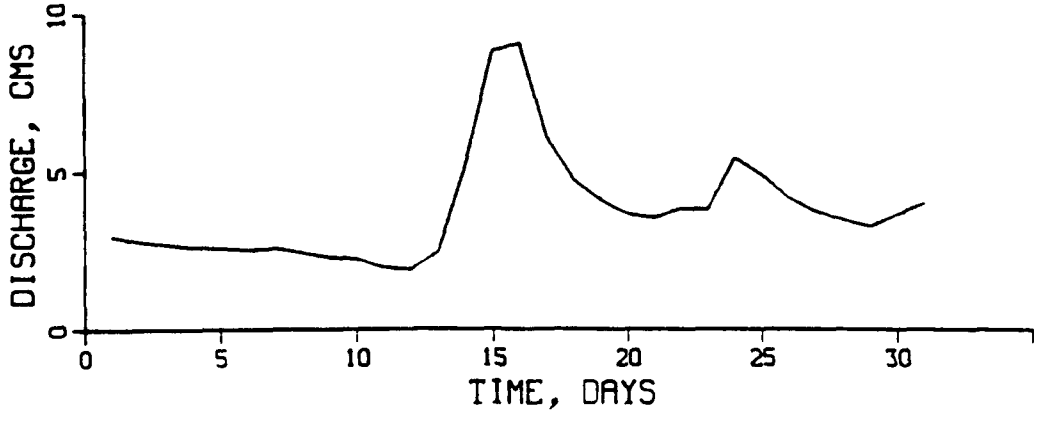

c. Rappahannock River

Figure 4. Freshwater inflows during September 1983. Day 0 is 1 September. (Sheet 1 of 3)

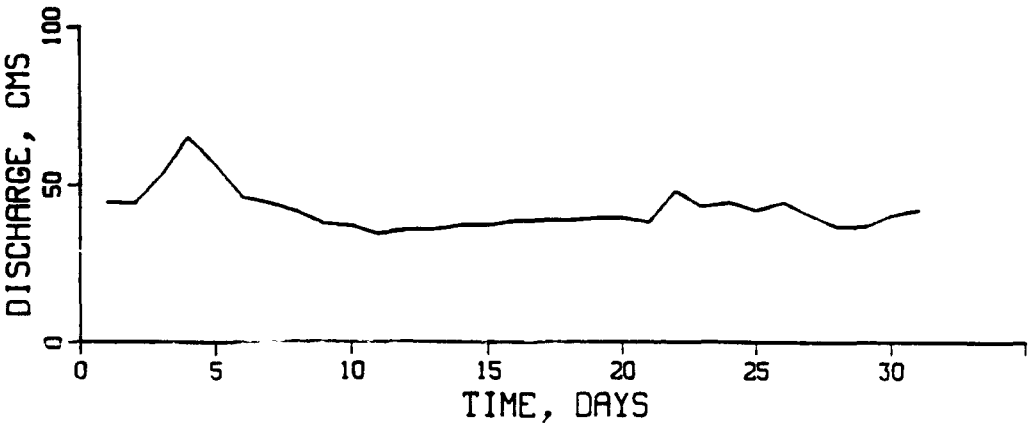

d. Potomac River

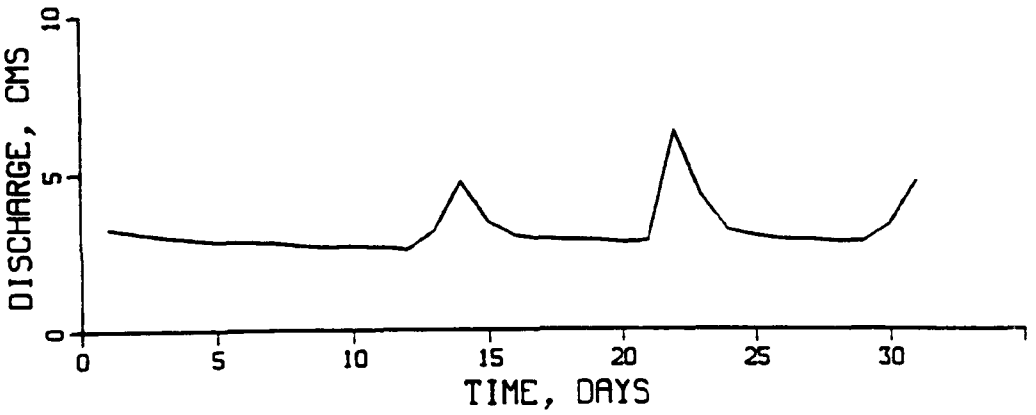

e. Patuxent River

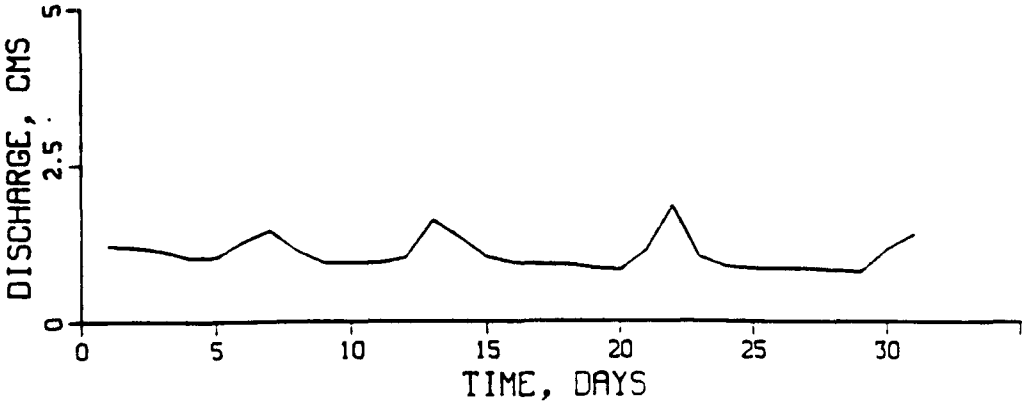

f. Patapsco River

Figure 44. (Sheet 2 of 3)

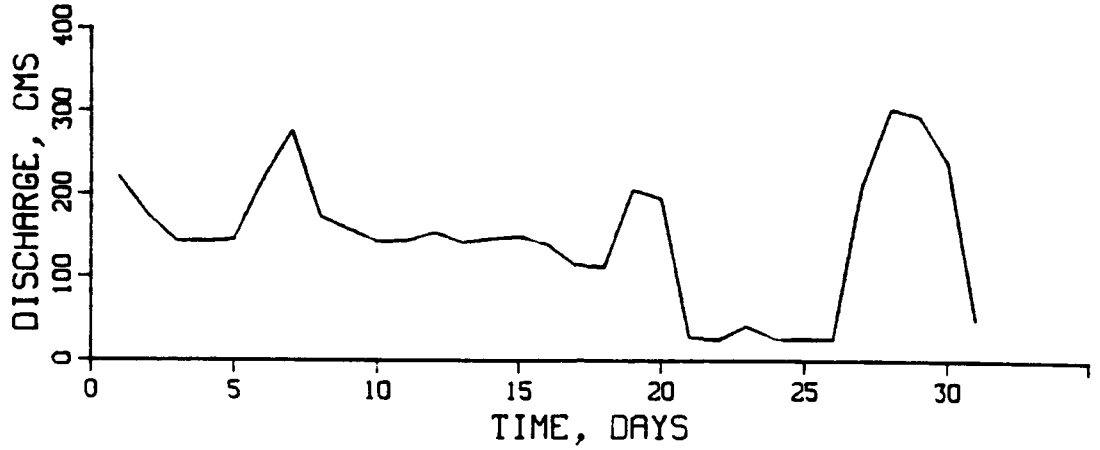

g. Susquehanna River

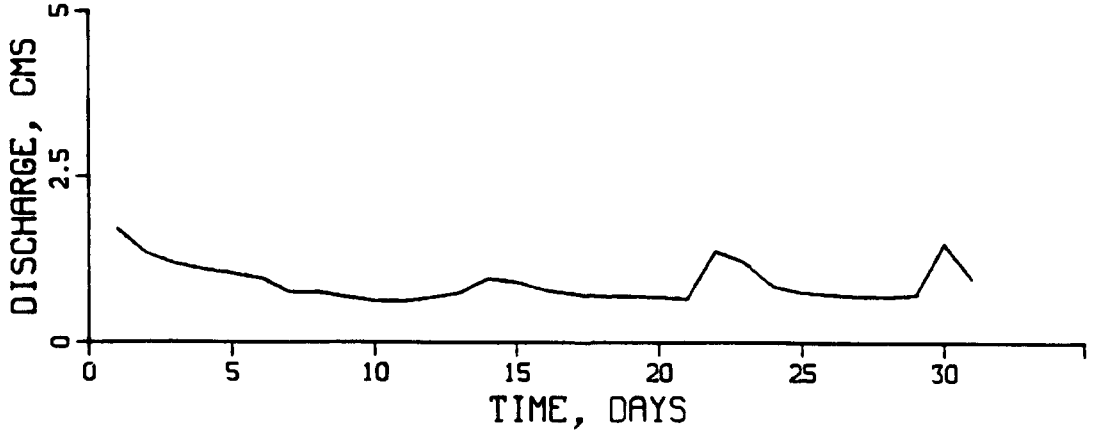

h. Choptank River

Figure 44. (Sheet 3 of 3)

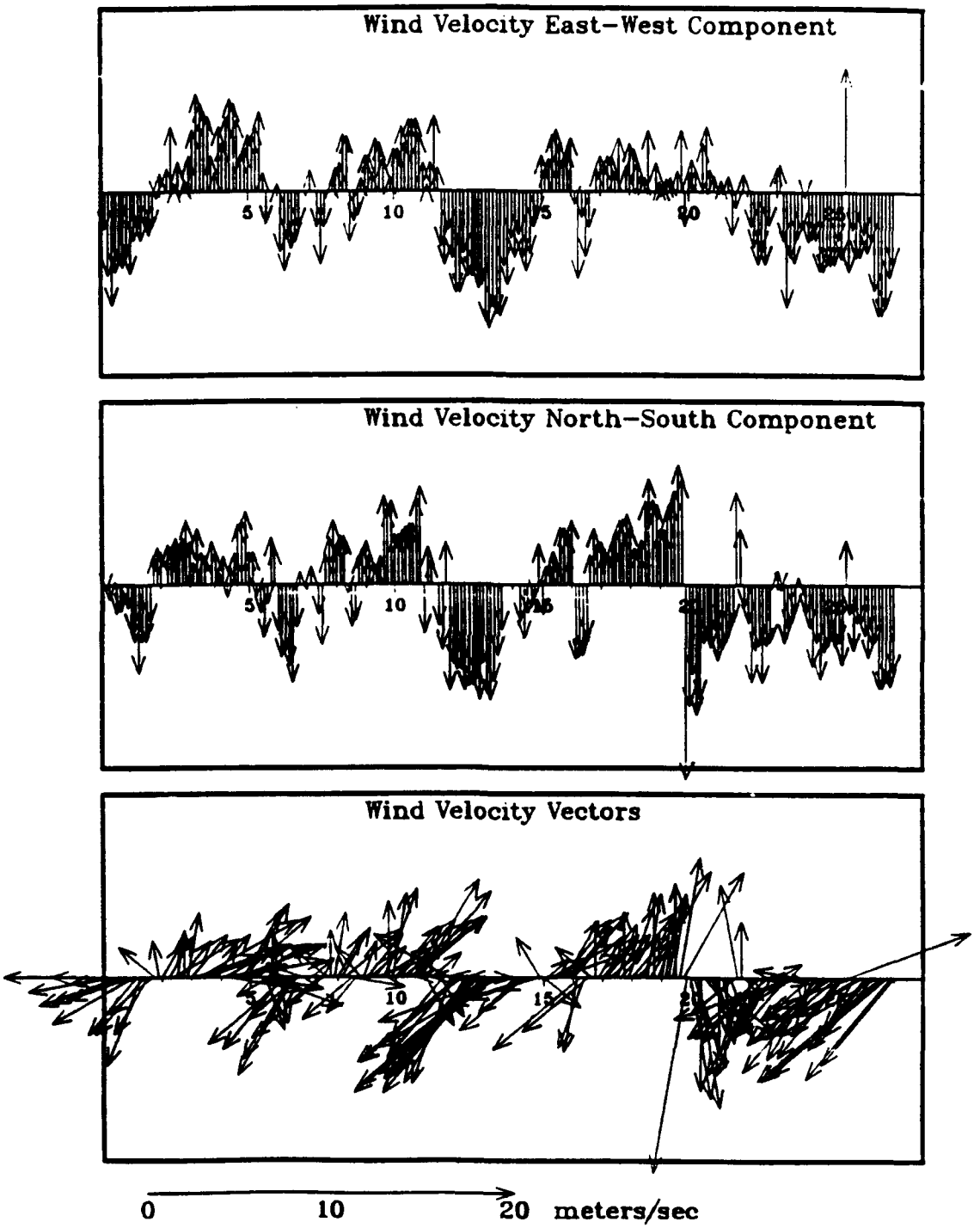

Figure 45. Wind data at the Norfolk International Airport during September 1983. Day 0 is 1 September.

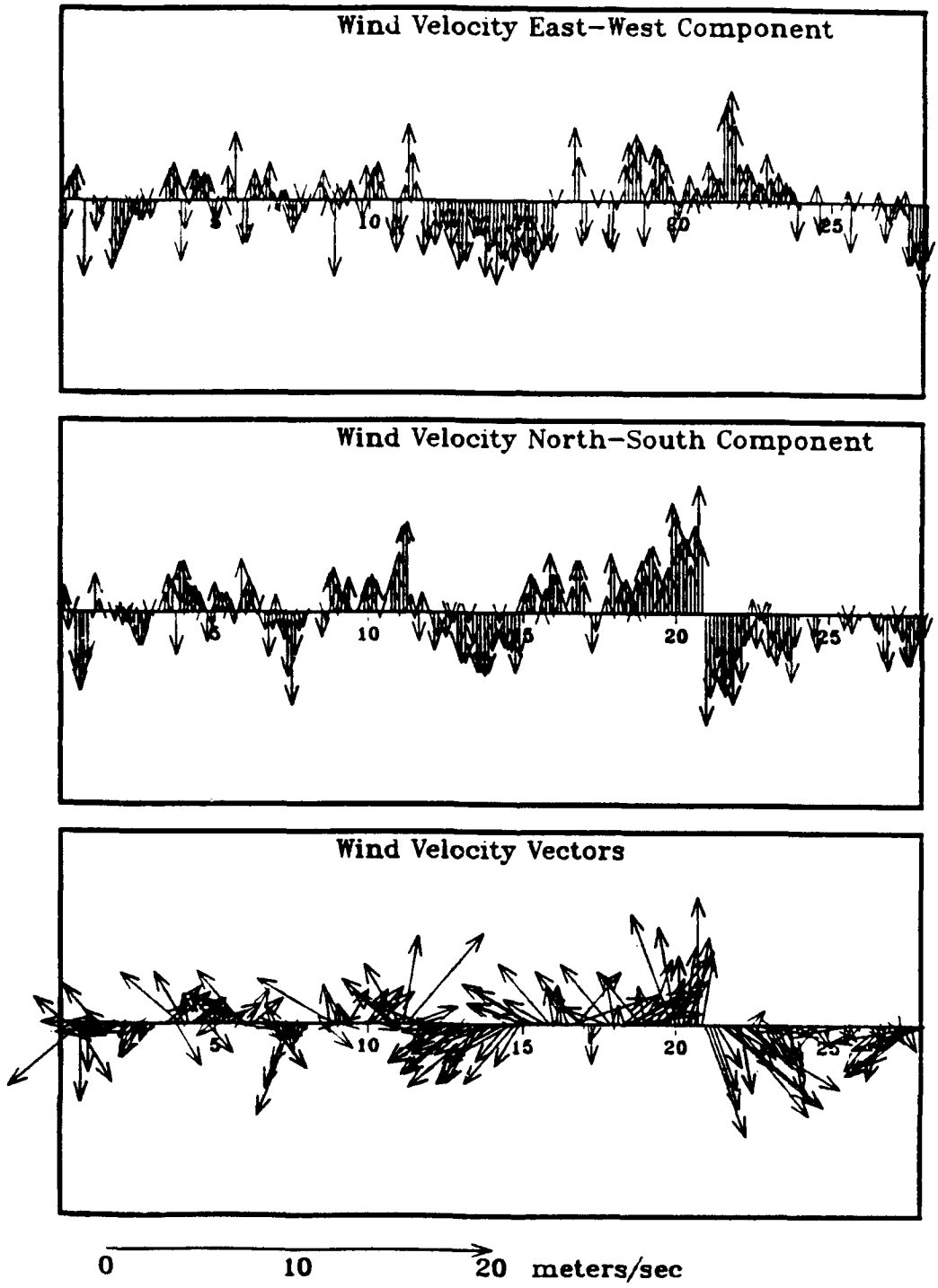

Figure 46. Wind data at the Patuxent River Naval Air Station during September 1983. Day 0 is 1 September.

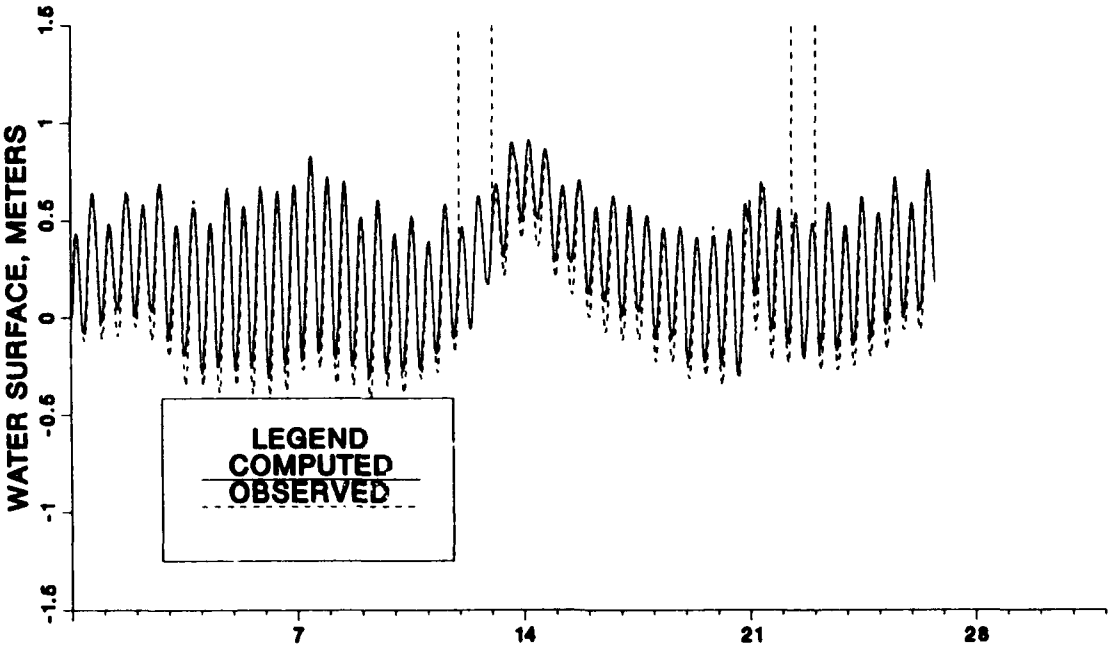

Figure 47. Comparison of computed and recorded tide at Hampton Roads, VA, during September 1983

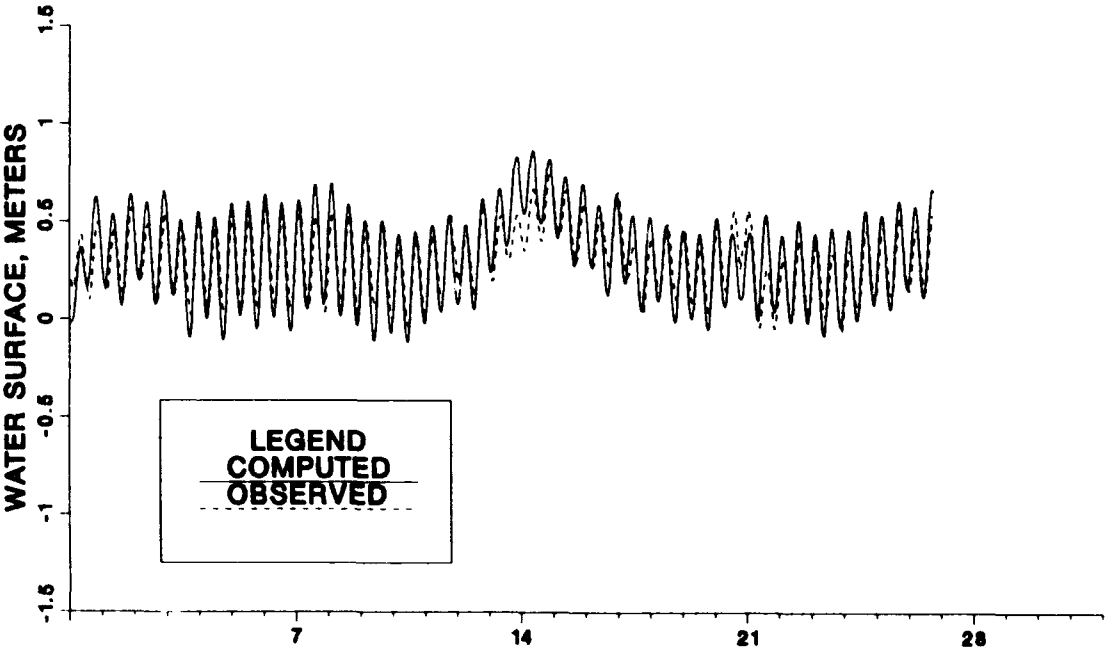

Figure 48. Comparison of computed and recorded tide at Lewisetta, VA, during September 1983

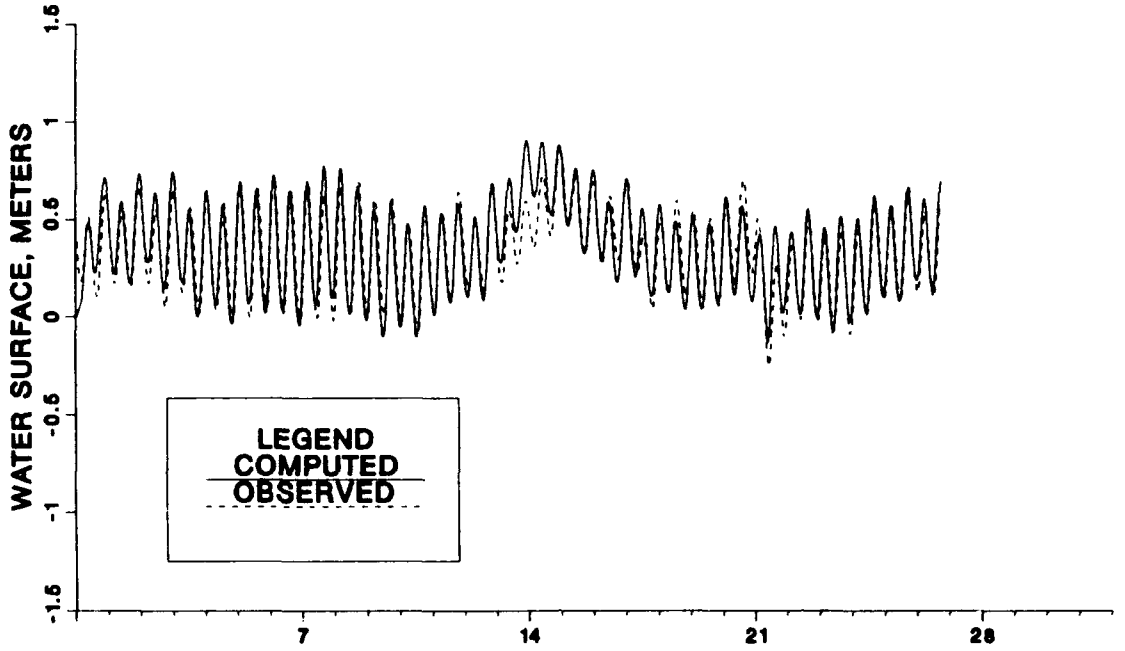

Figure 49. Comparison of computed and recorded tide at Colonial Beach, VA, during September 1983

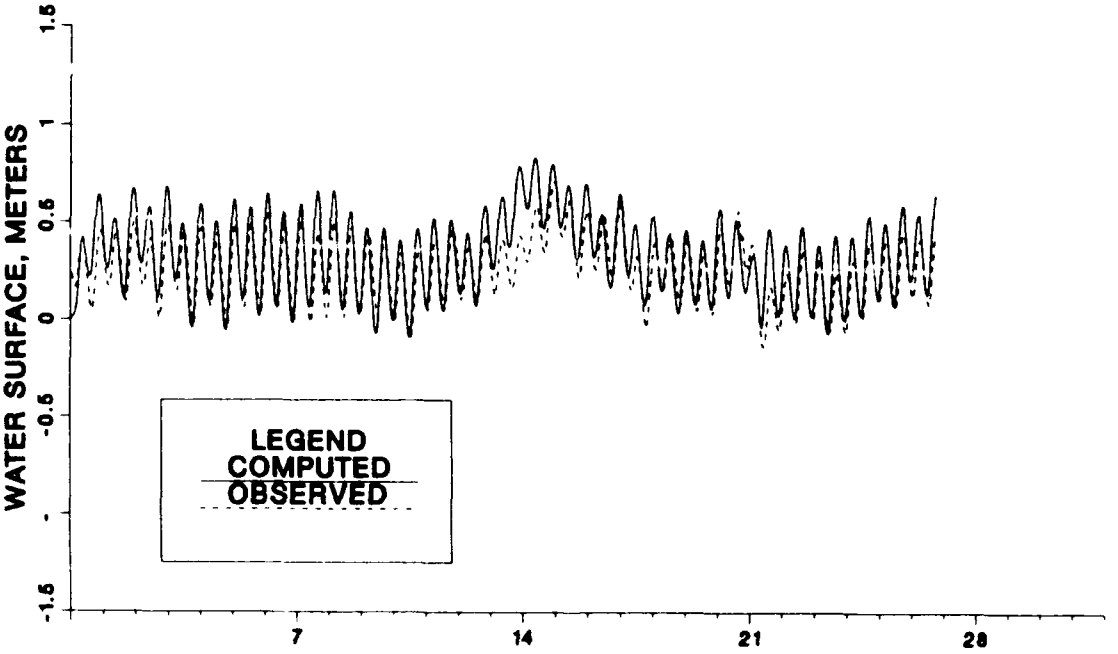

Figure 50. Comparison of computed and recorded tide at Solomons, MD, during September 1983

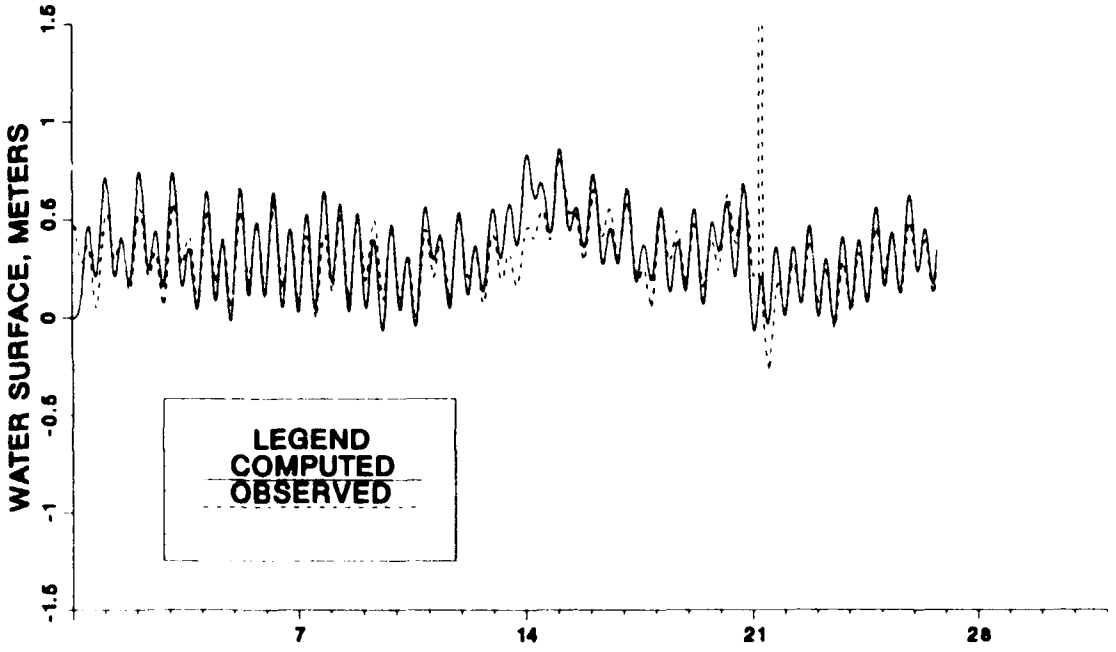

Figure 51. Comparison of computed and recorded tide at Annapolis, MD, during September 1983

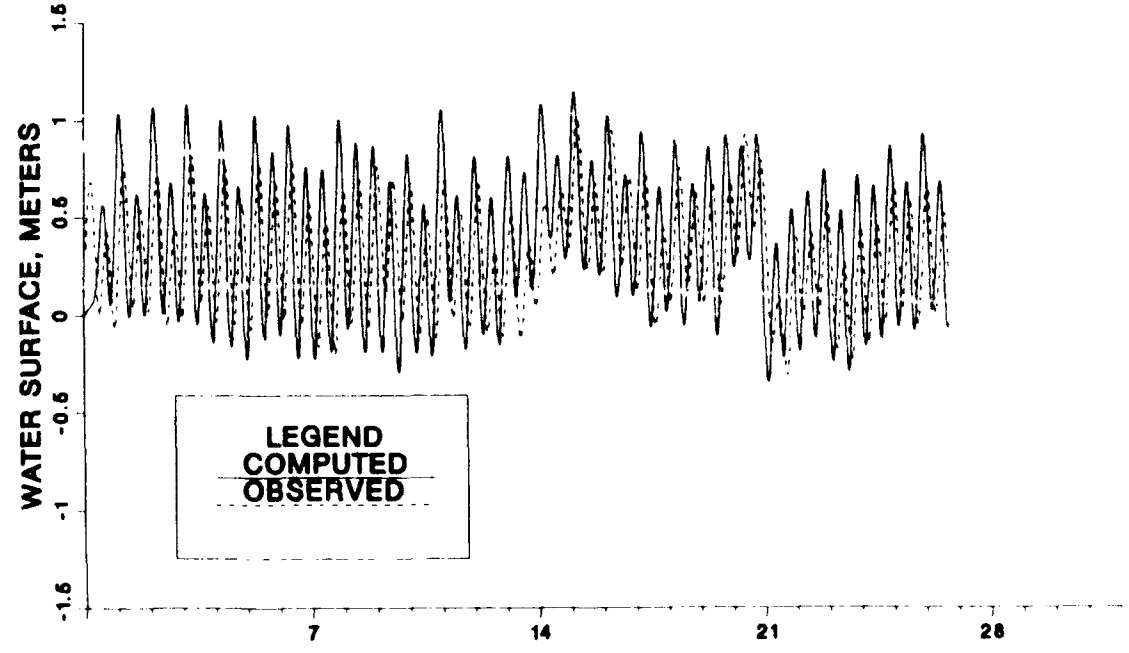

Figure 52. Comparison of computed and recorded tide at Havre de Grace, MD, during September 1983

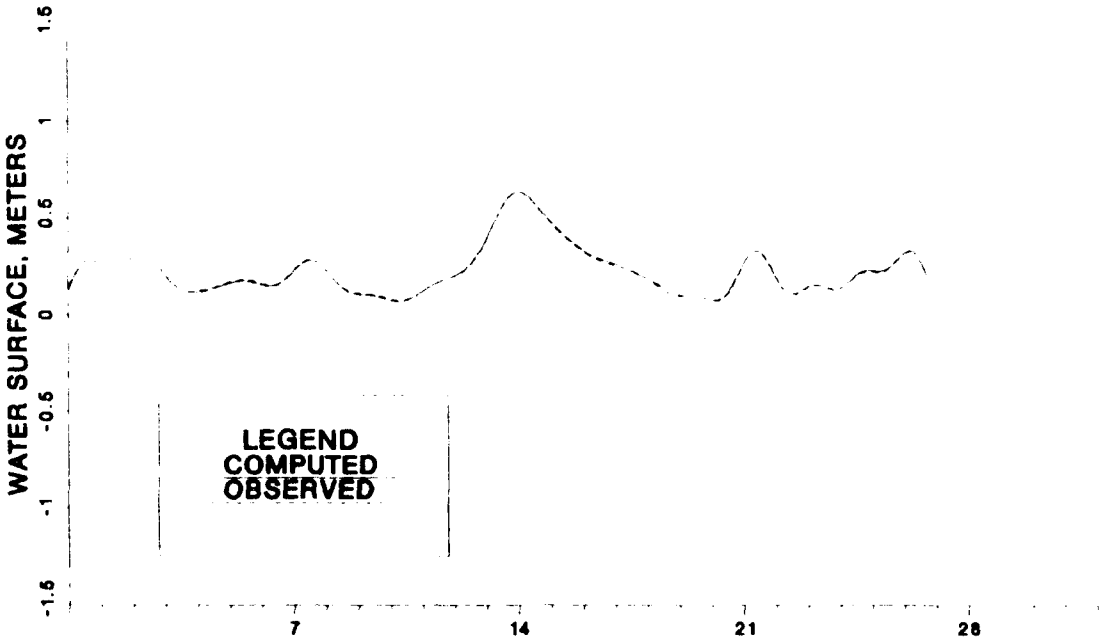

Figure 53. Filtered ocean boundary tide during September 1983

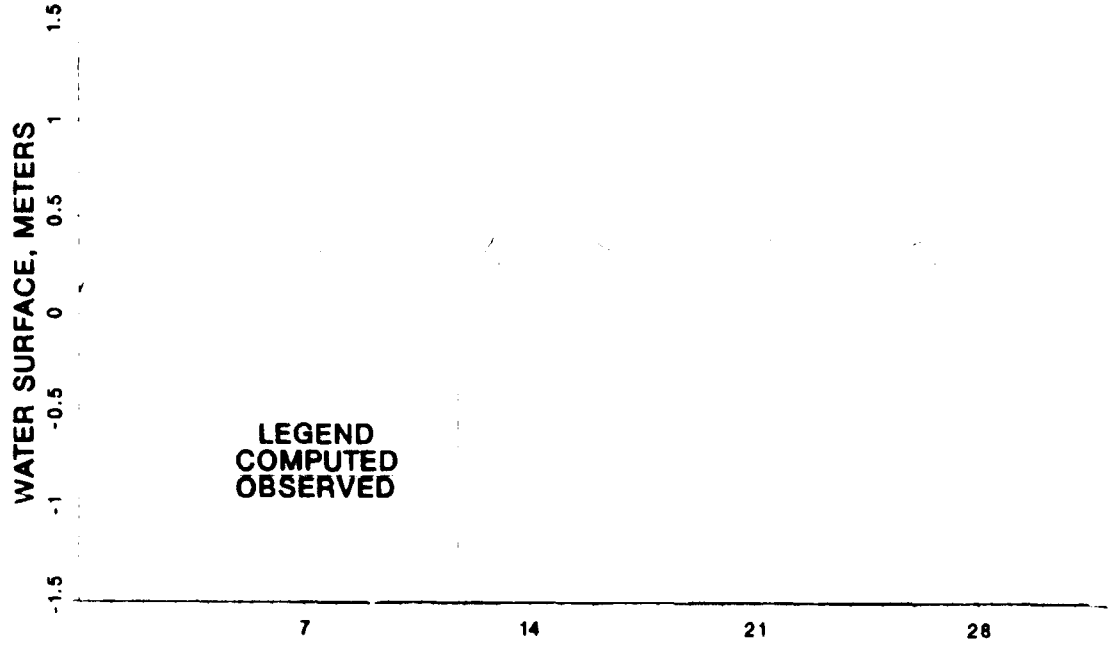

Figure 54. Comparison of filtered computed and recorded tide at Hampton Roads, VA, during September 1983

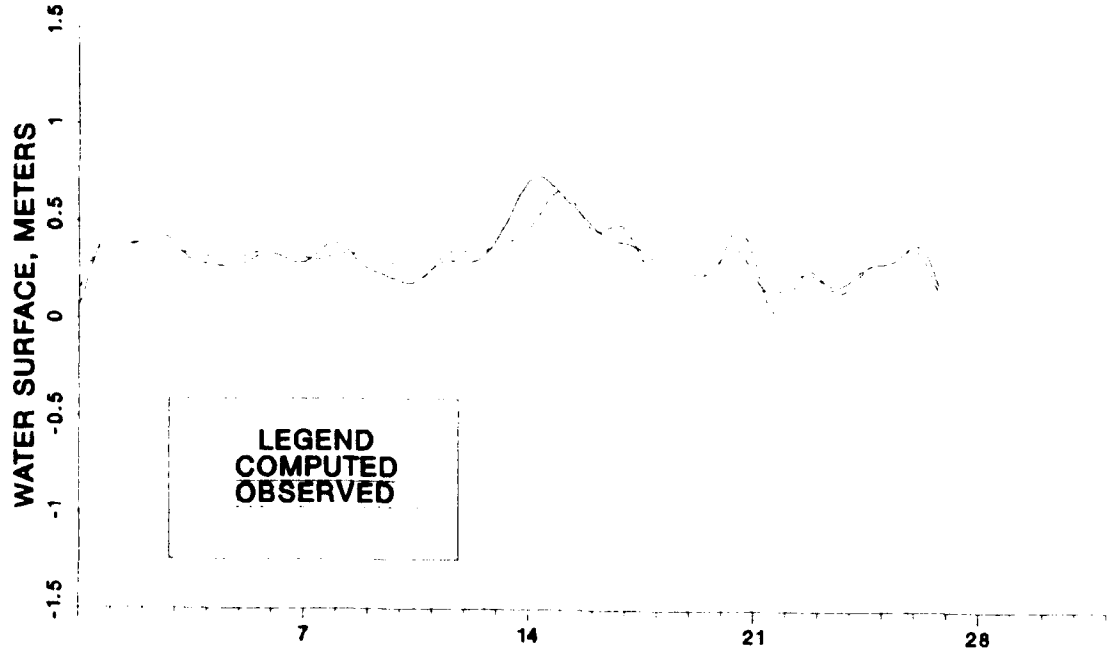

Figure 55. Comparison of filtered computed and recorded tide at Colonial Beach, VA, during September 1983

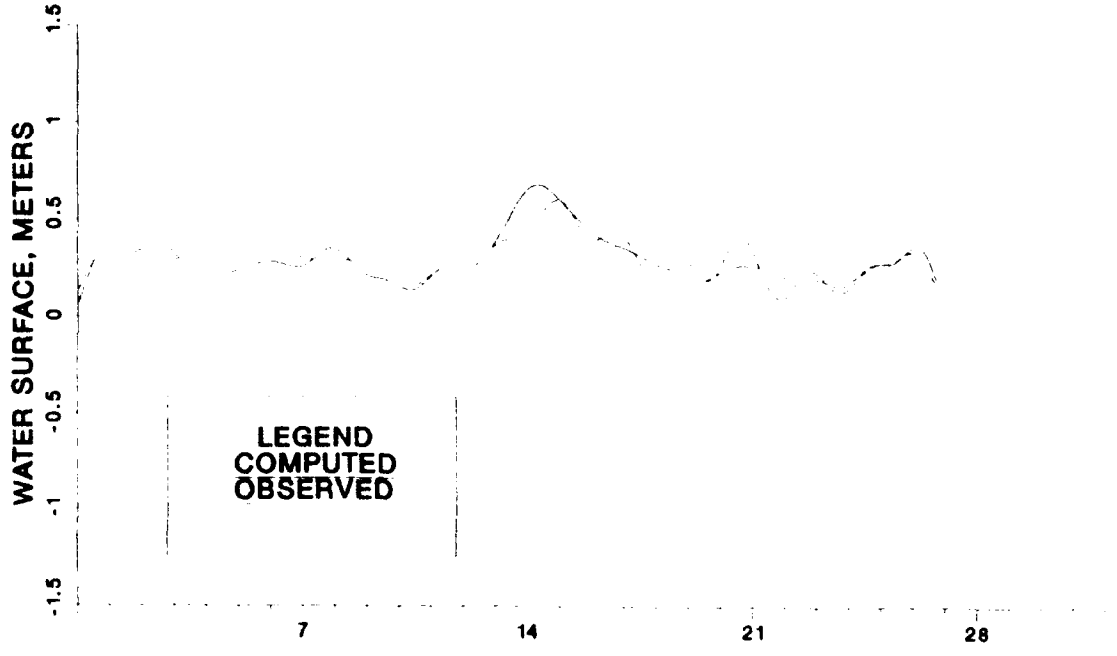

Figure 56. Comparison of filtered computed and recorded tide at Lewisetta, VA, during September 1983

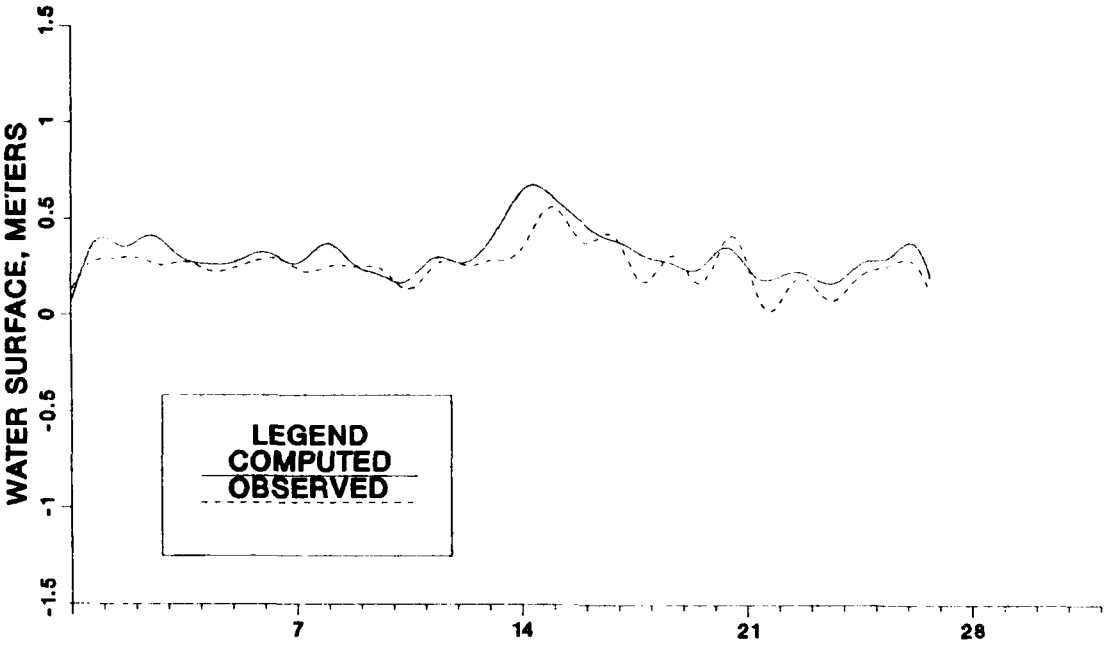

Figure 57. Comparison of filtered computed and recorded tide at Solomons, MD, during September 1983

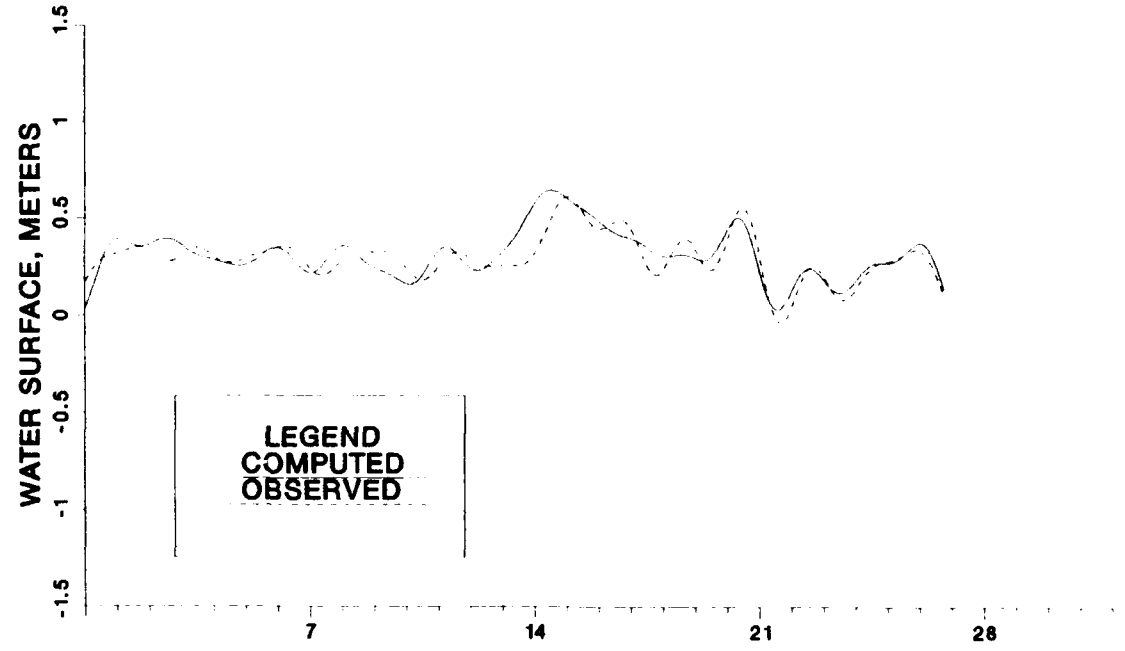

Figure 58. Comparison of filtered computed and recorded tide at Annapolis, MD, during September 1983

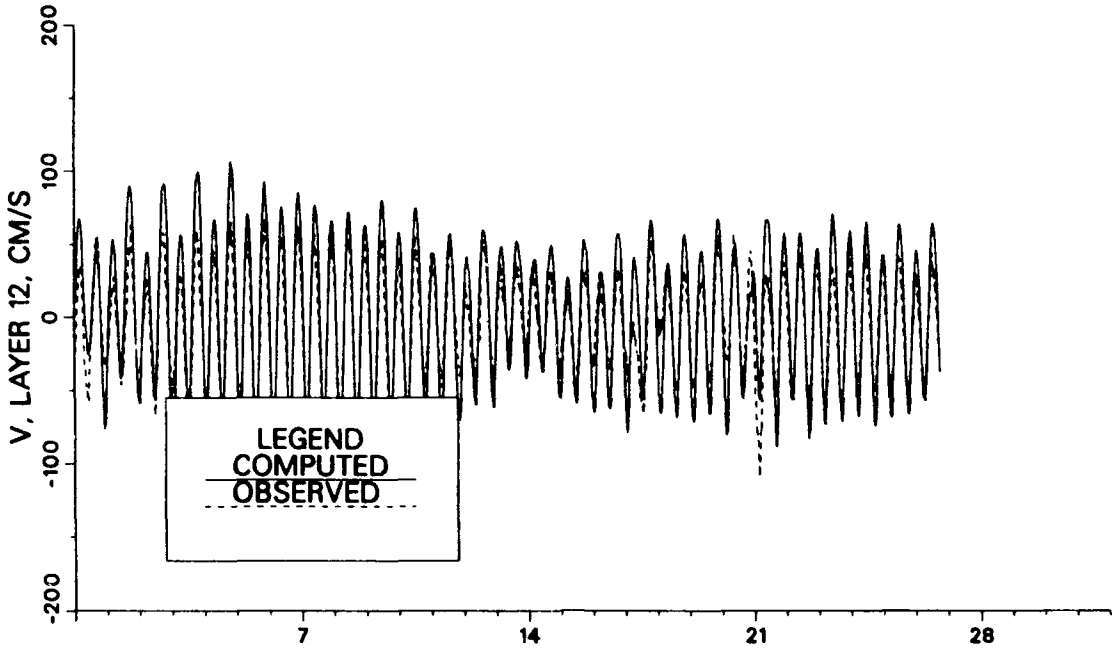

a. Depth = 17.5 ft

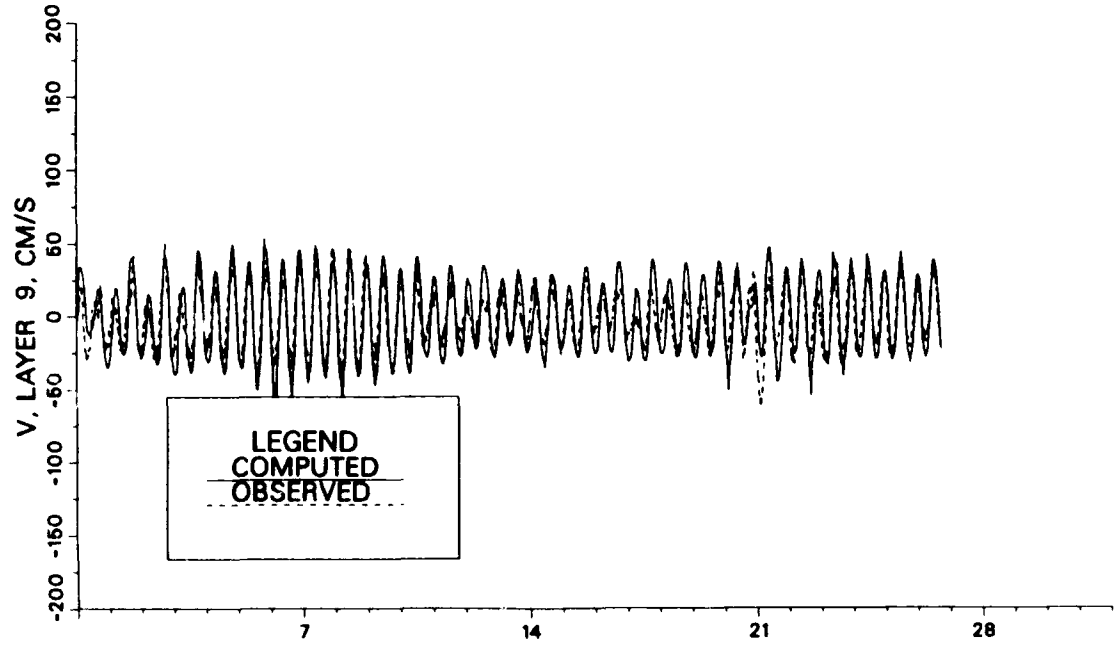

b. Depth = 32.5 ft

Figure 59. Comparison of computed and recorded velocity at station BE during September 1983

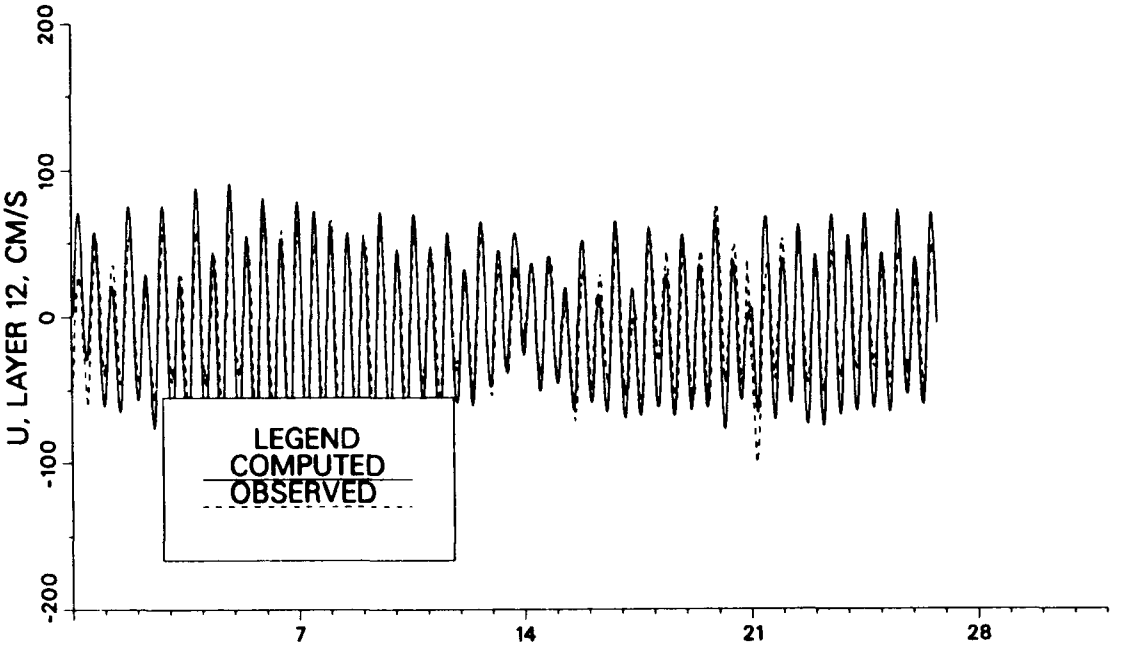

a. Depth = 17.5 ft

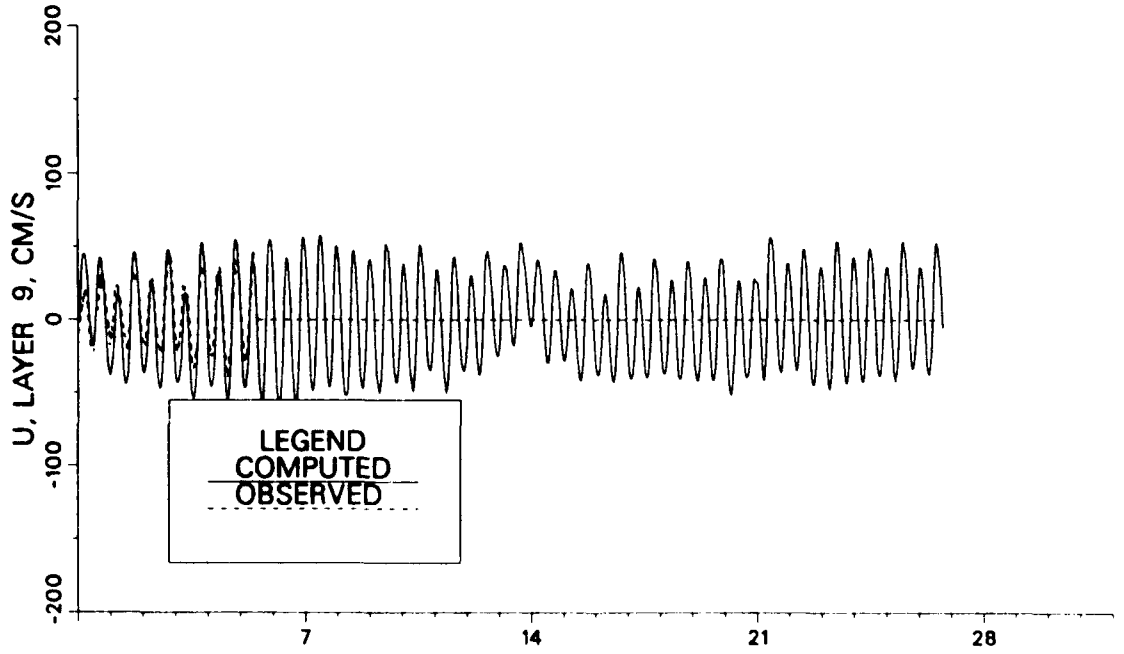

b. Depth = 32.5 ft

Figure 60. Comparison of computed and recorded velocity at station WT during September 1983

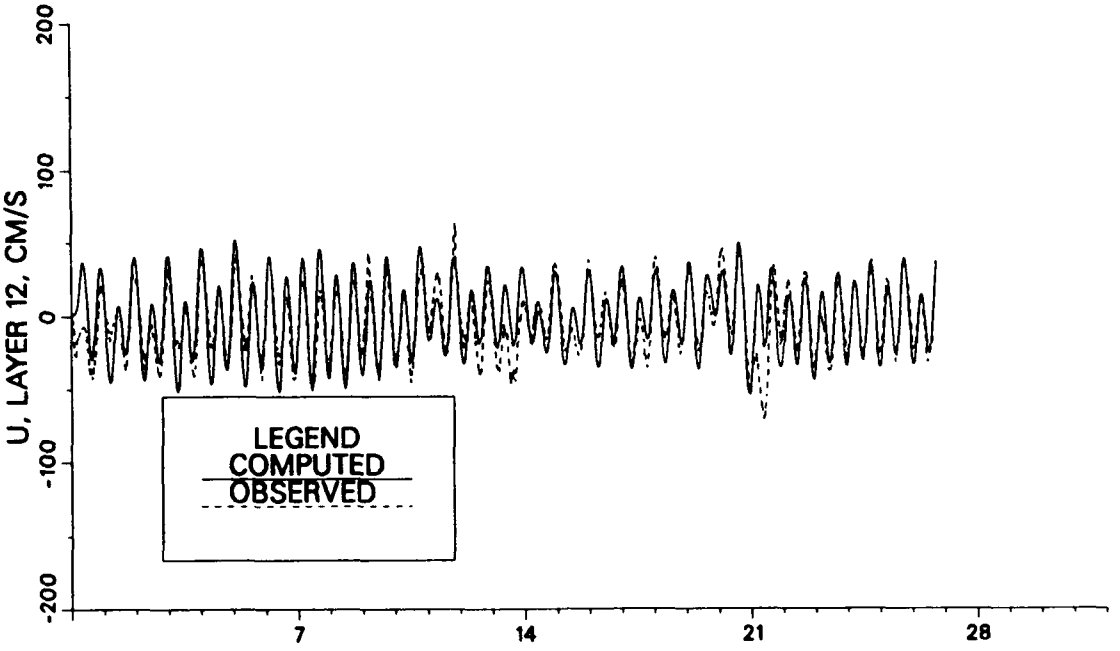

a. Depth = 17.5 ft

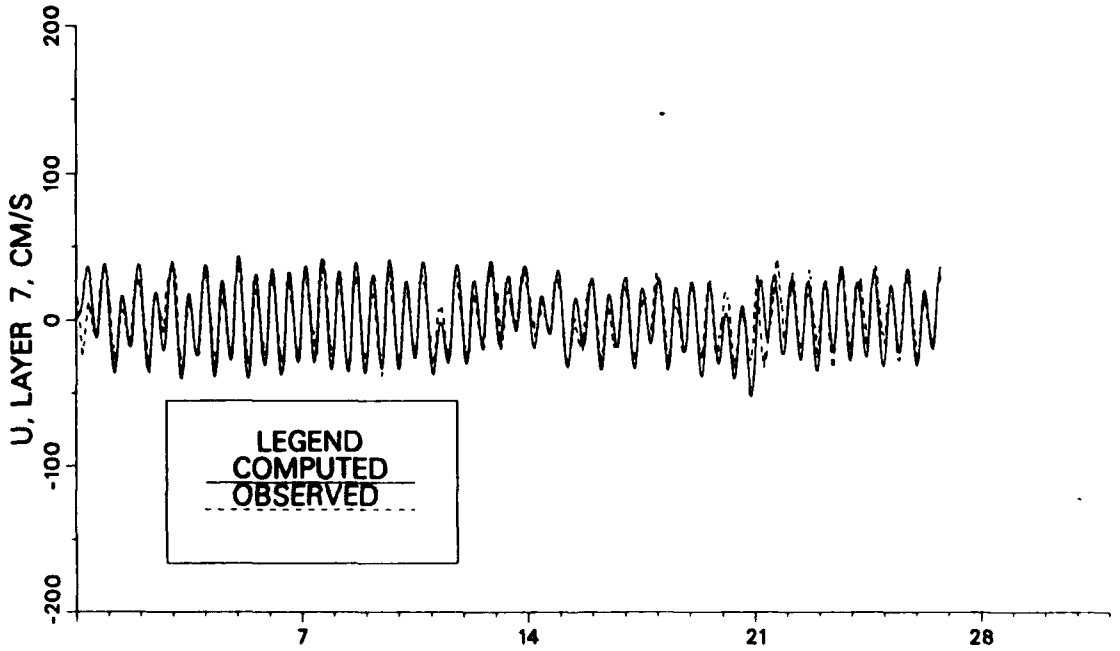

b. Depth = 42.5 ft

Figure 61. Comparison of computed and recorded velocity at station MB during September 1983

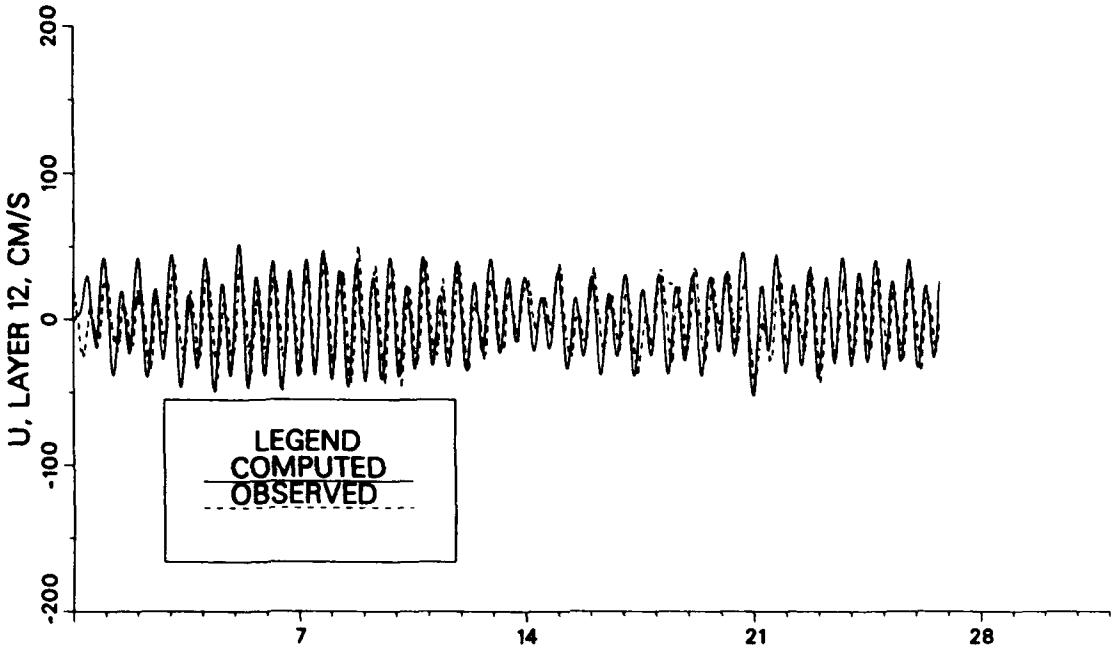

a. Depth = 17.5 ft

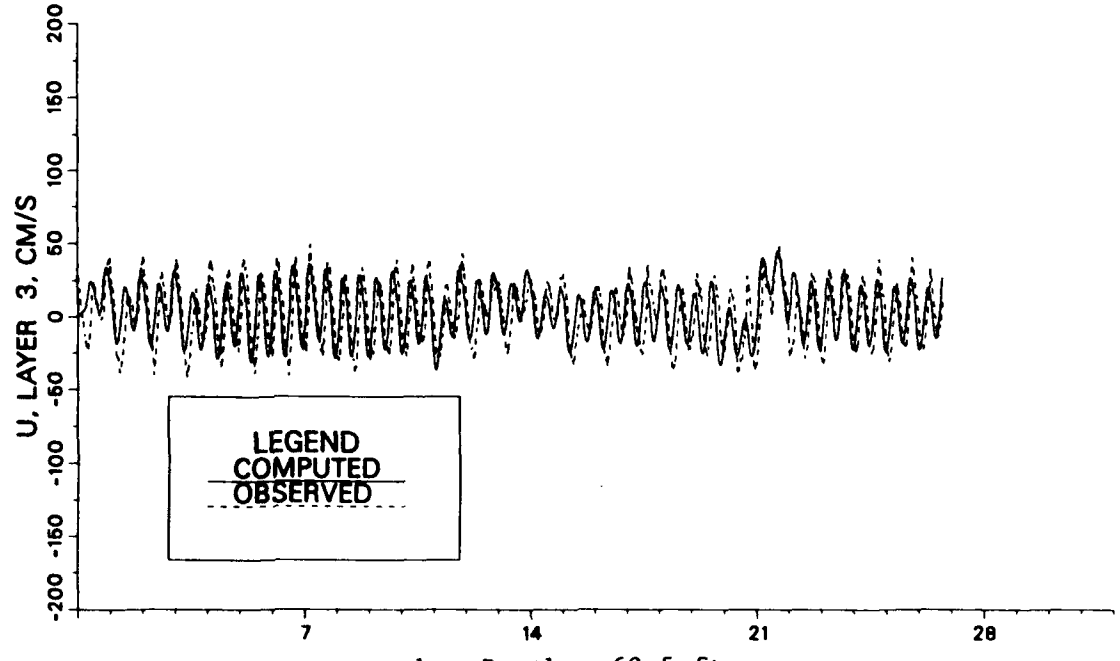

b. Depth = 62.5 ft

Figure 62. Comparison of computed and recorded velocity at station BB during September 1983

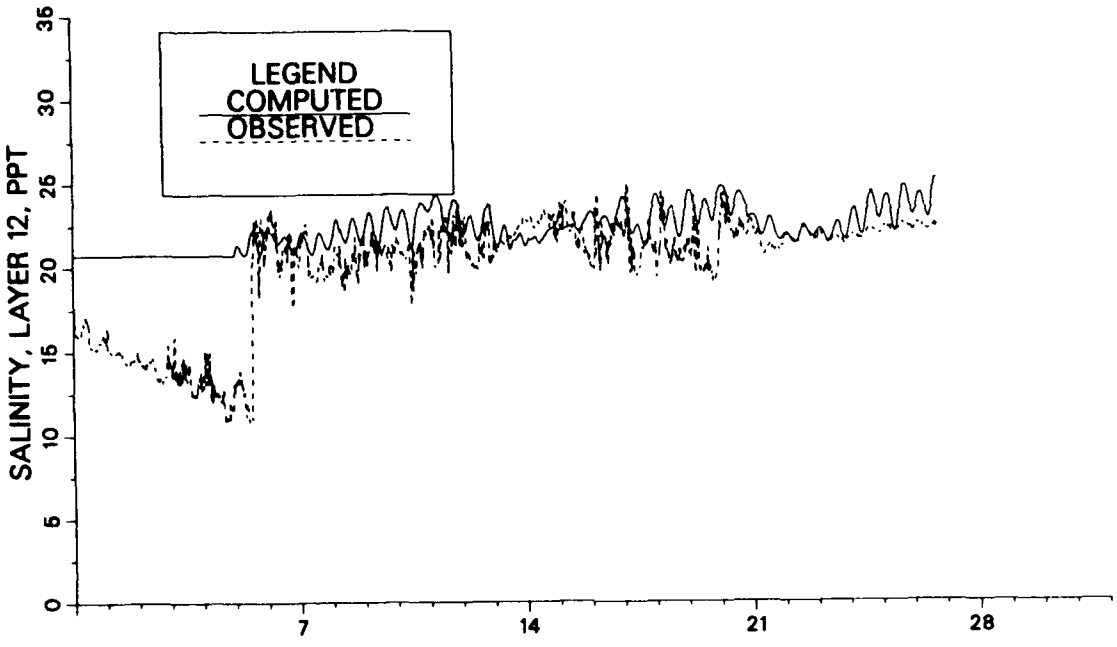

a. Depth = 17.5 ft

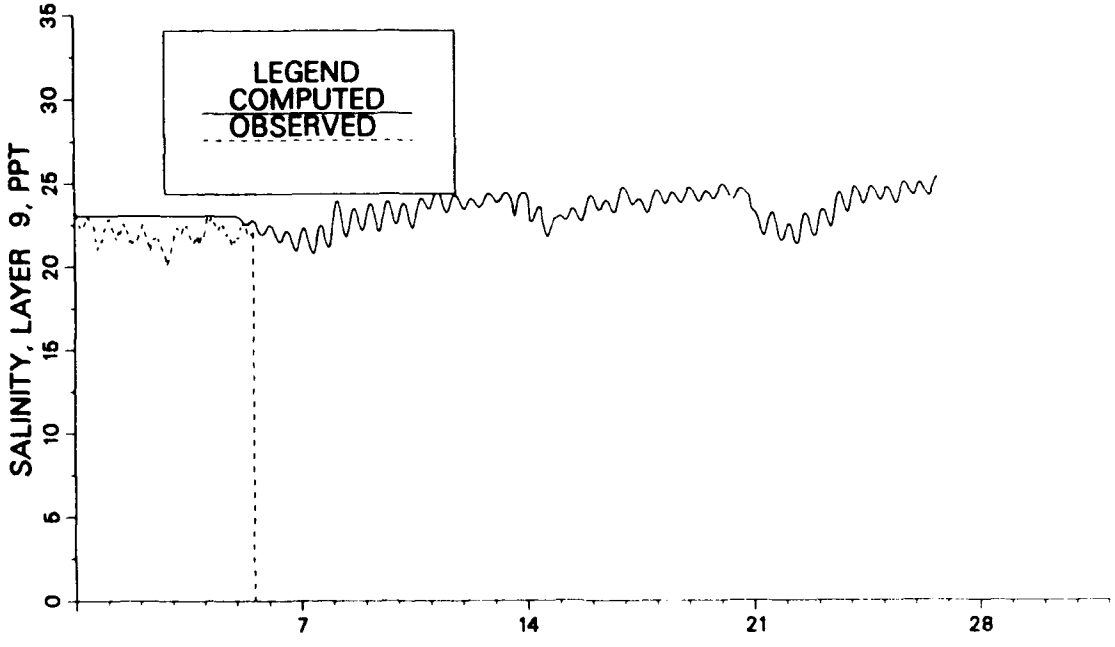

b. Depth = 32.5 ft

Figure 63. Comparison of computed and recorded salinity at station WT during September 1983

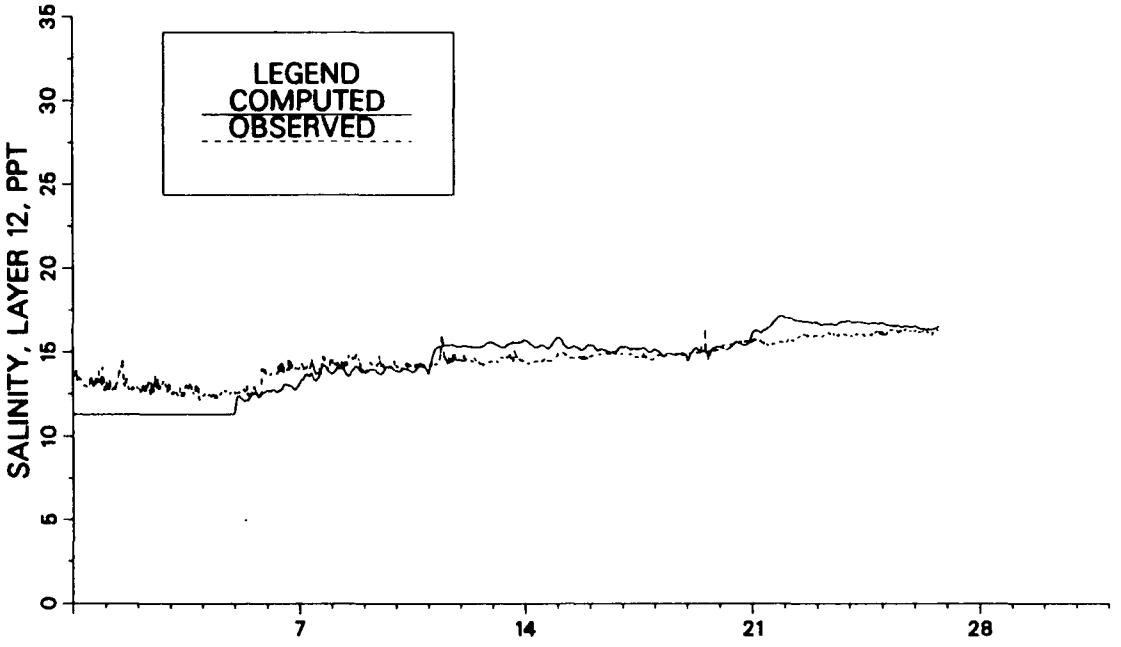

a. Depth = 17.5 ft

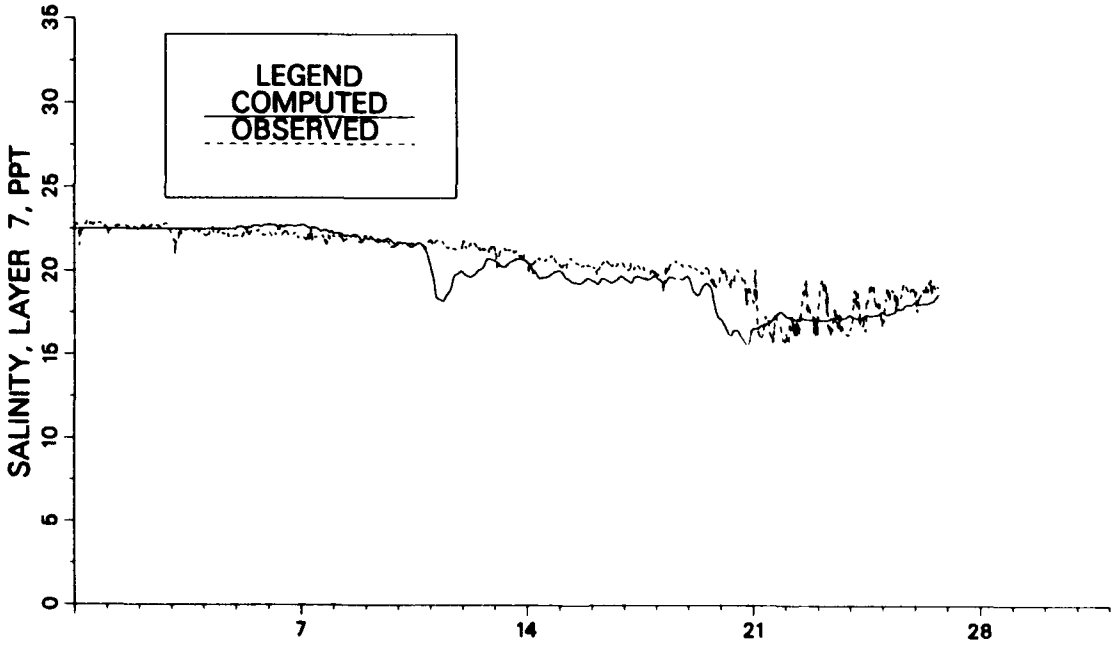

b. Depth = 42.5 ft

Figure 64. Comparison of computed and recorded salinity at station MB during September 1983

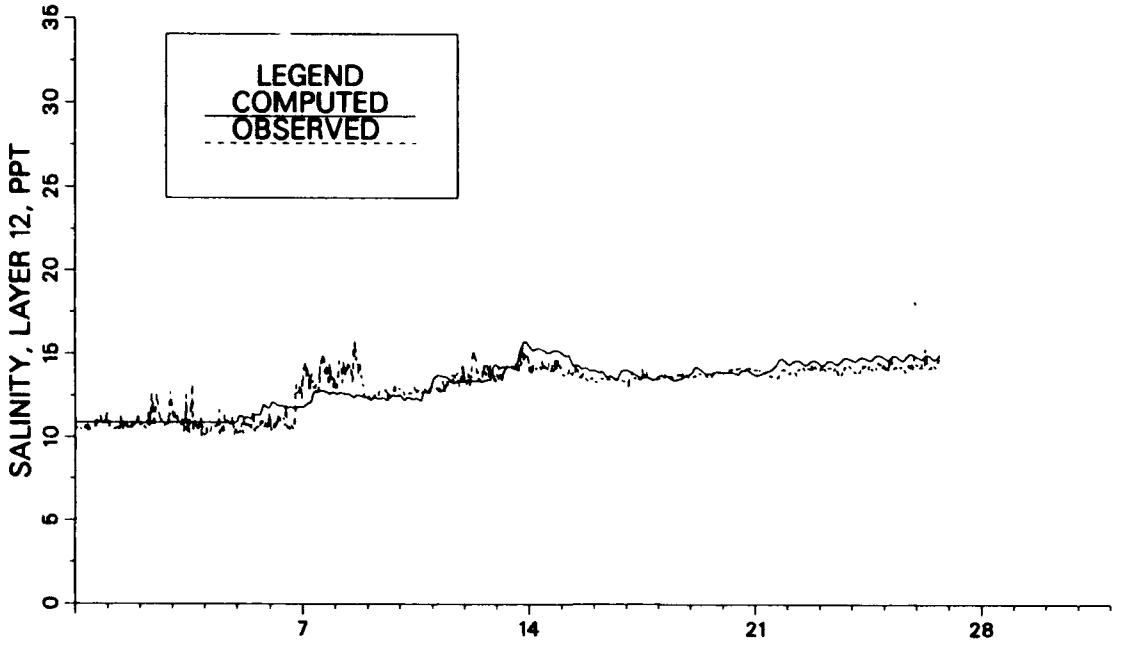

a. Depth = 17.5 ft

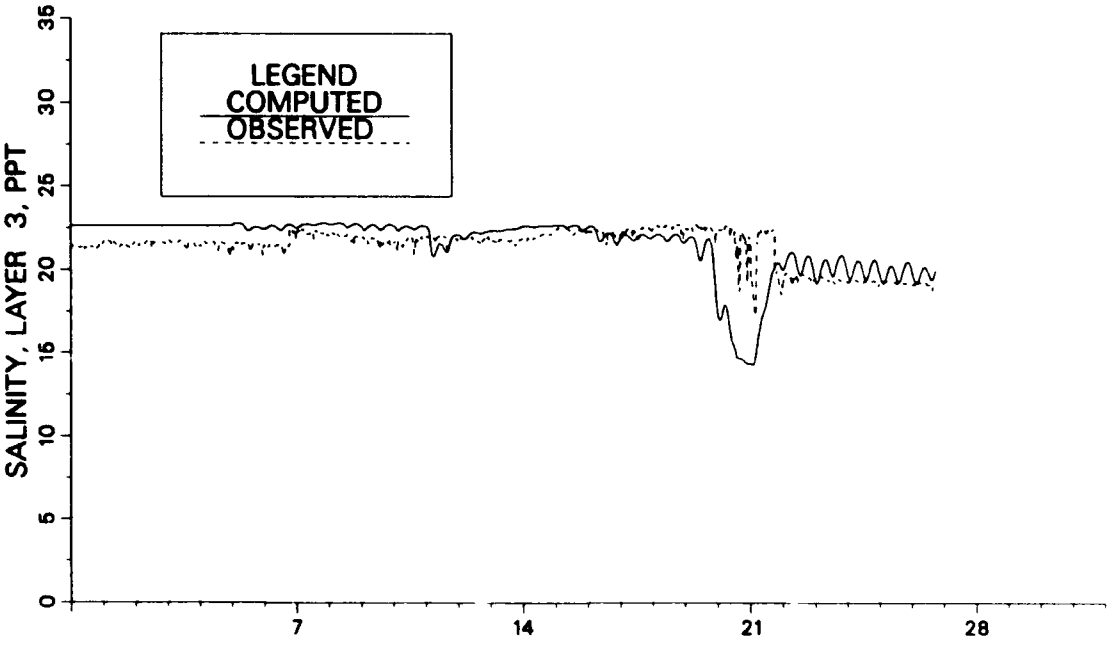

b. Depth = 62.5 ft

Figure 65. Comparison of computed and recorded salinity at station BB during September 1983

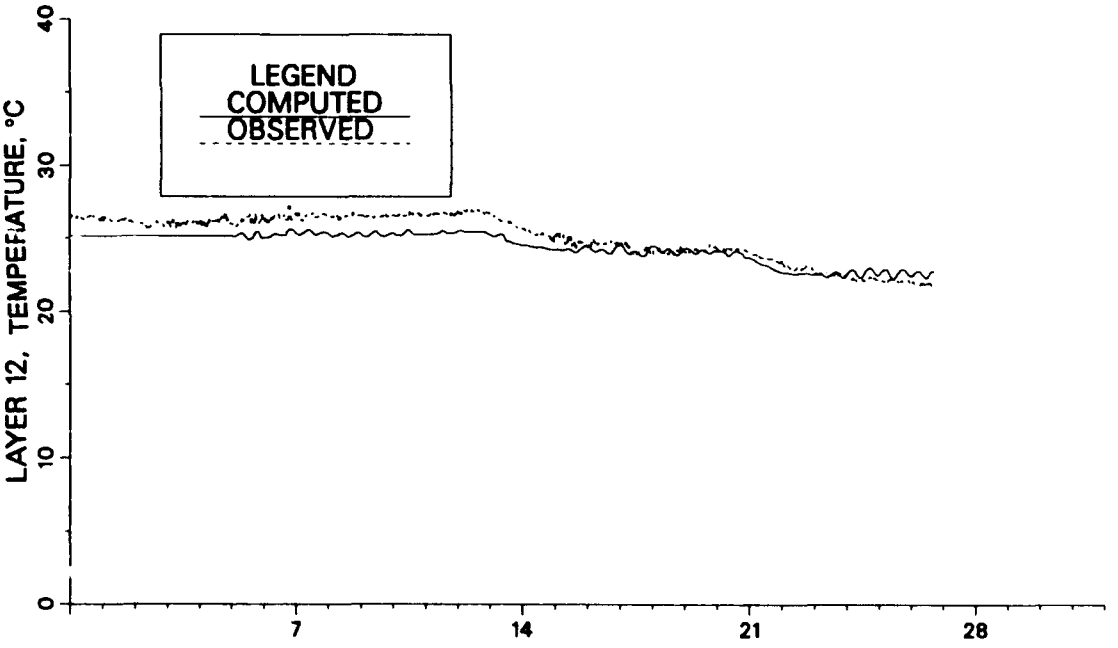

a. Depth = 17.5 ft

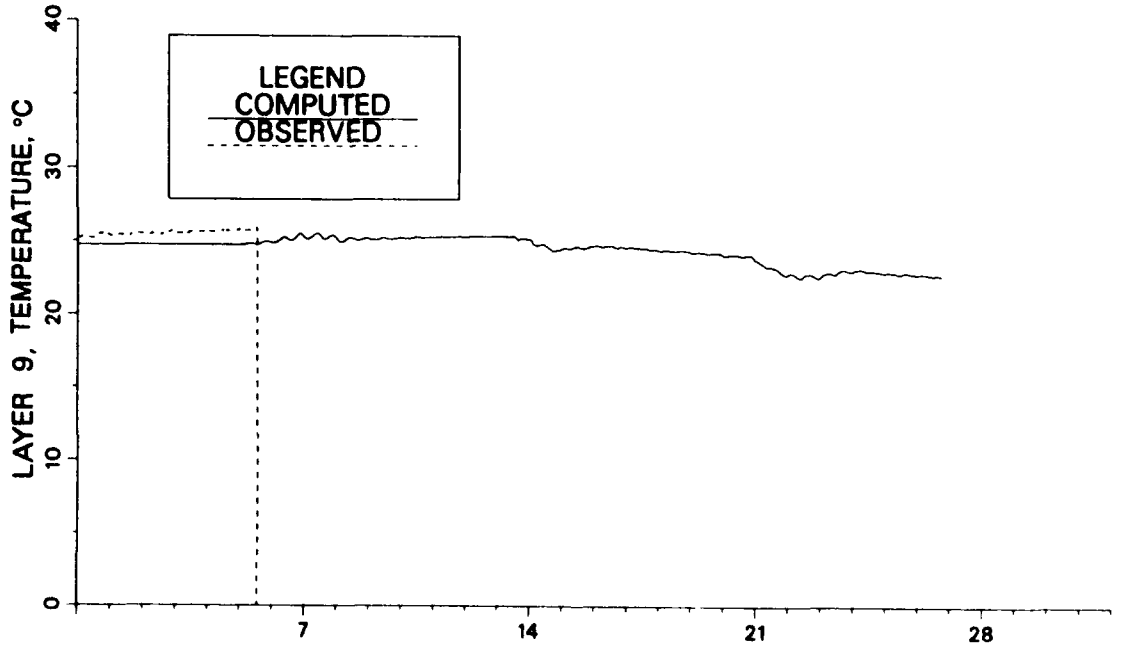

b. Depth = 32.5 ft

Figure 66. Comparison of computed and recorded temperature at station WT during September 1983

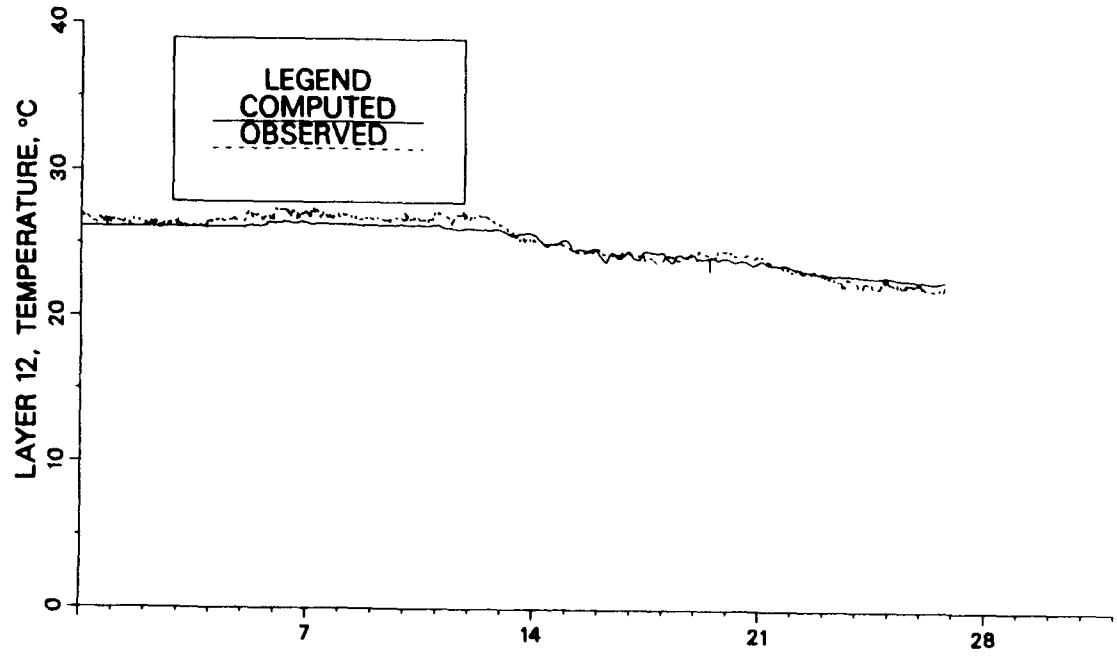

a. Depth = 17.5 ft

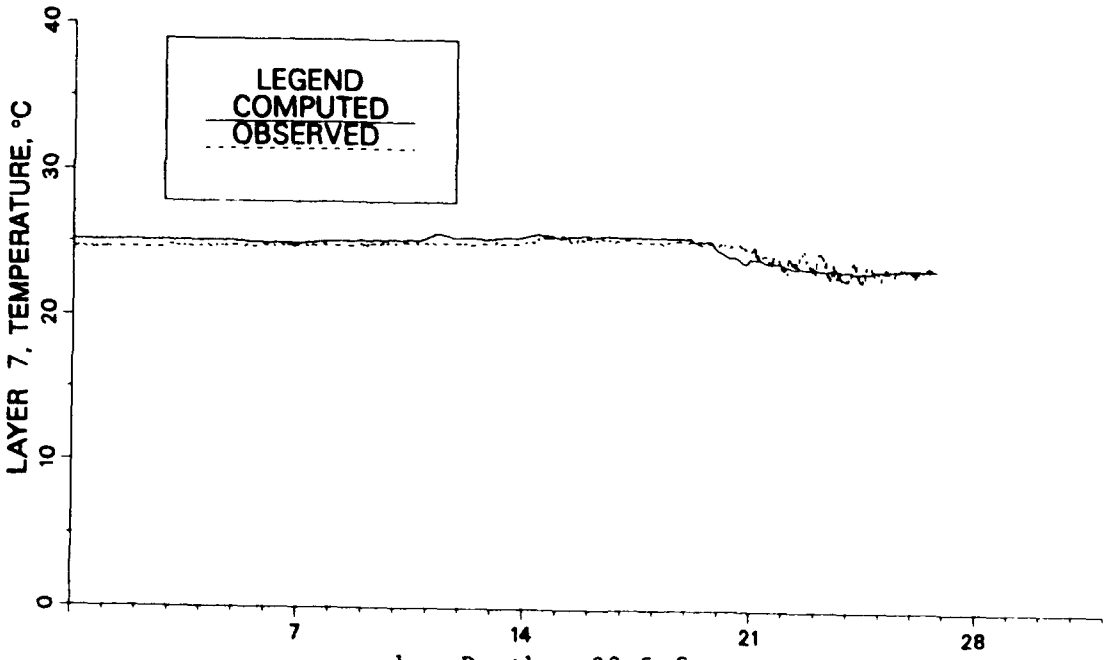

b. Depth = 32.5 ft

Figure 67. Comparison of computed and recorded temperature at station MB during September 1983

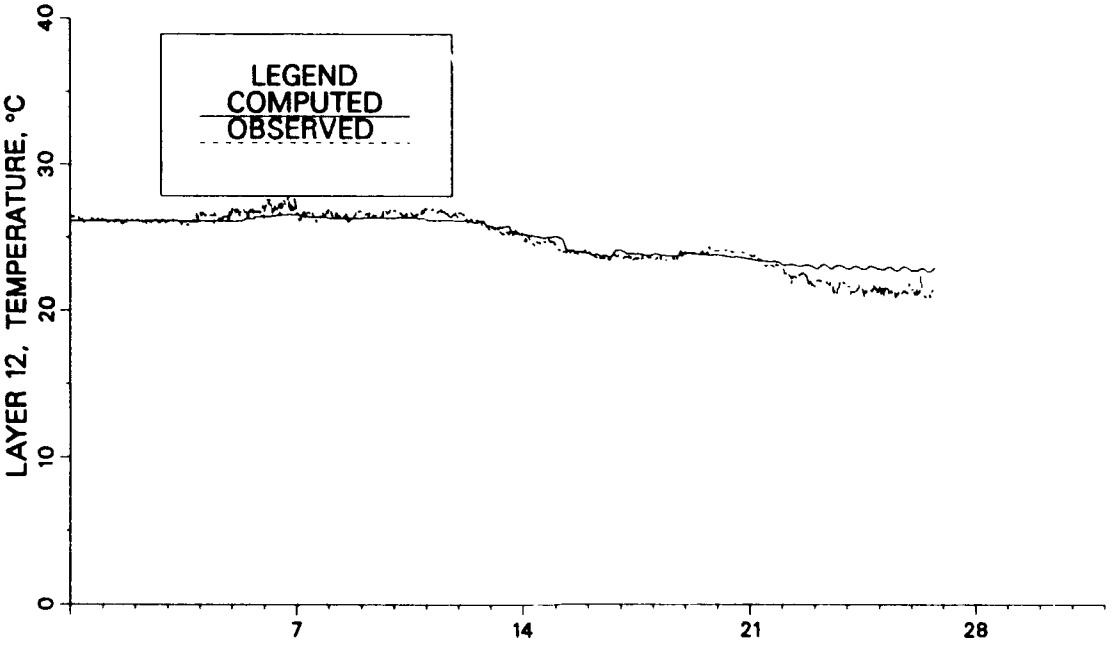

a. Depth = 17.5 ft

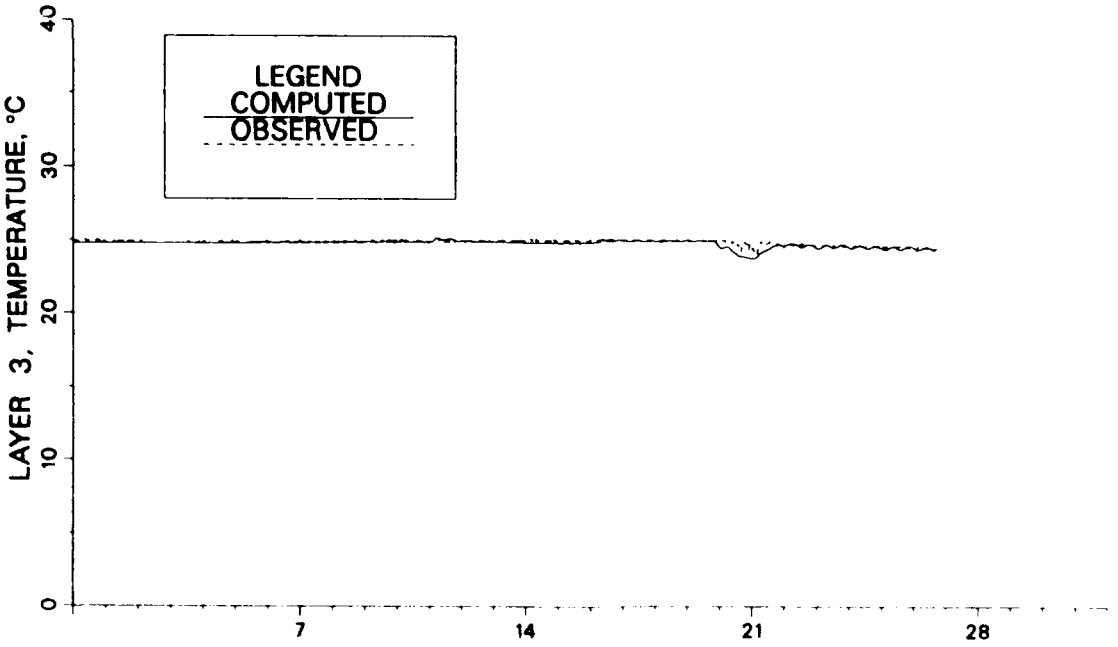

b. Depth = 62.5 ft

Figure 68. Comparison of computed and recorded temperature at station BB during September 1983

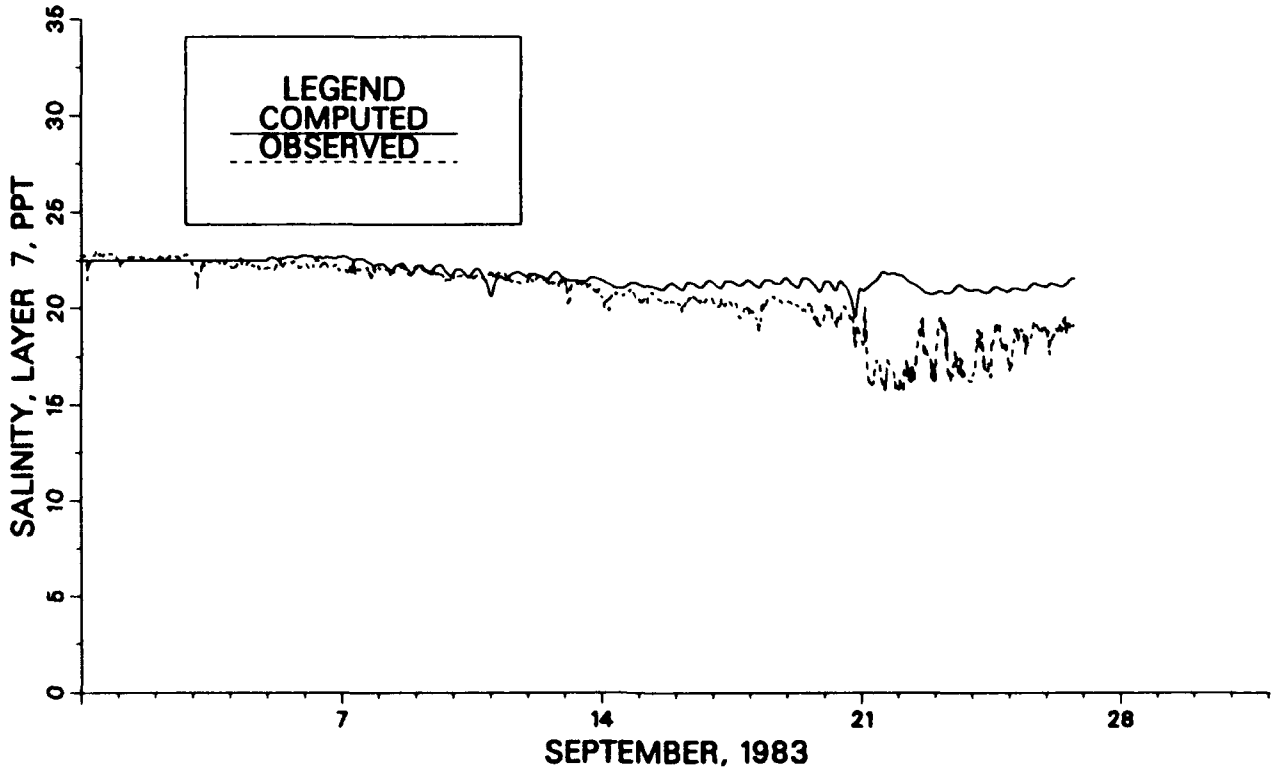

Figure 69. Comparison of computed and recorded salinity at a depth of 42.5 ft at station MB without the three-point smoothing

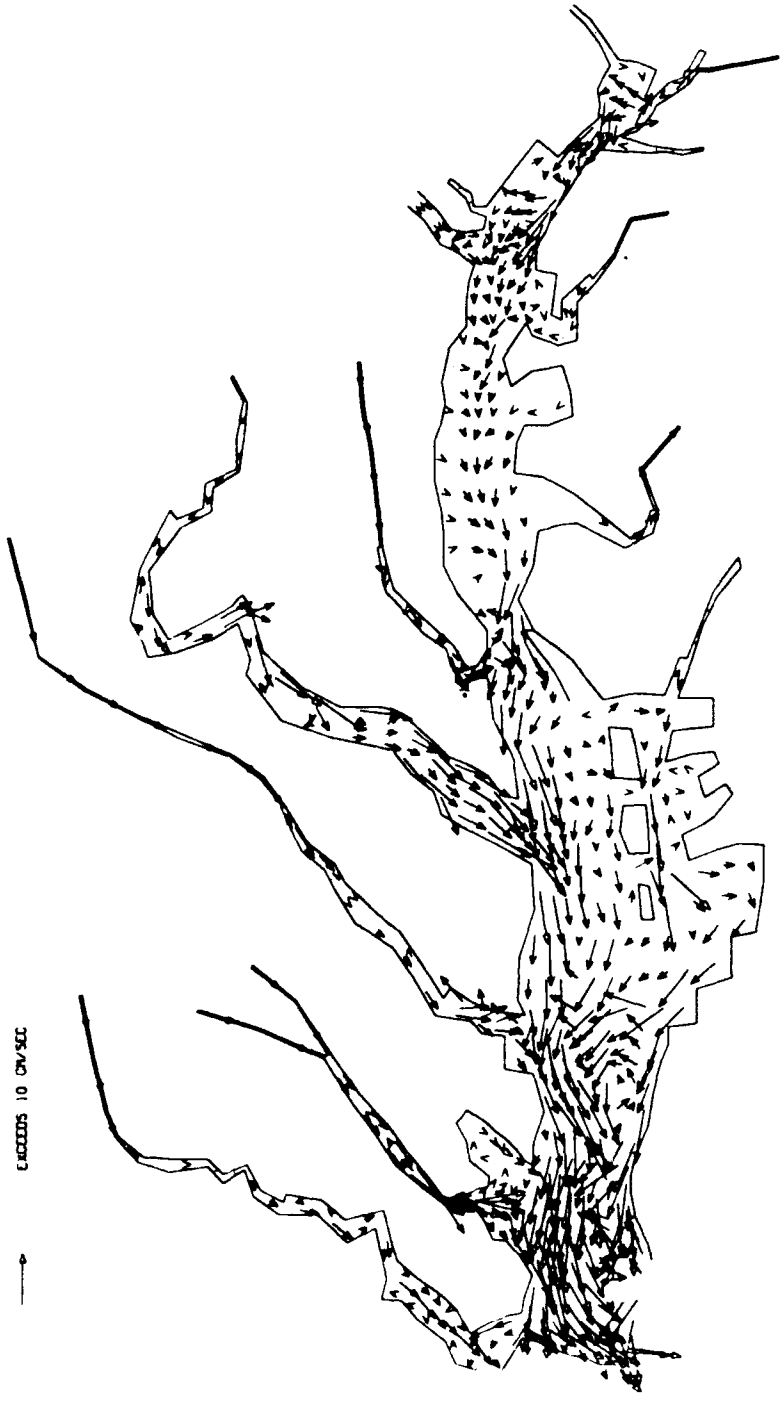

a. Near-surface

Figure 70. Computed residual currents from model during September 1983 (Continued)

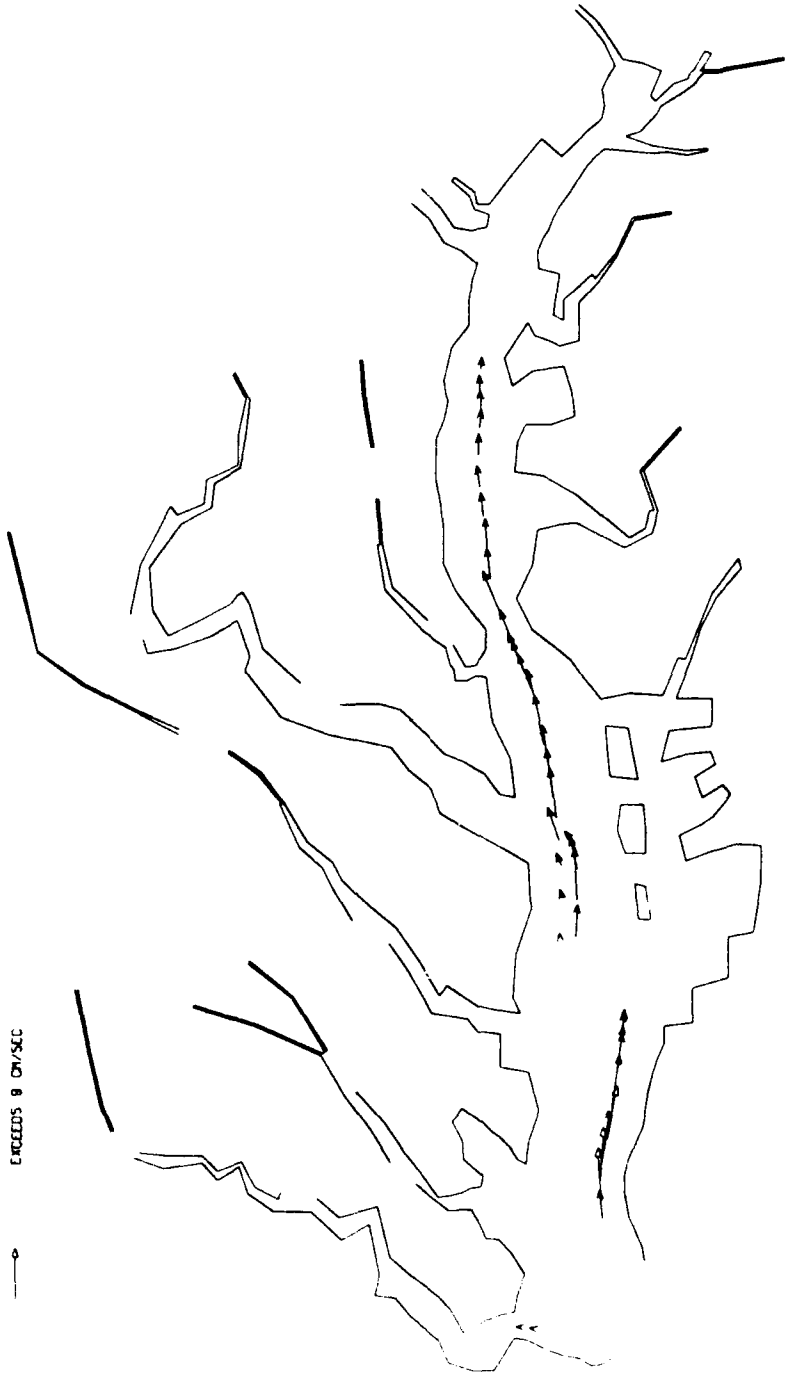

b. Near-bottom

Figure 70. (Concluded)

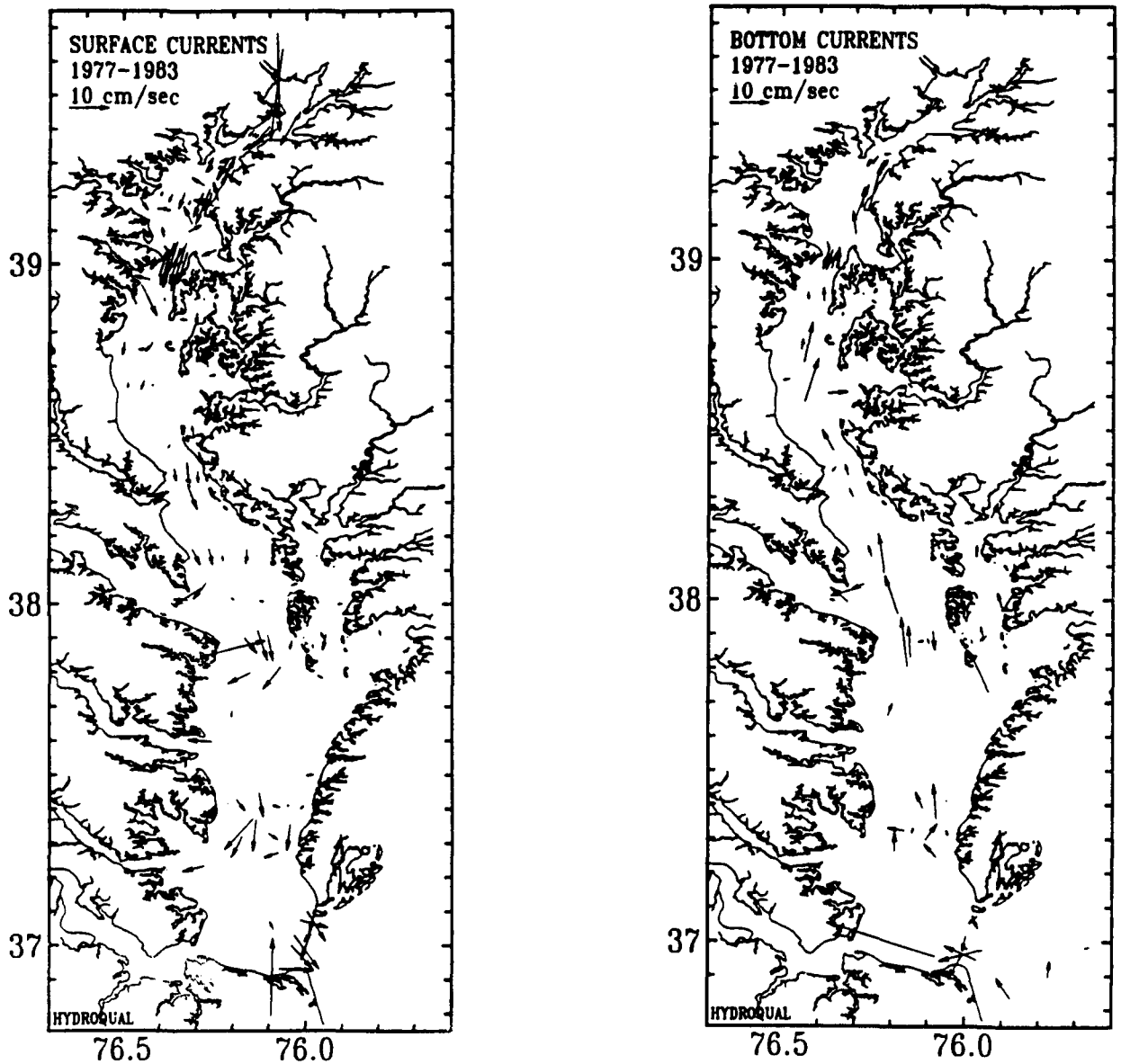

a. Near-surface b. Near-bottom

Figure 71. Computed residual currents from field data during 1977-1983

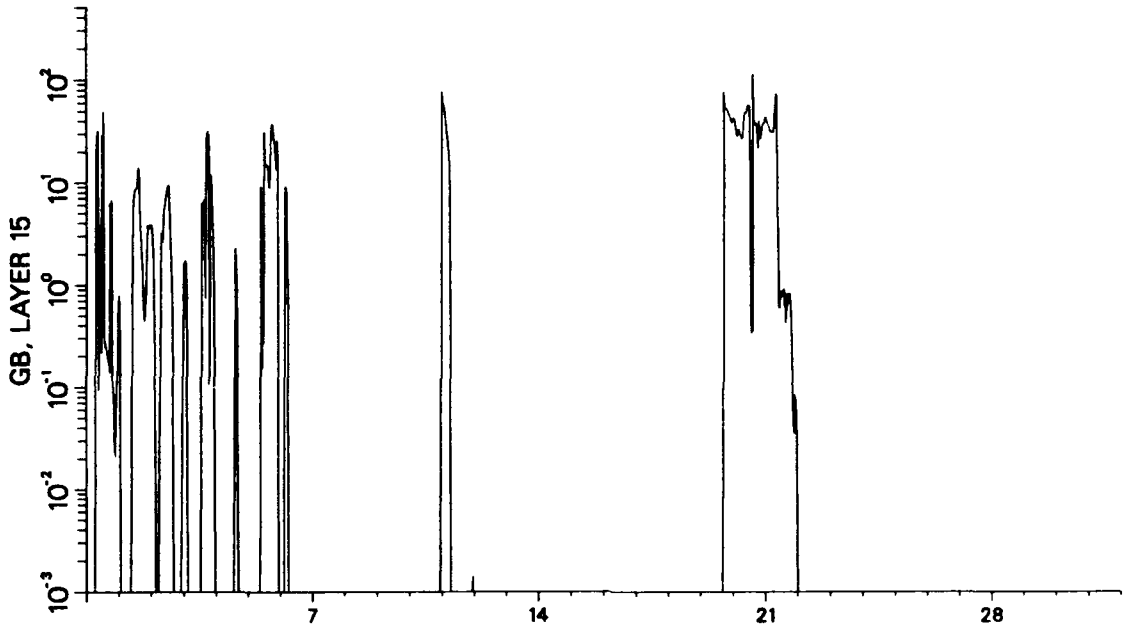

a. Depth = 2.5 ft

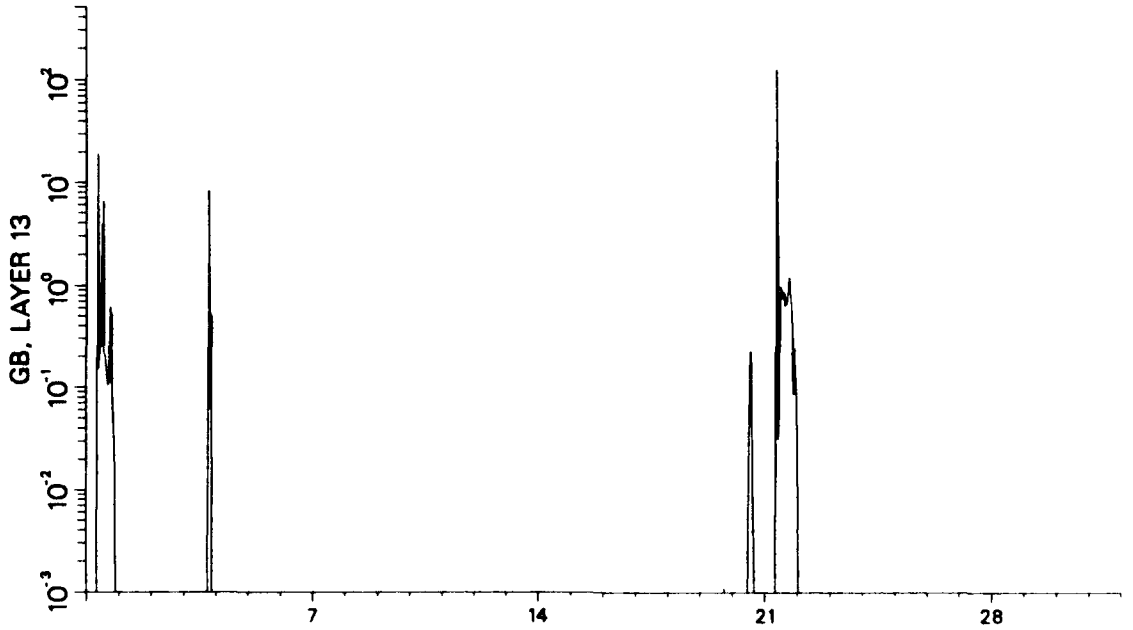

b. Depth = 12.5 ft

Figure 72. Eddy diffusivity GB at station MB computed during September 1983 (Sheet 1 of 3)

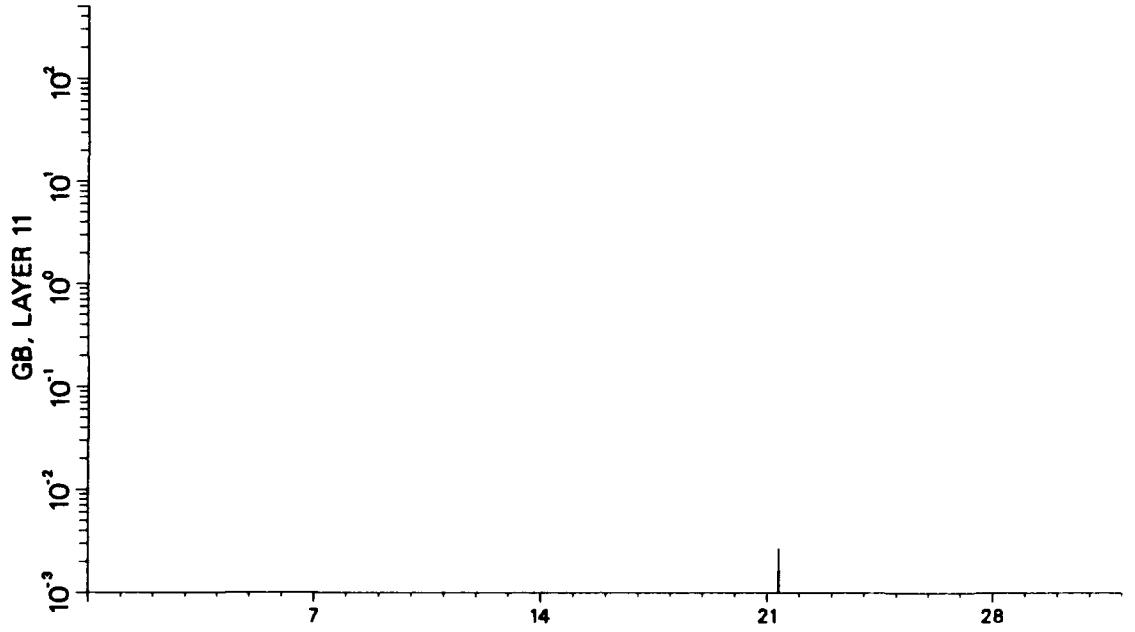

c. Depth = 22.5 ft

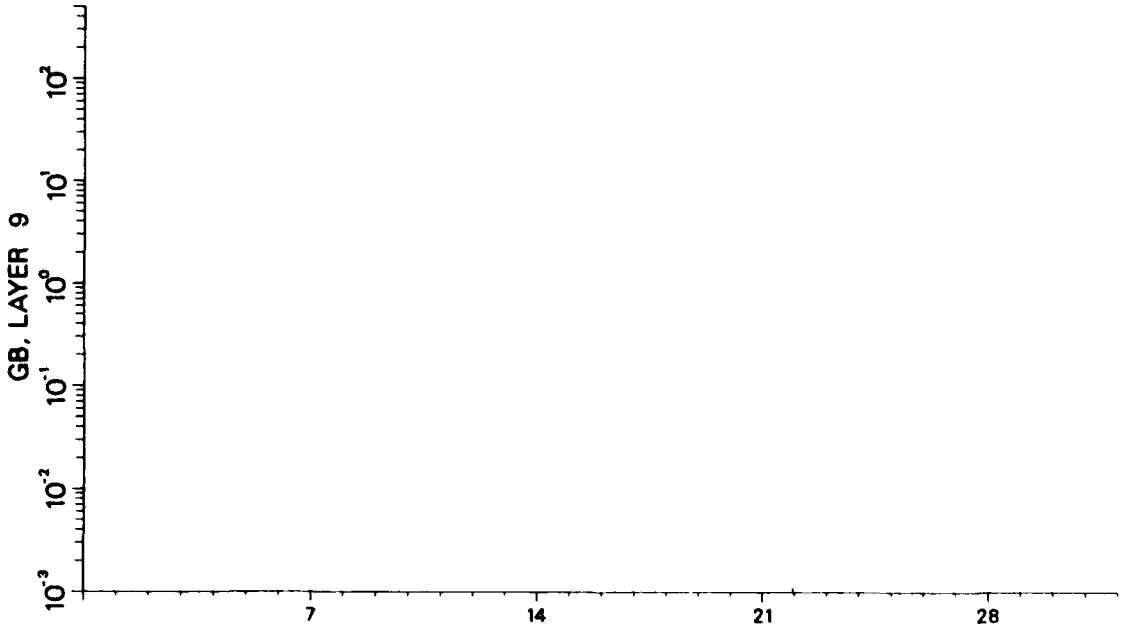

d. Depth = 32.5 ft

Figure 72. (Sheet 2 of 3)

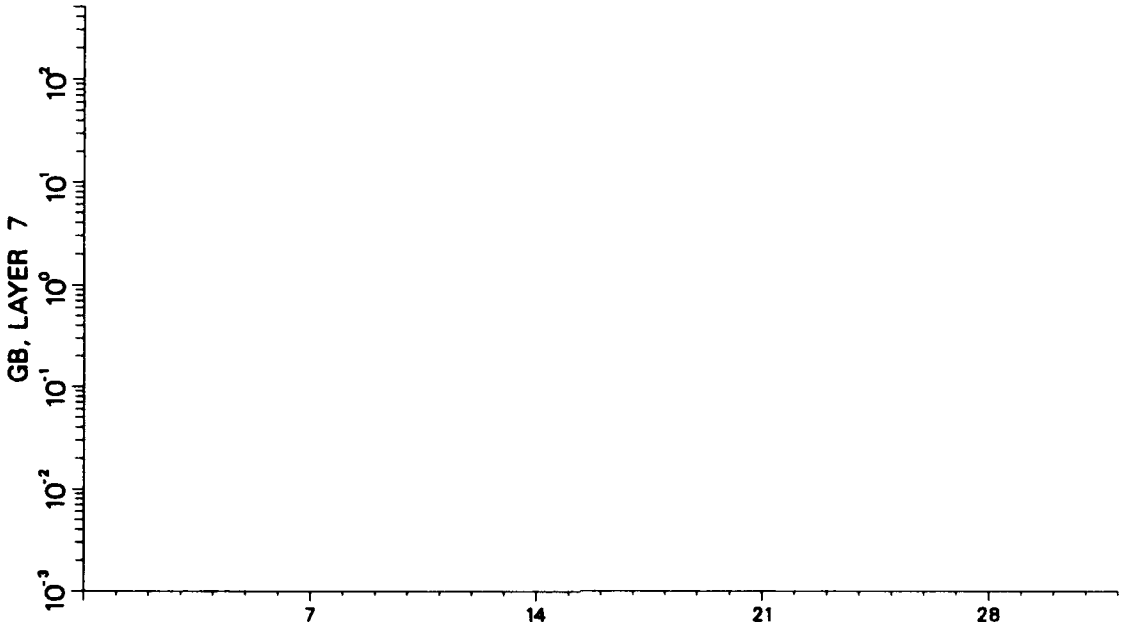

e. Depth = 42.5 ft

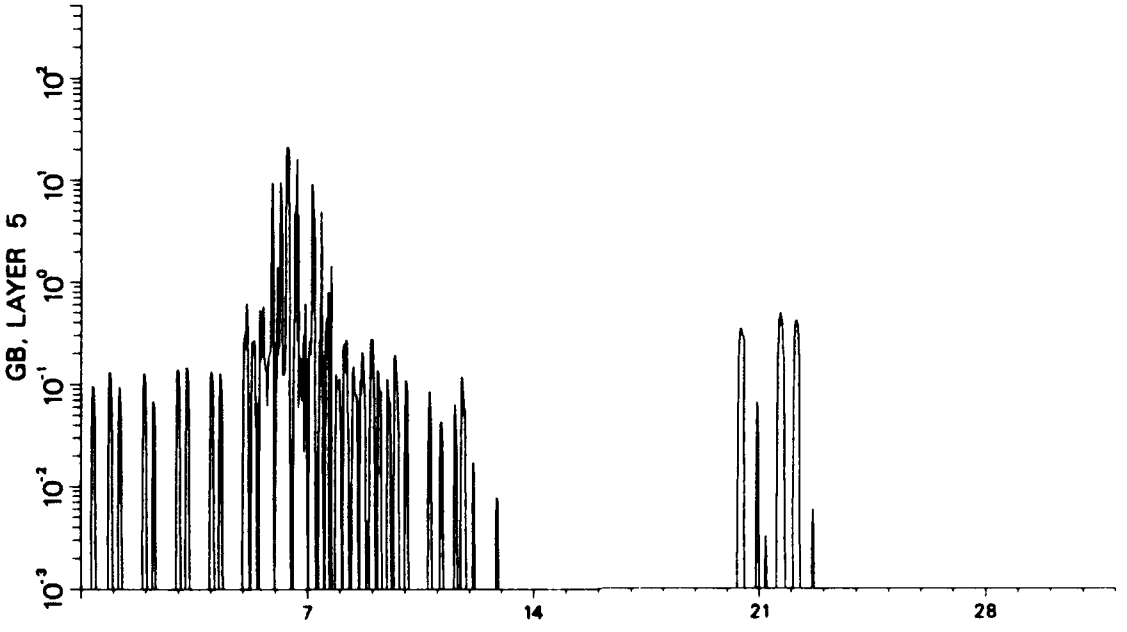

f. Depth = 52.5 ft

Figure 72. (Sheet 3 of 3)

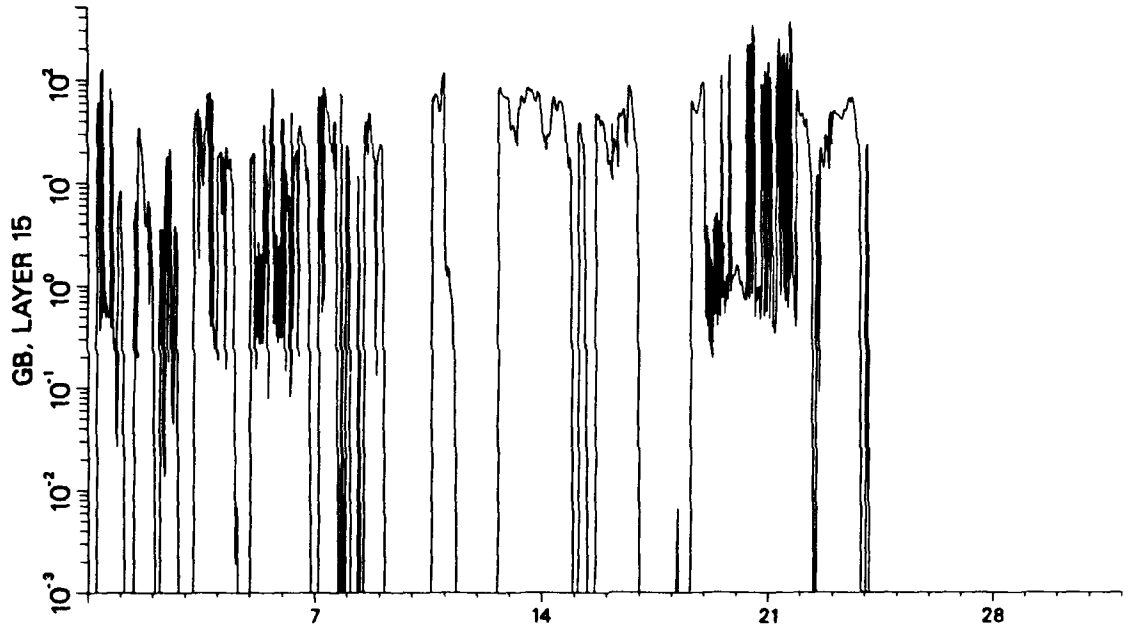

a. Depth = 2.5 ft

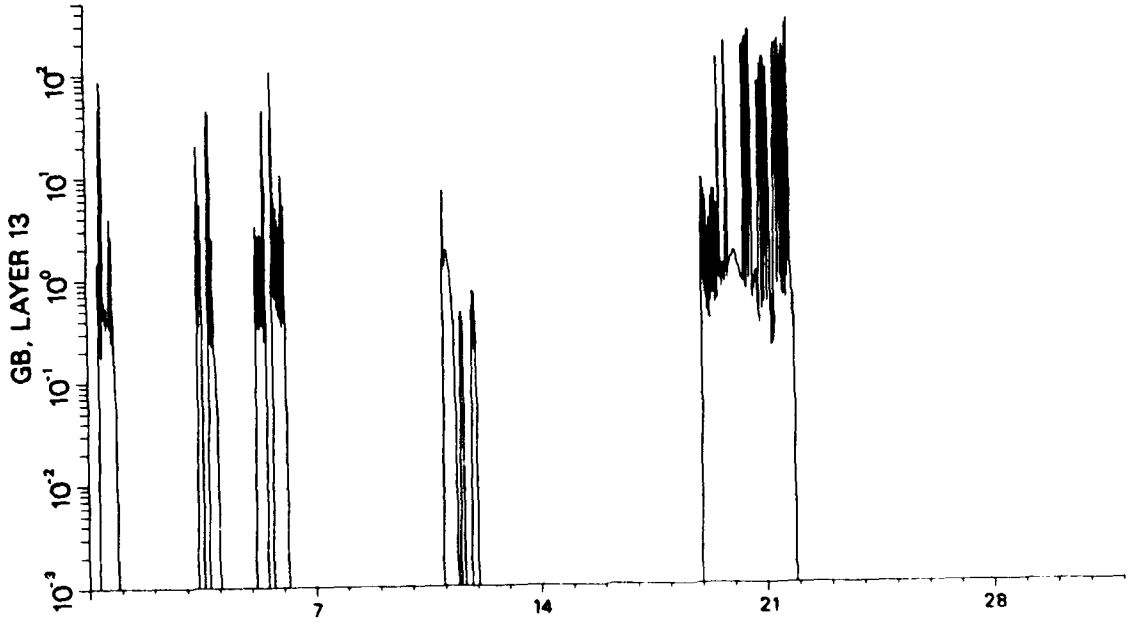

b. Depth = 12.5 ft

Figure 73. Eddy diffusivity GB at station BB computed during September 1983 (Sheet 1 of 4)

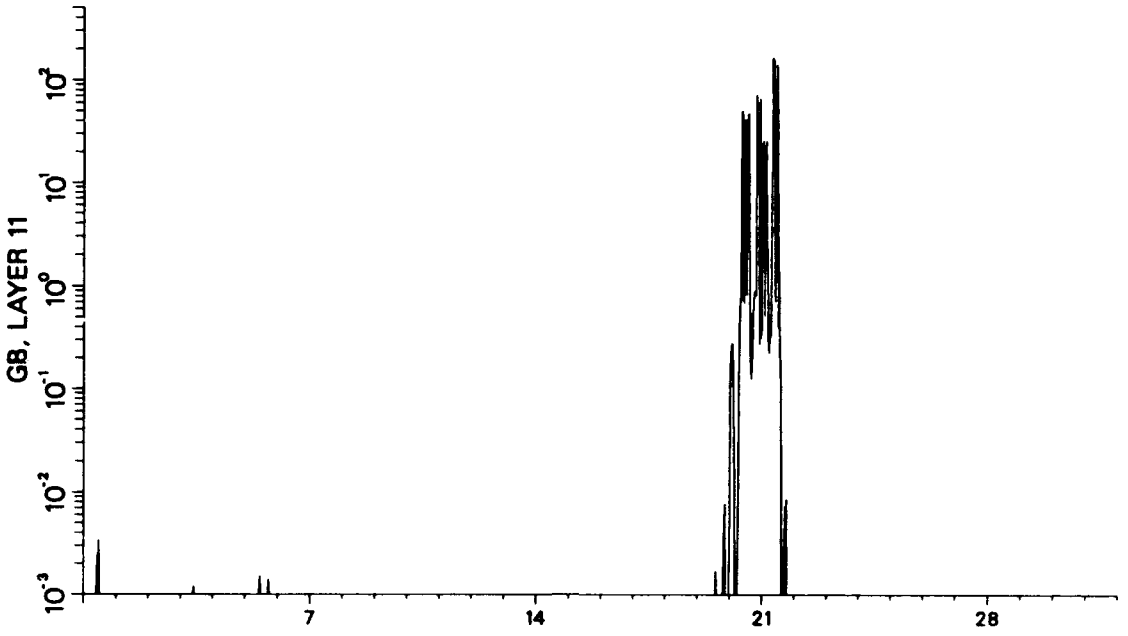

c. Depth = 22.5 ft

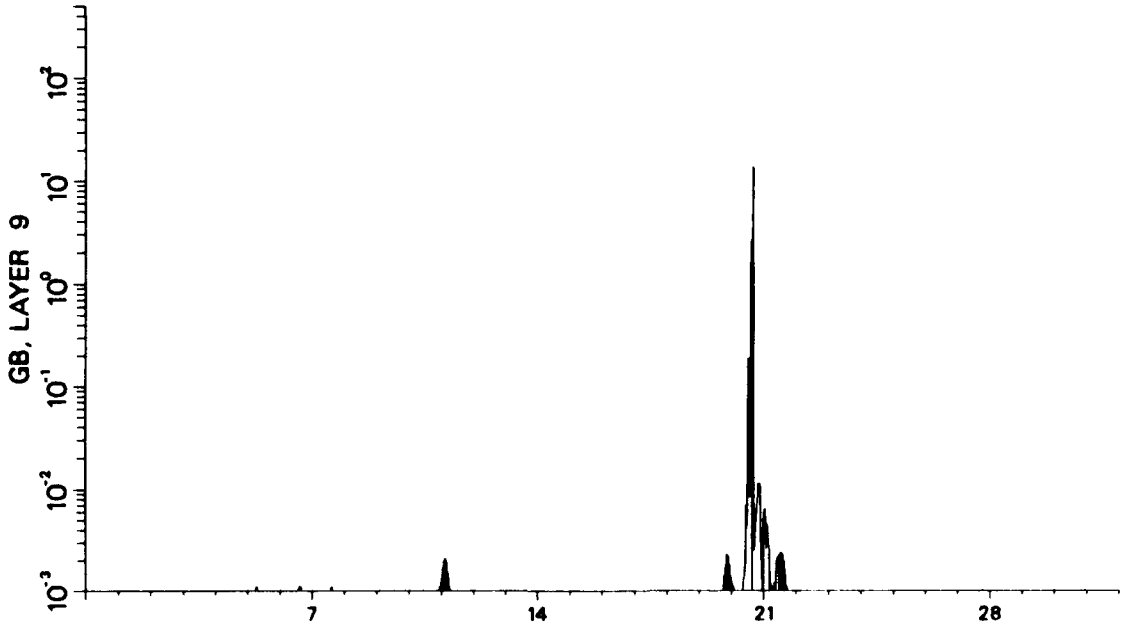

d. Depth = 32.5 ft

Figure 73. (Sheet 2 of 4)

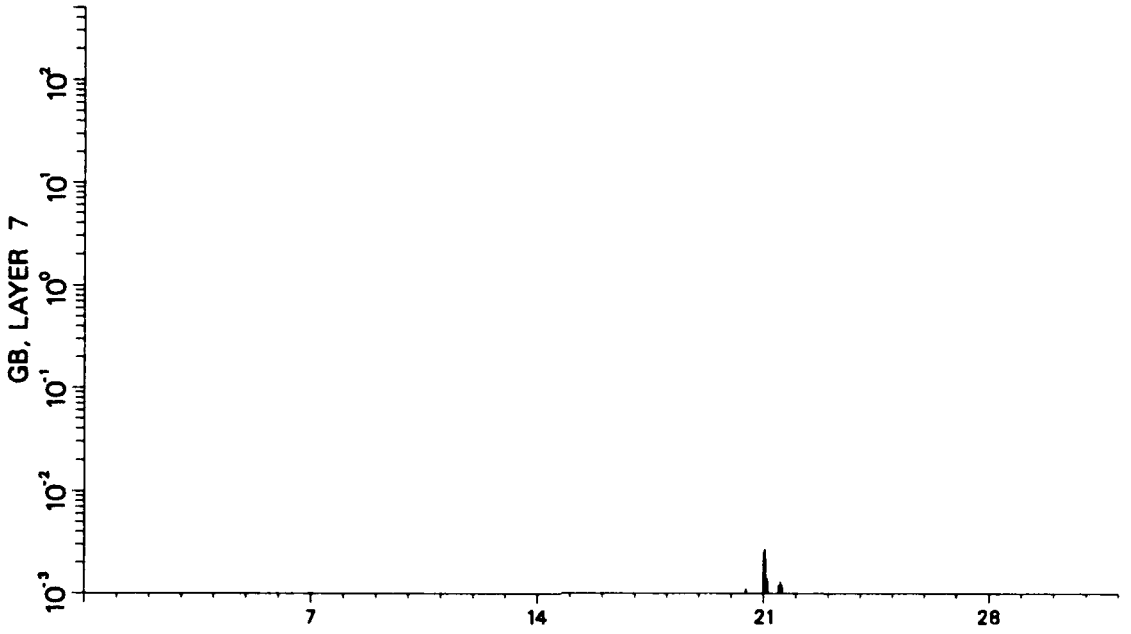

e. Depth = 42.5 ft

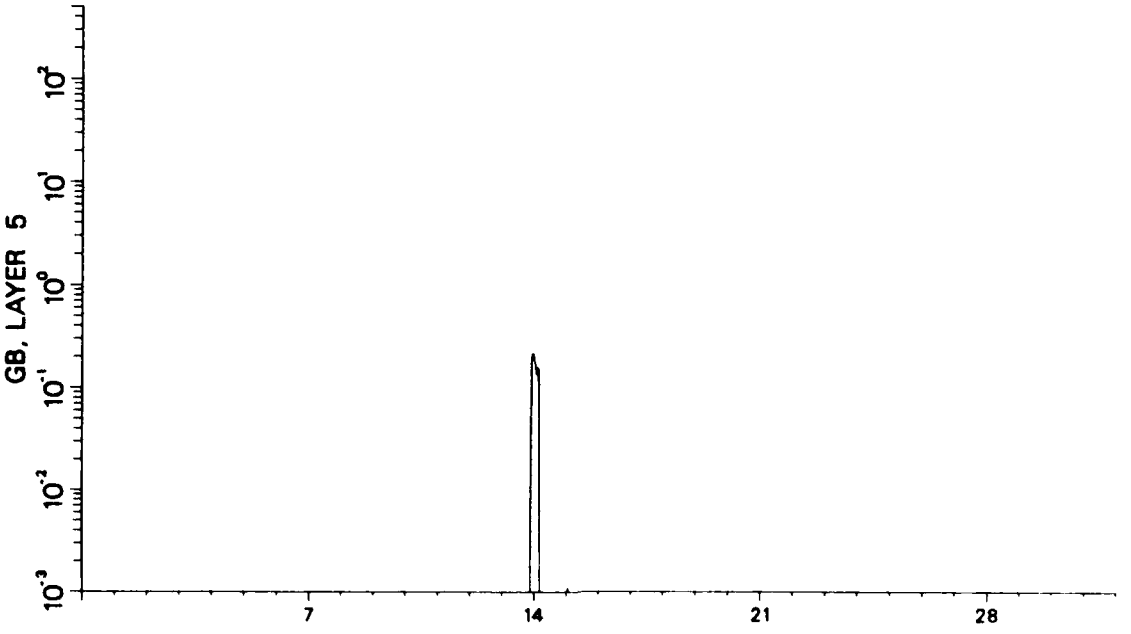

f. Depth = 52.5 ft

Figure 73. (Sheet 3 of 4)

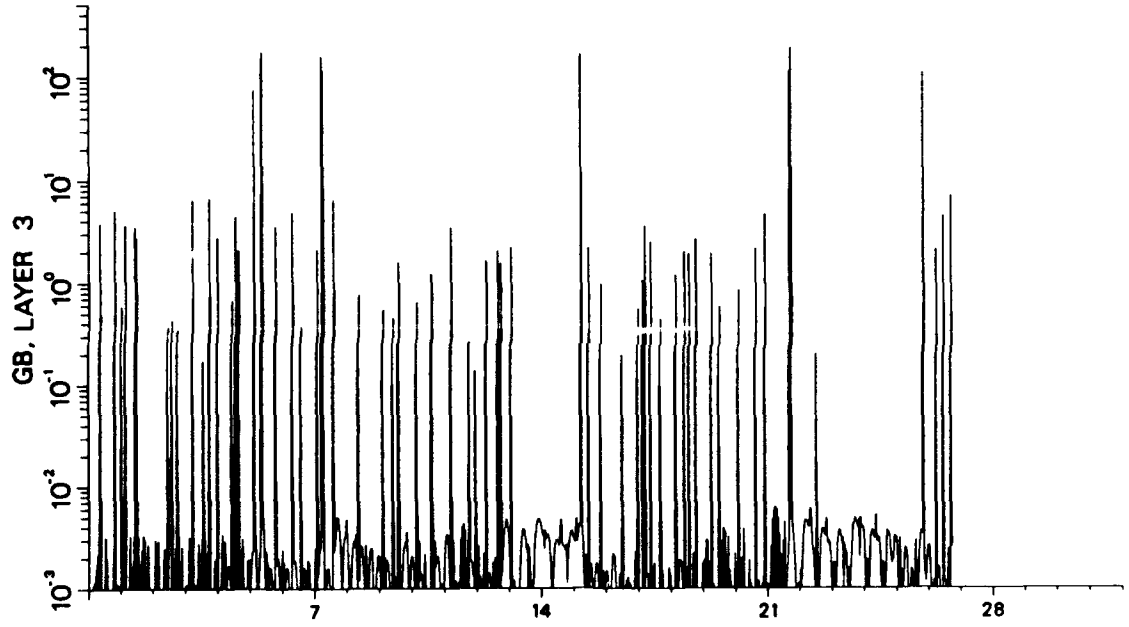

g. Depth = 62.5 ft

Figure 73. (Sheet 4 of 4)

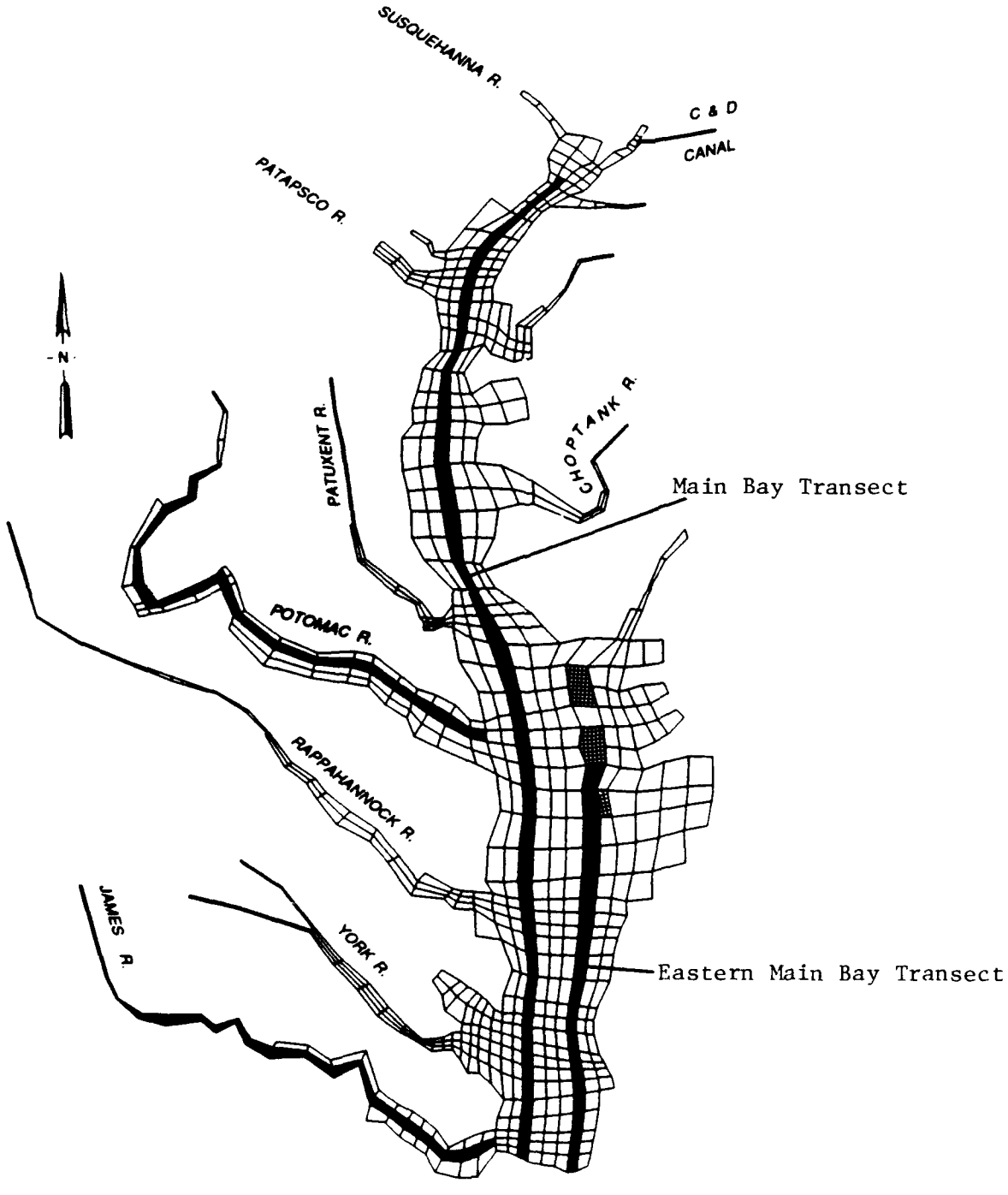

Figure 74. Longitudinal transects

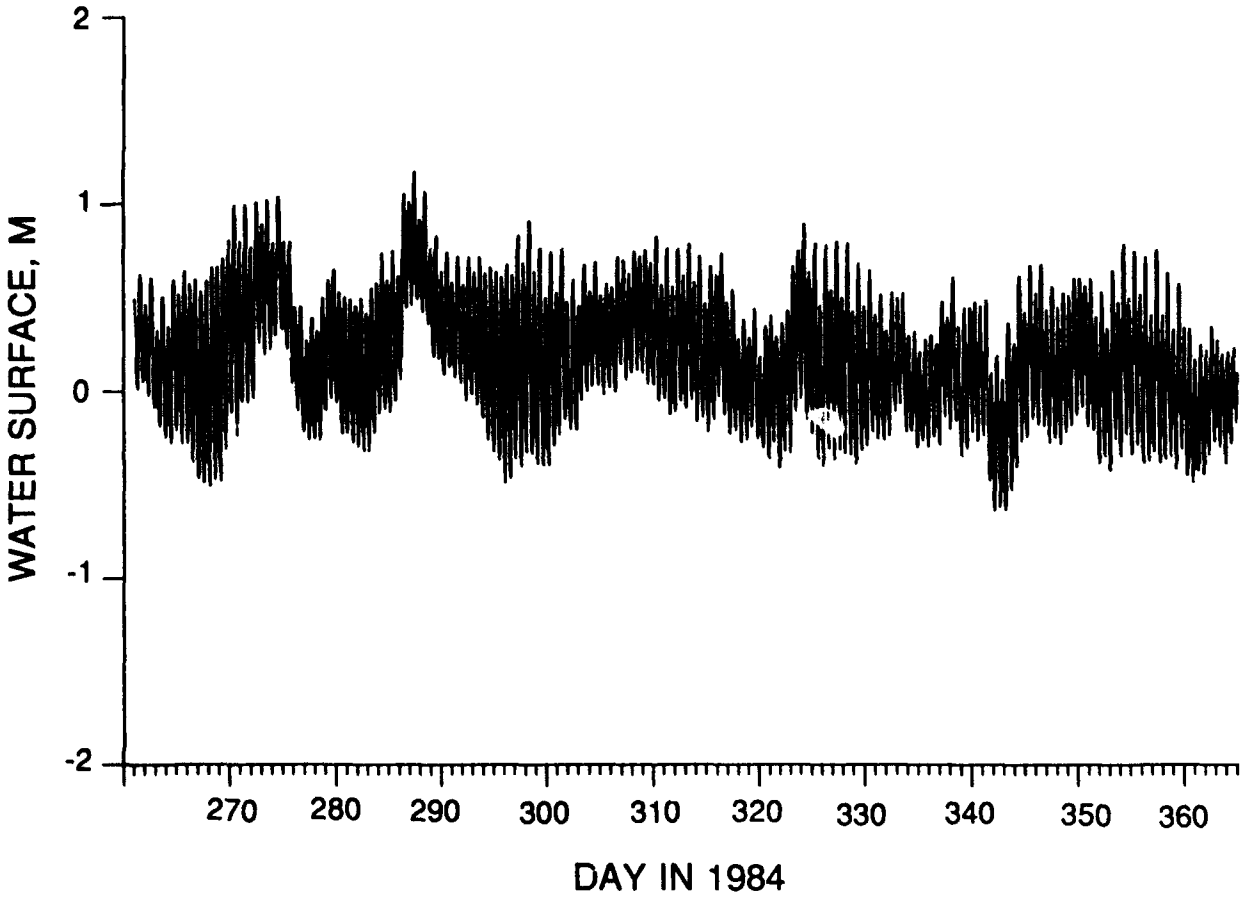

Figure 75. Ocean boundary tide at the Chesapeake Bay Tunnel during 1984

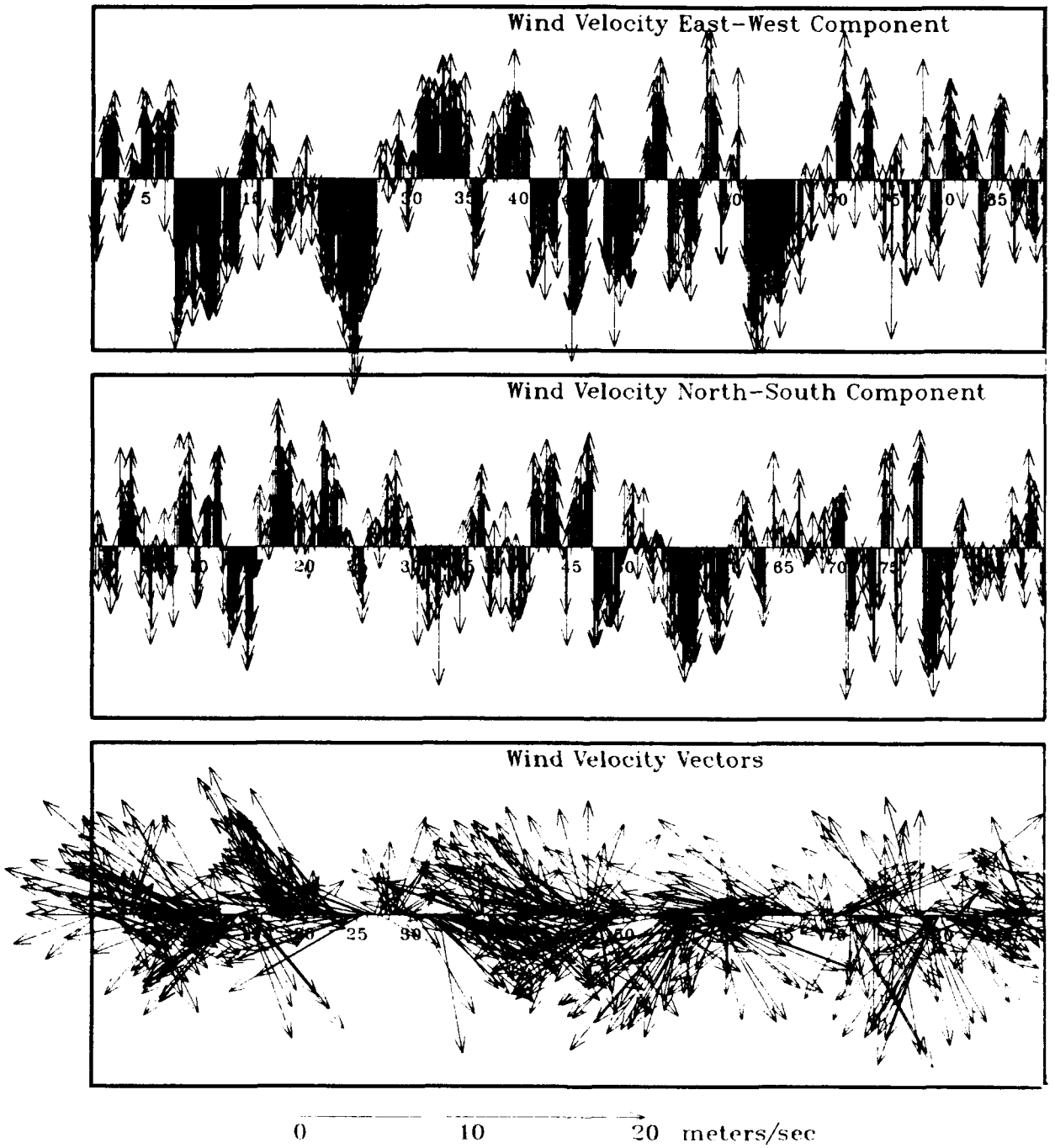

Figure 76. Wind data at the Norfolk International Airport during 1984. Day 0 corresponds to day 262 of 1984.

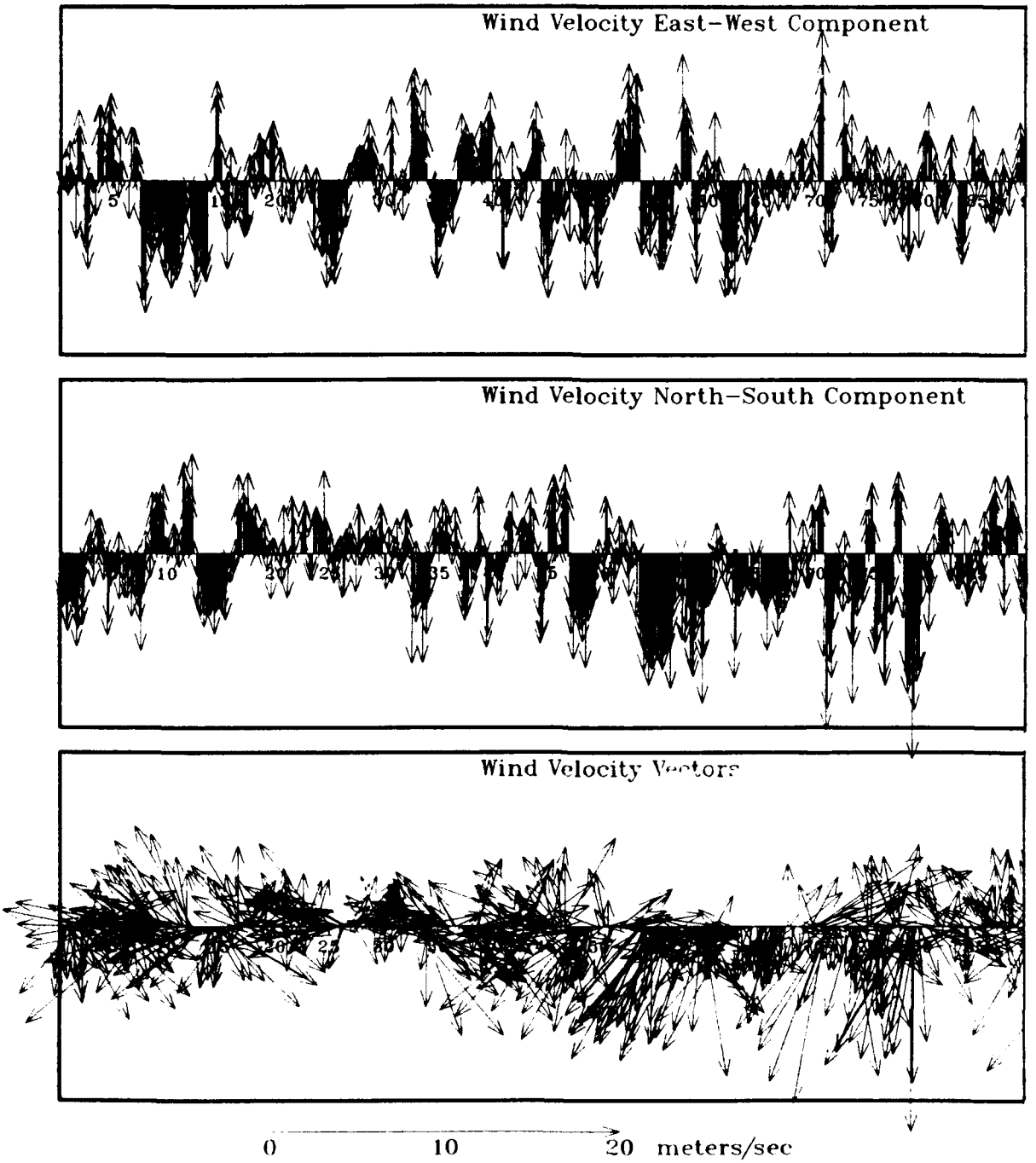

Figure 77. Wind data at the BWI station during 1984. Day 0 corresponds to day 262 of 1984.

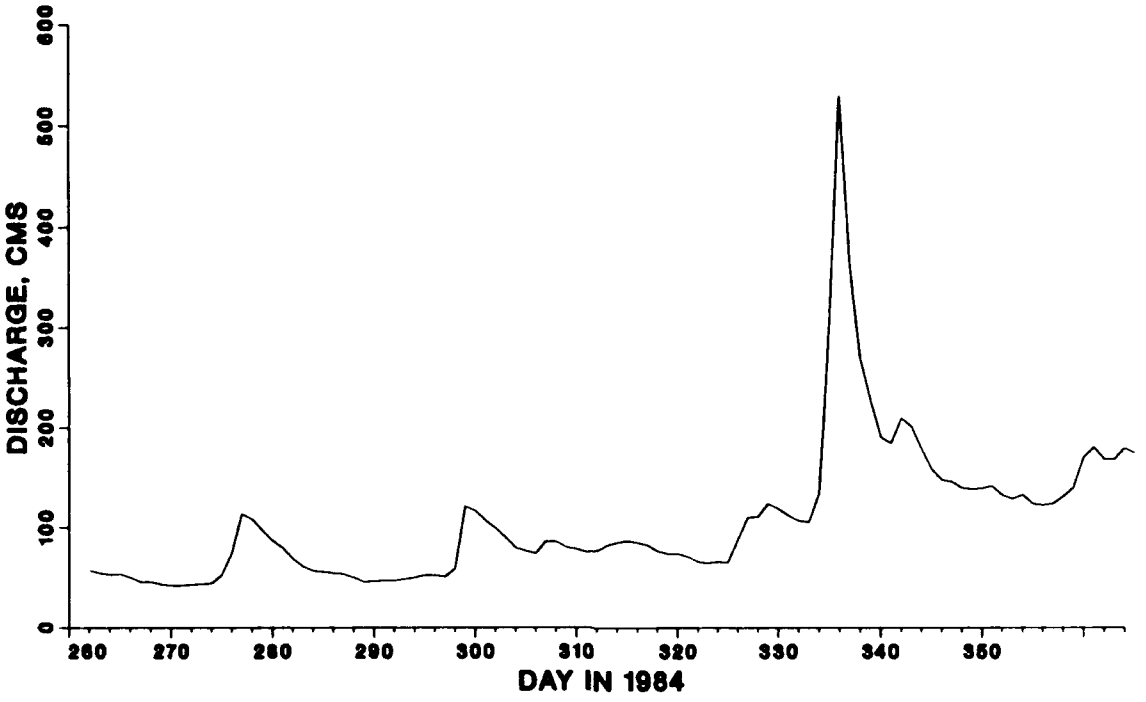

a. James River

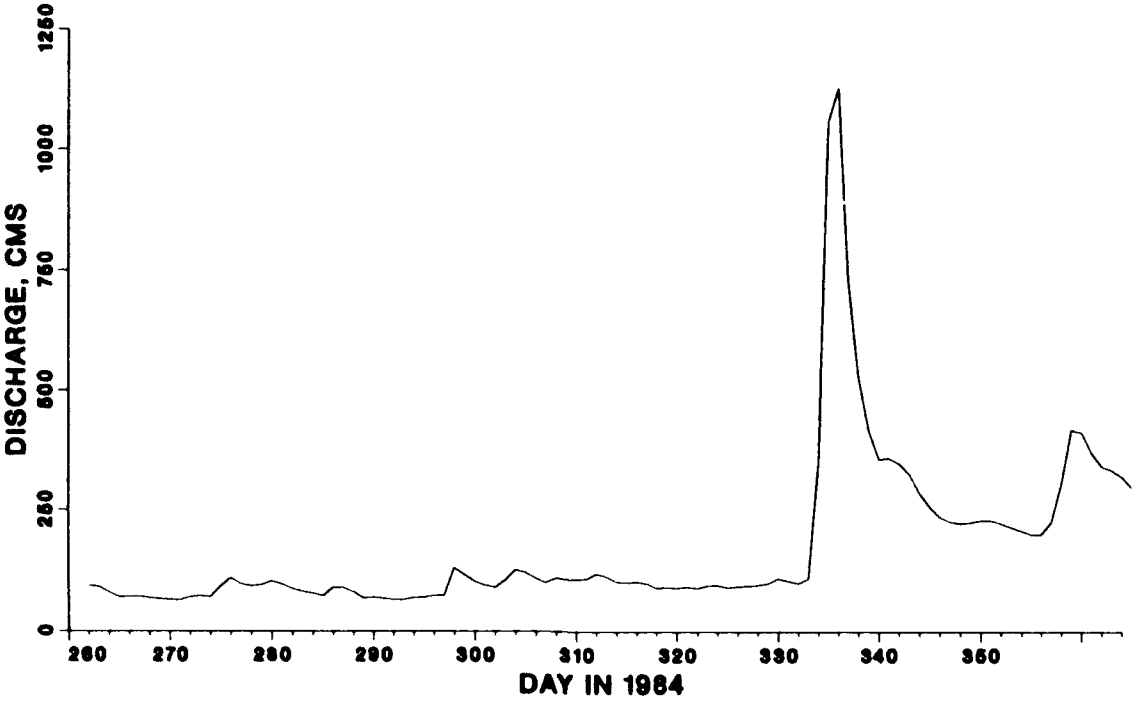

b. Potomac River

Figure 78. Freshwater inflows during 1984 (Continued)

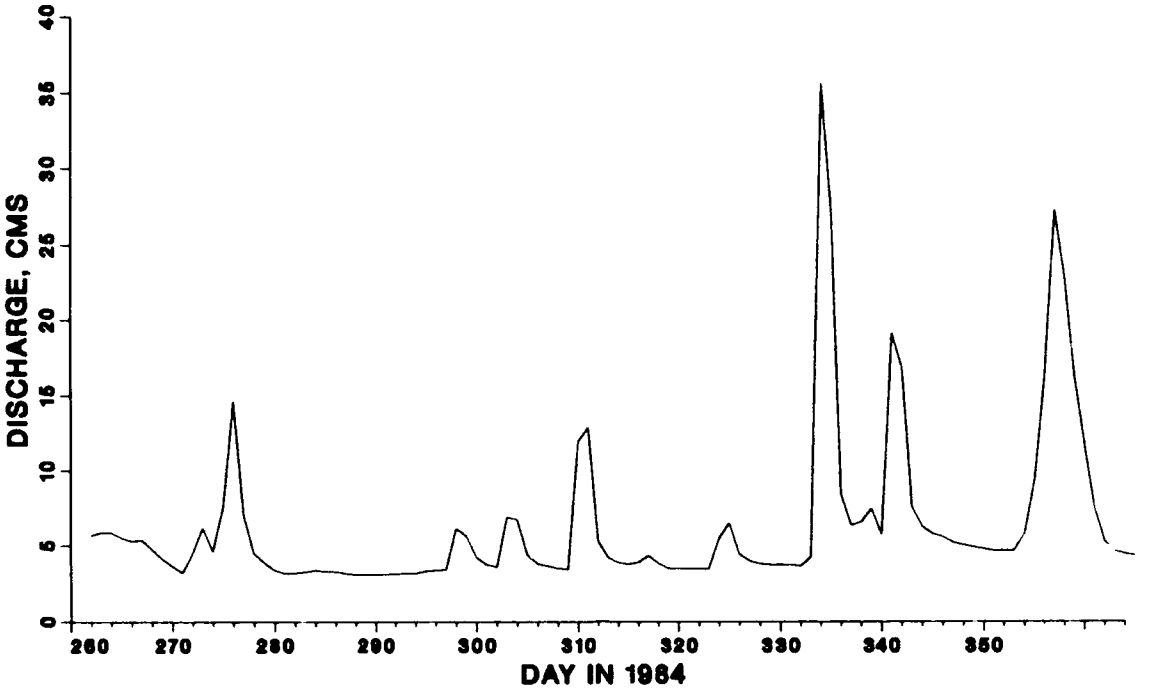

c. Patuxent River

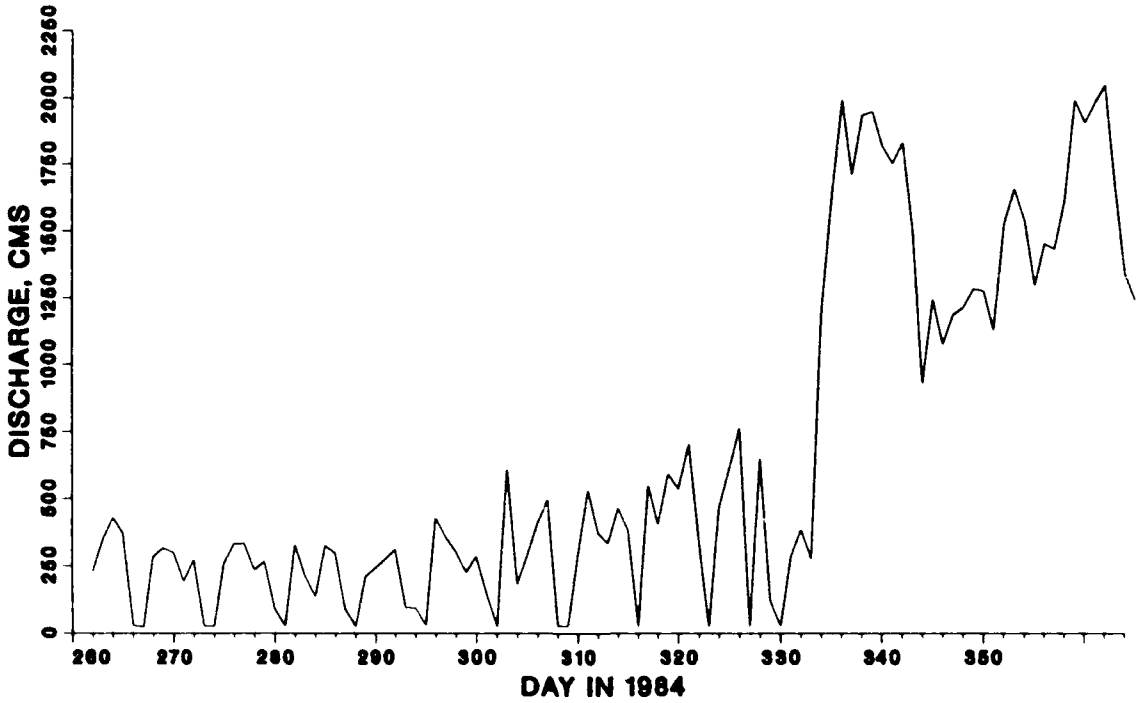

d. Susquehanna River

Figure 78. (Concluded)

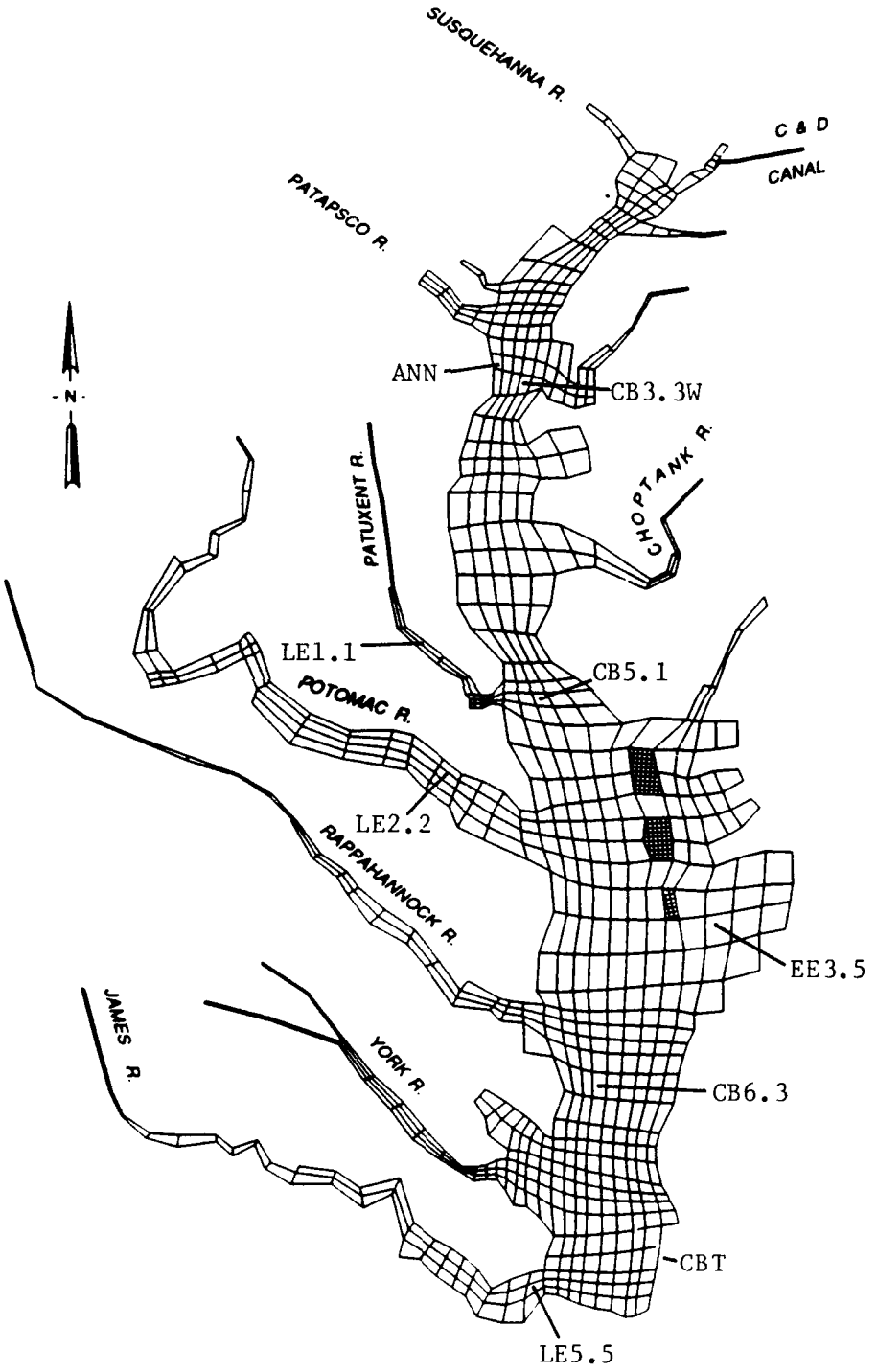

Figure 79. Data stations for 1984 data set

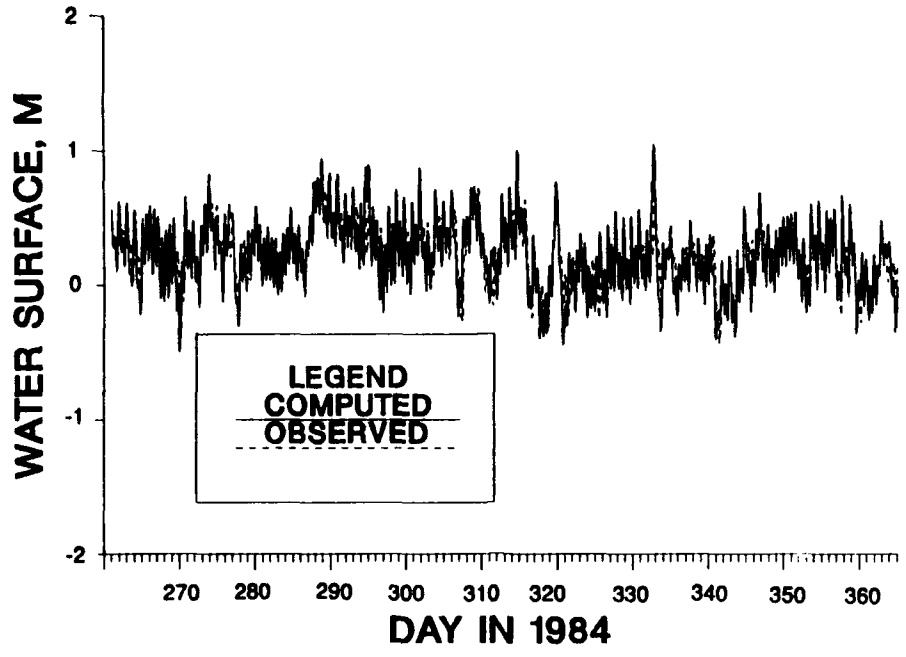

Figure 80. Comparison of computed and recorded tide at Annapolis, MD, during 1984

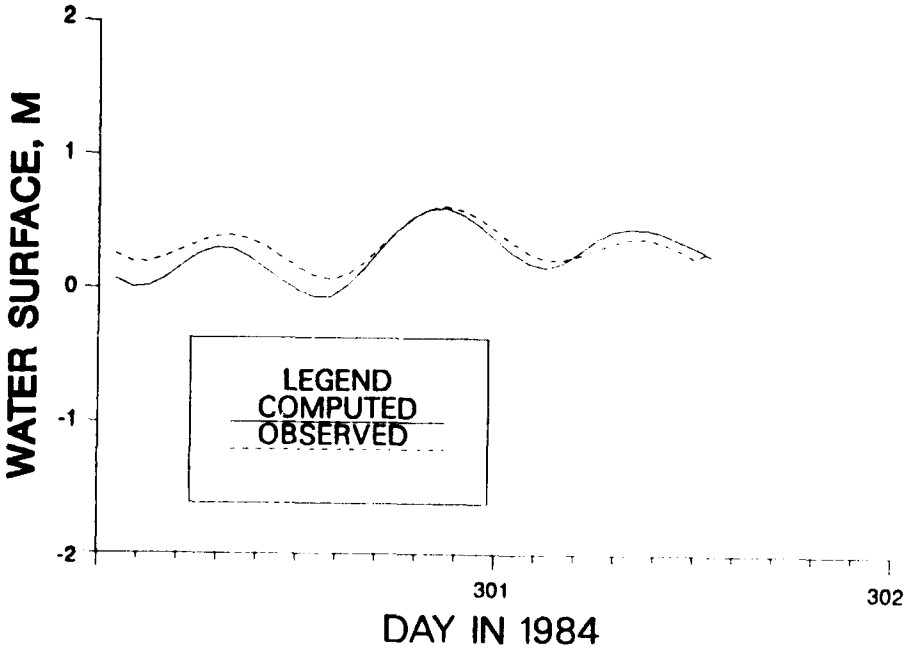

Figure 81. Comparison of computed and recorded tide at Annapolis, MD, near day 301 of 1984

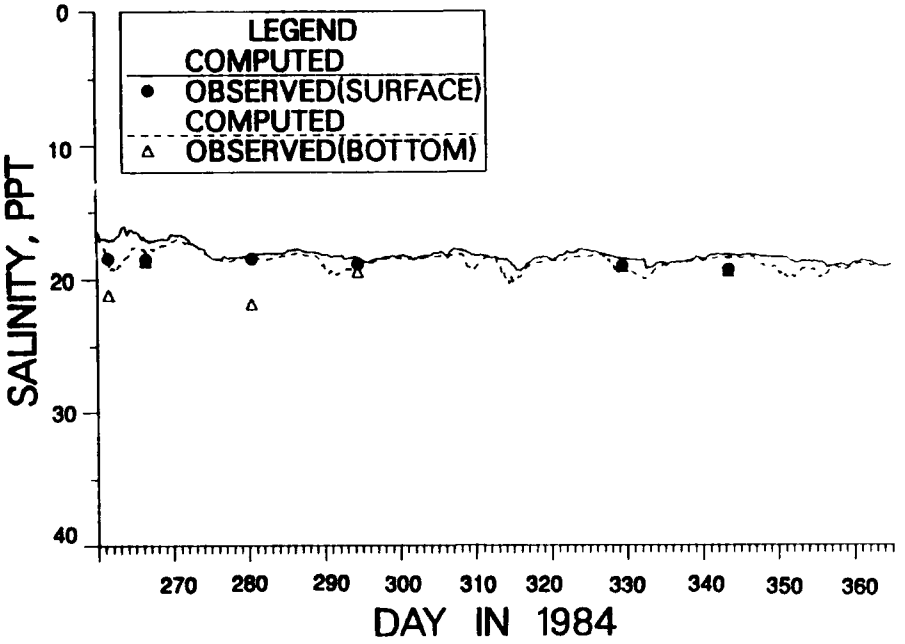

Figure 82. Comparison of computed and recorded salinity at station EE 3.5 during 1984

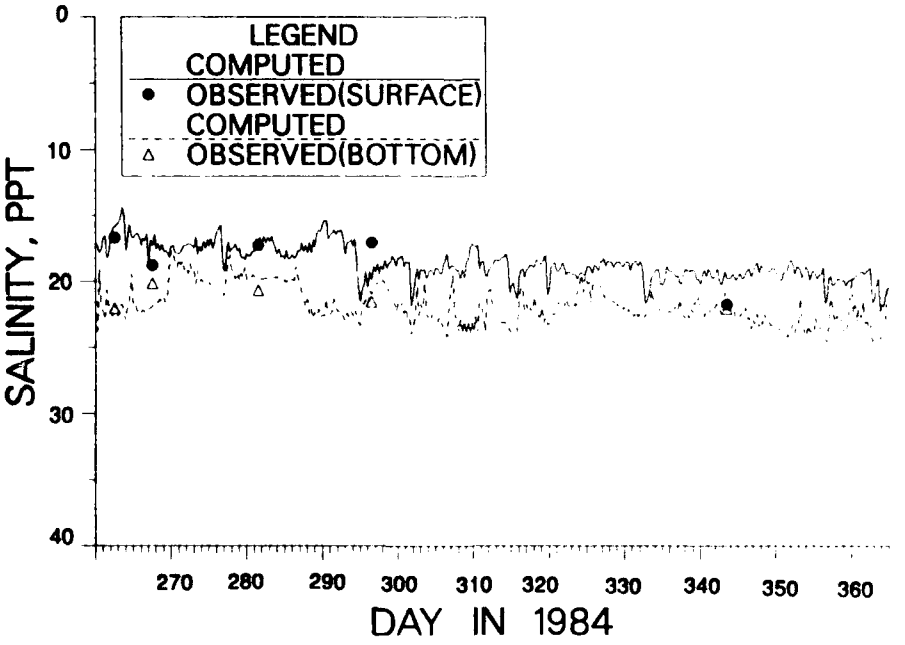

Figure 83. Comparison of computed and recorded salinity at station CB 6.3 during 1984

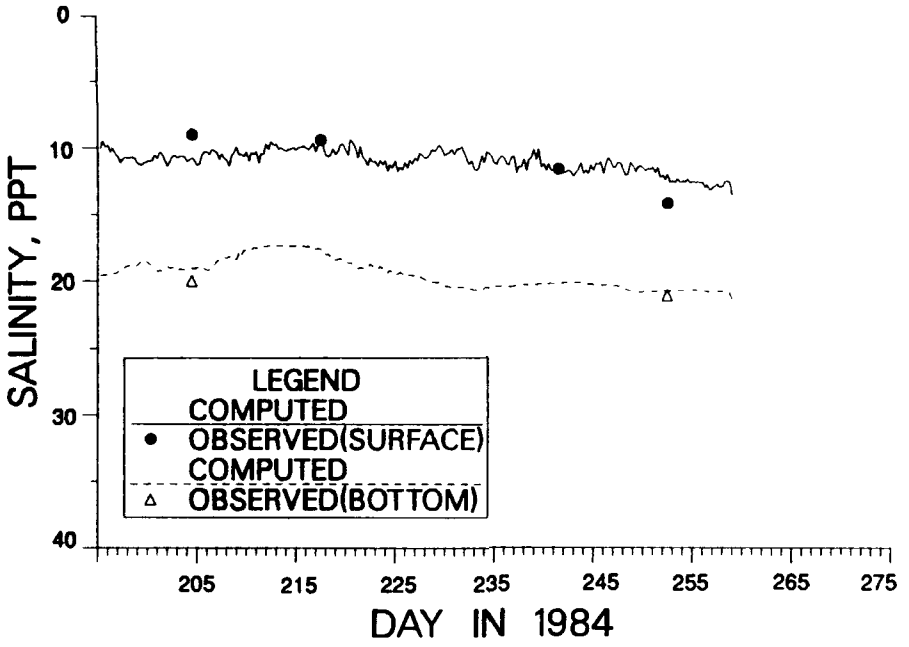

Figure 84. Comparison of computed and recorded salinity at station CB 5.1 during season 4 of 1984

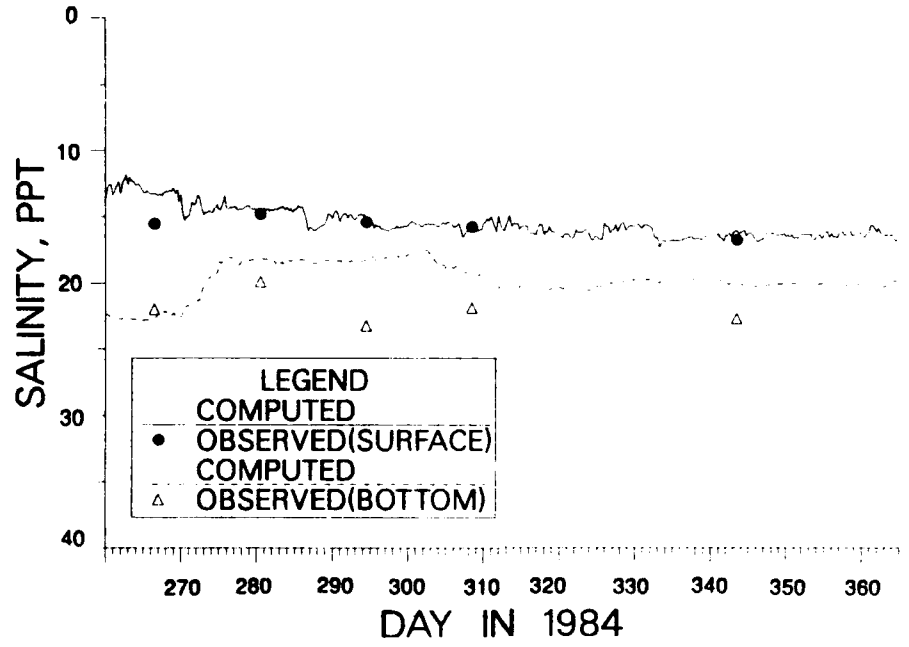

Figure 85. Comparison of computed and recorded salinity at station CB 5.1 during season 5 of 1984

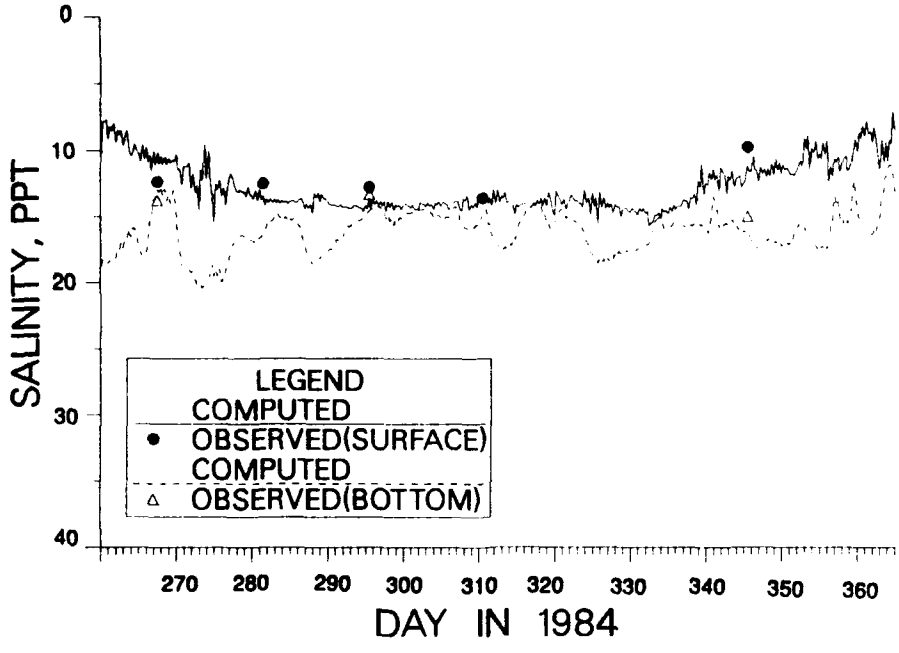

Figure 86. Comparison of computed and recorded salinity at station CB 3.3W during 1984

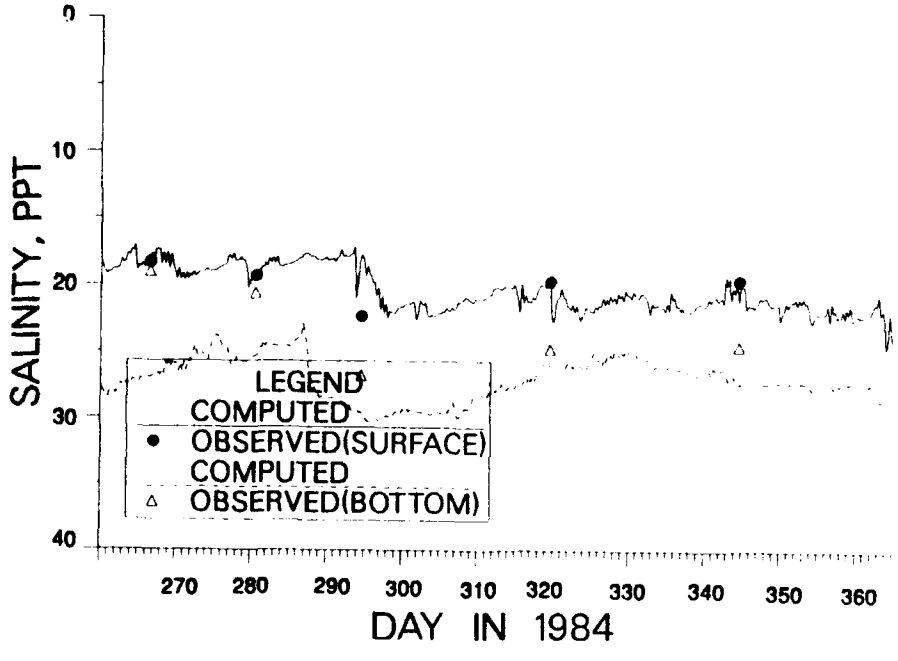

Figure 87. Comparison of computed and recorded salinity at station LE 5.5 during 1984

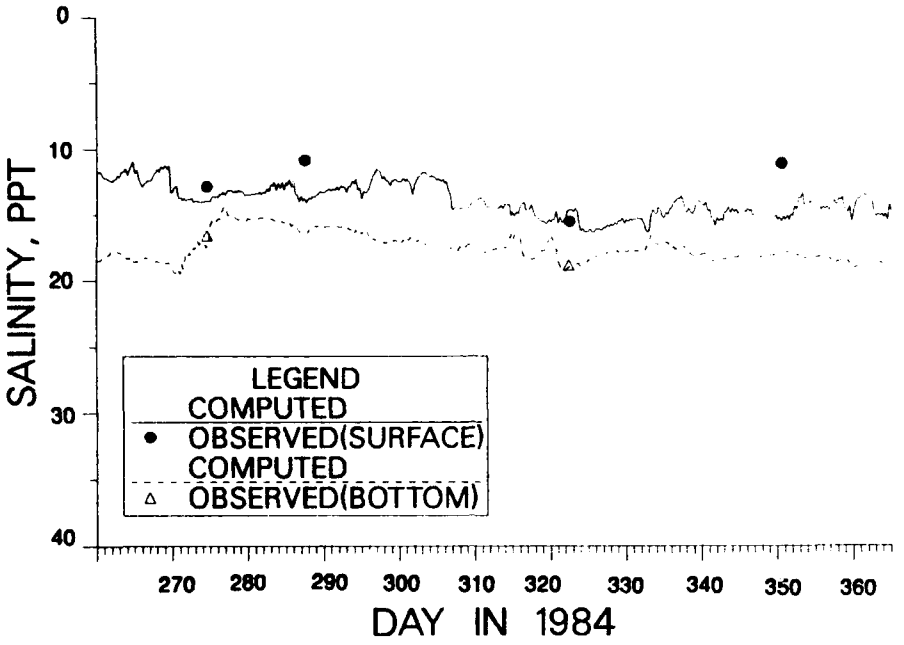

Figure 83. Comparison of computed and recorded salinity at station LE 2.2 during 1984

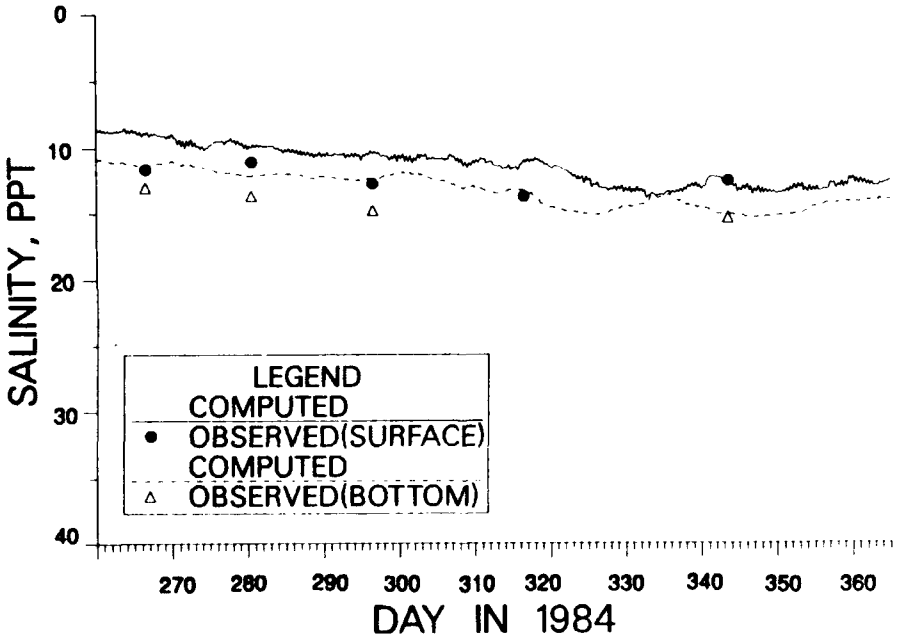

Figure 89. Comparison of computed and recorded salinity at station LE 1.1 during 1984

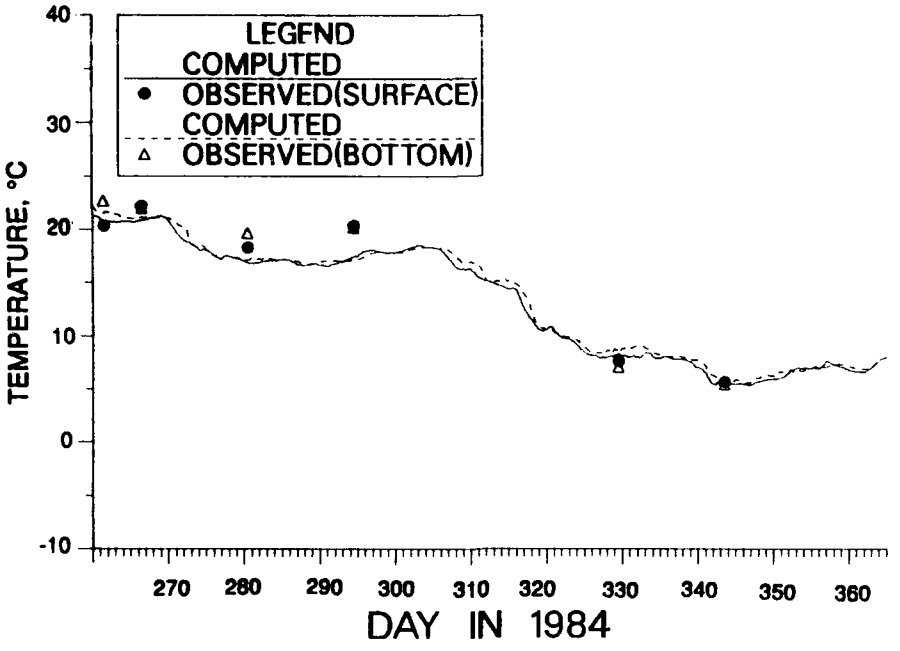

Figure 90. Comparison of computed and recorded temperature at station EE 3.5 during 1984

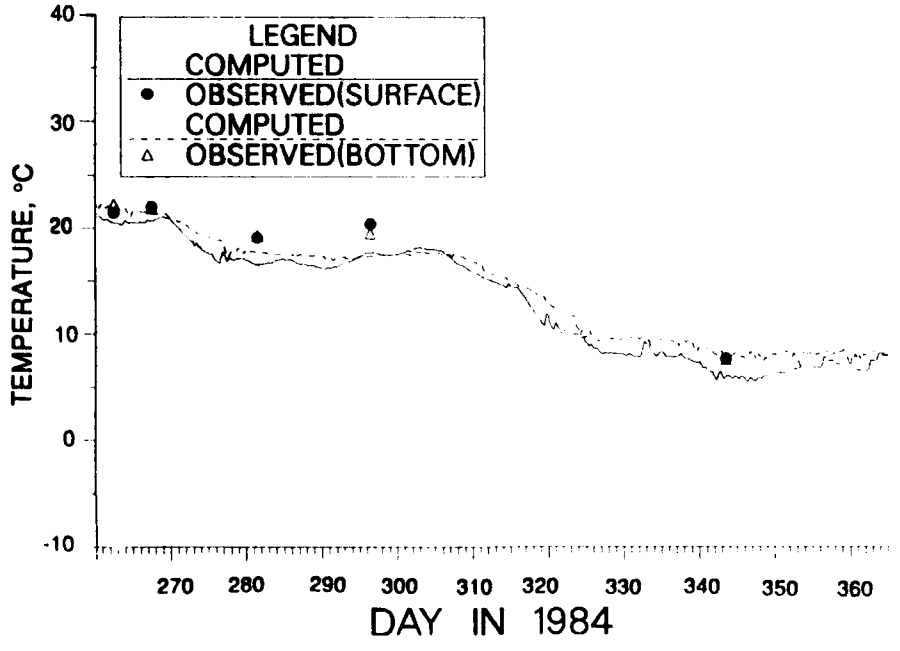

Figure 91. Comparison of computed and recorded temperature at station CB 6.3 during 1984

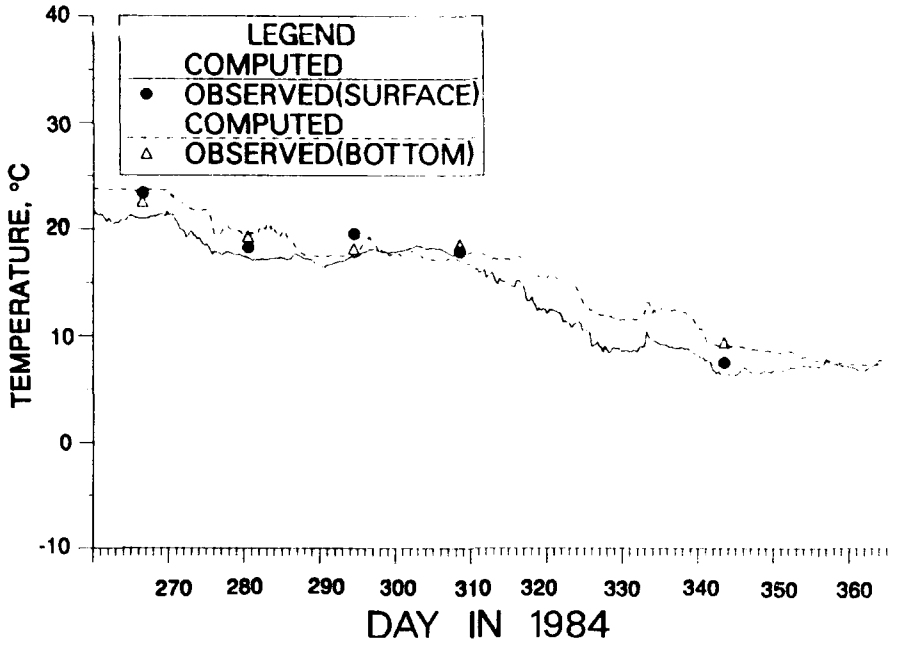

Figure 92. Comparison of computed and recorded temperature at station CB 5.1 during 1984

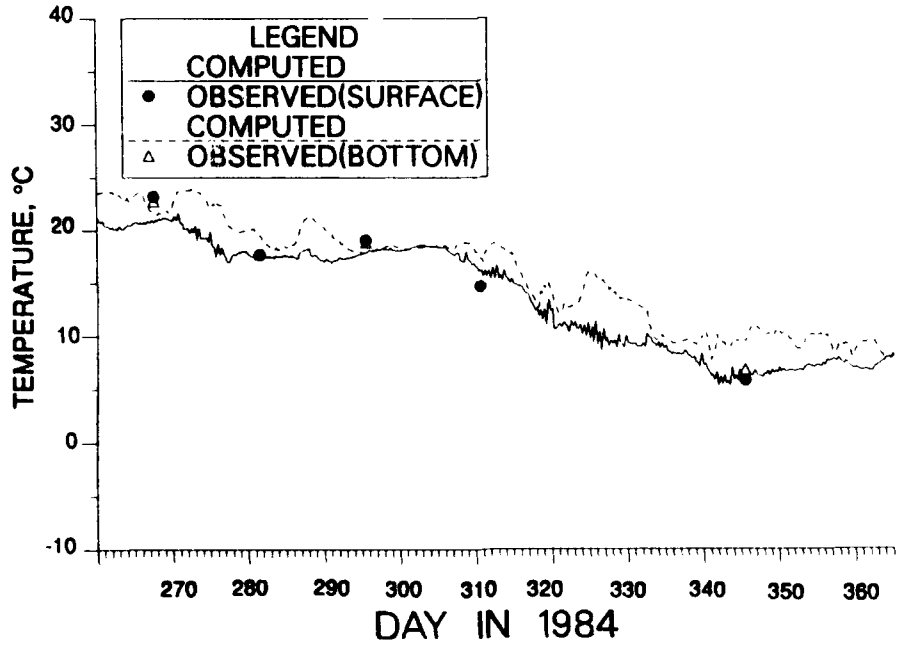

Figure 93. Comparison of computed and recorded temperature at station CB 3.3W during 1984

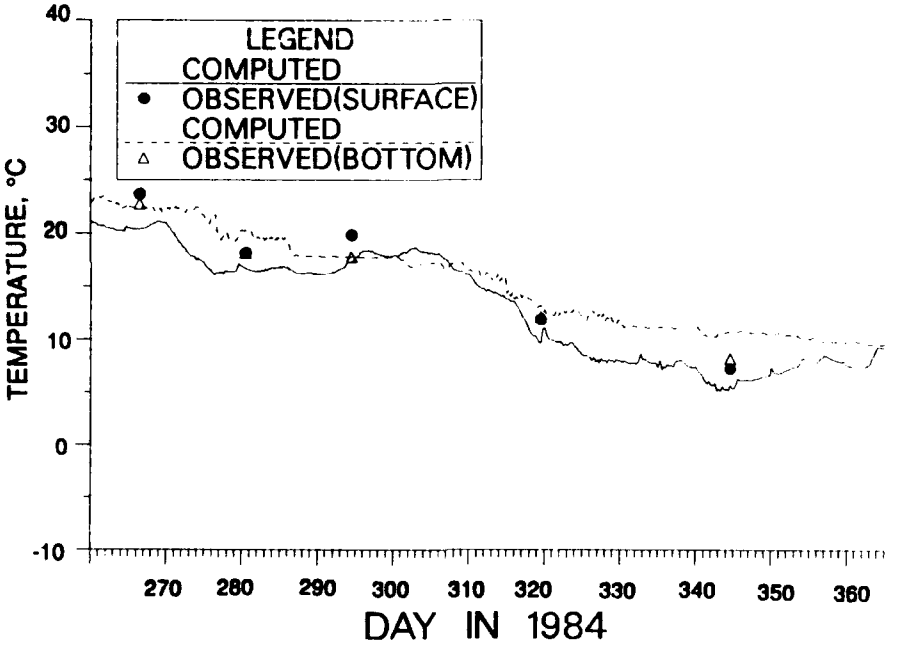

Figure 94. Comparison of computed and recorded temperature at station LE 5.5 during 1984

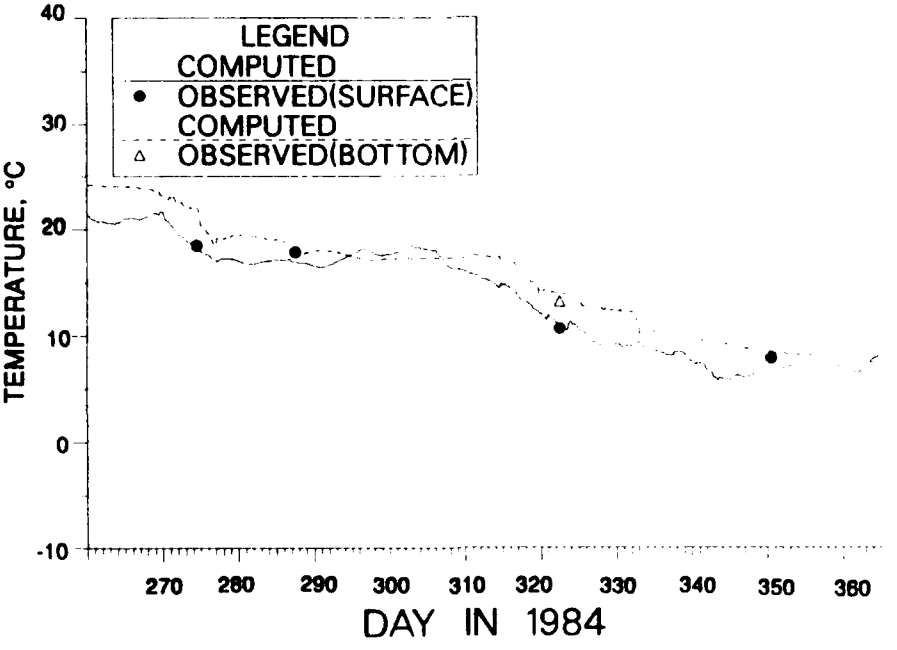

Figure 95. Comparison of computed and recorded temperature at station LE 2.2 during 1984

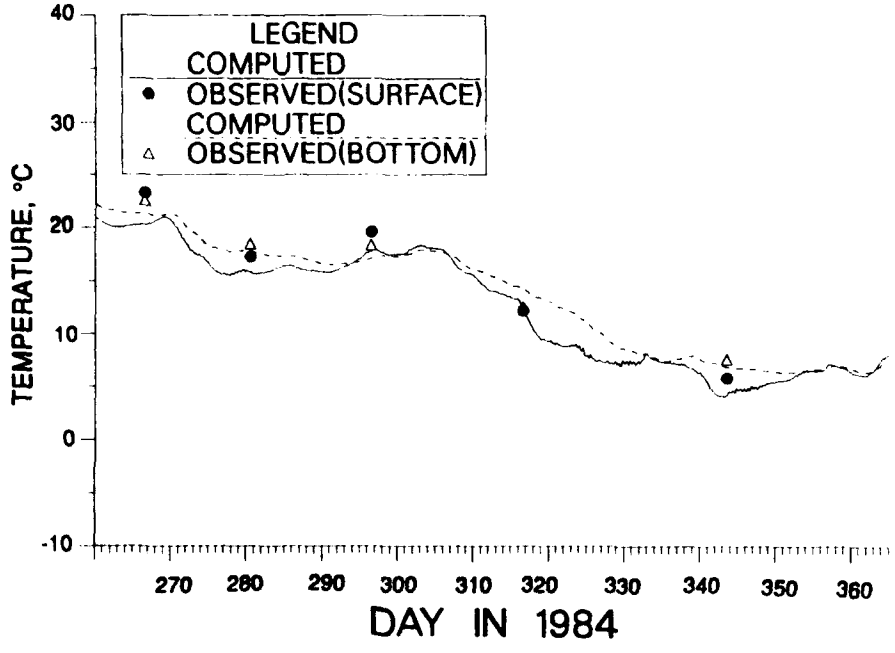

Figure 96. Comparison of computed and recorded temperature at station LE 1.1 during 1984

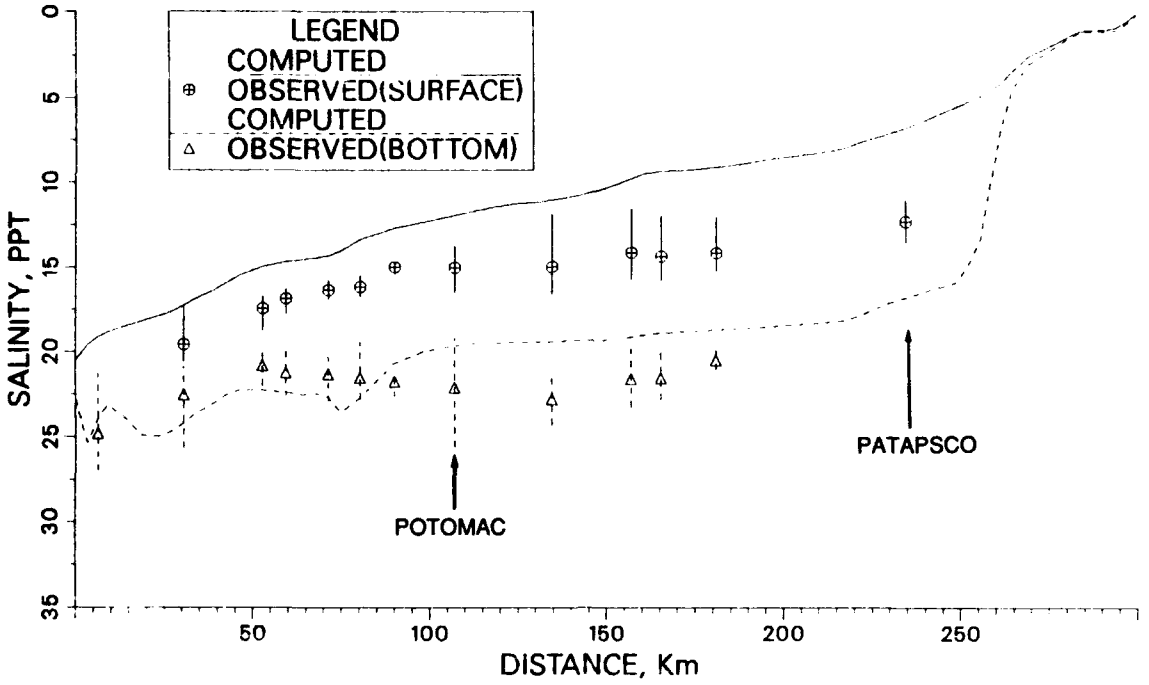

a. Season 4

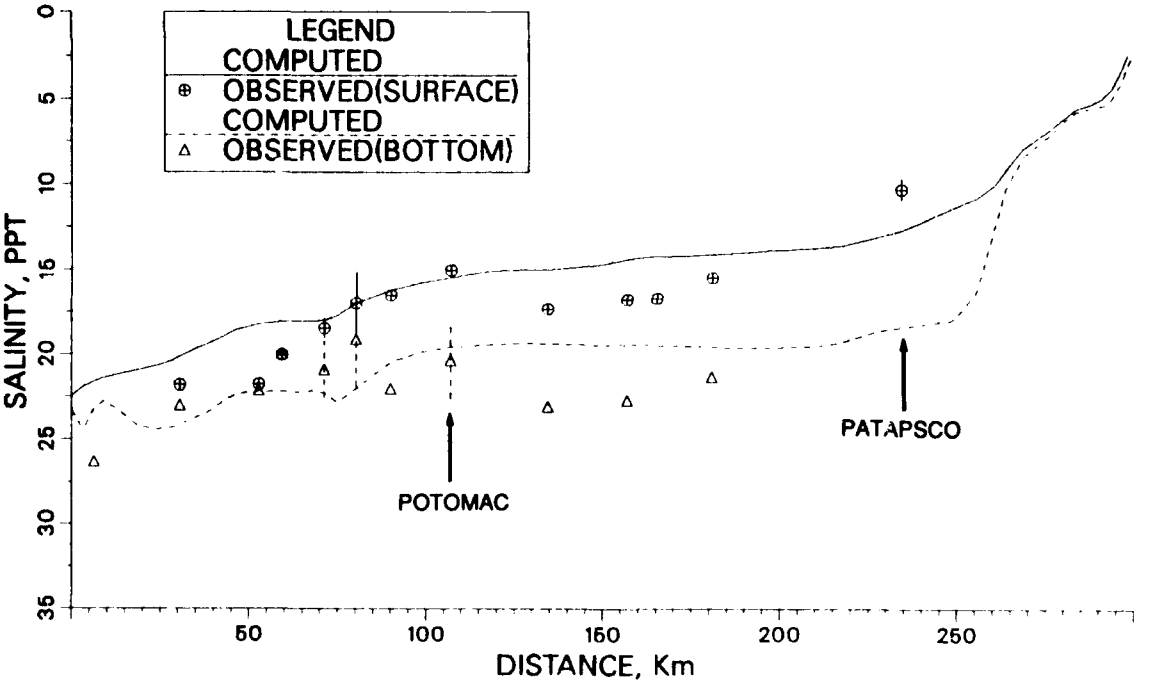

b. Season 5

Figure 97. Comparison of seasonally averaged salinities along the main bay during 1984

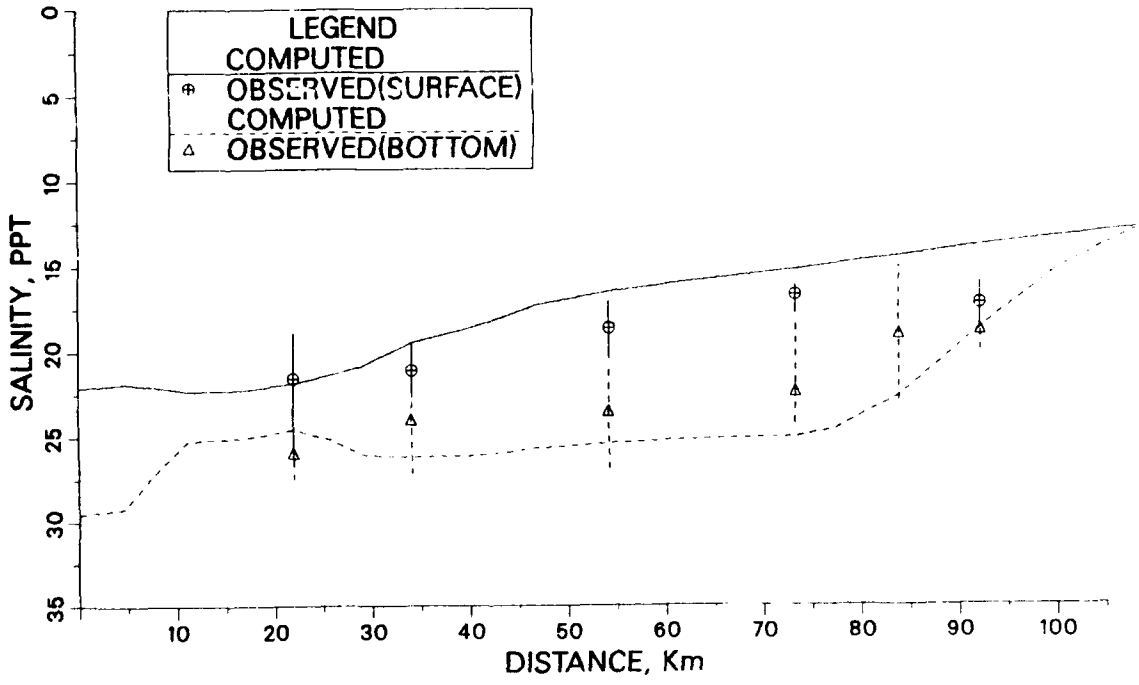

a. Season 4

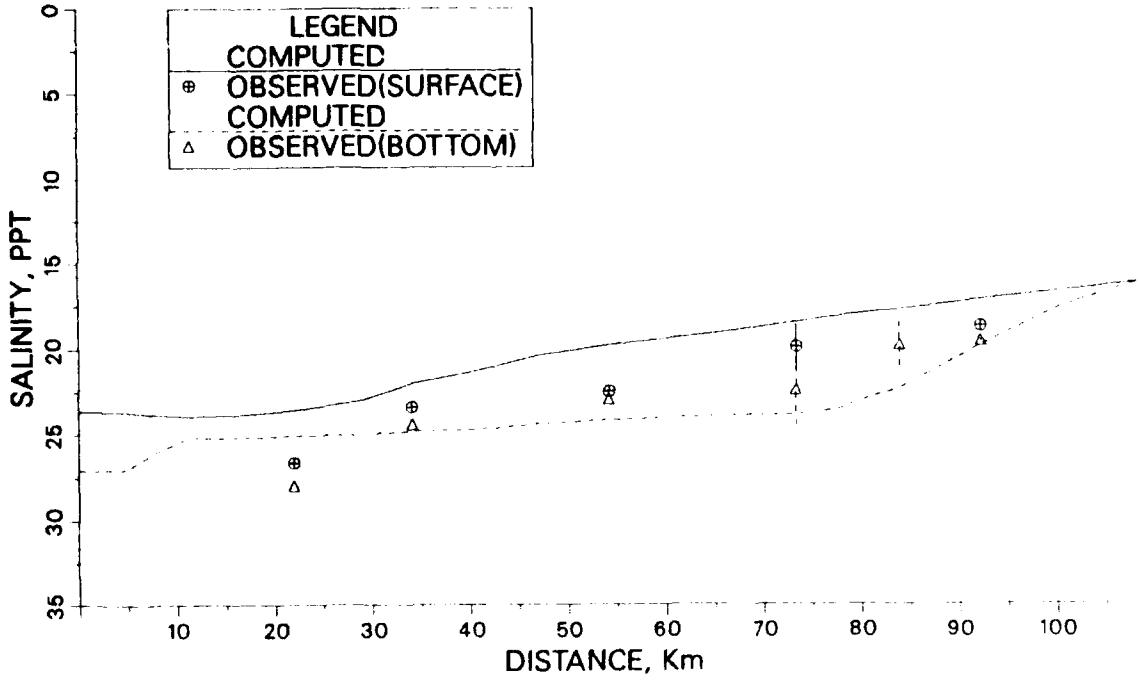

b. Season 5

Figure 98. Comparison of seasonally averaged salinities along the eastern main bay transect during 1984

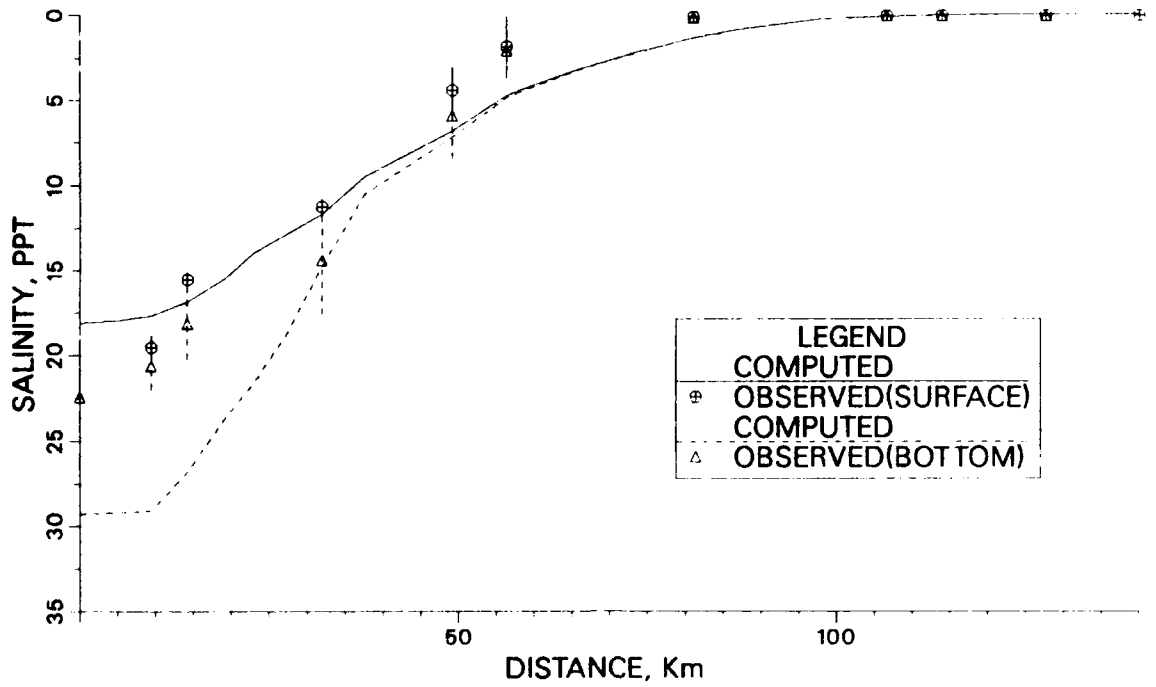

a. Season 4

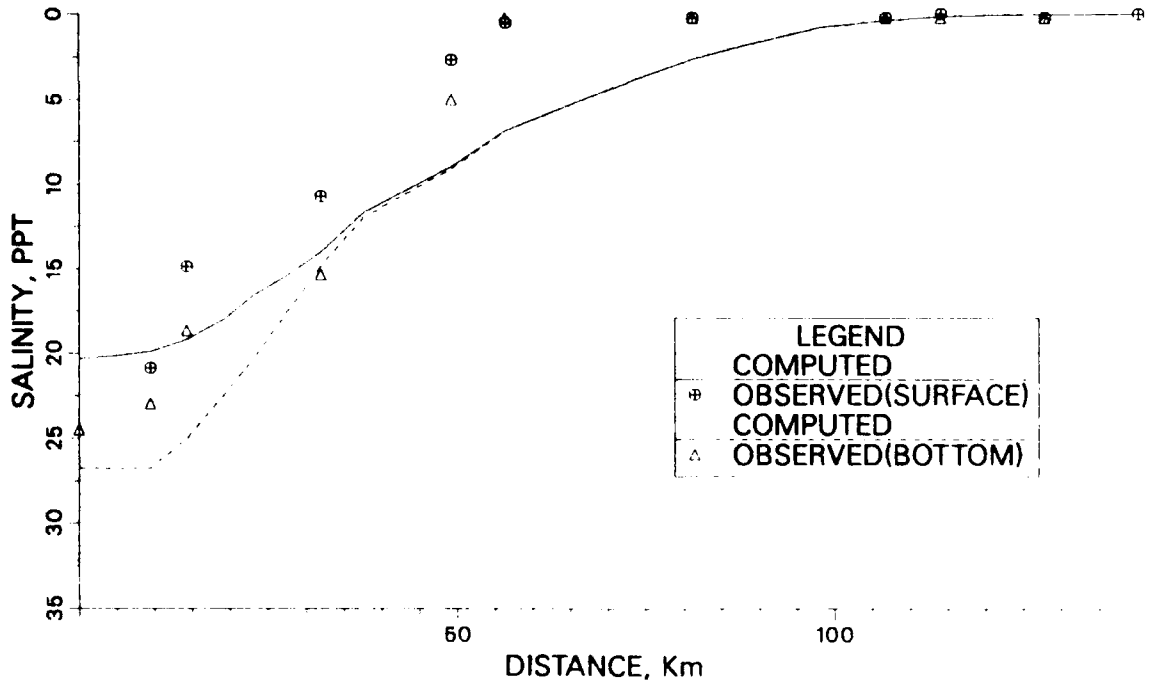

b. Season 5

Figure 99. Comparison of seasonally averaged salinities along the James River during 1984

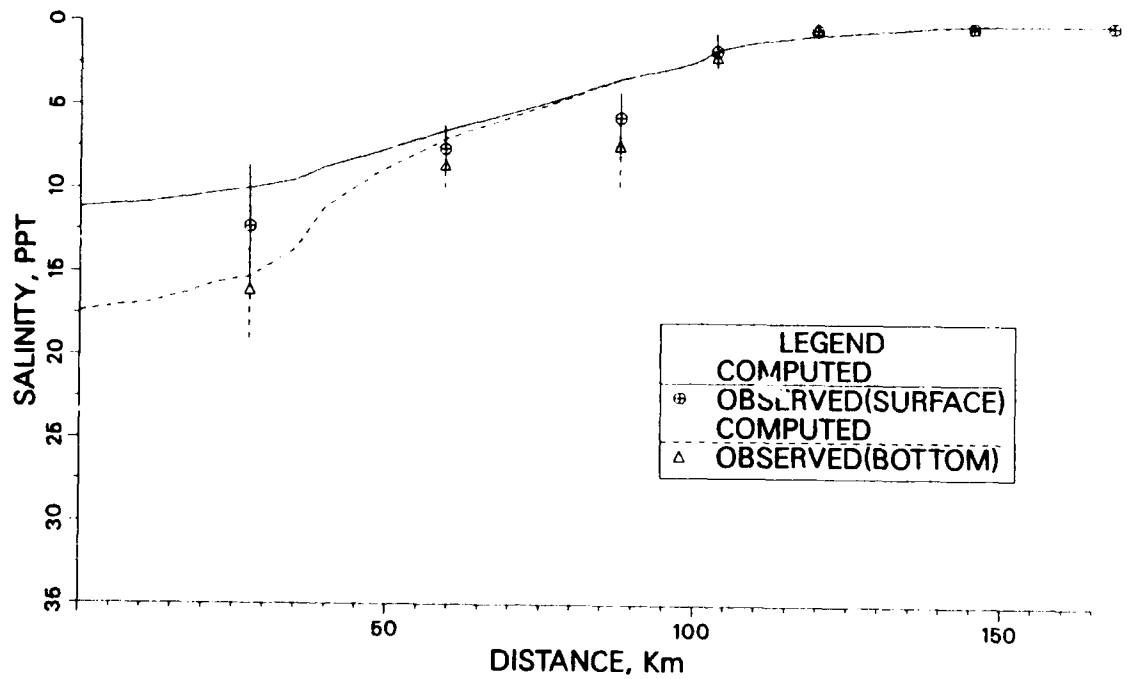

a. Season 4

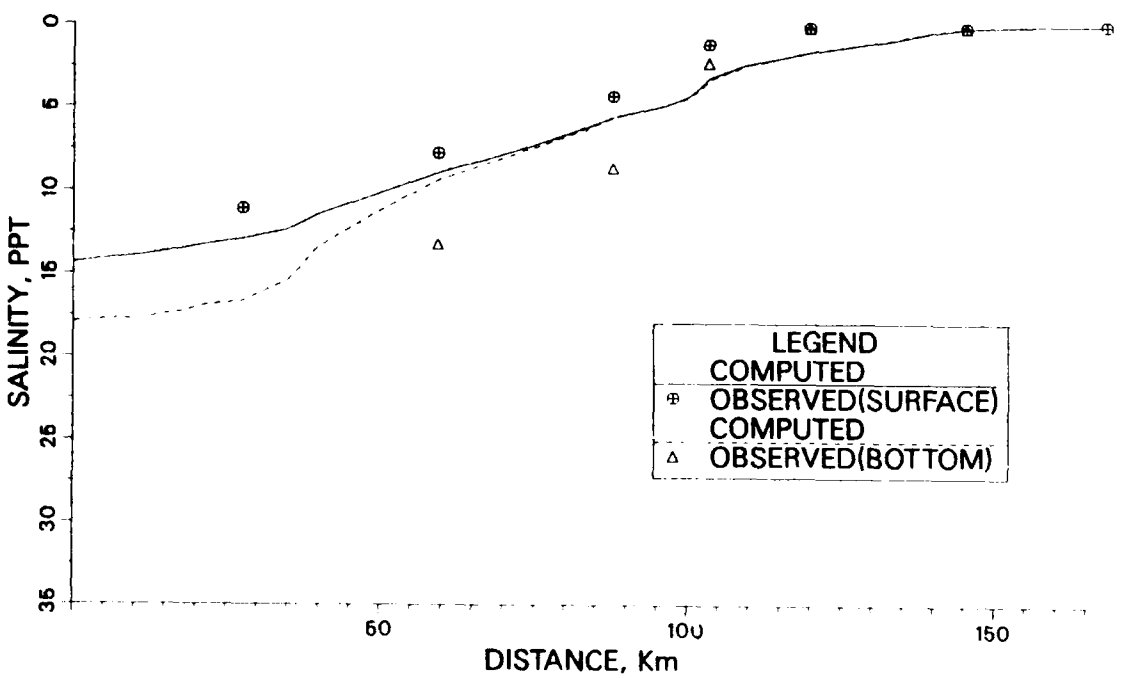

b. Season 5

Figure 100. Comparison of seasonally averaged salinities along the Potomac River during 1984

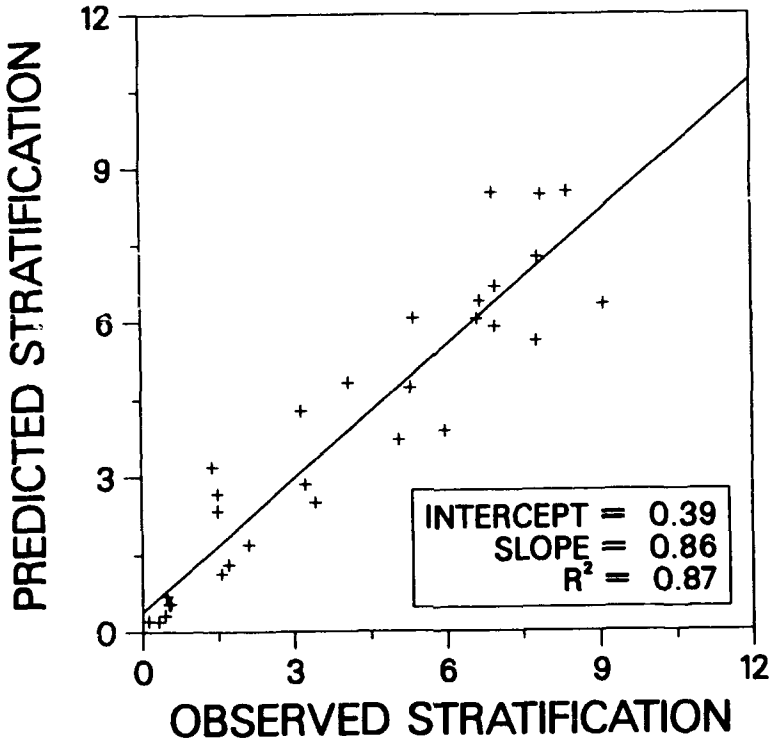

Figure 101. Comparison of computed and recorded stratification for all main bay stations during 1984

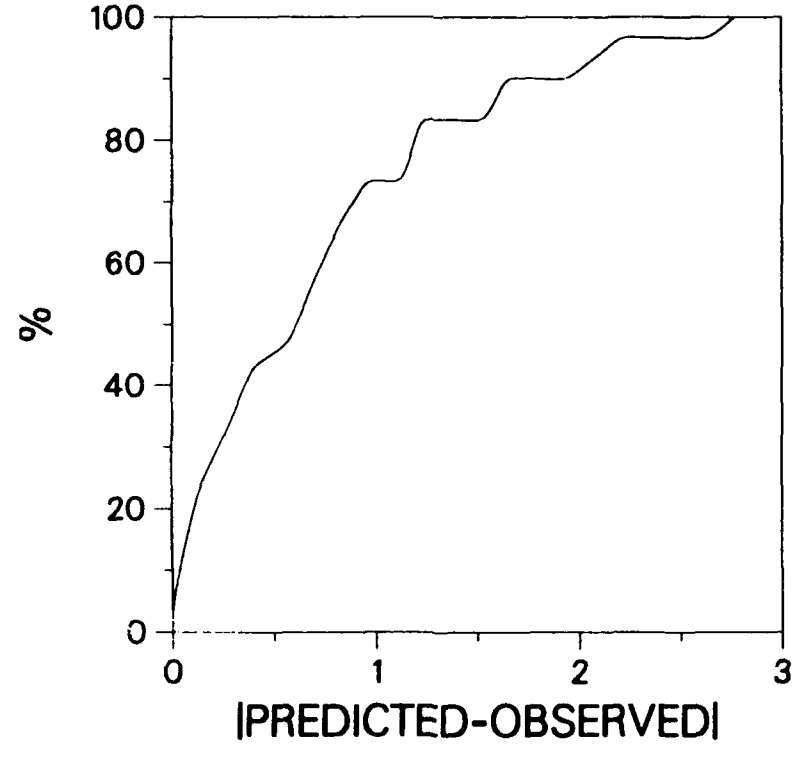

Figure 102. Frequency of occurrence of the error in the computed stratification for all main bay stations during 1984

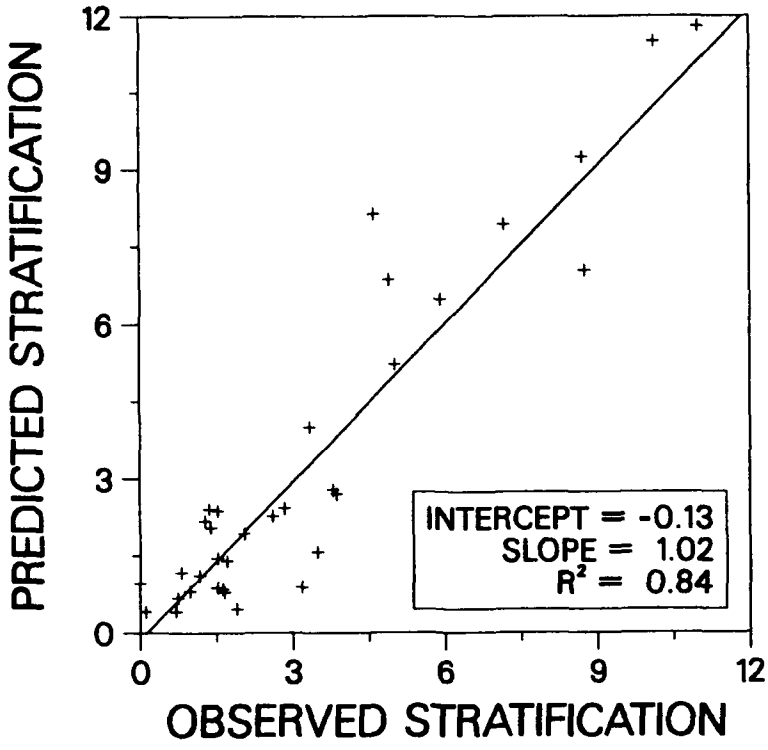

Figure 103. Comparison of computed and recorded stratification for all tributary stations during 1984

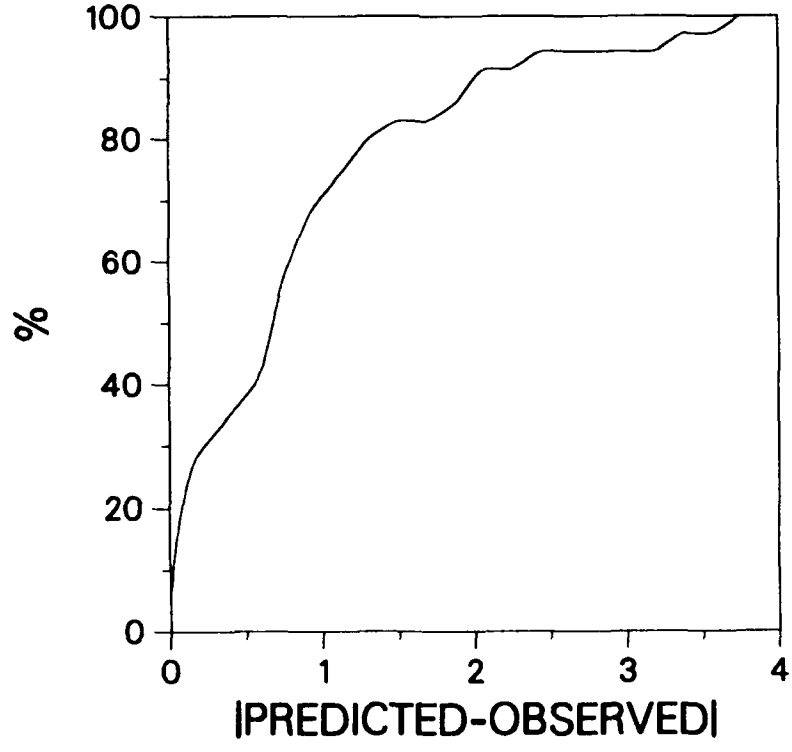

Figure 104. Frequency of occurrence of the error in the computed stratification for all tributary stations during 1984

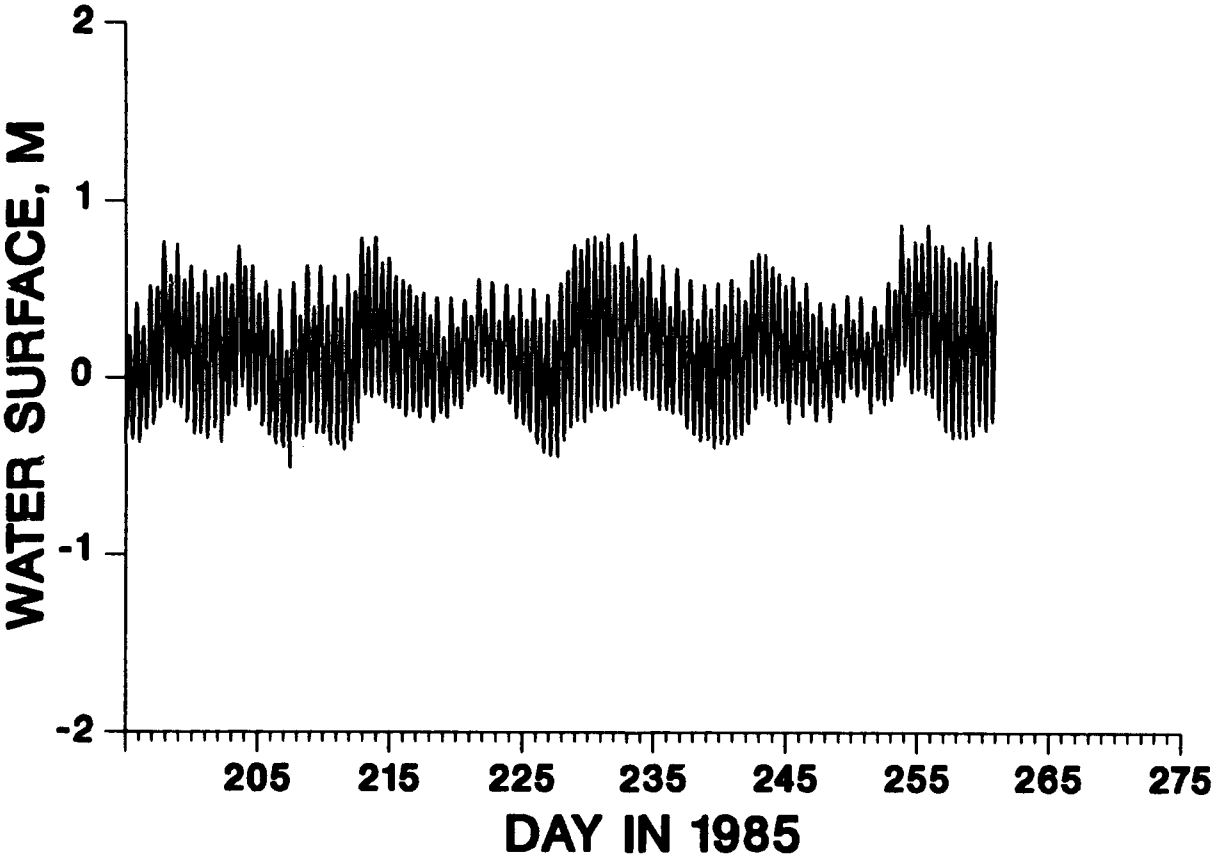

Figure 105. Ocean boundary tide at the Chesapeake Bay Tunnel during 1985

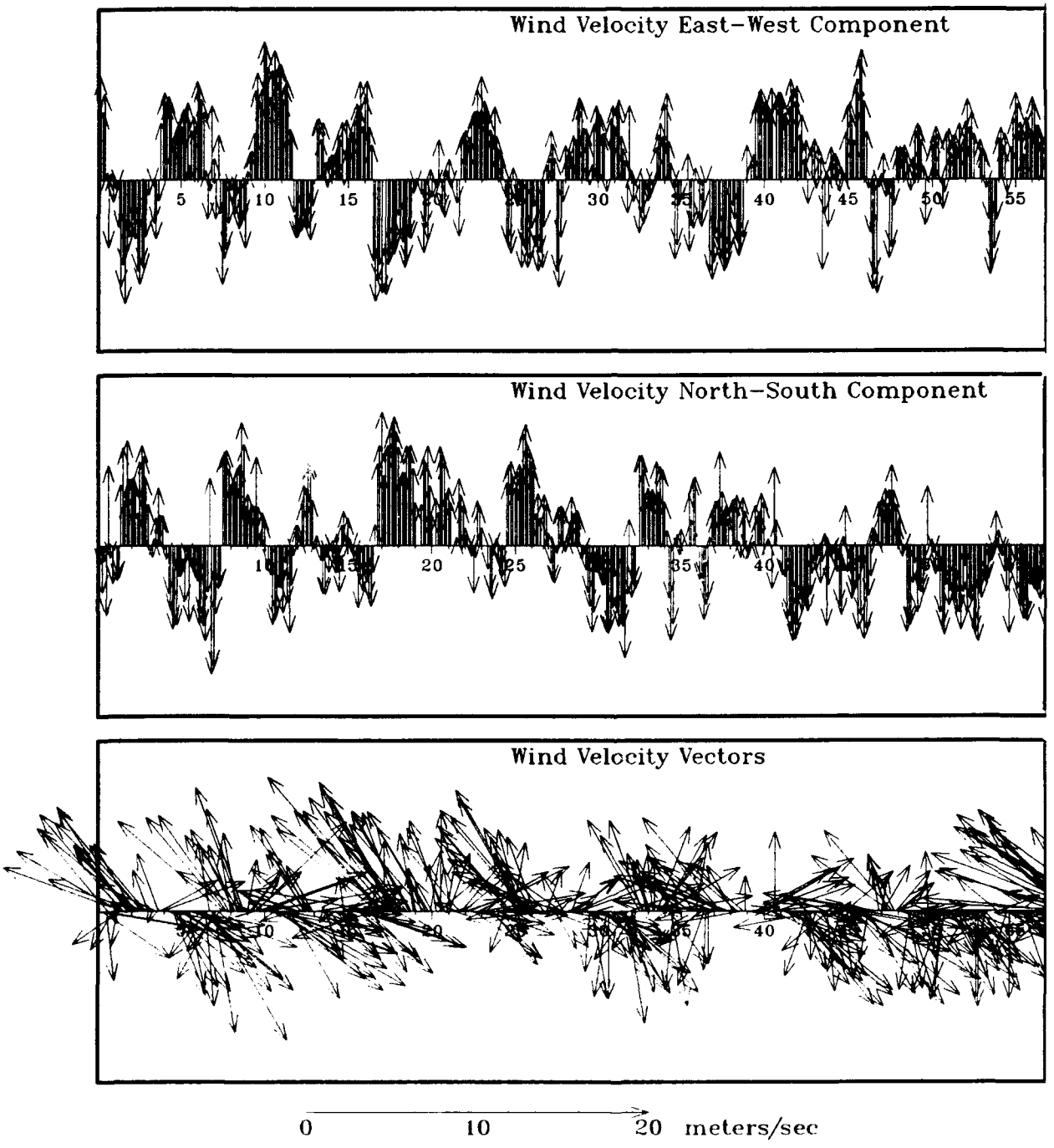

Figure 106. Wind data at the Norfolk International Airport during 1985. Day 0 corresponds to Day 195 of 1985.

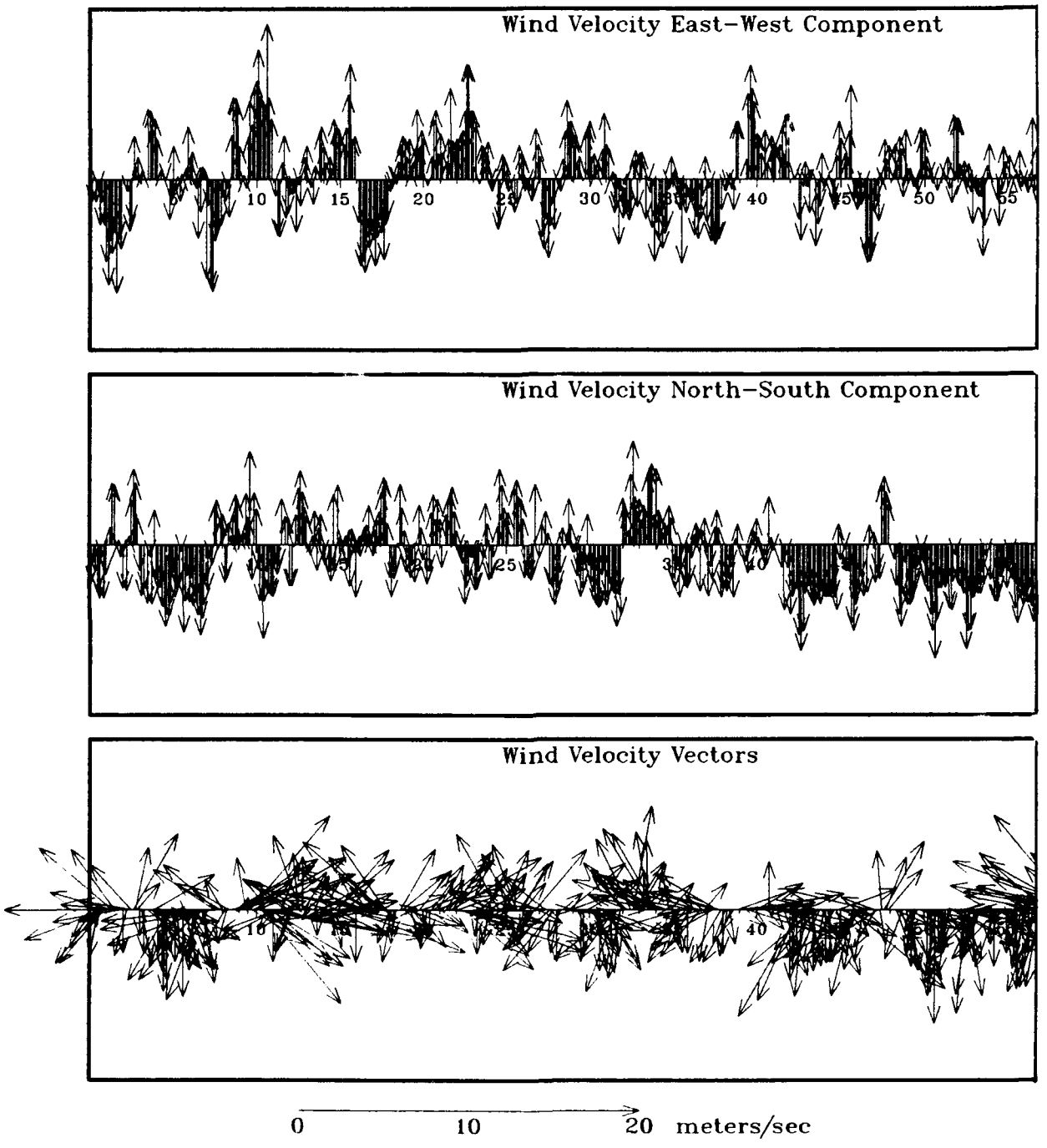

Figure 107. Wind data at the BWI Airport during 1985. Day 0 corresponds to Day 195 of 1985.

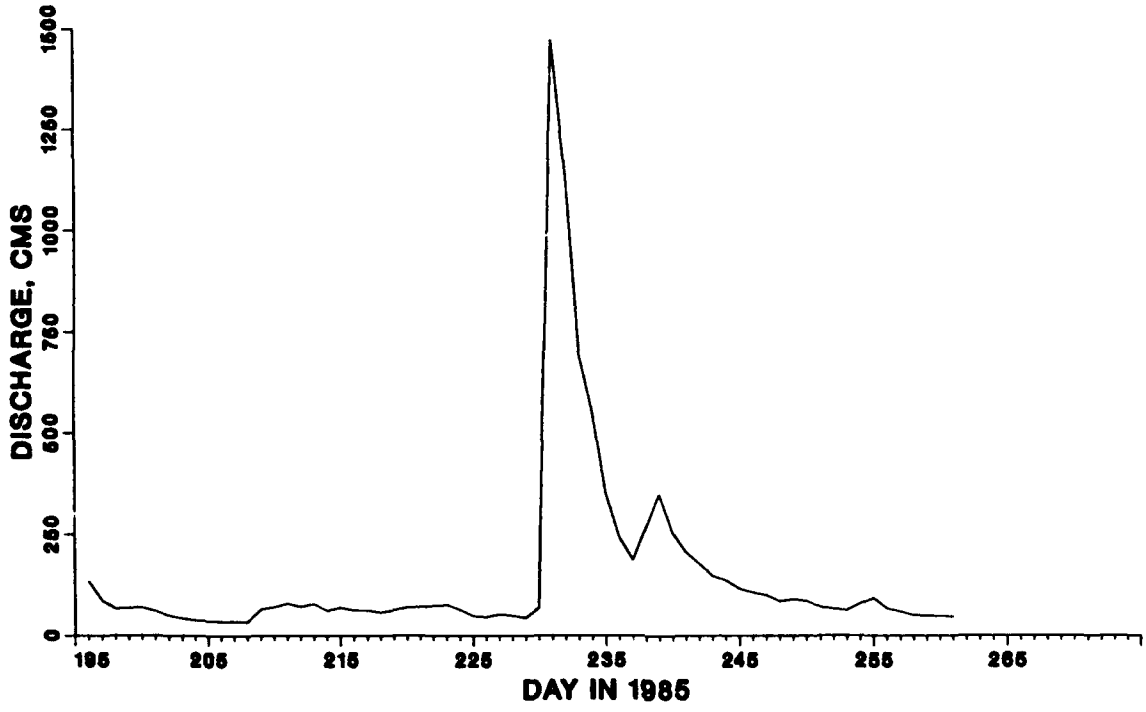

a. James River

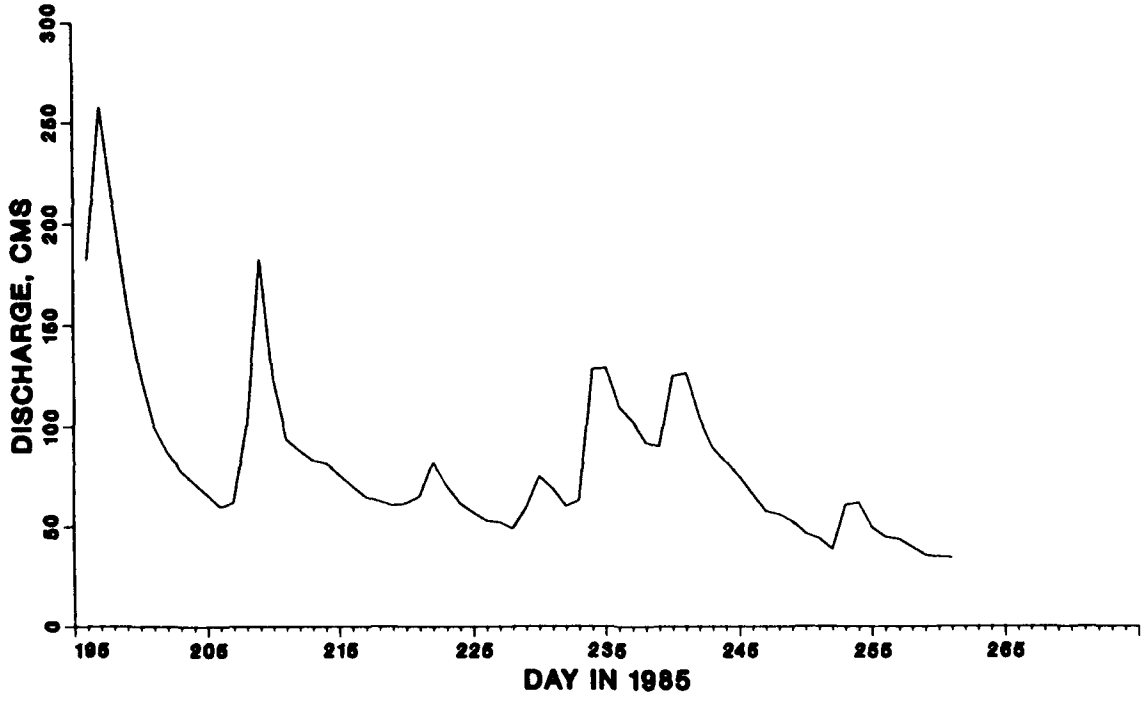

b. Potomac River

Figure 108. Freshwater inflows during 1985 (Continued)

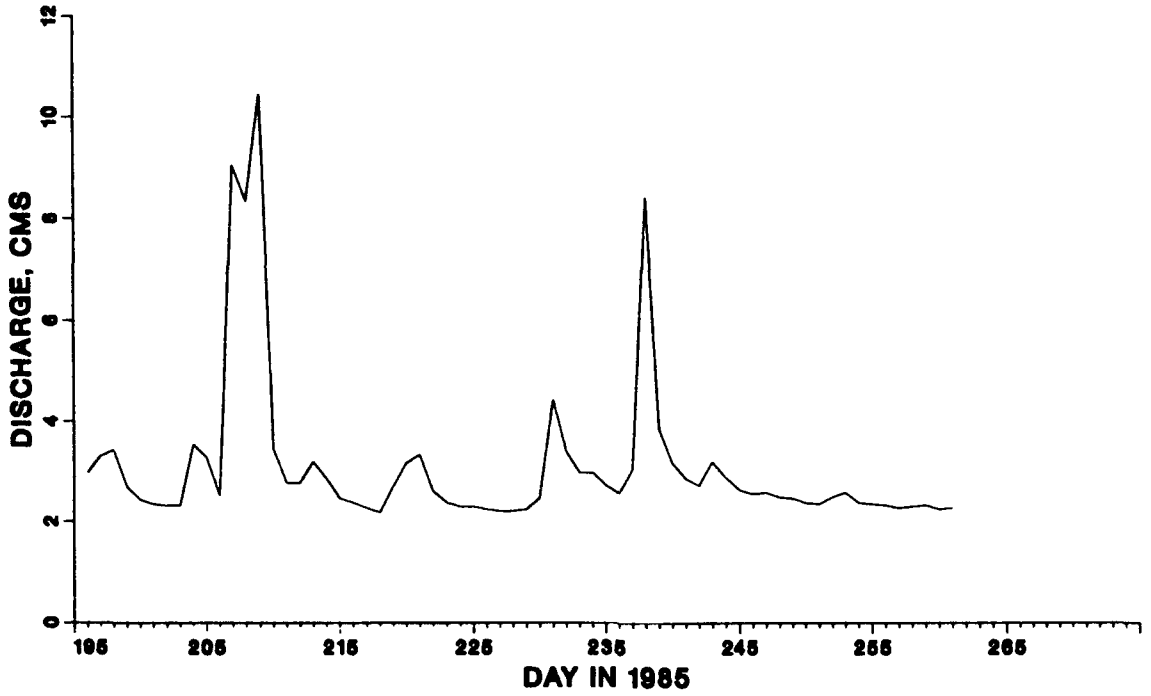

c. Patuxent River

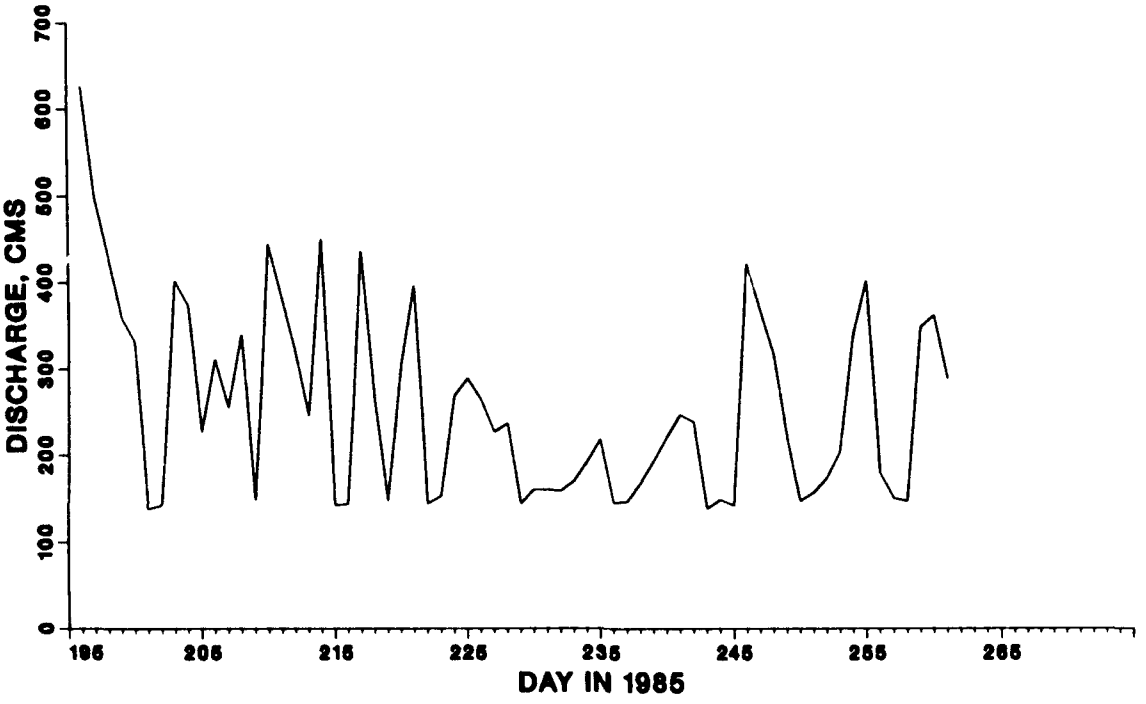

d. Susquehanna River

Figure 108. (Concluded)

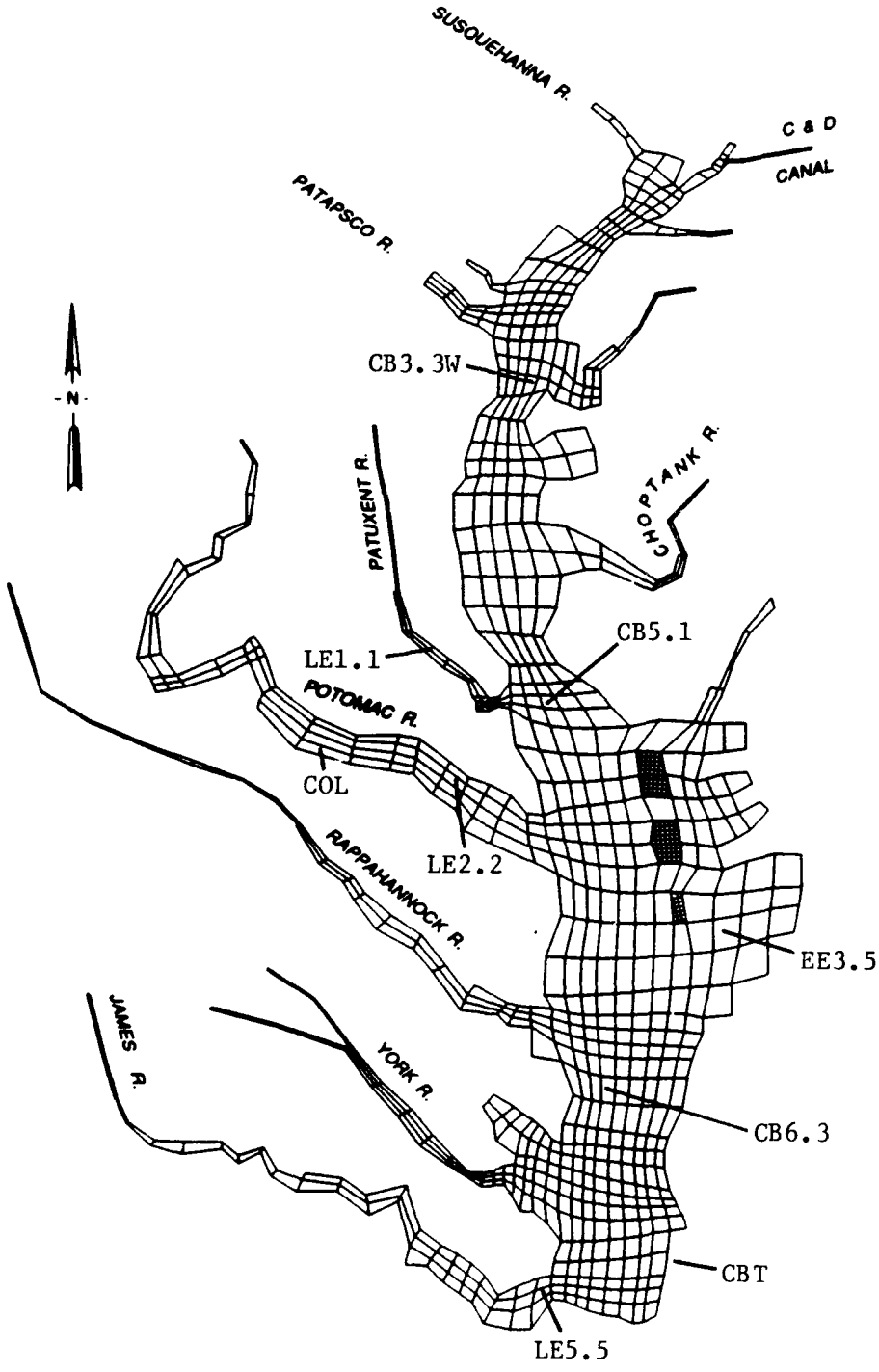

Figure 109. Data stations for the 1985 data set

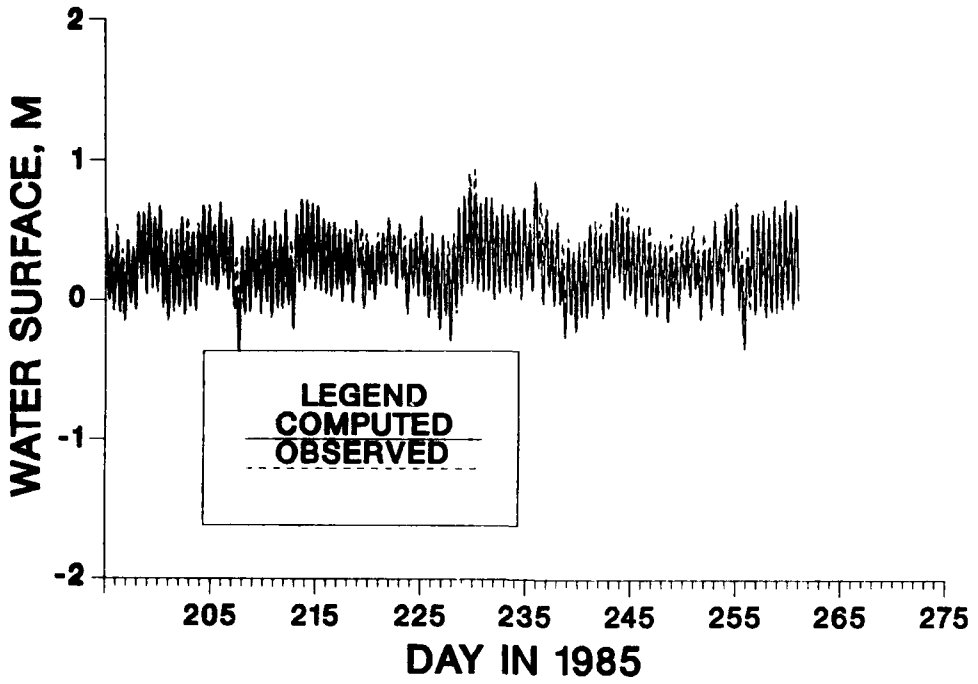

Figure 110. Comparison of computed and recorded tide at Colonial Beach, VA, during 1985

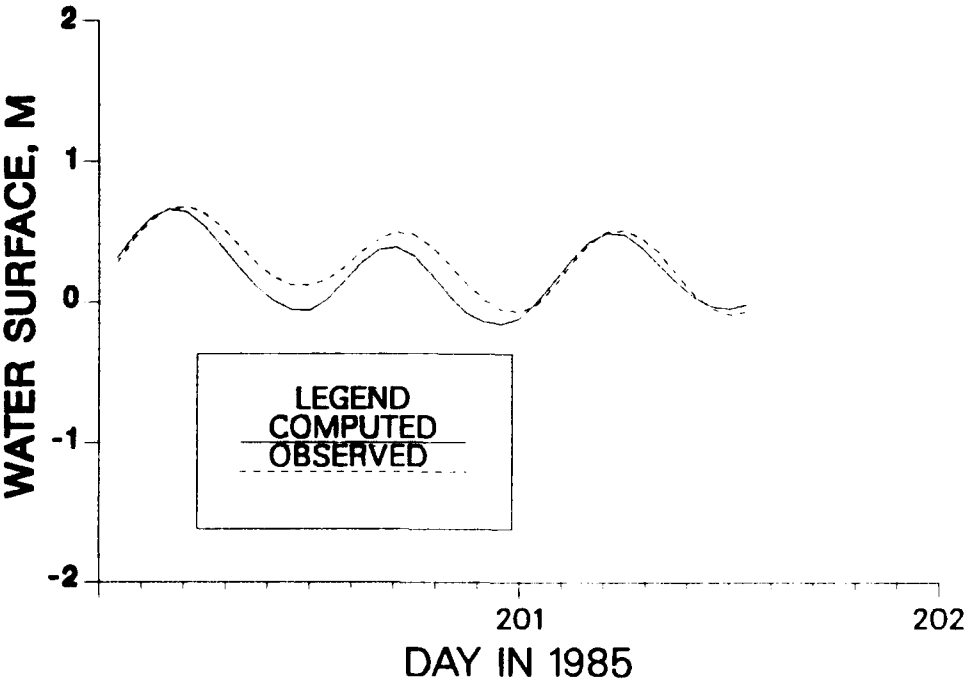

Figure 111. Comparison of computed and recorded tide at Colonial Beach, VA, near day 201 during 1985

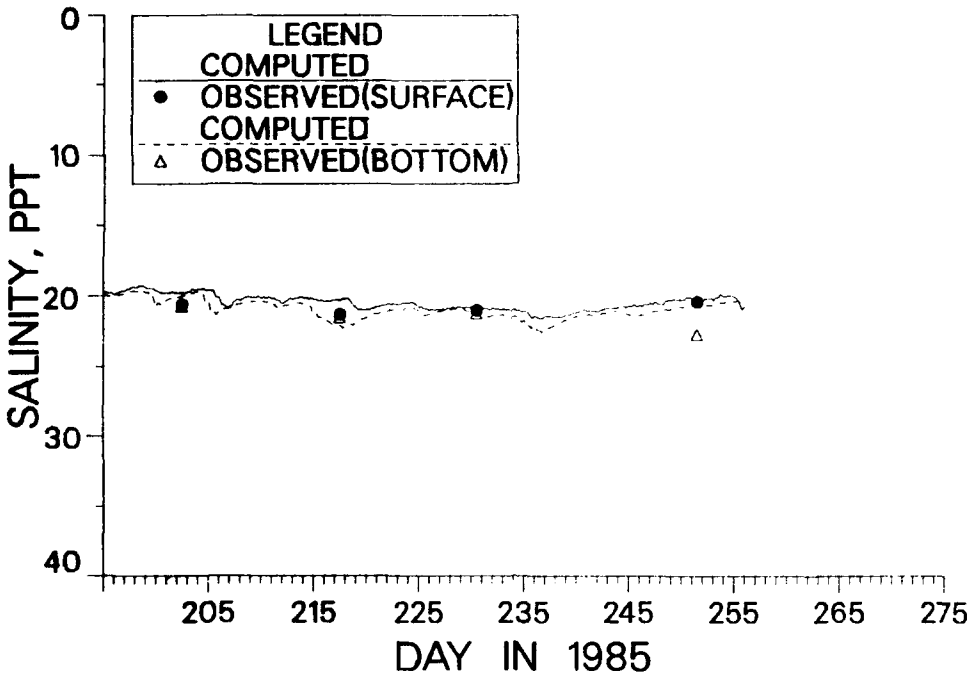

Figure 112. Comparison of computed and recorded salinity at station EE 3.5 during 1985

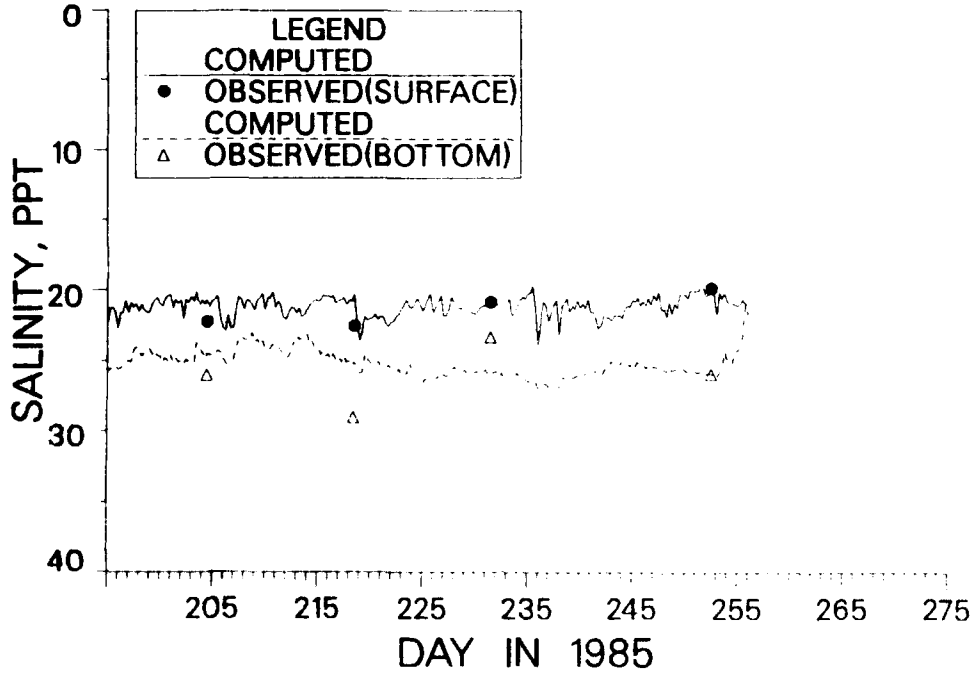

Figure 113. Comparison of computed and recorded salinity at station CB 6.3 during 1985

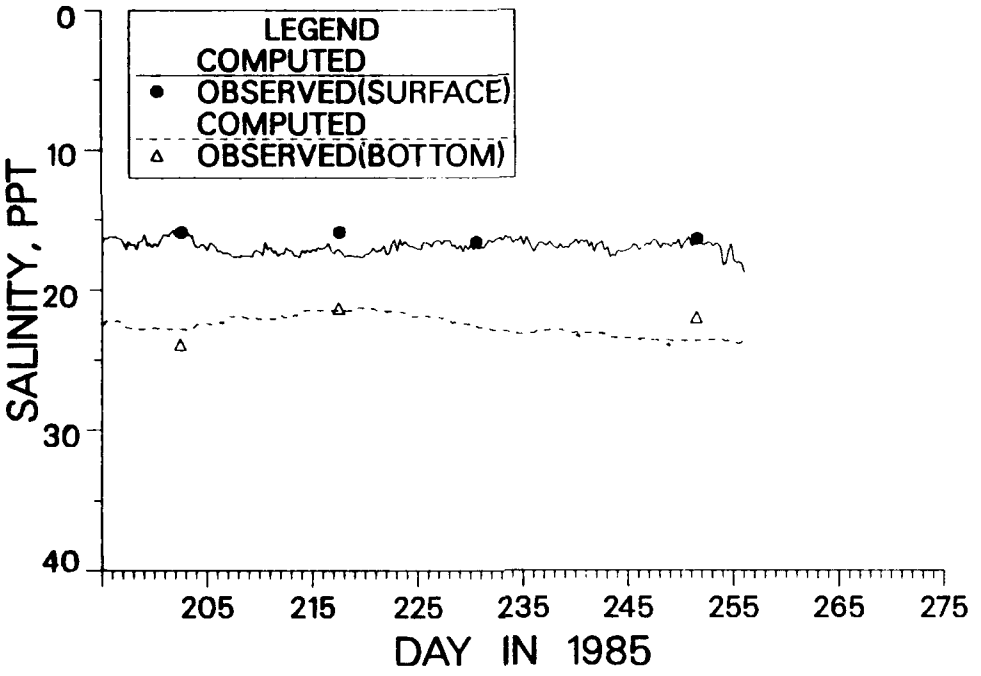

Figure 114. Comparison of computed and recorded salinity at station CB 5.1 during 1985

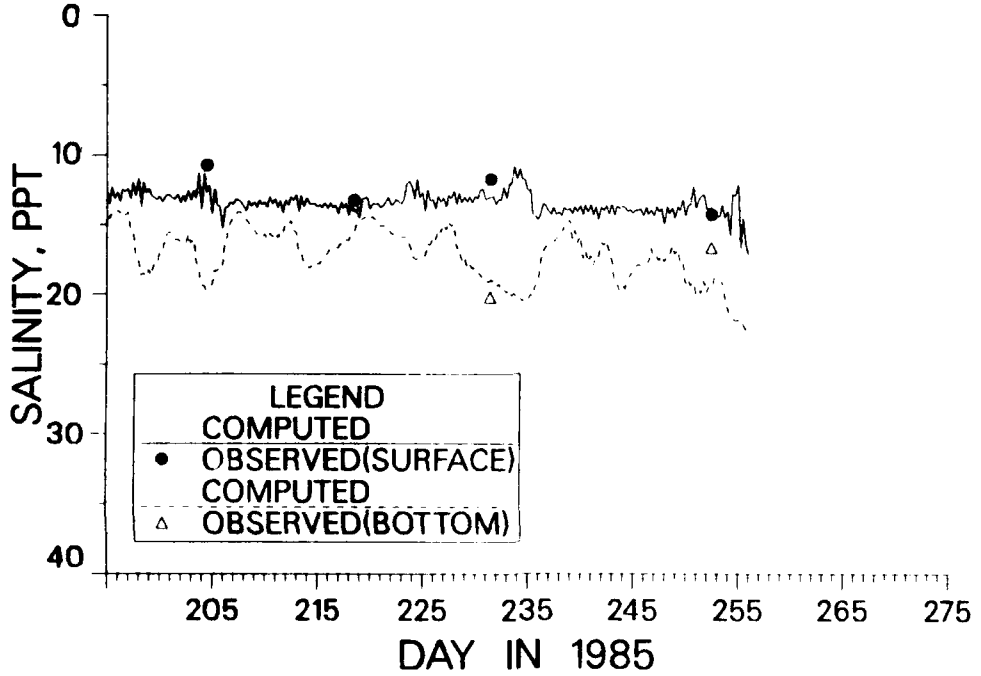

Figure 115. Comparison of computed and recorded salinity at station CB 3.3W during 1985

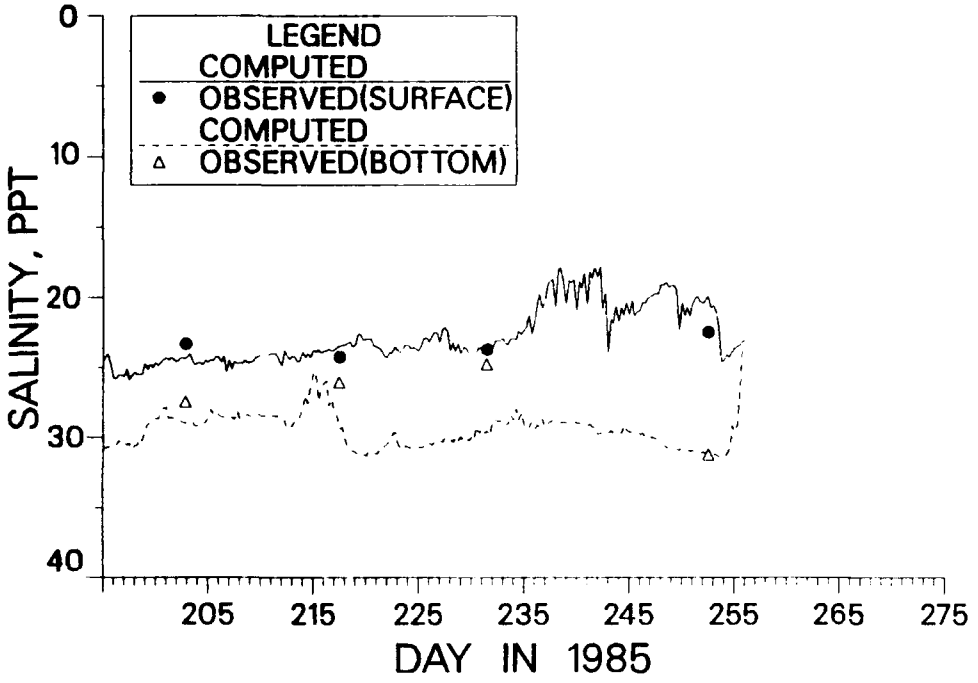

Figure 116. Comparison of computed and recorded salinity at station LE 5.5 during 1985

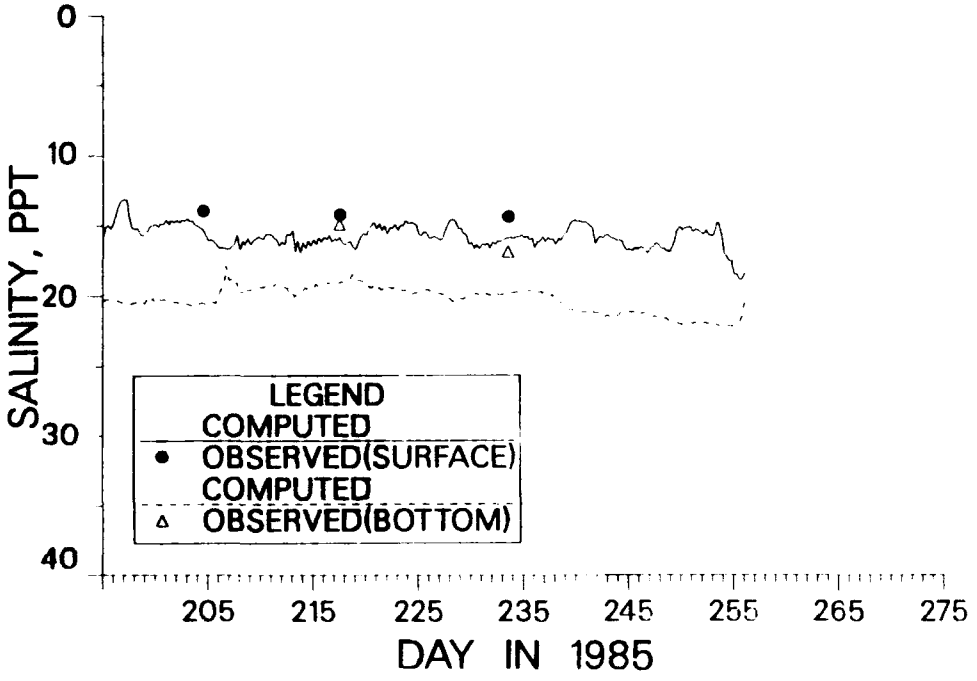

Figure 117. Comparison of computed and recorded salinity at station LE 2.2 during 1985

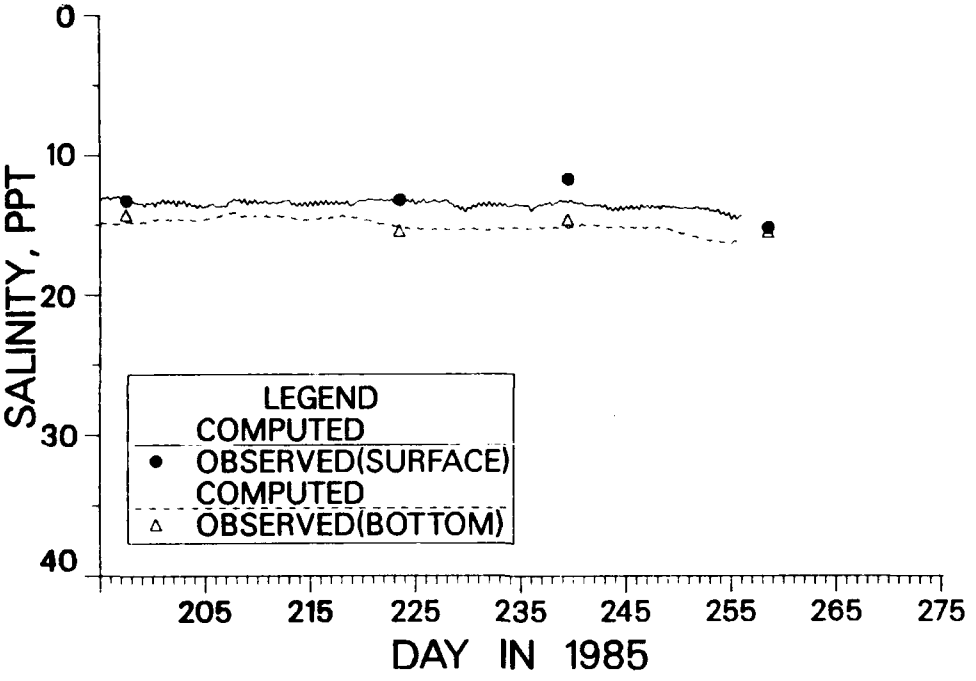

Figure 118. Comparison of computed and recorded salinity at station LE 1.1 during 1985

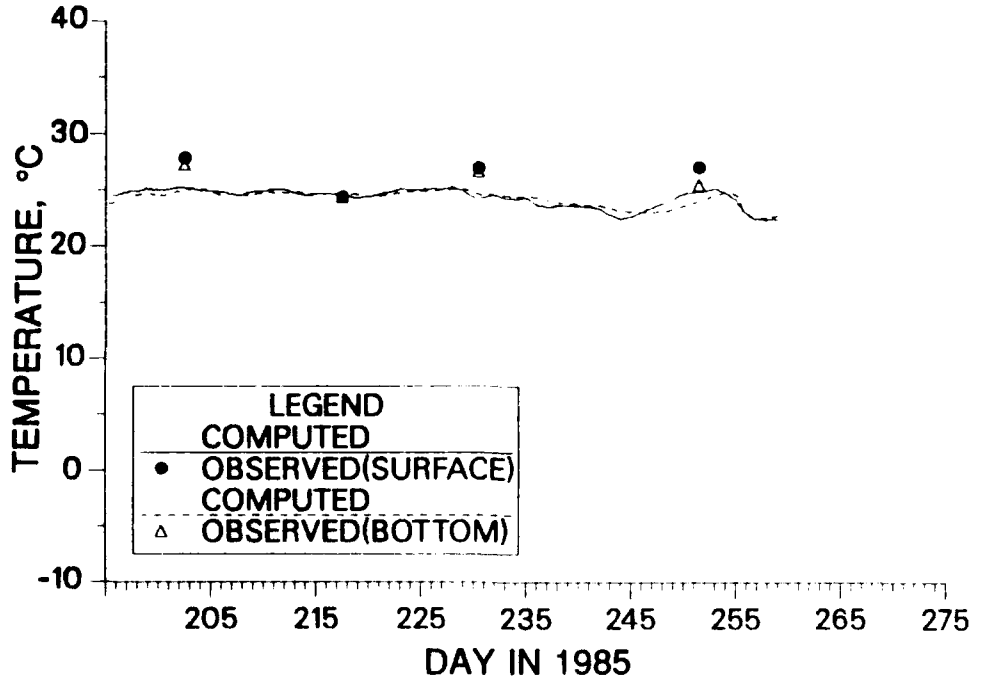

Figure 119. Comparison of computed and recorded temperature at station EE 3.5 during 1985

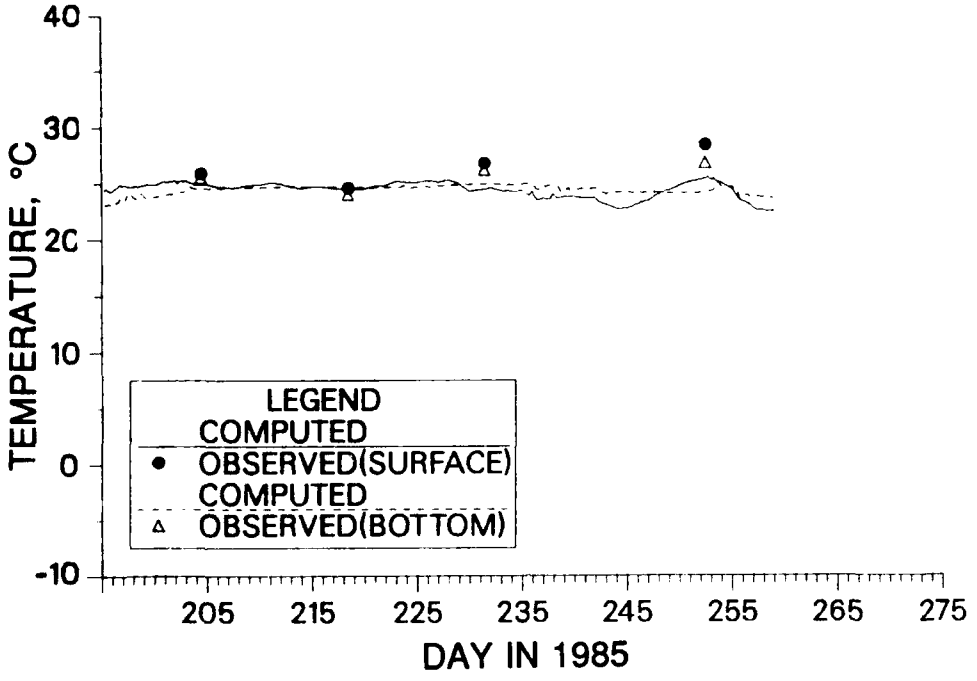

Figure 120. Comparison of computed and recorded temperature at station CB 6.3 during 1985

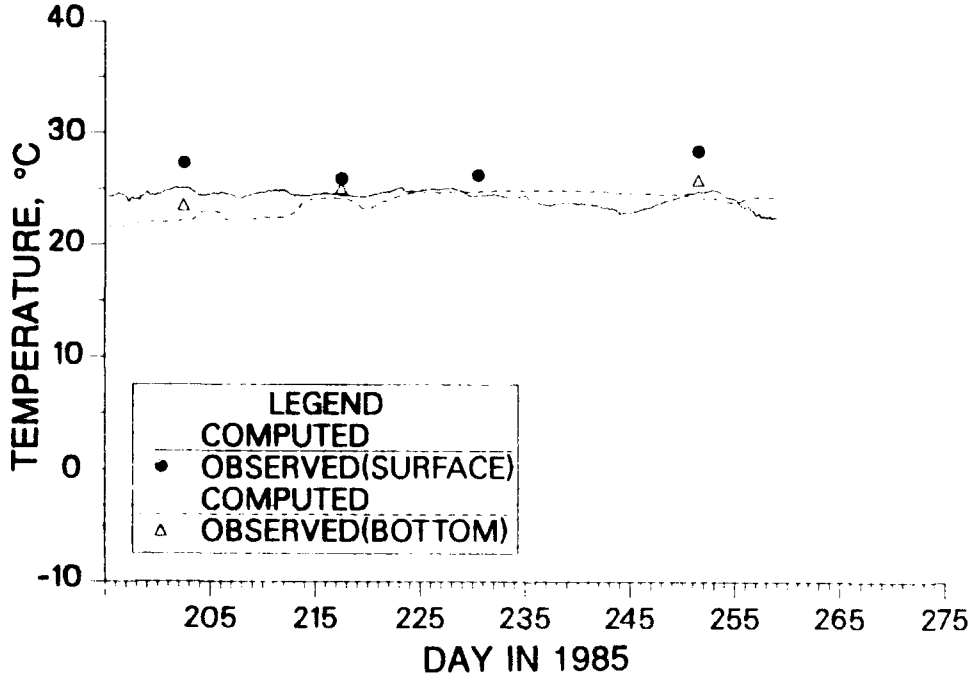

Figure 121. Comparison of computed and recorded temperature at station CB 5.1 during 1985

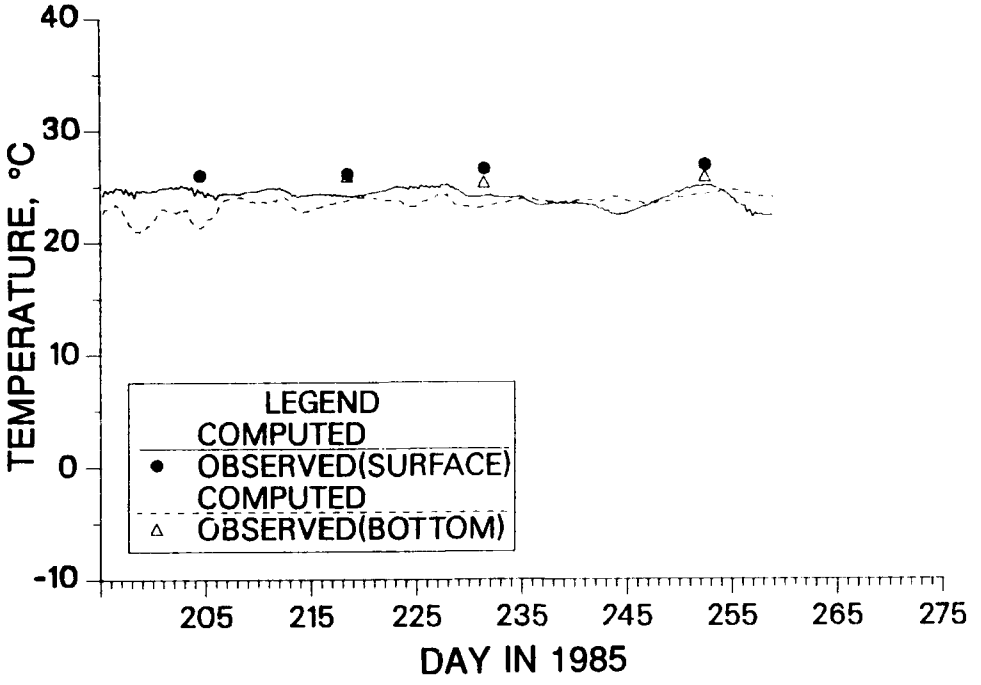

Figure 122. Comparison of computed and recorded temperature at station CB 3.3W during 1985

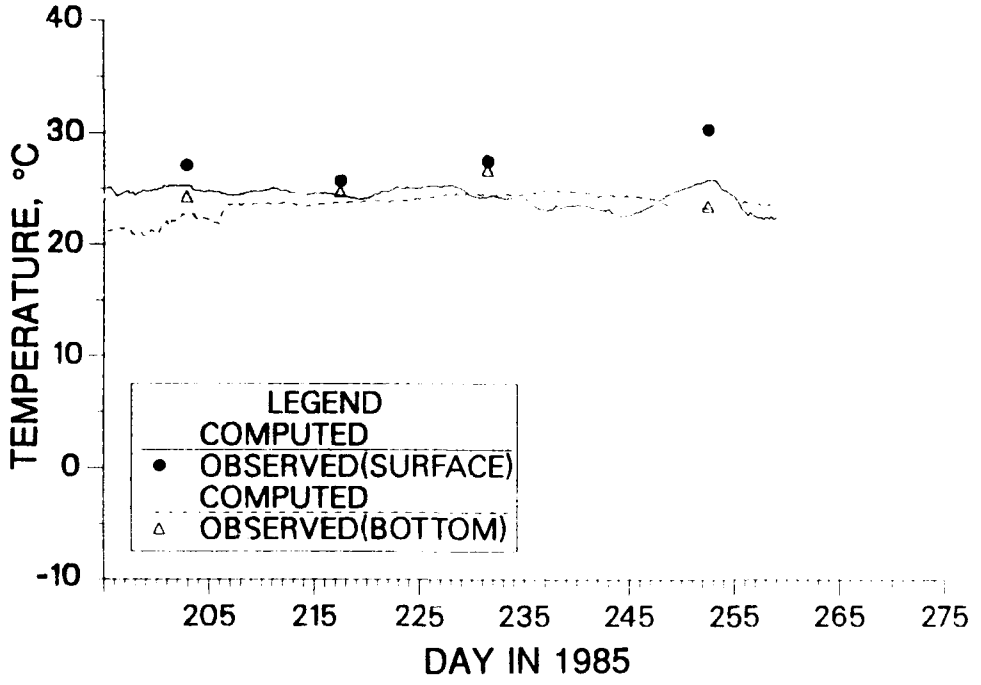

Figure 123. Comparison of computed and recorded temperature at station LE 5.5 during 1985

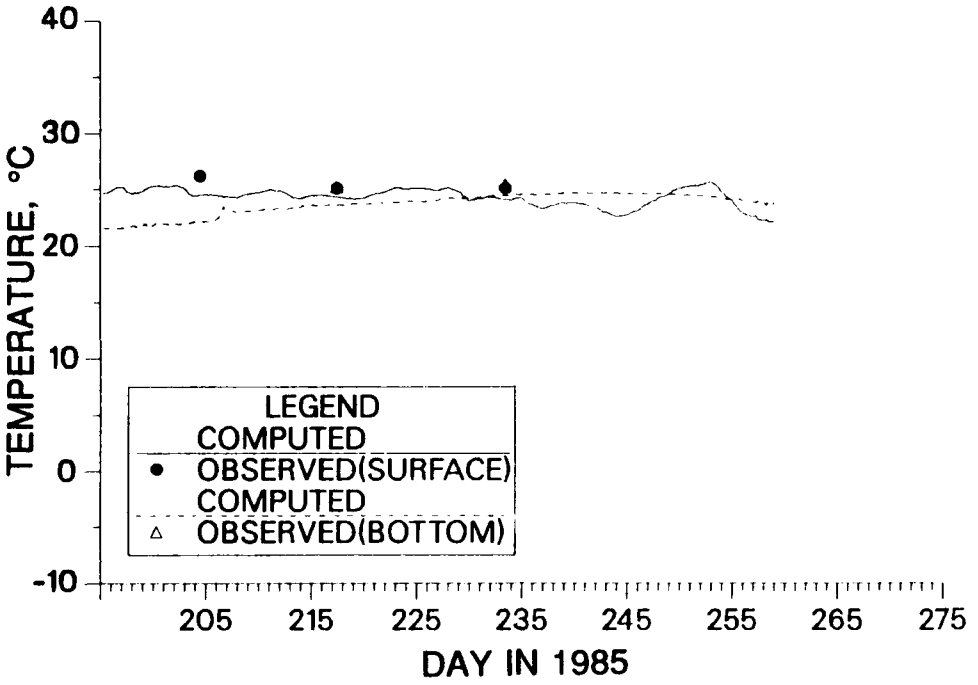

Figure 124. Comparison of computed and recorded temperature at station LE 2.2 during 1985

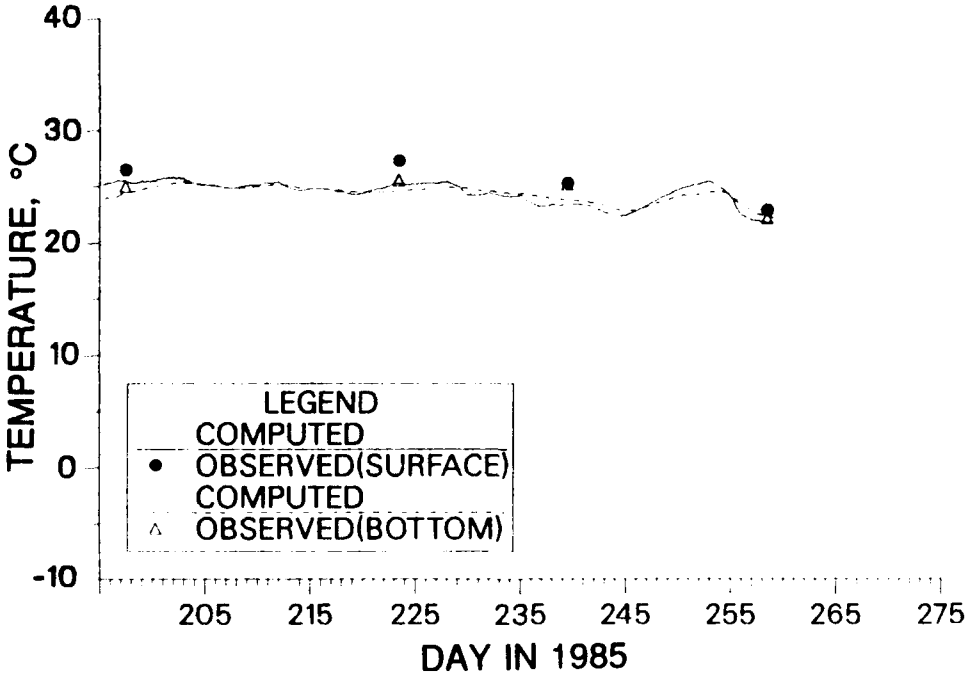

Figure 125. Comparison of computed and recorded temperature at station LE 1.1 during 1985

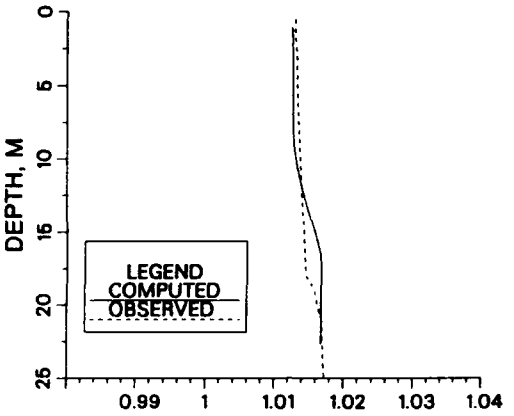

a. Day 42

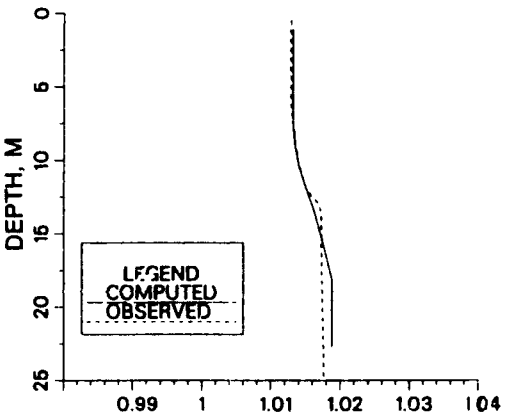

b. Day 140

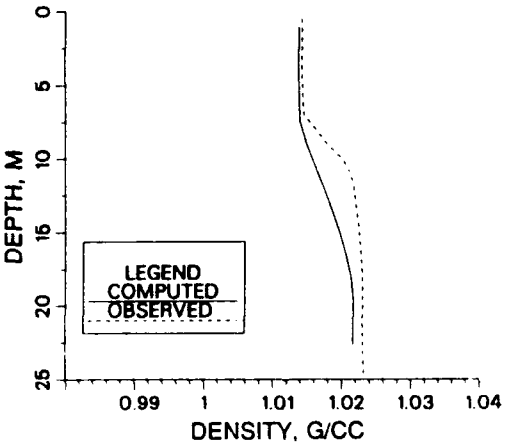

c. Day 203

Figure 126. Vertical profiles of water density at station CB 5.1 during 1985 (Continued)

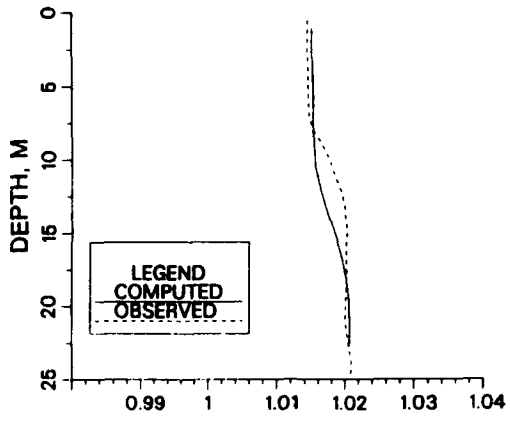

d. Day 218

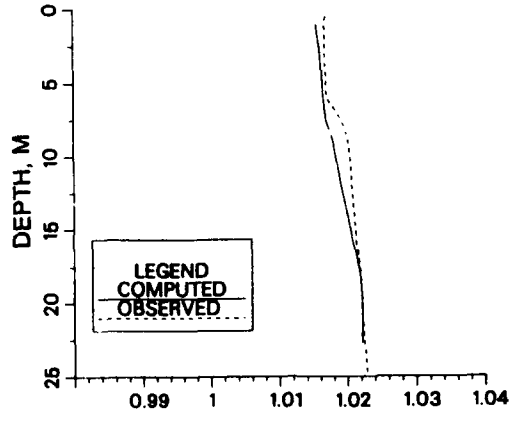

e. Day 266

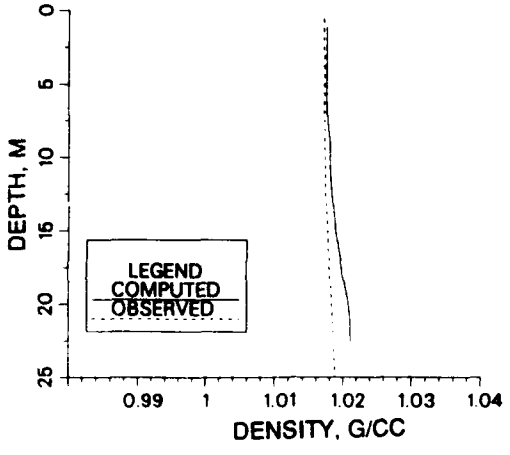

f. Day 316

Figure 126. (Concluded)

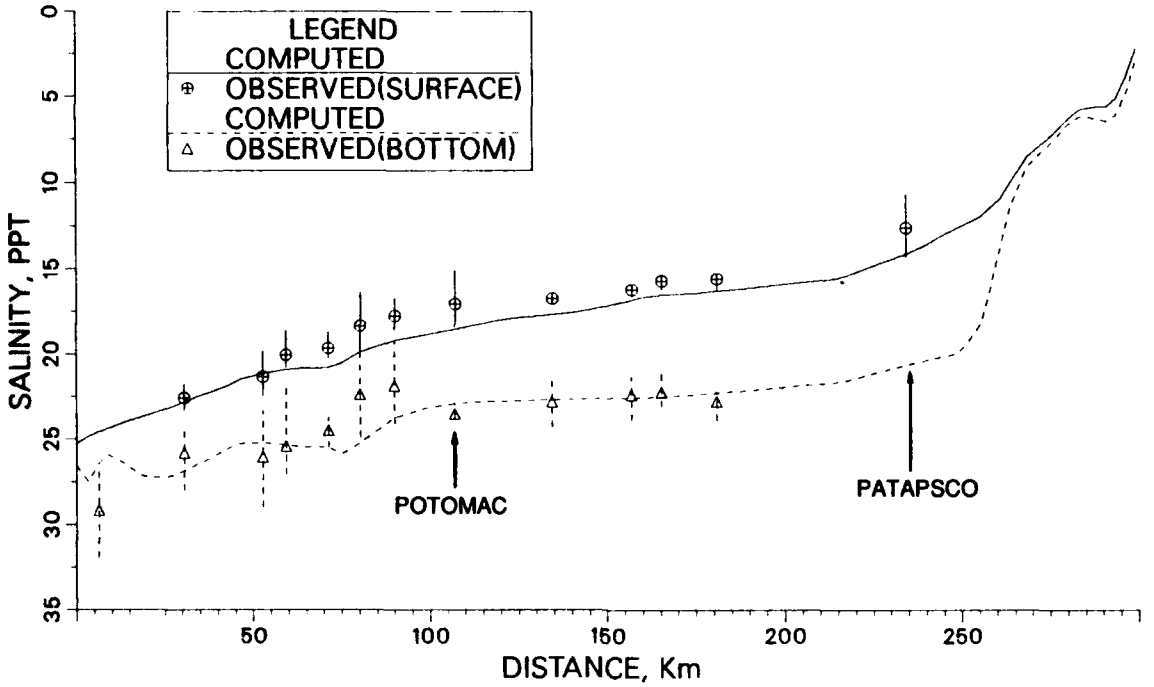

Figure 127. Comparison of seasonally averaged salinities along the main bay during 1985

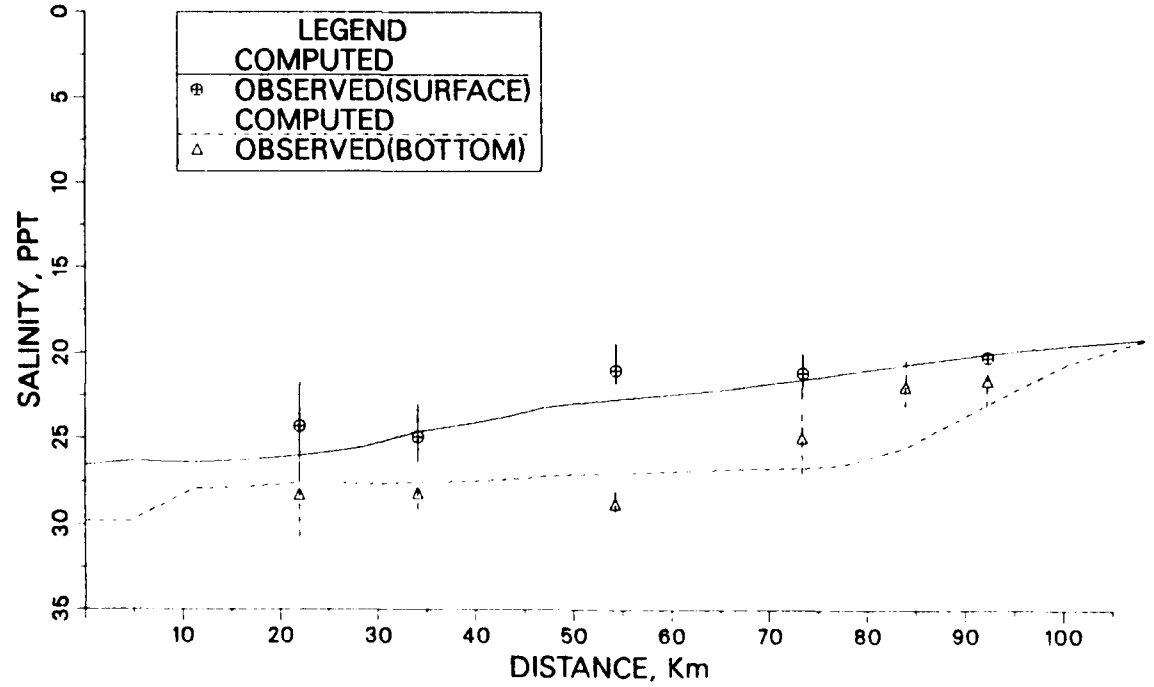

Figure 128. Comparison of seasonally averaged salinities along the eastern main bay transect during 1985

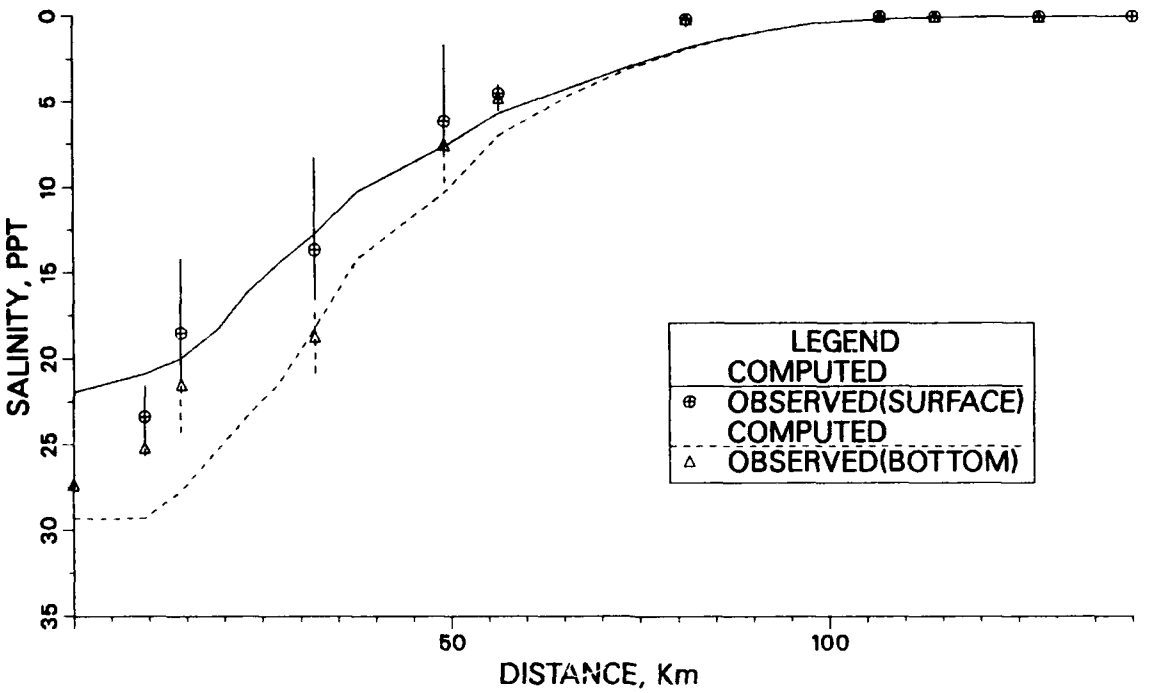

Figure 129. Comparison of seasonally averaged salinities along James River during 1985

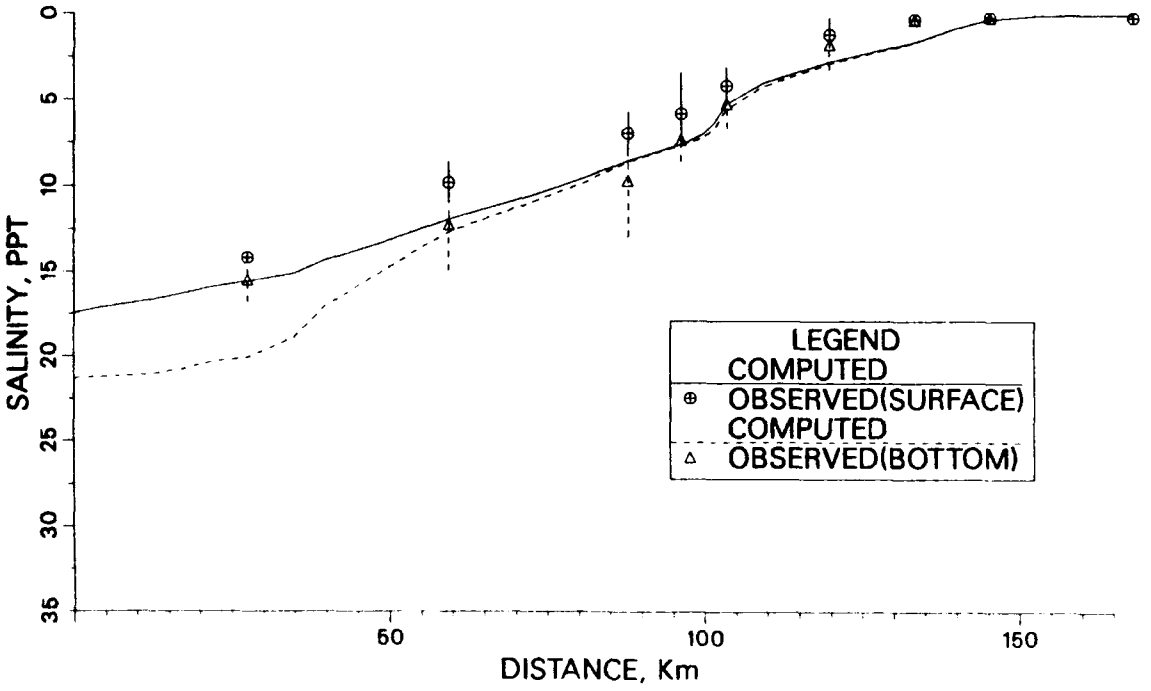

Figure 130. Comparison of seasonally averaged salinities along Potomac River during 1985

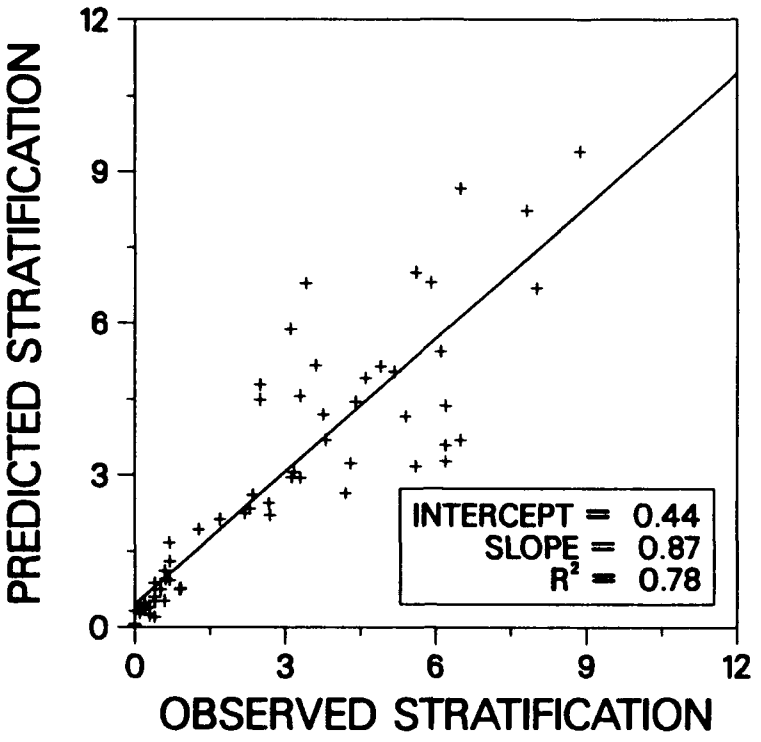

Figure 131. Comparison of computed and recorded stratification for all main bay stations during 1985

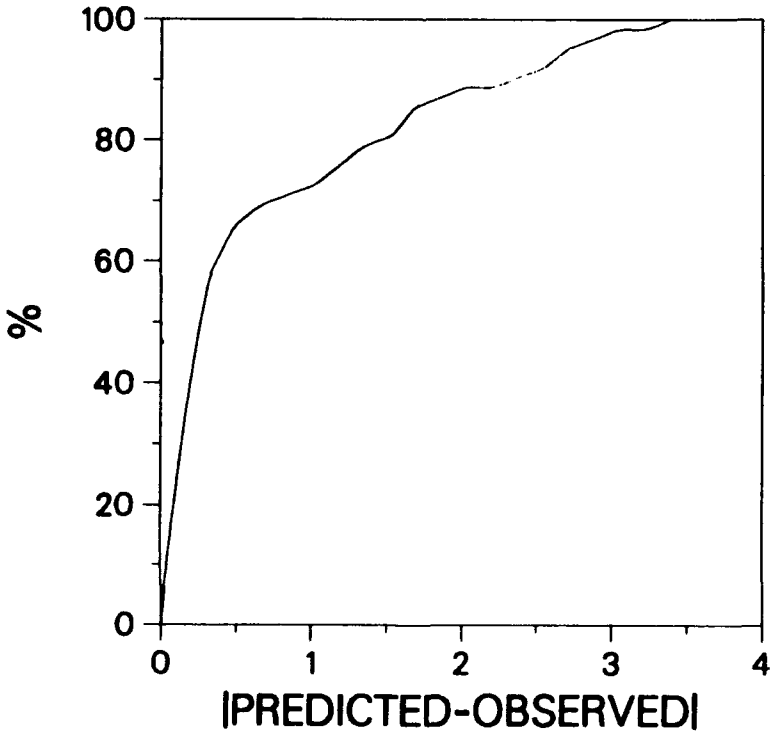

Figure 132. Frequency of occurrence of the error in the computed stratification for all main bay stations during 1985

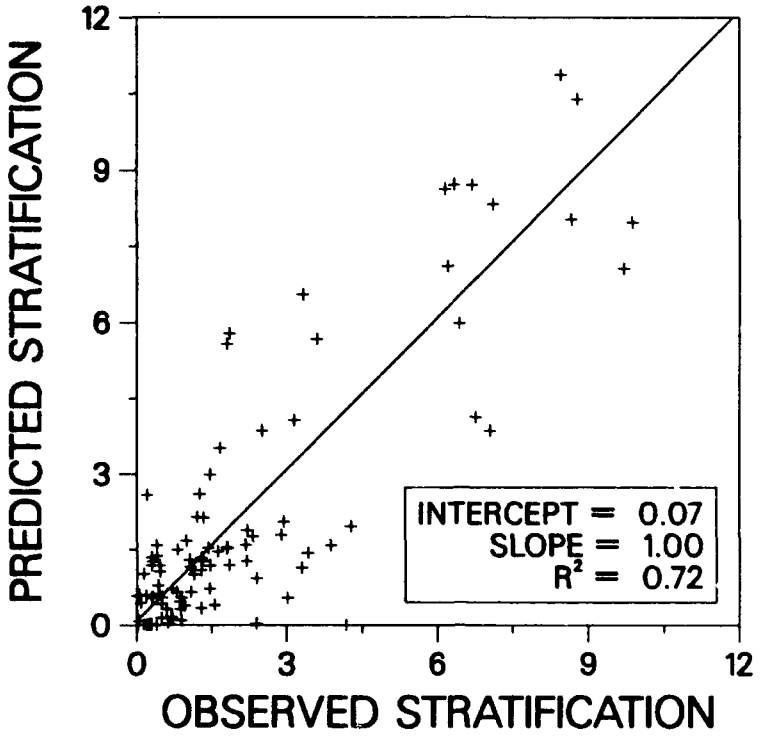

Figure 133. Comparison of computed and recorded stratification for all tributary stations during 1985

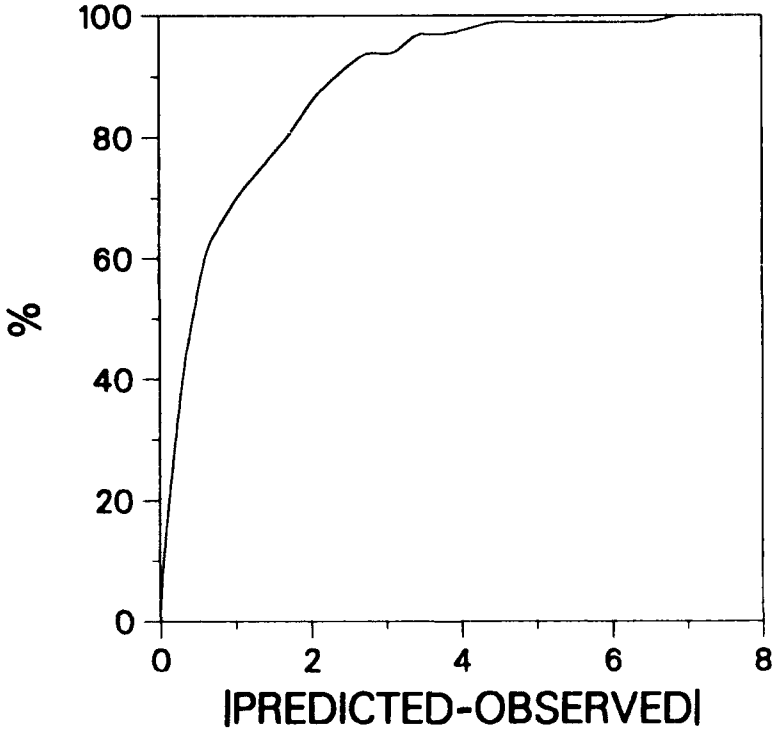

Figure 134. Frequency of occurrence of the error in the computer stratification for all tributary stations during 1985

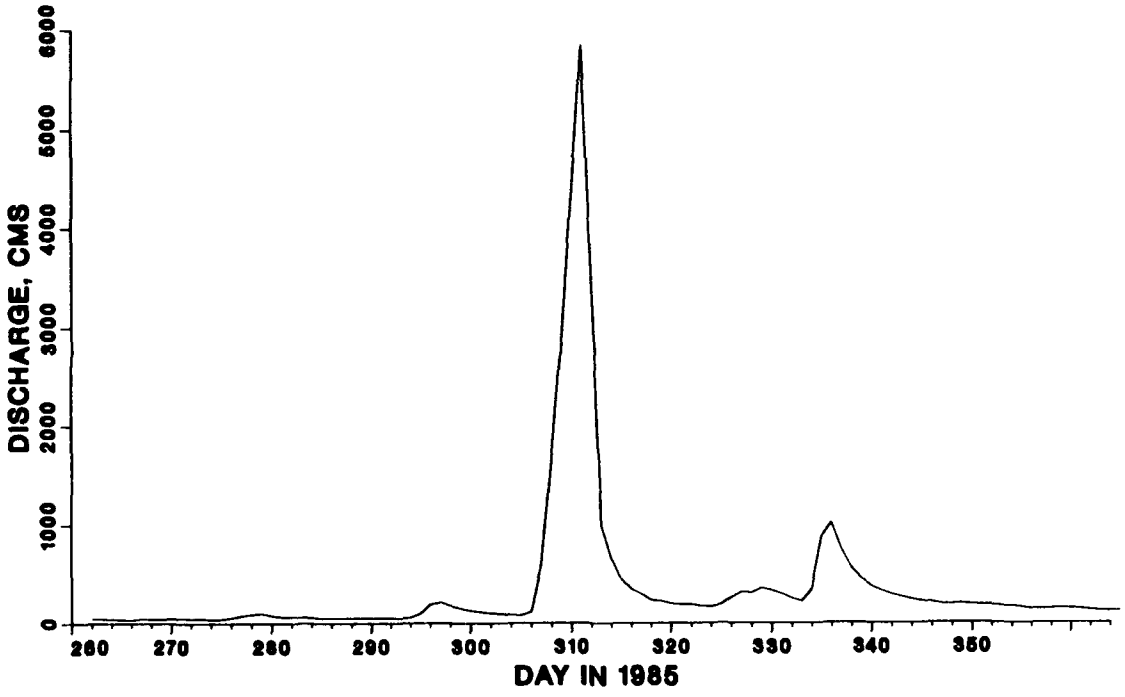

Figure 135. Freshwater inflow on James River during 1985 storm event

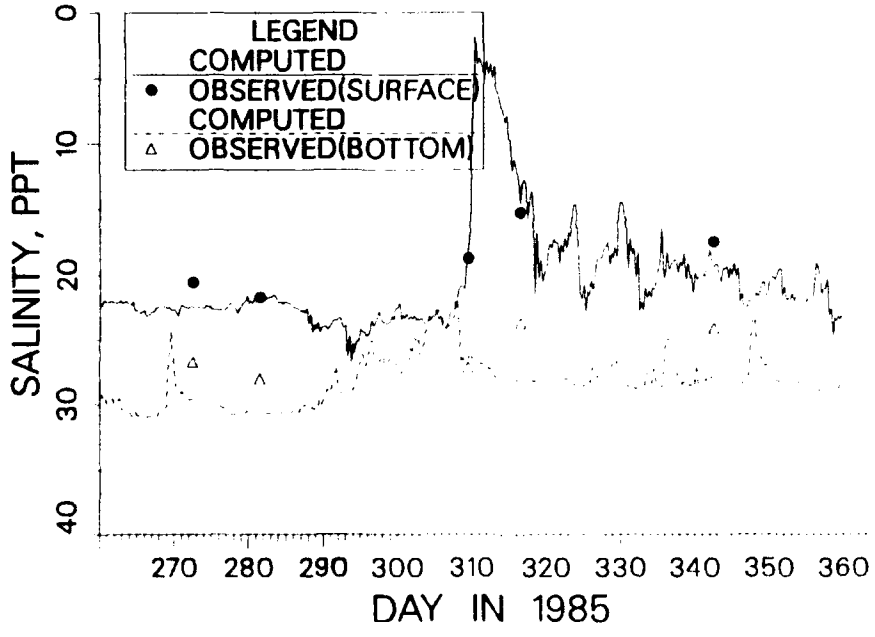

Figure 136. Comparison of computed and recorded salinity at station LE 5.5 during 1985 storm event

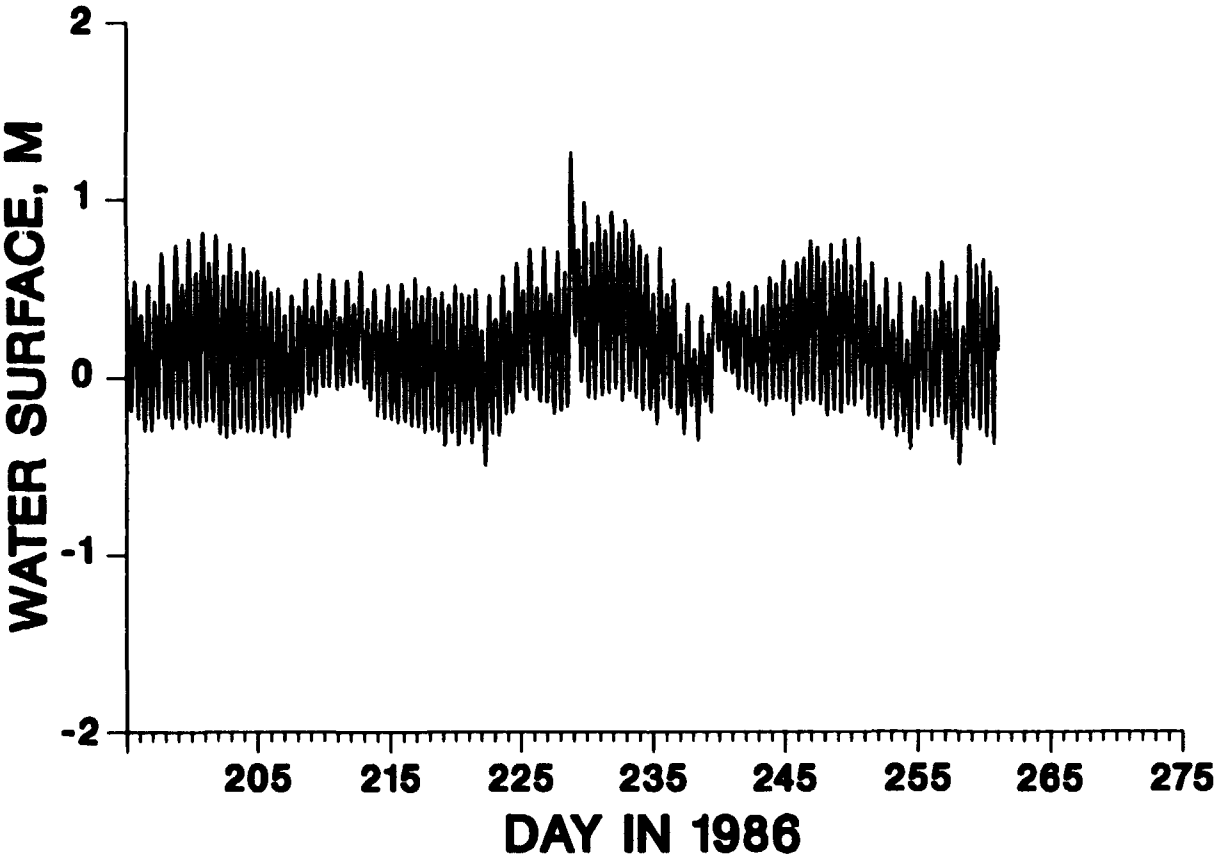

Figure 137. Ocean boundary tide at the Chesapeake Bay Tunnel during 1986

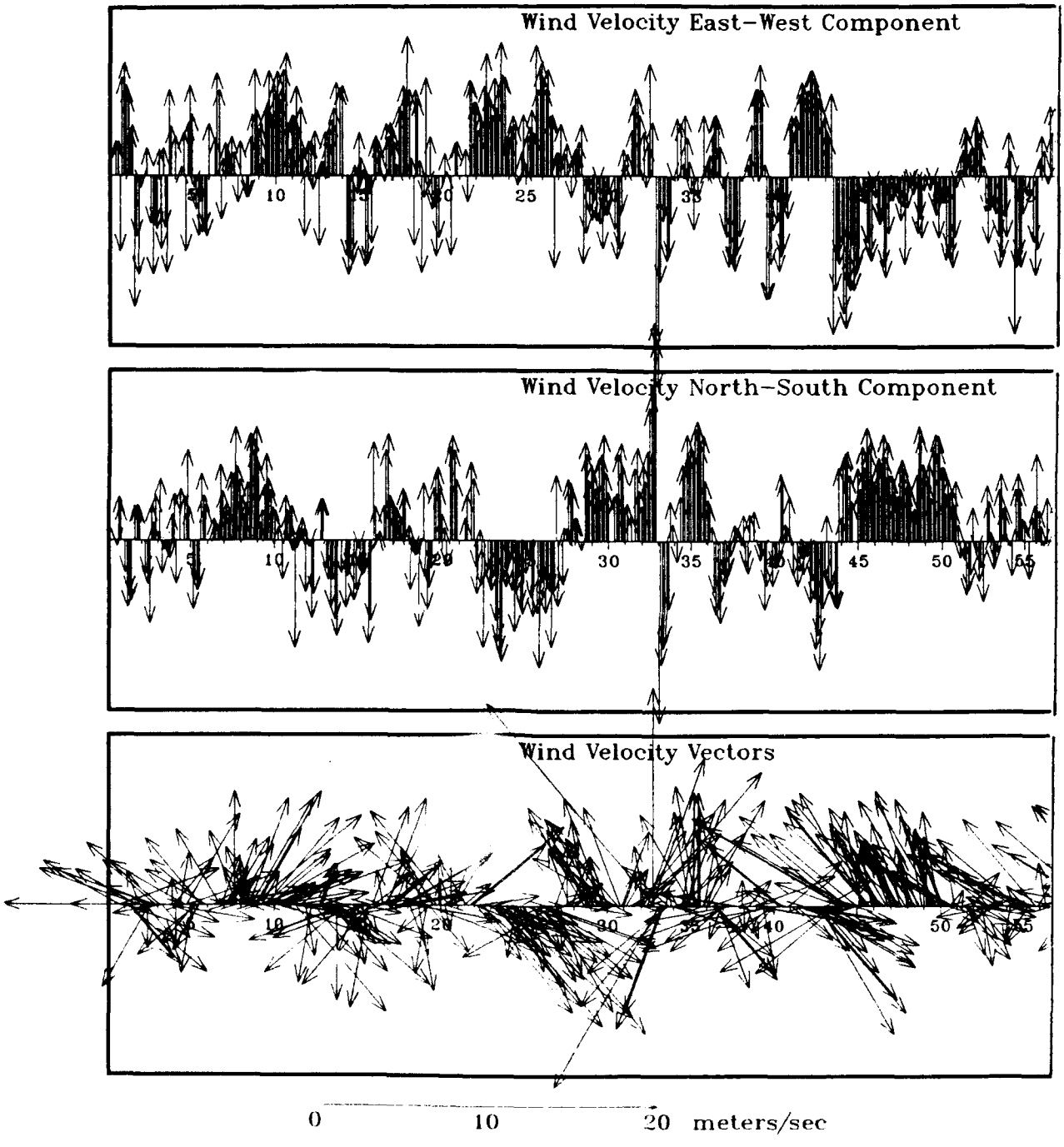

Figure 138. Wind data at the Norfolk International Airport during 1986. Day 0 corresponds to Day 195 of 1986.

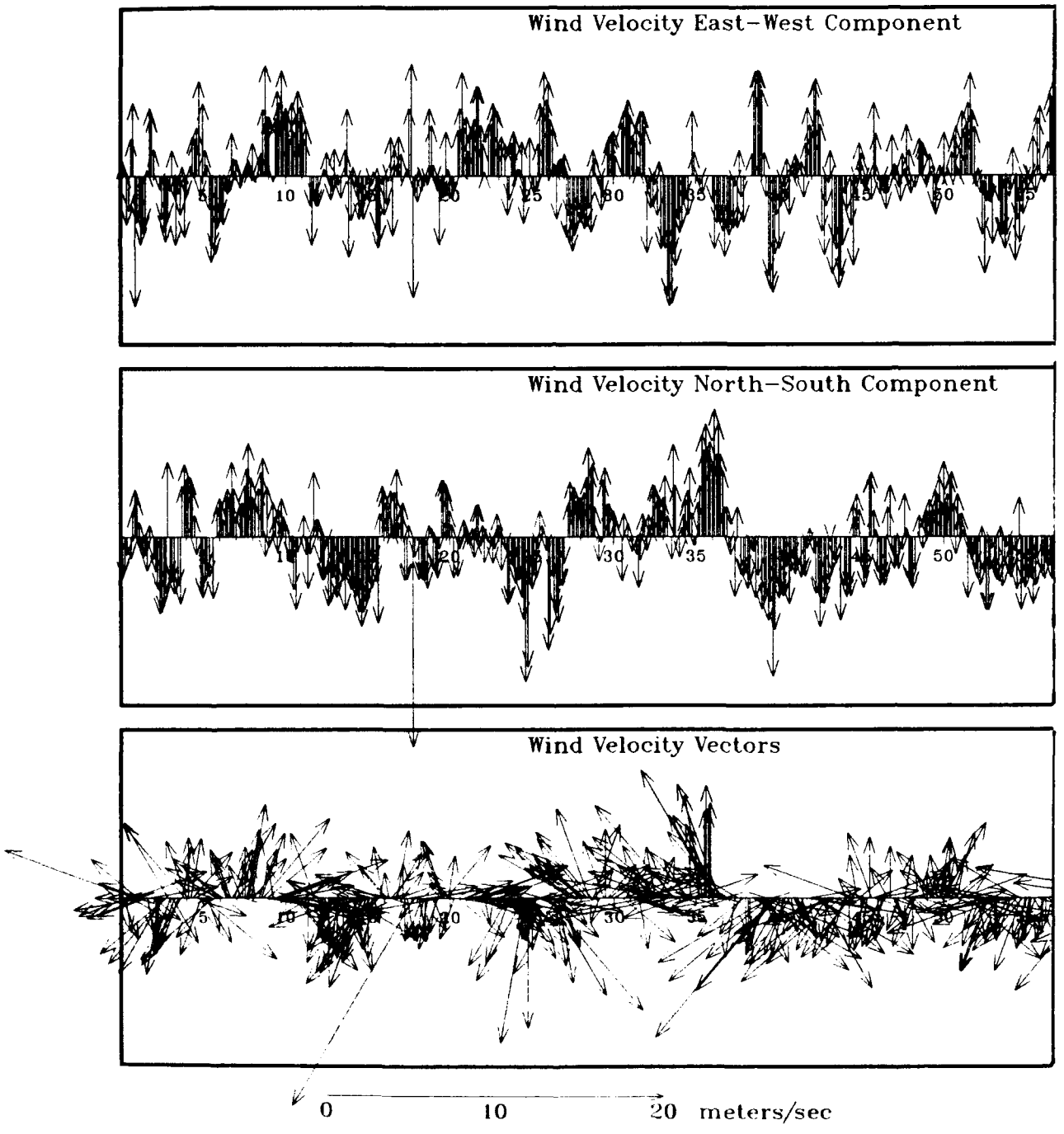

Figure 139. Wind data at the BWI Airport during 1986. Day 0 corresponds to Day 195 of 1986.

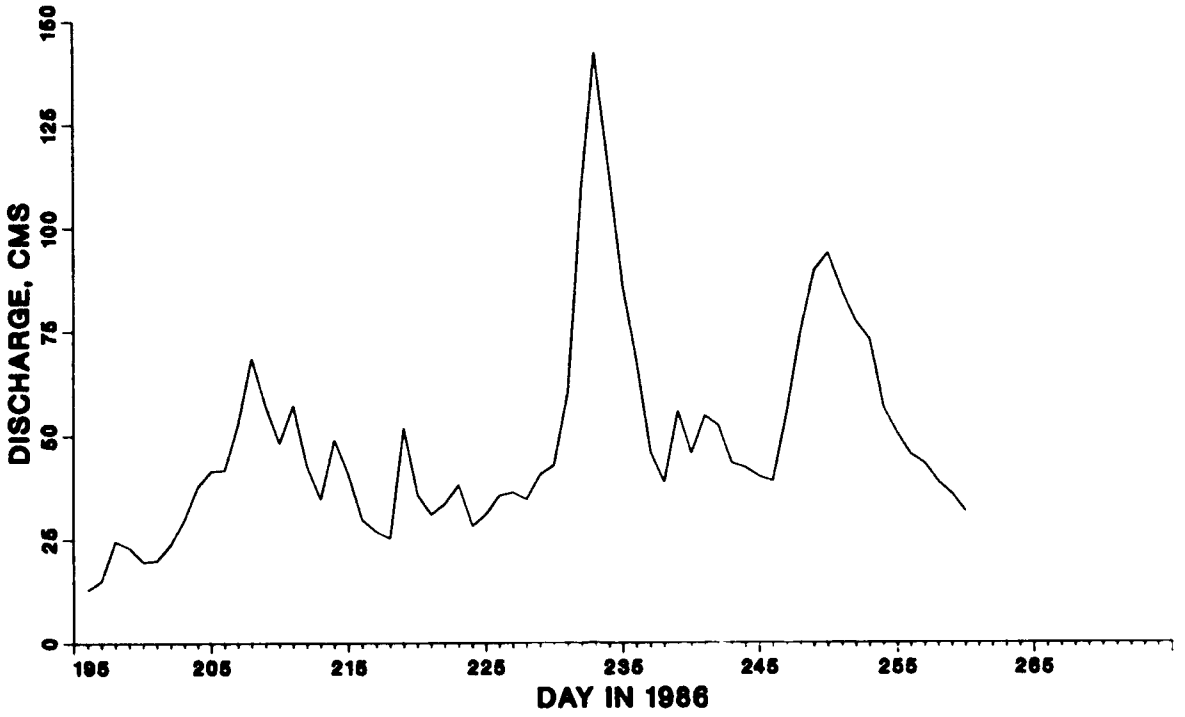

a. James River

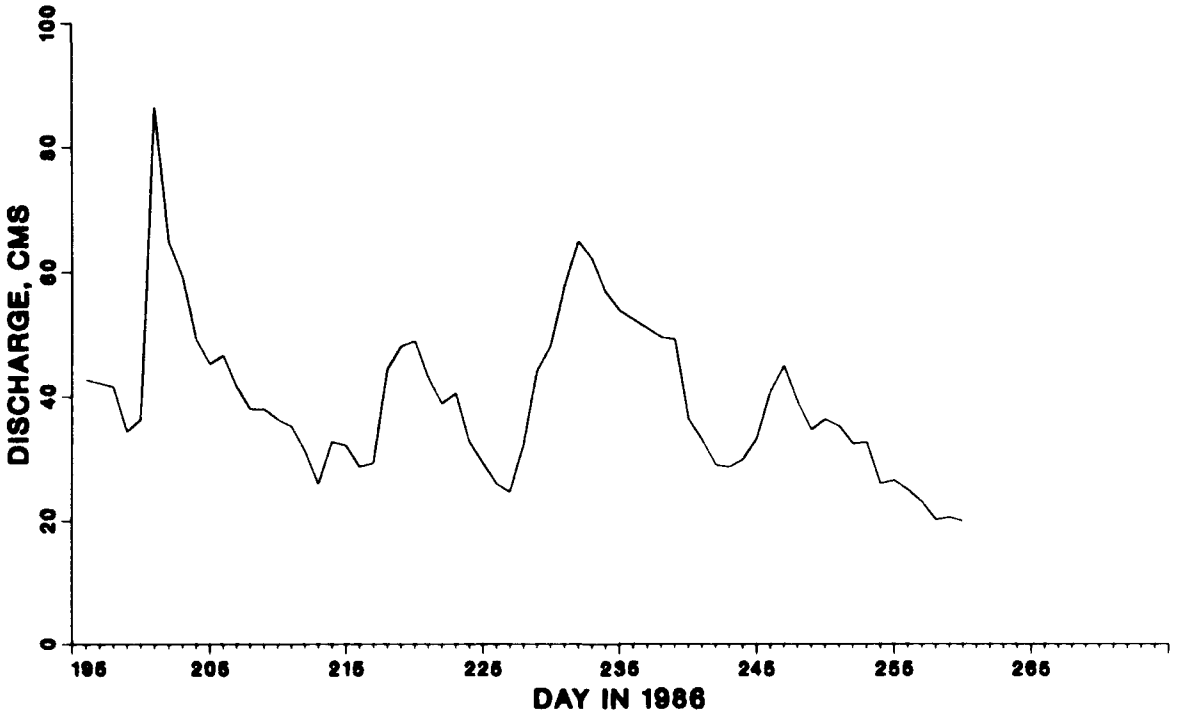

b. Potomac River

Figure 140. Freshwater inflows during 1986 (Continued)

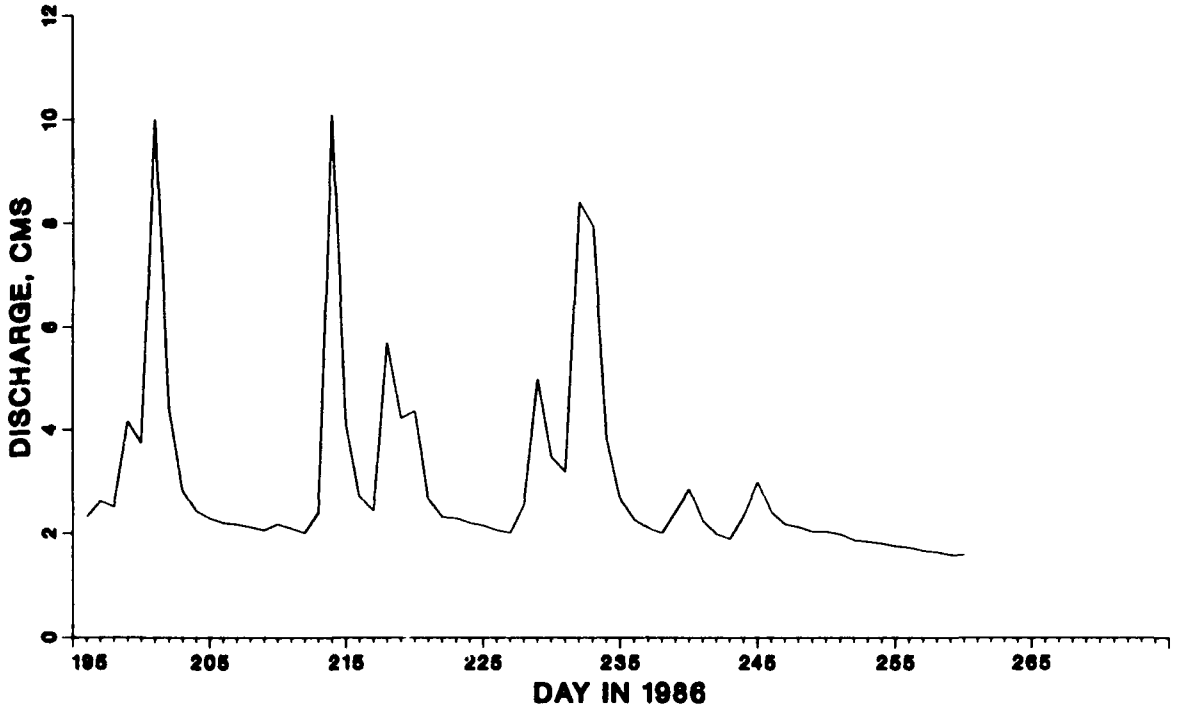

c. Patuxent River

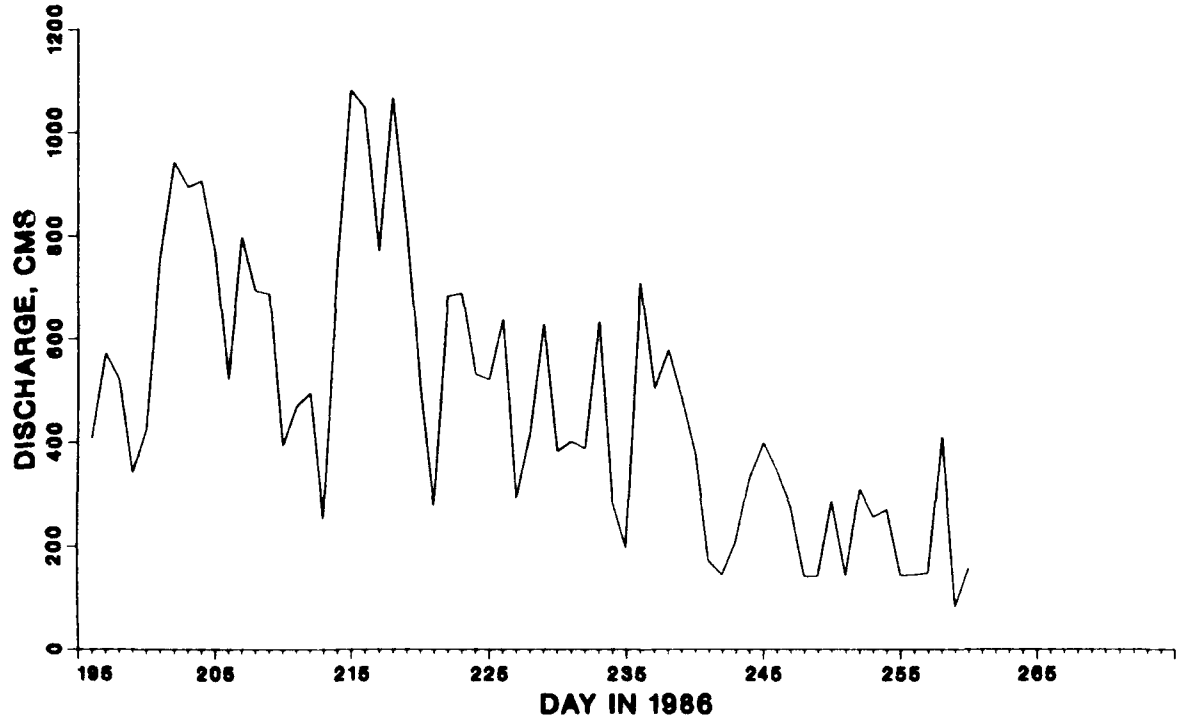

d. Susquehanna River

Figure 140. (Concluded)

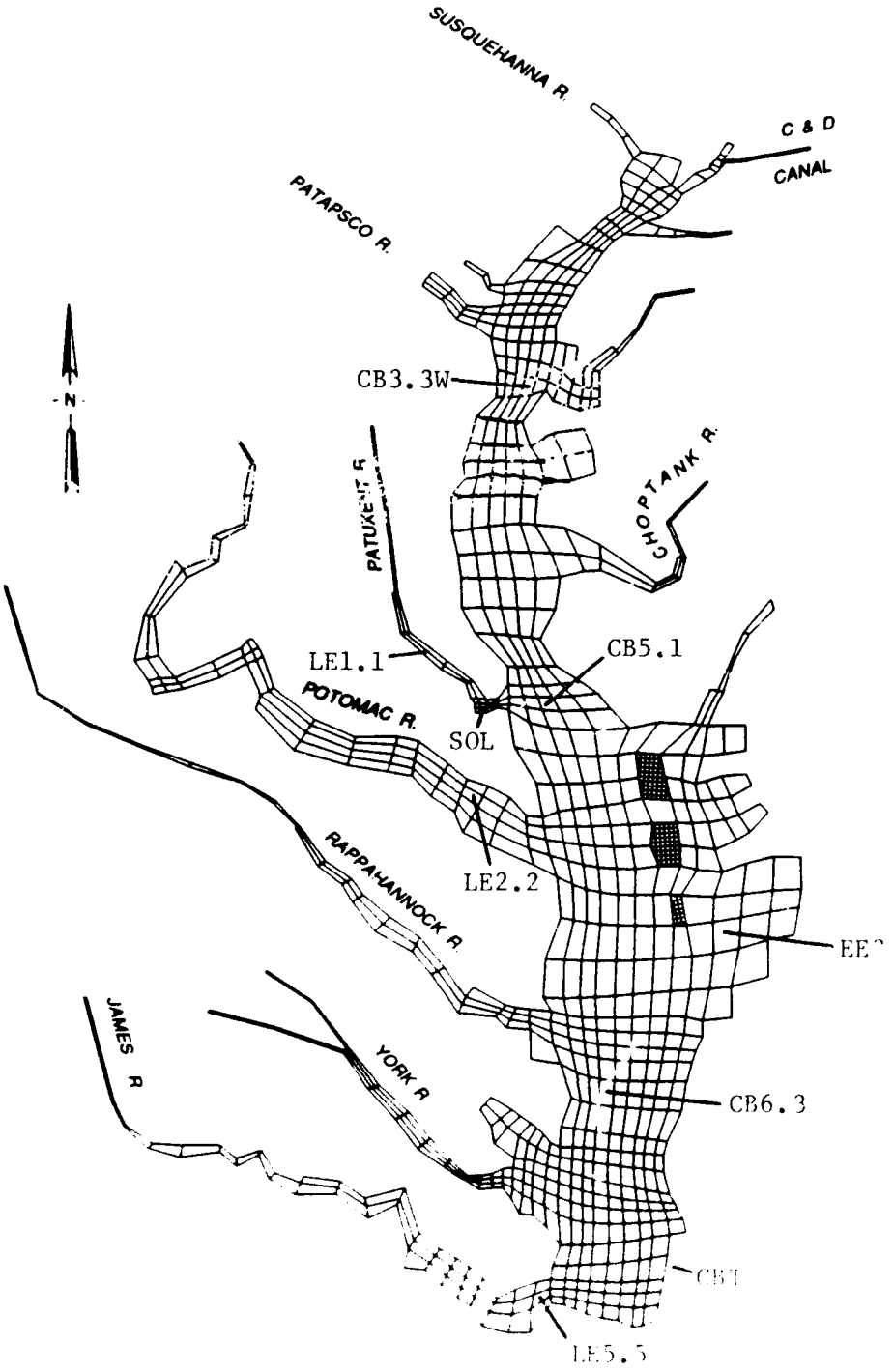

Figure 141. Data stations for the 1986 data set

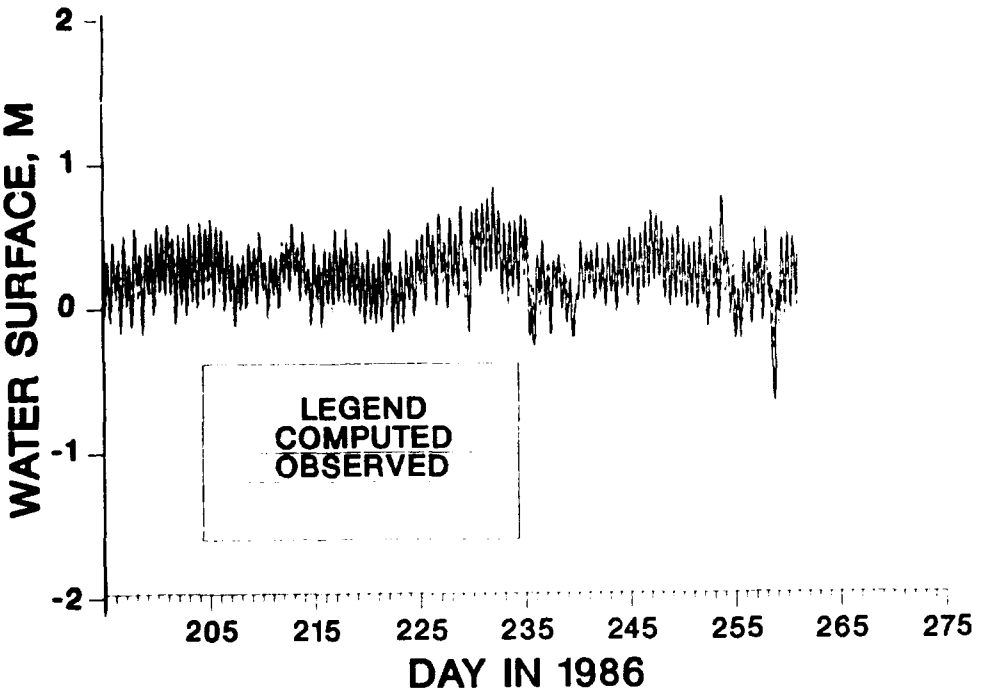

Figure 142. Comparison of computed and recorded tide at Solomons, MD, during 1986

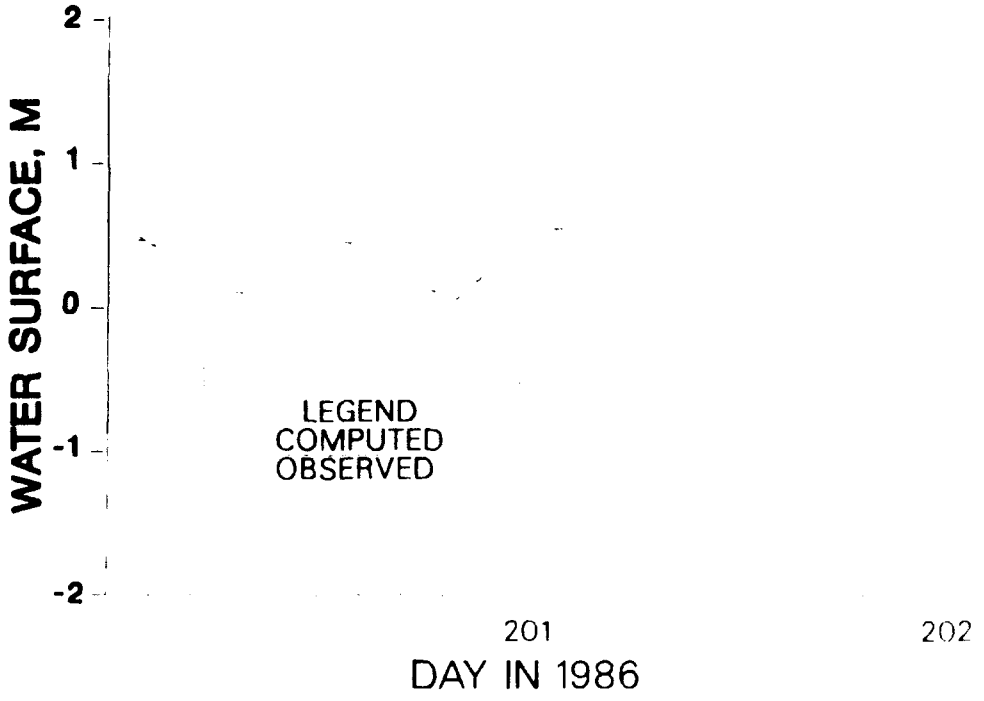

Figure 143. Comparison of computed and recorded tide at Solomons, MD, near day 201 of 1986

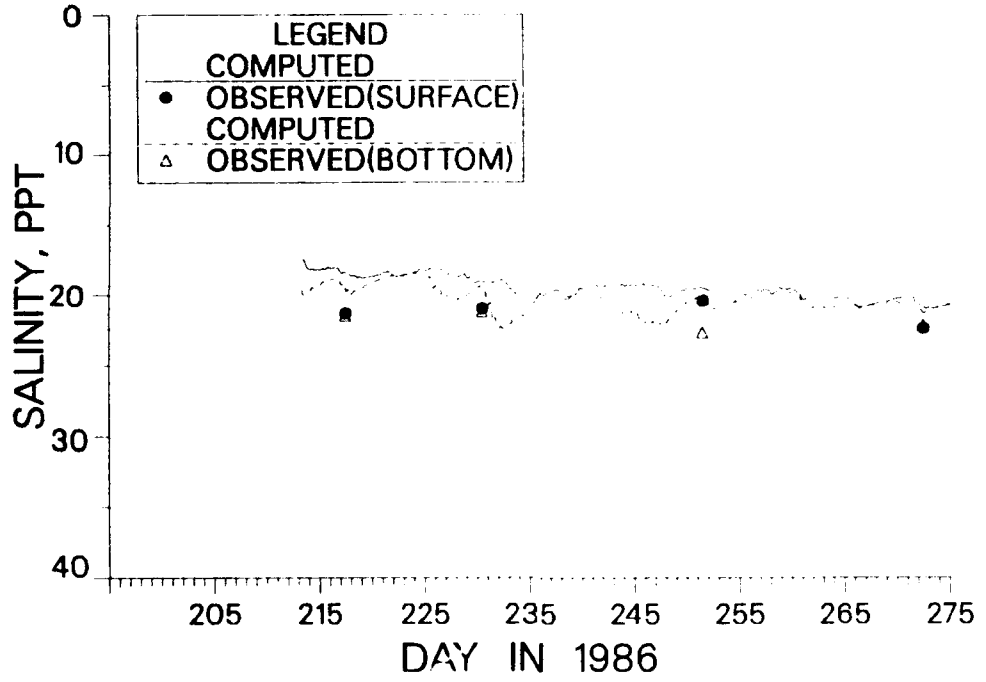

Figure 144. Comparison of computed and recorded salinity at station EE 3.5 during 1986

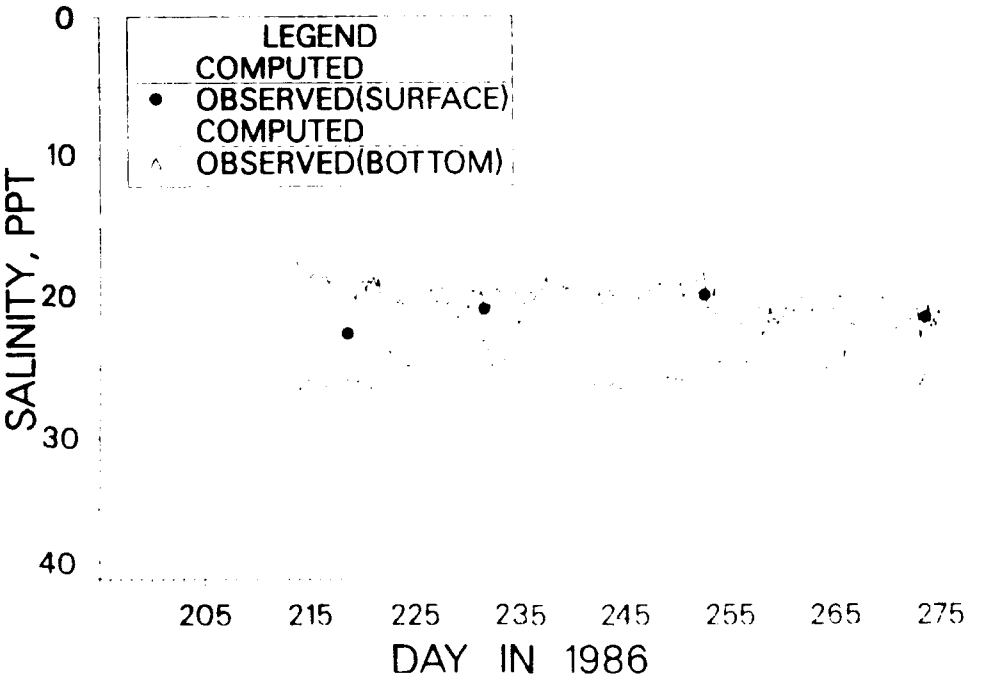

Figure 145. Comparison of computed and recorded salinity at station CB 6.3 during 1986

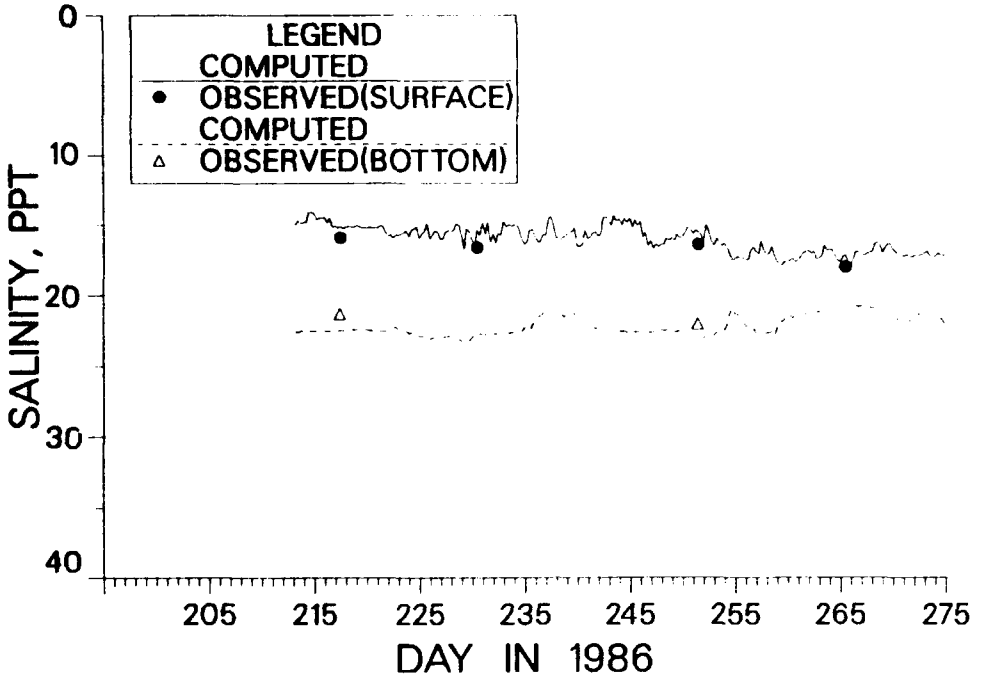

Figure 146. Comparison of computed and recorded salinity at station CB 5.1 during 1986

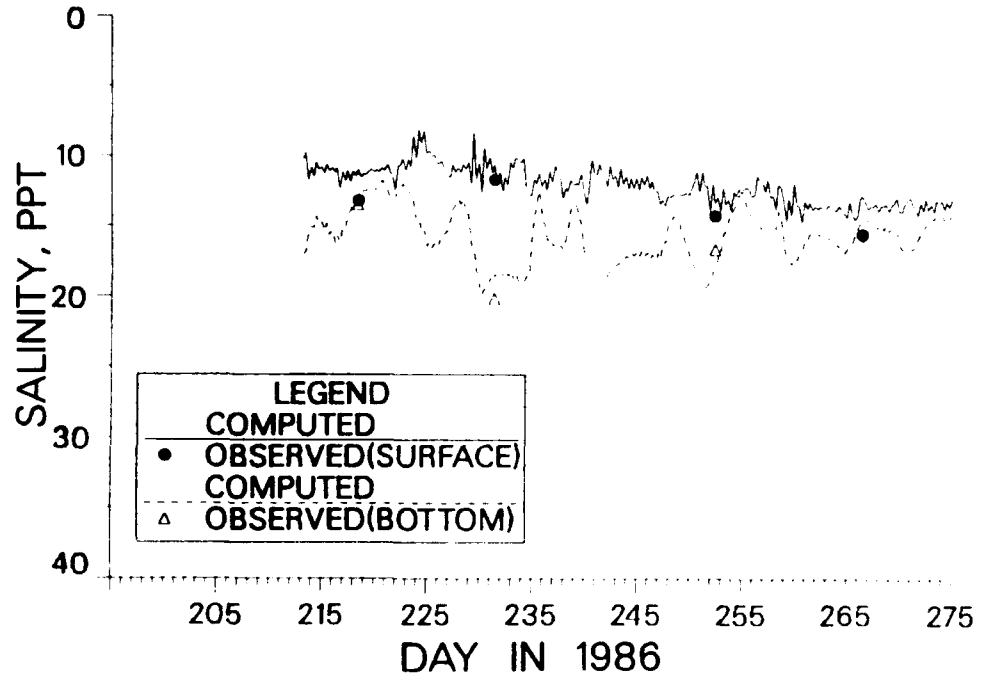

Figure 147. Comparison of computed and recorded salinity at station CB 3.3W during 1986

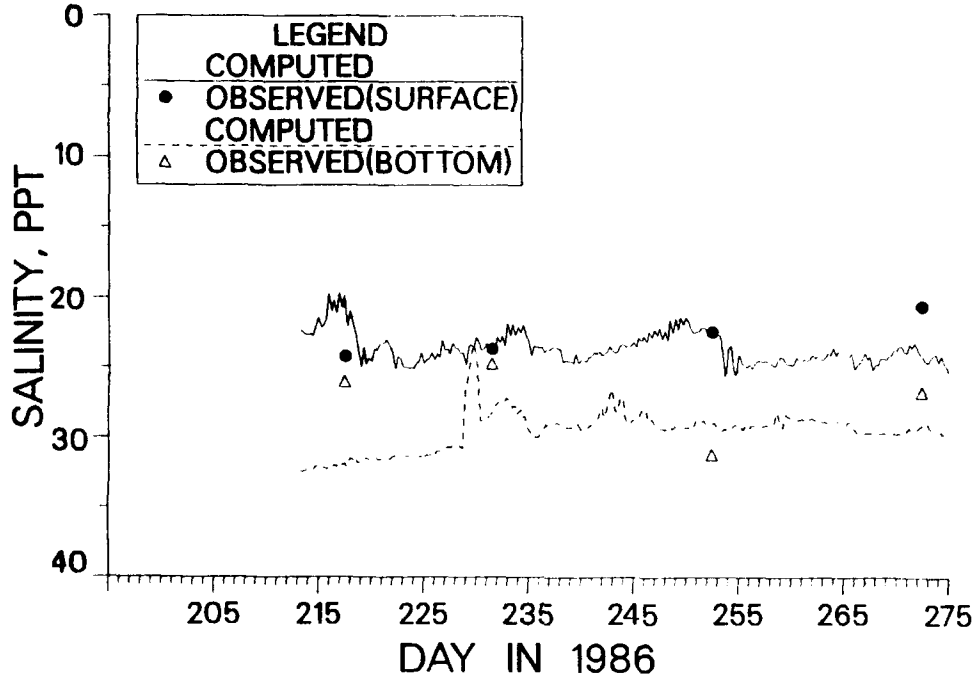

Figure 148. Comparison of computed and recorded salinity at station LE 5.5 during 1986

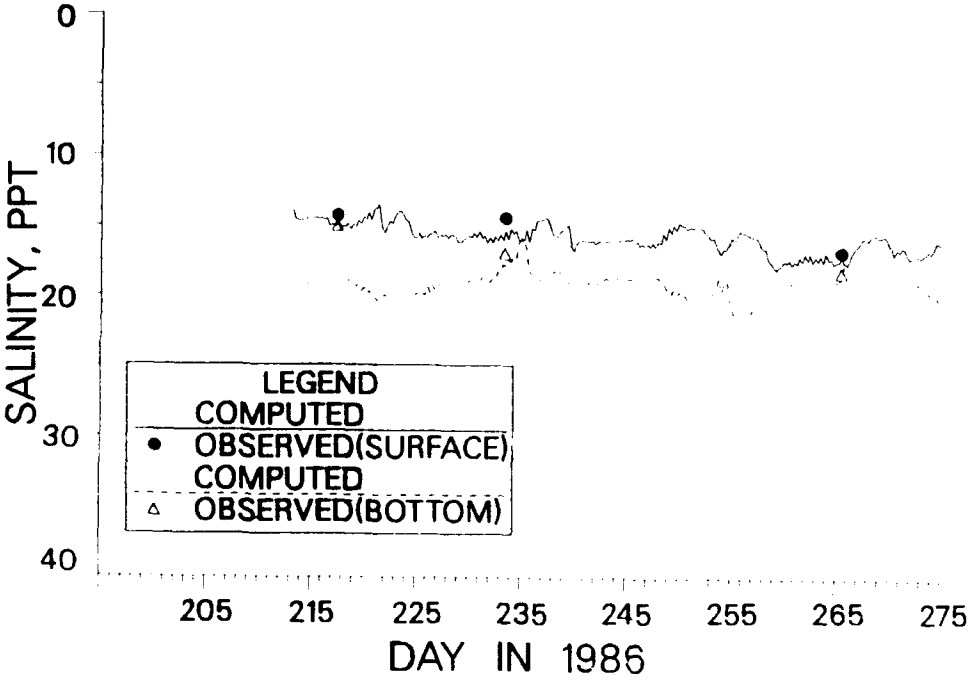

Figure 149. Comparison of computed and recorded salinity at station LE 2.2 during 1986

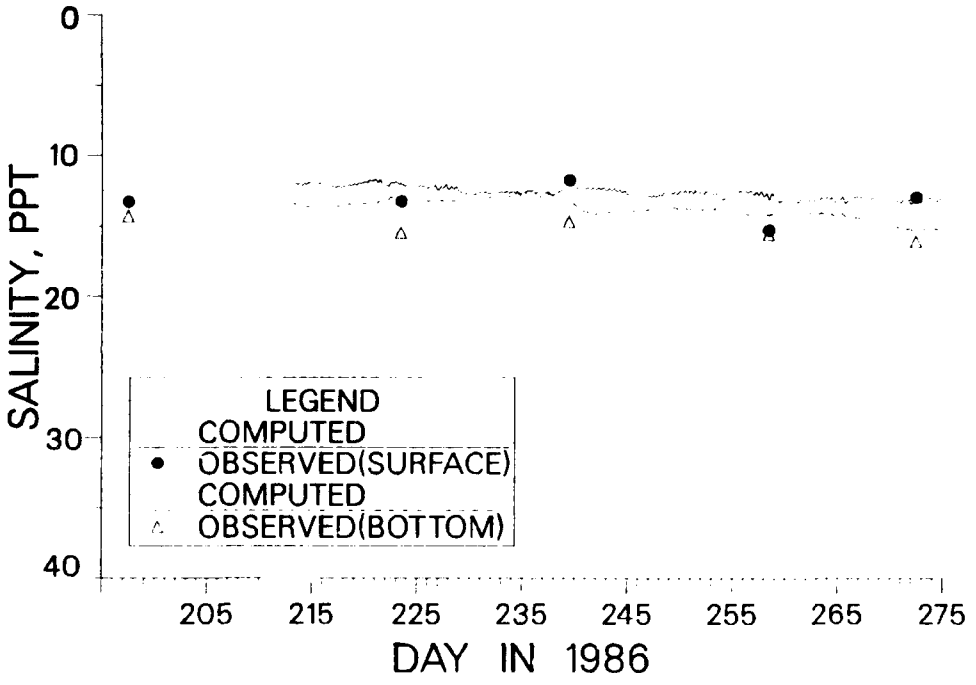

Figure 150. Comparison of computed and recorded salinity at station LE 1.1 during 1986

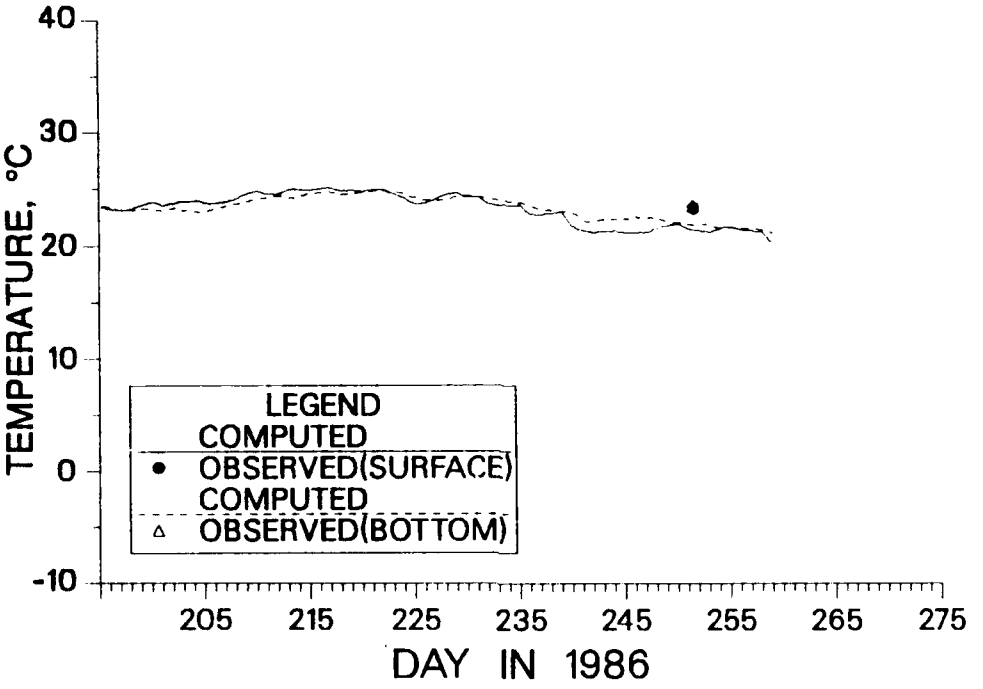

Figure 151. Comparison of computed and recorded temperature at station EE 3.5 during 1986

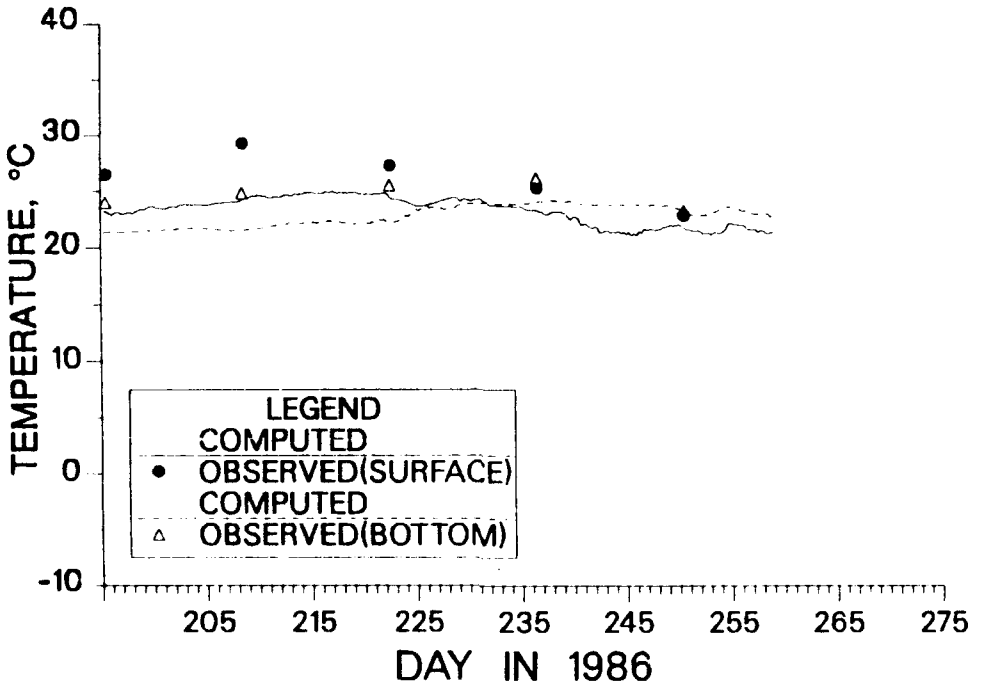

Figure 152. Comparison of computed and recorded temperature at station CB 5.1 during 1986

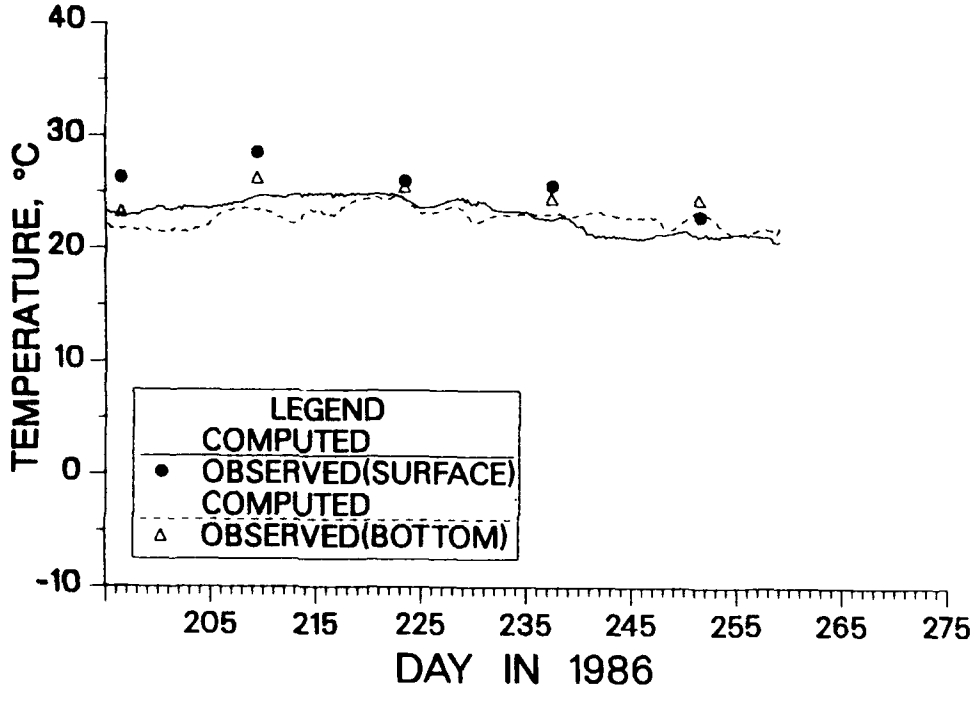

Figure 153. Comparison of computed and recorded temperature at station CB 3.3W during 1986

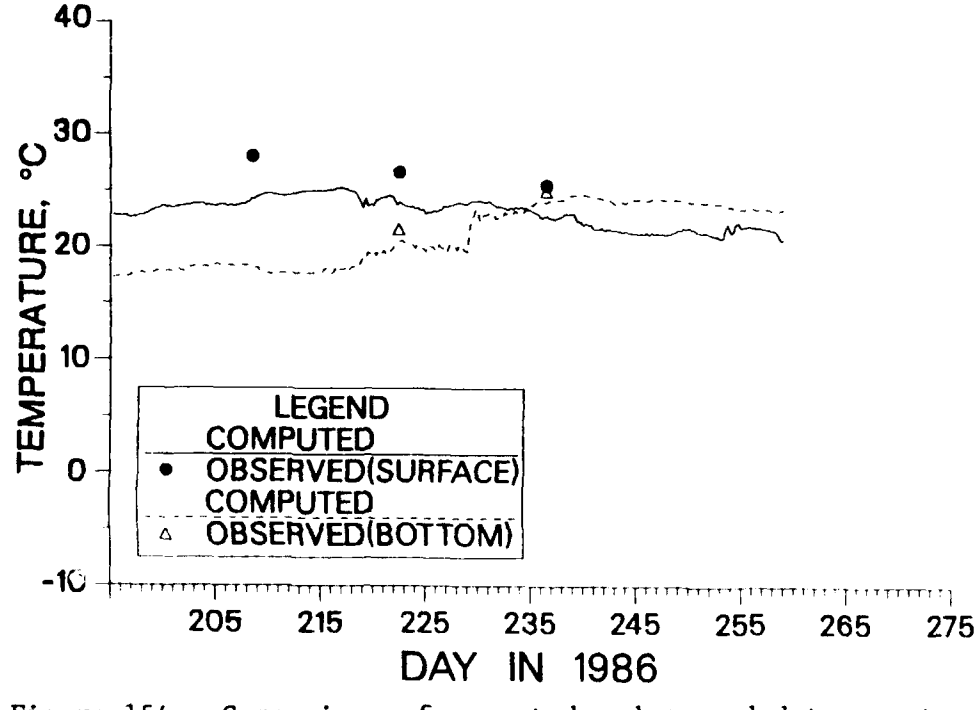

Figure 154. Comparison of computed and recorded temperature at station LE 5.5 during 1986

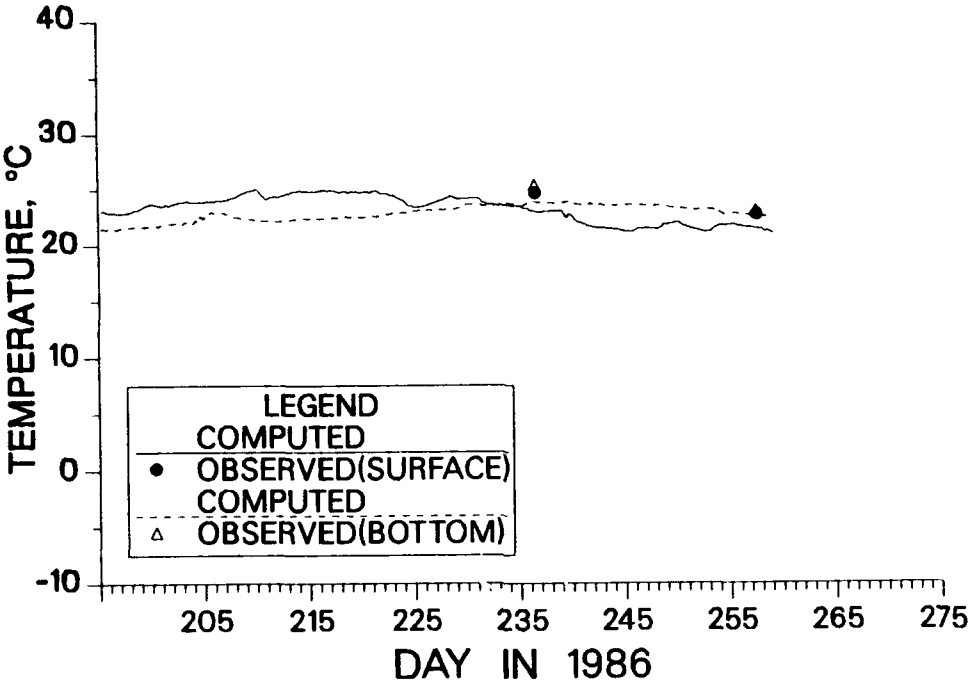

Figure 155. Comparison of computed and recorded temperature at station LE 2.2 during 1986

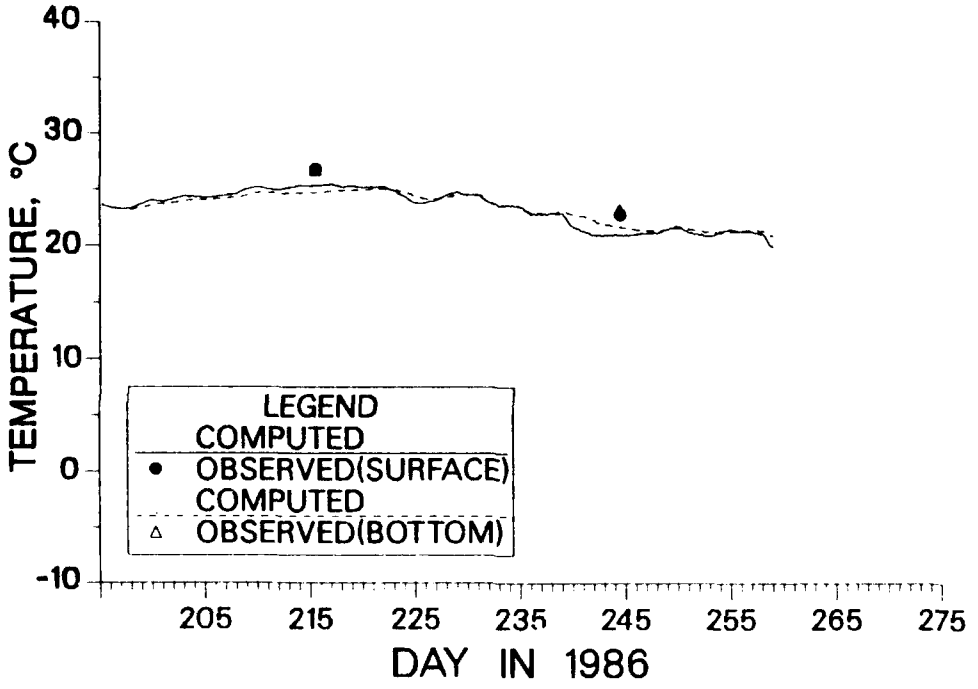

Figure 156. Comparison of computed and recorded temperature at station LE 1.1 during 1986

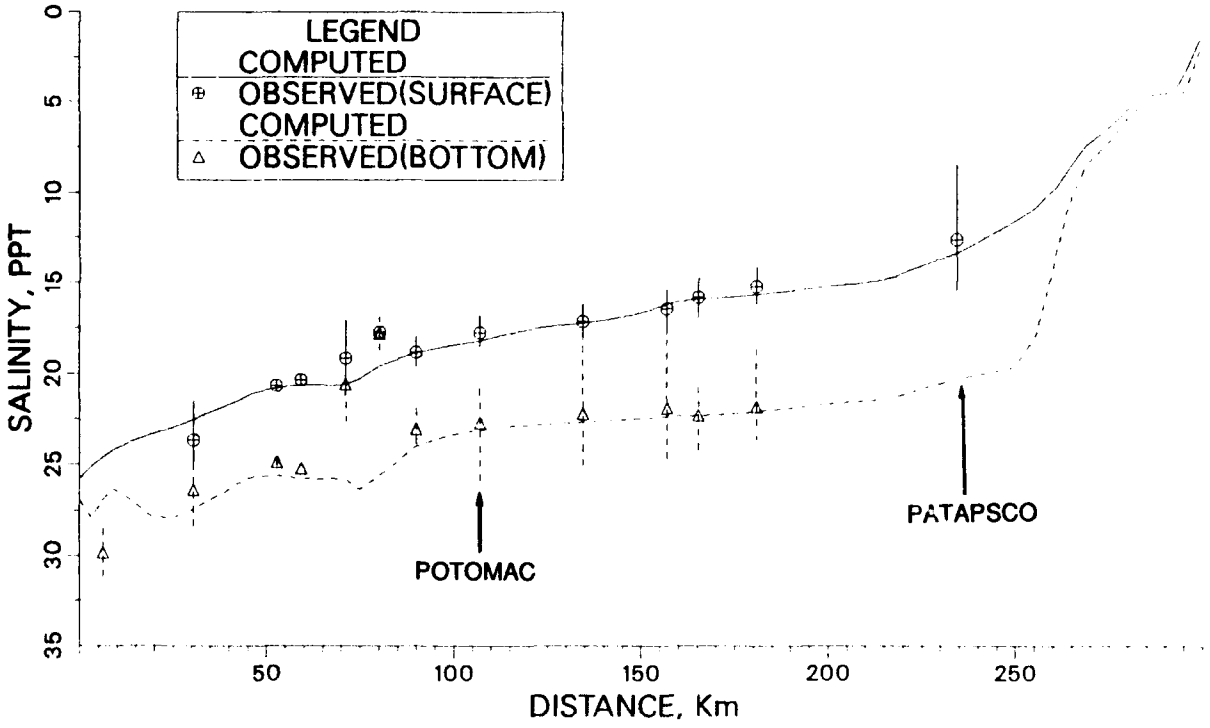

Figure 157. Comparison of seasonally averaged salinities along the main bay during 1986

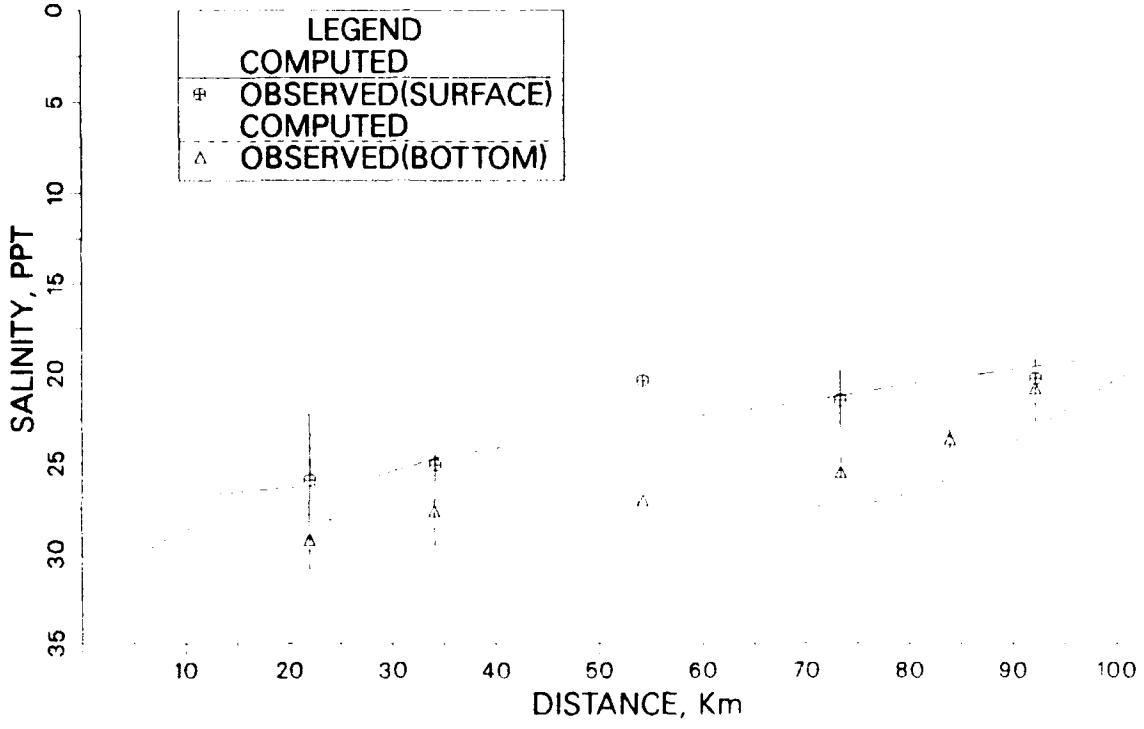

Figure 158. Comparison of seasonally averaged salinities along the eastern main bay transect during 1986

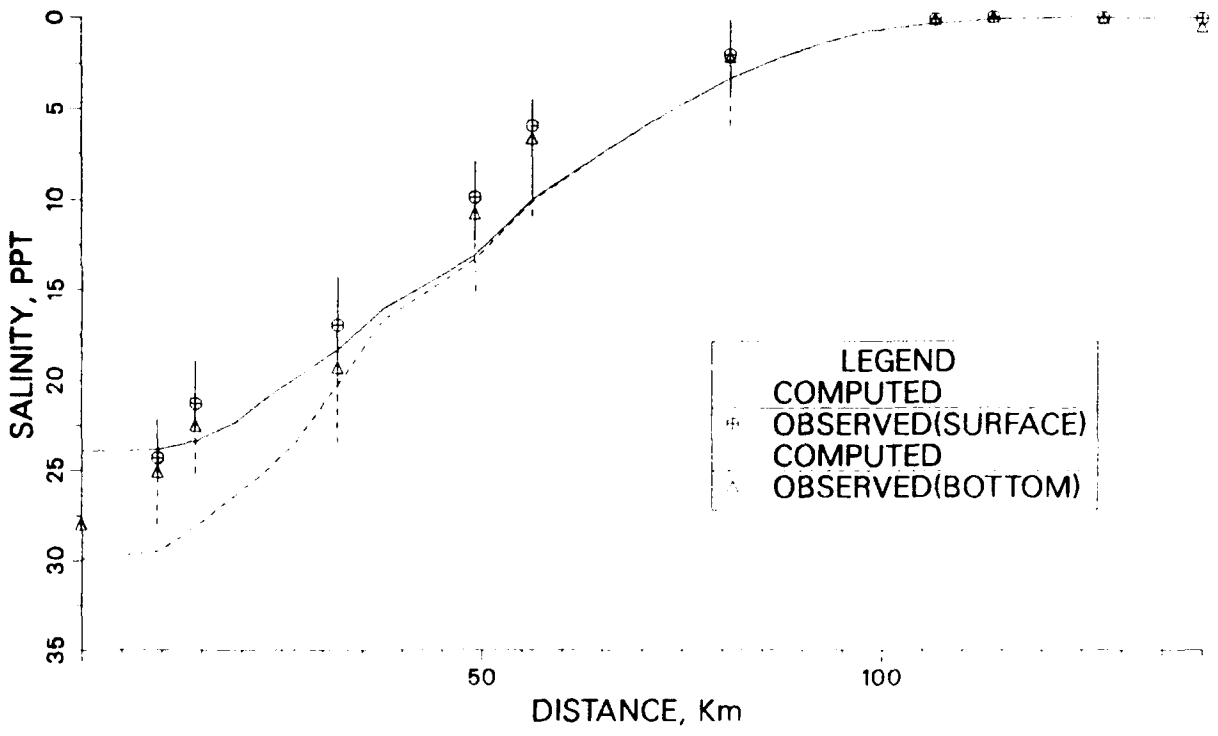

Figure 159. Comparison of seasonally averaged salinities along the James River during 1986

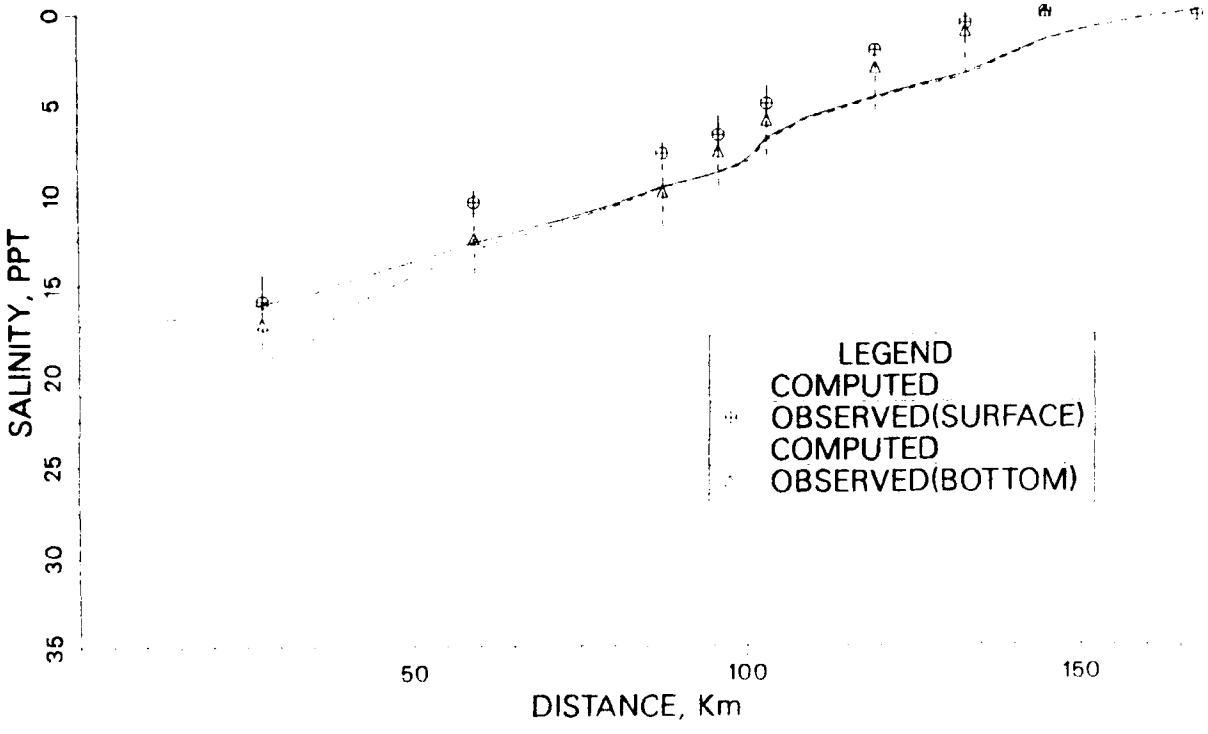

Figure 160. Comparison of seasonally averaged salinities along the Potomac River during 1986

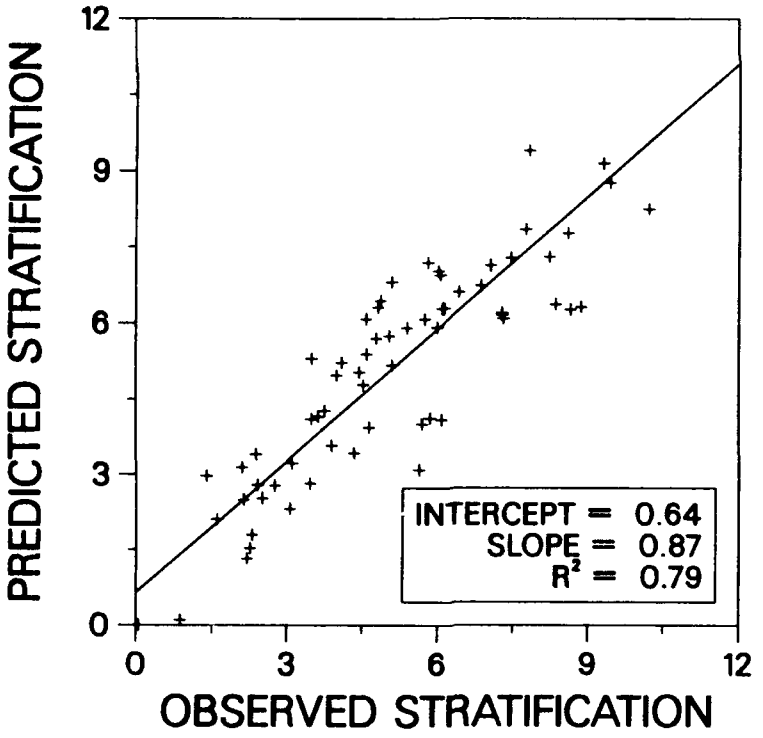

Figure 161. Comparison of computed and recorded stratification for all main bay stations during 1986

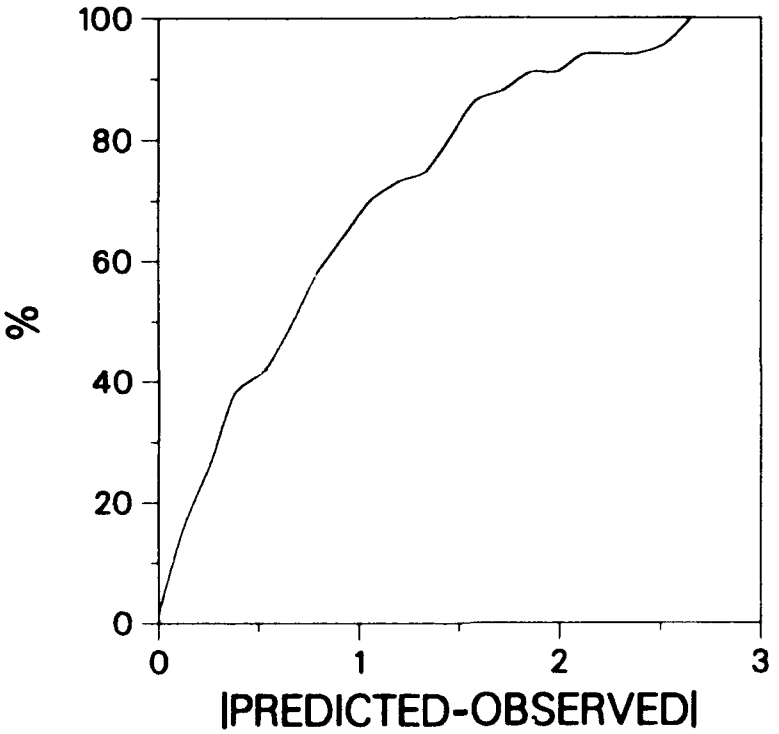

Figure 162. Frequency of occurrence of the error in the computed stratification for all main bay stations during 1986

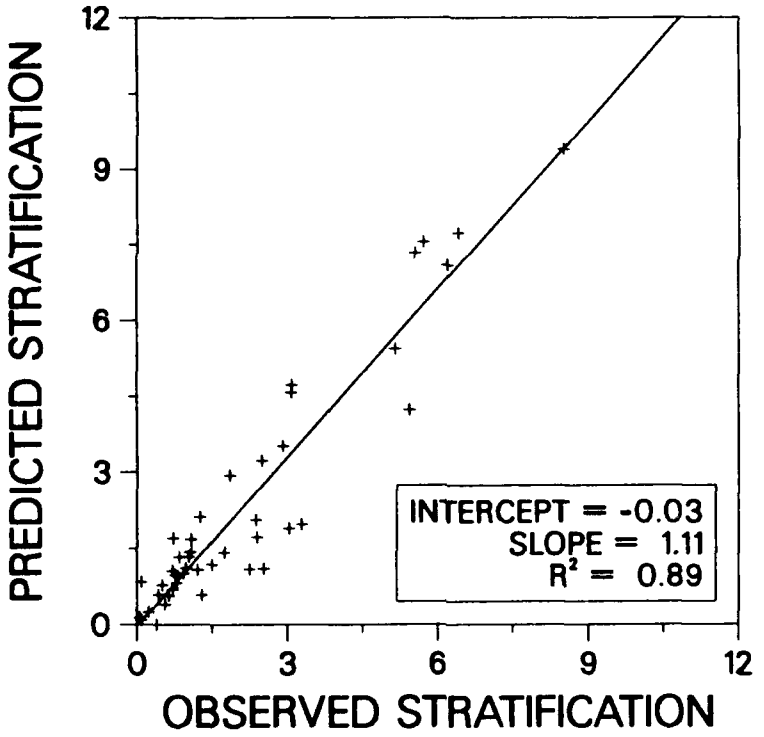

Figure 163. Comparison of computed and recorded stratification for all tributary stations during 1986

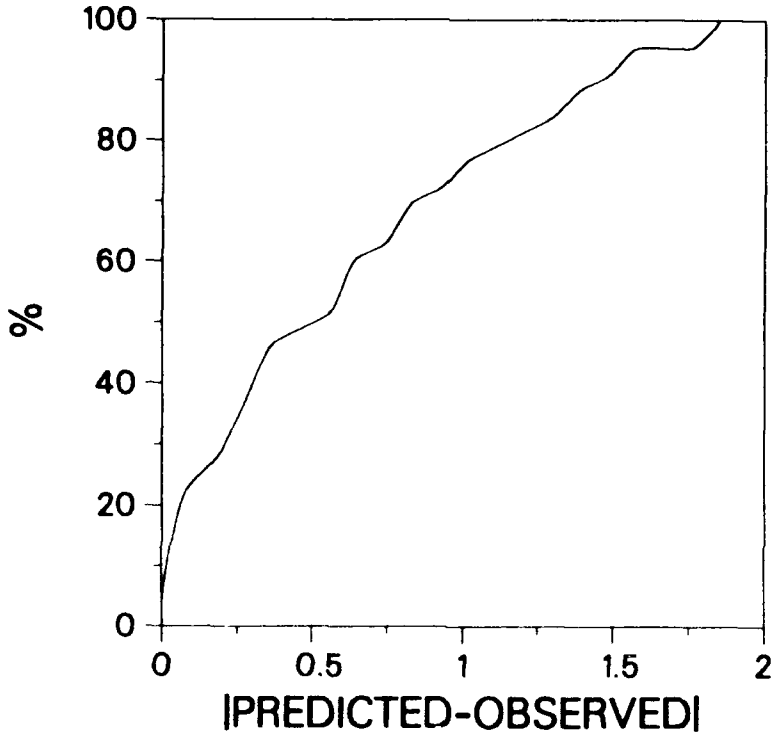

Figure 164. Frequency of occurrence of the error in the computed stratification for all tributary stations during 1986

APPENDIX D: NOTATION

A_v, K_v	Vertical turbulent eddy coefficients
ARE	Average relative error
C	Surface drag coefficient; conductivity
C_d	Bottom friction coefficient
D	Eddy diffusivity or viscosity
f	Coriolis parameter
g	Acceleration due to gravity
h	Layer thickness
H	Total water depth
k	von Karman constant
K	Surface heat exchange coefficient
MAE	Mean absolute error
MBE	Mean bias error
M_i	Model results
N	Brunt-Vaisala frequency; number of data points
O_i	Observed data
Ri	Richardson number
RMSE	Root mean square error
S	Salinity
t	Time
T	Temperature
T_e	Equilibrium temperature
u,v	Horizontal components of Cartesian velocity
u′,v′,w′	Turbulent velocity fluctuations
$\bar{u},\bar{v}$	Components of contravariant velocity
$\bar{U},\bar{V}$	Vertically integrated contravariant unit flows
$\bar{u}_1,\bar{v}_1$	Horizontal contravariant velocity components next to the bottom
w	Vertical component of velocity
W	Wind speed
x,y,z	Cartesian coordinates
z_o	Bottom roughness height
ζ	Water-surface elevation
Λ	Macroscale of turbulence
ξ,η	Boundary-fitted coordinates

ρ	Water density
$\tau_{b_\xi}, \tau_{b_\eta}$	Components of bottom shear stress
$\tau_{s_\xi}, \tau_{s_\eta}$	Components of surface shear stress